

Study of Interaction of Entrained Coal Dust Particles in Lean Methane – Air Premixed Flames

A Master Thesis Submitted to the Faculty of the
Worcester Polytechnic Institute
in partial fulfillment of the requirements for the
Degree of Master of Science in
Fire Protection Engineering

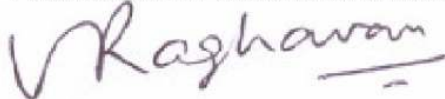
September 2011


Yanxuan Xie


Approved:



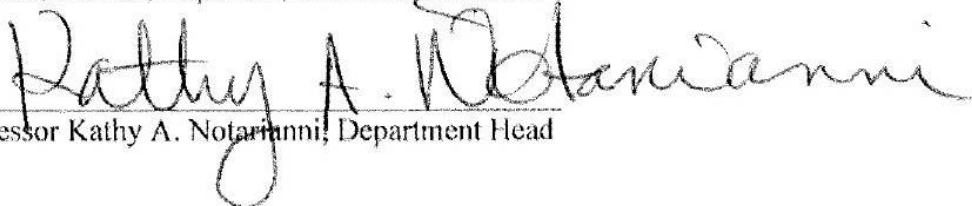
Professor Ali S. Rangwala, Advisor



Professor Raghavan Vasudevan,
Indian Institute of Technology, Co-Advisor



Alfonso Ibarreta, Exponent, Committee Member



Professor Kathy A. Notarianni, Department Head

Contents

Acknowledgement	3
Chapter 1	4
Chapter 2.....	7
Chapter 3.....	15
Chapter 4.....	35
Appendices.....	37
Appendix A: Experimental Apparatus Details.....	37
A.1 Experimental Equipment	37
A.2 Procedures of Conducting Experiment for Study.....	46
Appendix B: Algorithm for Angle Measurement	48
B.1 Description of the Algorithm using Matlab	48
B.2 Developed Algorithm (Matlab Code)	49
Appendix C: Experimental Data	54
C.1 Pressure Drop Calculation for Dust Injector.....	54
C.2 Dust Entrainment Data for Dust Injector	55
C.3 Summary Sheet of Flame Cone Angle for Experiment.	58
C. 4 Pictures and Entrainment Data.....	62

Acknowledgement

This work is funded by **National Science Foundation (NSF) Award #0846764** and the author like to give the special thanks to NSF.

The author likes to thank the research advisors **Professor Rangwala Ali**, and **Professor Raghavan Vasudevan**. Without their devotion, this study cannot be completed.

The Higgins Lab machinist **Neil Whitehouse** provided invaluable guidance in the manufacture of experiment parts throughout this project. I would also like to acknowledge the help of **Professor Andy Klein** (ECE) in assisting me with the algorithm for cone angle measurement. **Professor Simon Evans** (ME) provided helpful information on the shadowgraph set-up. **Professor Robert Zalosh** was instrumental in getting us free samples of coal dust and providing valuable input. The support from my lab-mates of Combustion Lab, **Scott Rockwell**, **Kulbhushan Joshi**, **Brian Elias** and **Minkyu Lee** are also appreciated. I would like to thank all of them.

The author also like to thank to **American Electric Power (AEP)** for supplying the coal dust and **Retsch (Jacqui Town)**for providing research equipment (sieve shaker and ultrasonic cleaner) at half of the full price.

Chapter 1

Introduction

In industries that manufacture, transport, process and/or use combustible dusts, accidental dust deflagrations represent a real hazard to both personnel and equipment. Among all the dust deflagrations, coal mine explosion is a worldwide phenomenon that causes a high number of casualties each year. An example is the recent coal mine explosion in West Virginia (April 5, 2010) killing 29 miners and considered as one of the most disastrous mining accidents in US history. Interestingly, most coal mine explosions often involve both a methane deflagration combined with fugitive coal dust (coal particles that are small enough to be easily suspended in air $\sim 100 \mu\text{m}$) that is collected by the combustion wave as it progresses through the mine. The evolution of coal mine explosion usually has three different stages: 1. a small methane-air explosion (fire damp) is generated due to various ignition sources, such as sparks caused by mining equipment; 2. the pressure blast disperses the dust deposited on various surfaces of mine tunnels; 3 the methane-air flame interacts with the coal dust suspended in the air.

The objective of this work is to use a lab-scale experiment to study the interaction of coal dust particles and premixed methane-air flame at lean conditions. Specifically, the influence of coal dust particle size, number density on the laminar burning velocity of the flame is analyzed. It is observed that (in the laminar regime) a particle size less than $25 \mu\text{m}$ is required to cause an increase in the burning velocity for the particular type of coal dust examined in this study (Pittsburgh seam coal). The reason for the promotion of the burning velocity is mainly due to the volatiles released by the coal dust particles due to heat transferred from the flame which causes a local increase in the equivalence ratio. The small particle size ($<25 \mu\text{m}$) ensures that the additional heat evolved due to the release of volatiles is greater than that absorbed by the particles. A mathematical model is developed to analyze this behavior and good agreement is observed with theory and experiment. Ultimately, given reliable property data for a particular type of dust, the model can be used as a predictive tool to analyze the hazard associated with any kind of dust.

A novel dust injector is developed as the first part of the thesis. The design of the dust injector is inspired by Bunsen burner where the venturi effect is used to entrain the dust and create a dust-gas mixture. The performance of the novel dust injector is investigated and presented in Chapter 2. The results show that there is an optimum area for the side openings for dust entrainment, at which the injector performance will be the best. The entrainment rate is found to be a non-linear function of the flow-rate for low air flow-rates (till around 9.4 gram per minute) and for higher air flow-rates it becomes a linear function.

The second part of the thesis involves analyzing the change in laminar burning velocity by using a dust burner based on the injector. This study is presented in Chapter 3 of this thesis. In this study, the changes of laminar burning velocity with particles are investigated experimentally and theoretically. The laminar burning velocity of the coal dust-methane-air mixture is determined by taking a shadowgraph of the resulting flame and using the cone-angle method. The results show that the addition of coal dust in methane-air premixed flame reduces the laminar burning velocity at particle sizes of 53 to 63 μm and 75 to 90 μm . However, burning velocity promotion is observed for 0 to 25 μm particles at a methane-air equivalence ratio $\phi = 0.80$. A mathematical model is developed to analyze the influence of particle – gas - flame interaction. The model successfully predicts the change of laminar burning velocity at various dust concentrations.

Based on the observations made in the study, a Conclusions and Future Work section is included as Chapter 4. The Appendices contain additional information about the study and experiment data. The detailed information about experiment equipment and test procedures are available in Appendix A. The algorithm used for cone angle measurement in this study is provided in Appendix B. Appendix C contains additional experimental data, including entrainment data for Chapter 2, cone angle measurements, and images that are used to obtain laminar burning velocity using the cone-angle method in Chapter 3.

The following publications and conference papers have resulted from this work:

Peer Reviewed Publications

1. Y. Xie, V. Raghavan, A. S. Rangwala, "**Naturally Entraining Solid Particle Injector,**" *Powder Technology, Vol. 213, pp. 199-201, 2011 (Short Communication)*
2. Y. Xie, V. Raghavan and A. S. Rangwala, "**Interaction of Coal Dust Particles on Lean Premixed Methane-air Flames,**" *Combustion and Flame (Under Review)*

Conference Papers

1. **Y. Xie, V. Raghavan, and A.S. Rangwala, "Study of Interaction of Entrained Coal Dust Particles in Lean Methane - Air Premixed Flames,"** 7th U.S. National Combustion Meeting, Atlanta, Georgia, Mar 20-23, 2011.
2. **Y. Xie, V. Raghavan, and A.S. Rangwala, "Study of Interaction of Entrained Coal Dust Particles in Lean Methane - Air Premixed Flames,"** Eastern States Combustion Meeting, University of Connecticut, Storrs, 9-12, Oct 2011.

Chapter 2

Naturally Entraining Solid Particle Injector

Y. Xie, V. Raghavan, A. S. Rangwala, "Naturally Entraining Solid Particle Injector," *Powder Technology, Vol. 213, pp. 199-201, 2011 (Short Communication)*

Abstract

The objective of the present work is to develop and calibrate a novel, vertical solid particle injector that uses the pressure drop in the air flow across an orifice plate in a circular pipe, to naturally entrain micron-sized solid particles such as coal dust. The particles continuously drop from a feeder located outside the pipe into the orifice plate through peripheral (side) openings in the pipe, where they are carried upwards by the air flow accelerated near the orifice exit. Three types of designs for the peripheral openings, in terms of the shape, size and number are evaluated by testing which one of them results in maximum particle entrainment. The device is calibrated by recording the mass loss rate of the powder as a function of volumetric flow-rate of air. The results show that there is an optimum area for the side openings, at which the injector performance will be the best for the given pipe and orifice-hole sizes. The entrainment rate is found to be a non-linear function of the flow-rate for low air flow-rates (till around 9.4 grams per minute) and for higher air flow-rates it becomes an almost linear function.

Keywords: Particle or powder injector; Orifice plate; Pressure drop; Natural entrainment; Mass loss rate

1. Introduction

Injection of solid particles of different sizes into a fluidized flow device or in a pneumatic conveying process has applications in several chemical, food processing and energy related industries. The pulverized coal combustor, coal gasification systems, and dry-forming processes for paper are few examples. In these, there is a need to reliably meter the flow-rate of particle laden fluid mixtures. In pneumatic conveying, the solid particles are mixed with air either under the influence of gravitational force or due to the pressure force resulting from the pressure drop in an accelerating air flow. Typical materials used

for conveying are pulverized coal, ash, food grains, sand particles and dry chemicals [1]. Wagenknecht and Bohnet [2] were the first and foremost to study an injector type particle feeder. In their study, a high-velocity air stream exists from a primary nozzle and entrains the particles into a secondary nozzle, where the necessary pressure is built up for conveying the particles. Following them, Chellappan and Ramaiyan [3] and Westaway et al. [4] carried out investigations on the effects of important design parameters of a gas-solid injector feeder, which can be used in pneumatic conveying systems. All these designs utilize a nozzle to create high velocity air flow that carries the solid particles. Apart from the pneumatic conveying application, powder dispensers are designed for particle size measurements [5], including that of aerosols. These devices are usually oriented horizontally. Recently, dry particle dispersion methods, process and the dispersion efficiency have been discussed in a review article by Masuda [6].

The techniques currently available have limited capability for fine control of feeding rate. In certain applications involving fuel characterization and energy studies, the quantity of particle injected has to be precisely known and the particles are to be fed in wide ranges of quantities. In these cases, there is a need to have a particle injecting device, which allows for simple and precise control of both fluid flow and particle feed rates. A typical solid-particle injector is designed, developed and calibrated in this study. This injector, which is oriented upwards, utilizes the venturi effect observed when the flow passes through a reduced area passage such as in orifice plates, converging and diverging passages and nozzles. An orifice plate is used to create the venturi effect in this study because of ease of manufacture and cost effectiveness. The entire setup consists of a pipe having an orifice plate, connected to another pipe having openings of on its periphery from which the powder is easily fed into the orifice plate, and an extension pipe connected to this, to make the particle laden air flow develop further. Furthermore, since the powder does not pass through the orifice hole, erosion of the hole is prevented. The control of the powder feed rate is basically achieved by varying the air flow-rate and/or by changing the area of the side openings in the pipe. Three design configurations are studied and a thorough calibration is done for each case for varying air flow-rates.

2. Solid-Particle Injector

The injector device comprises of three parts:

1. A lower pipe with an orifice plate. A straight hole, sharp edged orifice has been employed.
2. A middle section, which is a pipe with openings in its periphery and with a dust feeder.
3. A pipe on the top of the middle section to further develop the flow.

The assembly is shown in Fig. 1. The upper (124.5 mm long and 3.3 mm thick) and lower (135.5 mm and 3.3 mm thick) pipes can be inserted to the middle section and socket head screws are used to secure these sections intact (Fig. 1). The top end of the lower pipe has an orifice plate of 1 mm thickness with a hole at its center having a diameter of 1 mm. The length of the middle section is 50.8 mm. It has provisions to insert the top and lower pipes at its top and lower ends. The middle section has peripheral openings as shown in Fig. 1. Both the number and size of these openings have been varied in this study.

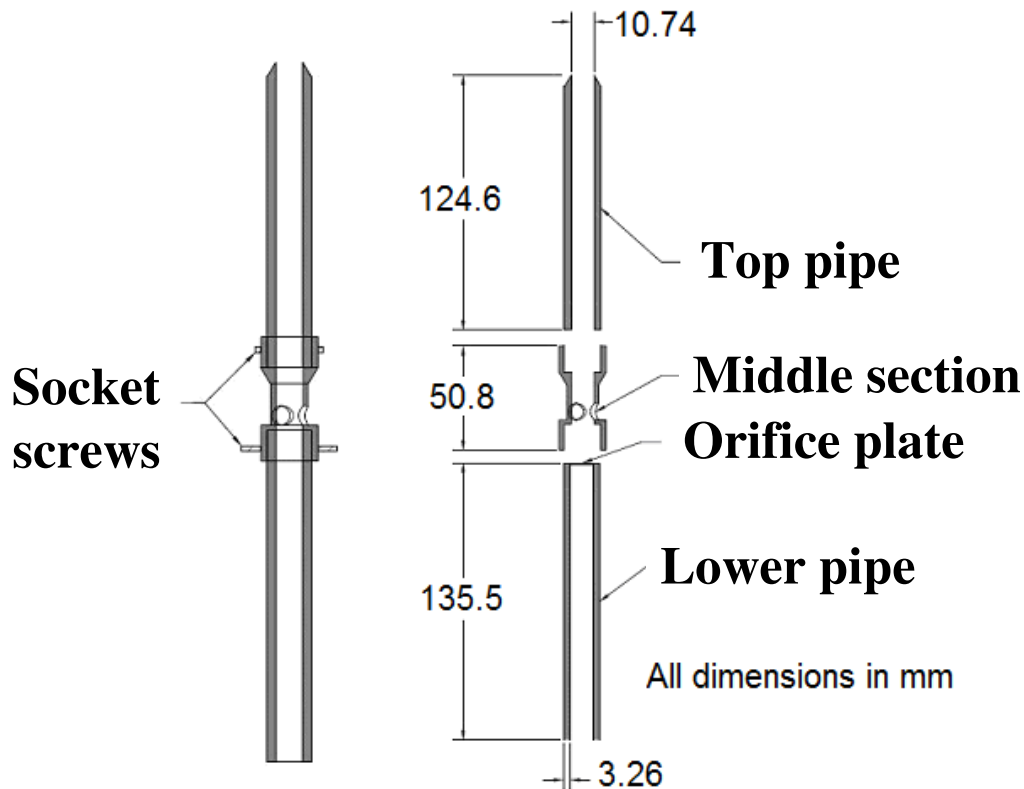


Figure 1: Solid particles injector

To study the effects of size and number of openings in the middle section, three different middle sections are used:

1. First middle section (case 1) has six circular openings each with a diameter of 5 mm, amounting to a total particle-feed area of 118 mm^2 .
2. The second one (case 2) has three circular openings with 8 mm diameter each and a total opening area of 151 mm^2 .
3. The third middle section (case 3) consists of three rectangular openings each with an area of 90 mm^2 and a total opening area of 270 mm^2 .

A particle feeder which comprises of an inverted hollow 60° inverted cone made of acrylic is connected around the middle section as shown in Fig. 2. The feeder is open at the top and has a smooth surface to minimize frictional losses. The feeder rests on the outer portion of socket screws.

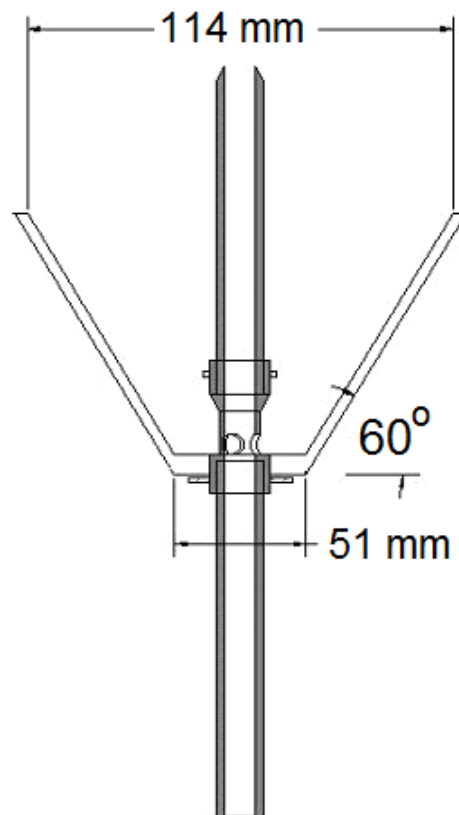


Figure 2: Injector with particle feeder

3. Experimental Setup and Procedure

A schematic of the experimental setup is shown in Fig. 3. Air is supplied with an upstream pressure of 5 psig (34474 Pa) to the lower pipe through a pressure regulator, valve and air flow meter. The air flow meter can supply air at flow-rates ranging from 0 liters per minute (lpm) to 10 lpm in increments of 0.5 lpm. The accuracy of the flow meter at its highest flow-rate is within $\pm 4\%$. Pittsburgh seam coal dust is used in the present study, and has a particle size in the range of 90 - 106 micro-meters (μm), a reported constant sphericity value of 0.73 [6], and a bulk density of 0.553 g/cm^3 . A particle collection pan of 300 mm diameter, as shown in Fig. 3, is used to collect the particles injected out of the top pipe. The injector and the particle feeder are secured in a support frame as shown in Fig. 3 and the entire assembly is weighed using a Cole Palmer load cell (capacity of 4.2 kg with a sensitivity of 0.01 g). The uncertainty in the mass measurement is $\pm 0.03 \text{ g}$. The ring stand is used to support the collection pan so that the particles collected in the pan will not be weighed by the load cell.

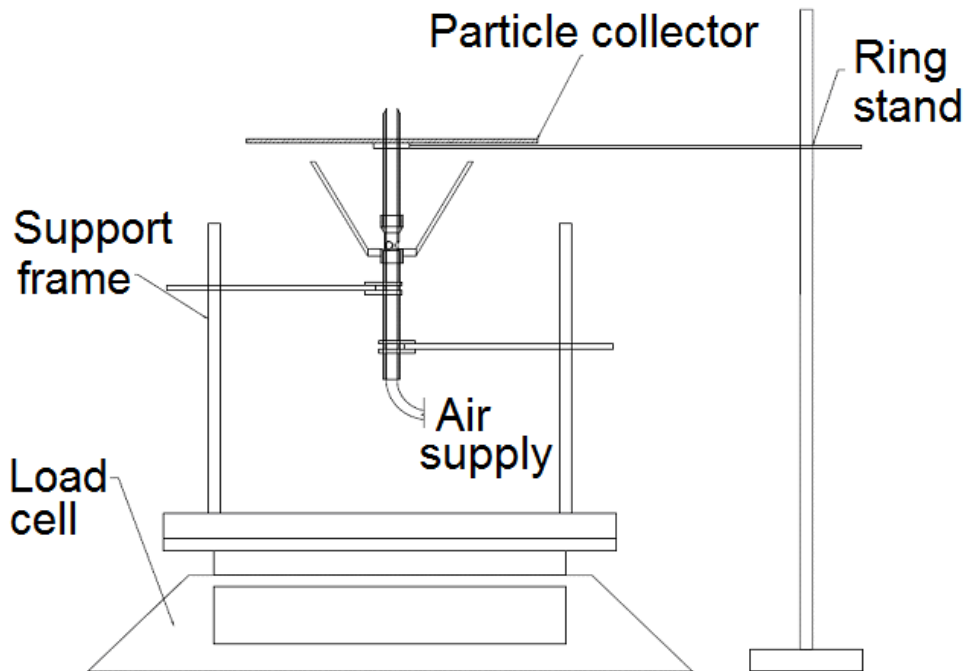


Figure 3: Schematic of experimental setup

The experiments are carried out in atmospheric temperature equal to 300 K. The experimental procedure comprises of fitting the desired middle section, filling the conical

feeder with coal dust and then turning the air supply on. The flow meter is set to deliver the desired air flow-rate and the load cell output is recorded as a function of time. The recording of the mass loss rate is continued for 5 minutes and then stopped. Each experiment is repeated at least three times to ensure consistent results within $\pm 2\%$. An instantaneous photograph showing particle injection and collection in the pan is presented in Fig. 4 (case 2: three circular openings with 8 mm diameter each at an air flow-rate of 5 lpm).



Figure 4: An instantaneous photograph showing particle injection and collection in the pan

4. Results and Discussions

The particle injection rate is mainly dependent on the flow-rate and the size of the side openings in the three middle sections studied. For each middle section, air flow-rate is varied from 1.57 grams per minute (gpm) to 15.7 gpm (1 lpm to 10 lpm). However, no entrainment is recorded for 1.57 gpm, irrespective of the middle section used. As flow-rate increases, the entrainment of coal dust into the pipe increases due to increased venturi effect. This is shown in Fig. 5, where the mass of dust injected (grams per minute) is plotted as a function of the air-flow rate in gpm. The variation of the coal dust injection rate is non-linear for air flow-rates up to 9.4 gpm. After this, as the air flow-rate increases, the dust injection rate follows an almost linearly increasing trend. For low air flow rates (< 9.4 gpm), the dust injection is found to be the highest for case 3 (three rectangular openings with a total area of 270 mm^2). For instance, at an air flow-rate of around 7.9

gpm, the entrainment for case 3 is around 15% more than that of case 2 and 50% more than that of case 1 (six circular openings each with a diameter of 5 mm). In fact at an air flow-rate of around 3.15 gpm (2 lpm), maximum deviation is recorded between case 3 and case 2 (35% more for case 3 than case 2) and between case 3 and case 1 (89% more for case 3 than case 1). When the air flow-rate is increased beyond 9.4 gpm (6 lpm), the variation between all the three middle section cases are almost the same with a maximum deviation within $\pm 3\%$. This shows that when the inertia of air is increased, venturi effect is increased and as a result, the air is capable of carrying the coal dust fed to the orifice plate irrespective of the side opening area. At low flow-rates, the pressure drop created due to venturi effect is partly overcome by the friction, which the inner surfaces of the holes offer to the coal dust flow. Therefore, the injection rate is higher for large openings where the friction effects are minimal. This means that the middle section opening area is critical only for lower air flow-rates and as the air flow-rate increases an optimum opening area can be employed, which in this case can be either case 2 or case 3. The usage of variable opening area, if designed carefully, can be employed to control the particle feeding rate even more precisely.

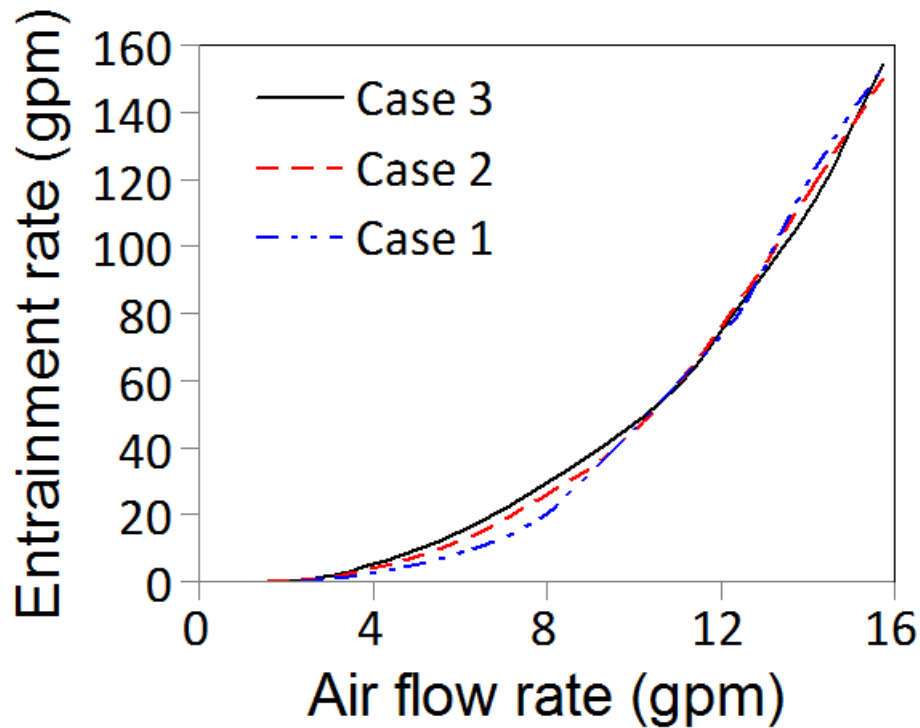


Figure 5: Particle entrainment rate in grams per minute (gpm) as a function of air flow-rate in gpm for all the three middle section cases

5. Conclusions

Design, development, and calibration of a novel solid particle injector have been reported. The injector uses the pressure drop in the air flow across an orifice plate fitted in a circular pipe (venturi effect), to naturally entrain micron-sized solid particles such as coal dust. Coal dust is continuously fed from a feeder located outside the pipe into the orifice plate through peripheral openings in the pipe. Three types of designs for the peripheral openings, in terms of the shape, size and number are evaluated by testing which one of them results in maximum particle entrainment, especially at lower air flow-rates. Calibration of the device is carried out by precisely recording the mass loss rate of the coal dust as a function of volumetric flow-rate of air. The results show that there is an optimum area for the side openings, at which the injector performance will be the best for the given pipe and orifice-hole sizes. The entrainment rate is found to be a non-linear function of the flow-rate for low air flow-rates (till around 9 grams per minute) and dependent on the net area of the openings. For higher air flow-rates, the entrainment becomes almost independent of the opening area and also it becomes an almost linear function.

References

1. EEUA, Pneumatic Handling of Powdered Materials, EEUA Handbook No. 15, Constable, London, (1963) p. 1.
2. U. Wagenknecht and M. Bohnet, Ger. Chem. Engg., 1 (1978) p. 298.
3. S. Chellappan and G. Ramaiyan, Powder Technology, 48 (1986) p. 141.
4. S. F. Westaway, C. R. Woodcock, J. S. Mason and L. S. Fox, Pneumatech 3, Third International Conference on Pneumatic Conveying Technology, Jersey, England, March 1987.
5. P. Tang, D. F. Fletcher, H. K. Chan and J. A. Raper, Powder Technology, 187 (2008) p. 27.
6. J.P. Mathews, S. Eser, P.G. Hatcher, and A.W. Scaroni, KONA Powder and Particles, 25 (2007) p.145.

Chapter 3

Study of Interaction of Entrained Coal Dust Particles in Lean Methane – Air Premixed Flames

Y. Xie, V. Raghavan and A. S. Rangwala, “**Interaction of Coal Dust Particles on Lean Premixed Methane-air Flames,**” Combustion and Flame (Under Review)

Abstract

This study investigates the interaction of micron-sized coal particles entrained into lean methane – air premixed flames. In a typical axisymmetric burner, coal particles are made to naturally entrain into a stream of the premixed reactants using an orifice plate setup. Pittsburgh seam coal dust, with three particle sizes in the range of 0 to 25 μm , 53 to 63 μm , and 75 to 90 μm is used. The effects of different coal dust concentrations (10 – 300 g/m^3) at three lean equivalence ratios, ϕ (methane-air) of 0.75, 0.80 and 0.85 on the laminar burning velocity are determined experimentally. The laminar burning velocity of the coal dust-methane-air mixture is determined by taking a shadowgraph of the resulting flame and using the cone-angle method. The results show that the addition of coal dust in methane-air premixed flame reduces the laminar burning velocity at particle size of 53 to 63 μm and 75 to 90 μm . However, burning velocity promotion is observed for 0 to 25 μm particles at $\phi = 0.80$. Two competing effects are assumed involved in the process. The first is burning velocity promotion effect that the released volatile increases the gaseous mixture equivalence ratio and thus the burning velocity. The second is the heat sink effect of the coal particles to reduce the flame temperature and accordingly the burning velocity. A mathematical model is developed based on such assumption and it can successfully predict the change of laminar burning velocity at various dust concentration. Furthermore, the implication of this study to coal mine safety is discussed.

NOMENCLATURE

A	Parameter characterizing rate of vaporization of particles, Eq. 2	n_s	Number of particles
B	Frequency factor characterizing rate of gas phase oxidation of gaseous fuel	\dot{n}_{air}	Number of mole of air per unit time
B	Burner base width	\dot{Q}	Heat release rate
C_p	Heat capacity of air	\dot{q}''	Heat flux to particles in Fig. 5
C_s	Heat capacity of solid particle	R	Gas constant
C_{total}	Heat capacity of particle-gas mixture	r	Mean radius of particles
c	Density	S_u	Burning velocity
E	Activation energy characterizing the gas phase reaction	T_b	Flame temperature based on original premix mixture
h	Heat of the flame cone	T_f	Flame temperature with particles
K	Heat conductivity of air	T'_f	Promoted flame temperature due to locally increased equivalence ratio
L_v	Latent heat of vaporization	T''_f	Reduced flame temperature due to heat sink effect of particles
M	Molecular mass	t_r	Residence time
m'''_{CH_4}	Mass of air presents in 1 m ³	U	Average flow velocity at burner nozzle
m'''_{air}	Mass of methane presents in 1 m ³	\dot{V}_{air}	Volumetric flow rate of air
m'''_{fuel}	Mass of fuel presents in 1 m ³	\dot{V}_{CH_4}	Volumetric flow rate of methane
m'''_v	Mass of vapor presents in 1 m ³	V	Volume
n	Temperature exponent characterizing rate of vaporization of coal particles in Eq. 2	\dot{w}'''_v	Rate of vaporization of fuel particles
		x	Spatial coordinate
		Z_e	Zeldovich number

Greek Symbols

α	Flame cone angle
ε	=1/ Z_e , expansion parameter
ρ	Density of the solid-gas mixture
ρ_s	Density of the particle
δ	Thickness of devolatilization zone
ϕ	Original gaseous mixture equivalence ratio
ϕ_s	Equivalence ratio of coal particles and air

Subscripts

b	Adiabatic condition based on original gas phase condition
d	Devolatilization
f	Flame
s	Solid particle
u	Conditions in the ambient condition
v	Vapor

1. INTRODUCTION

Many materials that are virtually non-flammable in bulk form become explosive if dispersed as a cloud of fine particles in air. From a combustion viewpoint this can be treated as both a benefit and a hazard. In industries that manufacture, transport, process and/or use combustible dusts, accidental dust deflagrations represent a real hazard to both personnel and equipment. An example is the recent coal mine explosion in West Virginia (April 5, 2010) killing 29 miners and considered as one of the most disastrous mining accidents in US history. Interestingly, most coal mine explosions often involve both a methane deflagration combined with fugitive coal dust that is collected by the combustion wave as it progresses through the mine. The physical and chemical processes involved during the travel of a combustion wave through a flammable gas-dust-air mixture are shown in Fig. 1. Three distinct steps are identified as shown in Fig. 1. First, the dust deposited on the floor, walls, and ceiling can be lifted up by the pressure blast of the initial methane explosion causing a cloud of dust to be suspended in the air. When the methane-air flame front meets the dust cloud, the coal particles pyrolyze and contribute volatile vapor to the methane-air mixture. The coal particles can also cause instabilities, which could potentially alter the structure of the premixed flame. Greenberg et al. [1] have shown that adding combustible liquid droplets to a gas flame can increase the burning velocity under certain conditions. Based on droplet concentration and size, Suard et al. [2] identified different spreading regimes for such droplet – gas – air flames. Goral et al. [3] studied upward propagation of flames in a lean methane-air mixture to which had been added inert particles (sand). It was found that the upward flame velocity increased with increasing sand grain size. And such increase was attributed mainly to the enhanced combustion due to the micro-turbulence generated in the wake of the falling particles. Wendt and Graves [4] studied the flammability of coal dust in a laminar opposed jet diffusion flame. However, the interaction between solid combustible dust particles and a gaseous premixed flame have been rarely investigated in combustion literature and are the focus of the current study.

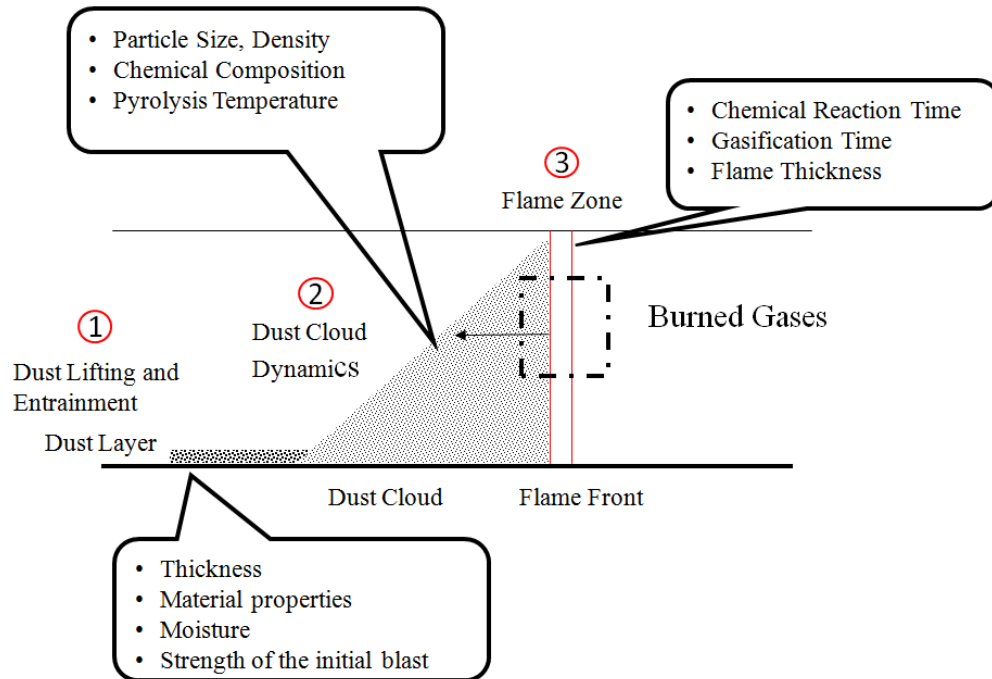


Fig. 1: Dust explosion process

2. EXPERIMENTAL APPARATUS

Fig. 2 (a) is a schematic of the experiment used for measurement of laminar burning velocity and dust entrainment rate. The design of such a burner is based on the Bunsen burner, with the difference that the side openings entrain coal dust particles flow instead of air. Specific details of the dust injection using such burner are discussed by Xie et al. [5]. The burner is made of a steel tube with inner diameter of 10.2 mm and wall thickness of 1.2 mm. A 1 mm thick acrylic plate with a 1 mm diameter orifice is installed inside the steel tube, 150mm away from the burner top. Entrainment of dust is achieved through three 7.5 mm wide and 9 mm long slot openings located above the orifice plate as shown in Fig. 2 (b). A brass jacket tube (highlighted in blue) whose inner diameter is 0.1mm larger than the outer diameter of the steel tube and secured by two socket head screws is used to adjust the opening size and thus the dust entrainment. The coal dust is filled in an inverted cone-shaped acrylic container which is also attached to the steel tube. The cone angle of the container is equal to 60° which represent the critical angle of repose of dust

particle size ranges used in this study. The repose angle was determined using an experimental method discussed by Botz et al. [6]. The adjustable burner and its attachments are secured in a support frame and the entire assembly is kept over the *Cole-Parmer Symmetry PR 4200* load cell. The load cell has a total weighing capacity of 4.2 kg with a sensitivity of 0.01 g and the factory uncertainty in the mass measurement is ± 0.03 g. A ring stand kept outside the load cell is used to support a collection pan. Pittsburgh seam bituminous coal dust with particle size in the range of 0 to 25 μm , 53 to 63 μm , and 75 to 90 μm are used in the experiment. The size ranges are obtained by *Retsch AS 300* sieve shaker. Compressed air and methane (99.99% purity) cylinders are used to supply the burner with an upstream pressure of 0.5 bar. Each gas flow is controlled by a *SIERRA Model 100* mass flow controller with an accuracy of $\pm 1\%$ of its flow capacity. The desired gases are mixed in a “tee” connection before it enters the burner.

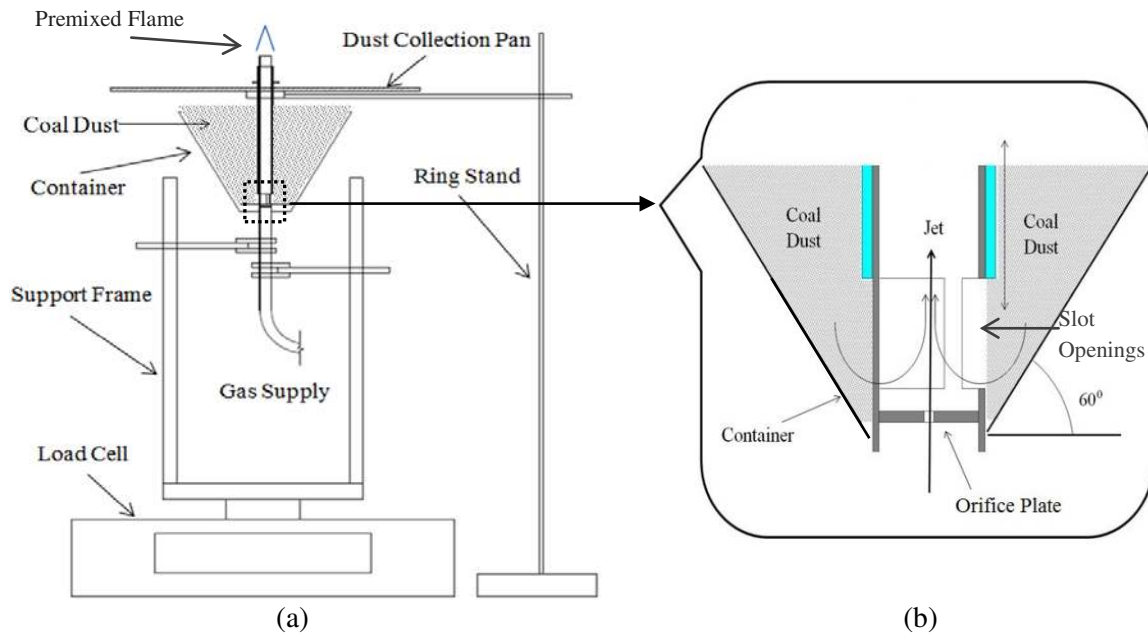


Fig. 2: Experiment apparatus: (a) dust burner and the weighing assembly; (b) the details of the dust entrainment mechanism

Direct shadowgraph technique is used to capture the flame cone with and without coal dust injection. The set-up is shown in Fig. 3. A 420 W projector lamp is converted into a

point light source and placed one focal length away from a double convex lens. A Canon EOS 5D single-lens reflex (SLR) camera with a macro-lens (Canon EF100/2.8 Macro USM) that has a minimum focal length of 31 mm is placed behind the flame along the center axis of the parallel light beam. The camera is manually adjusted where shutter speed of 1/4000 sec, ISO of 1600, and aperture of 2.8 are used for the optimization. A sample image of the actual flame and the corresponding shadowgraph image obtained by the macro-lens are shown in Fig. 4 (a) and 4 (b).

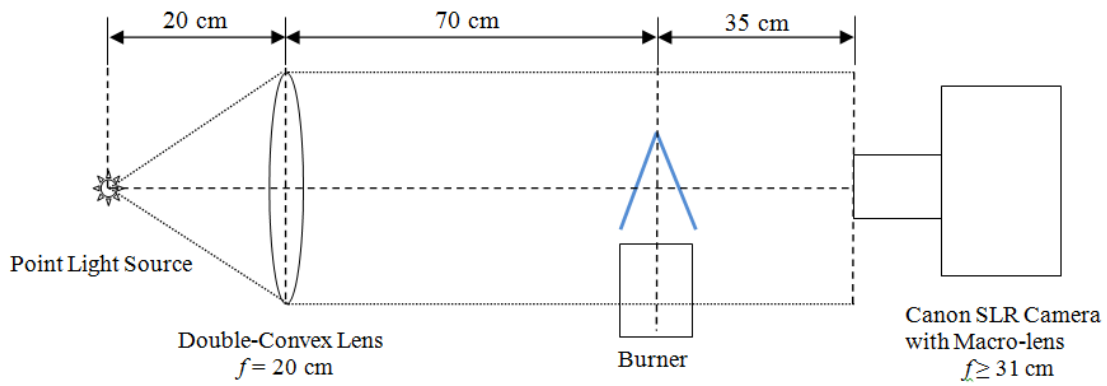


Fig. 3: Shadowgraph set-up

The main advantage of the shadowgraph is that it can capture clearly the flame cone even when the flame is loaded with high concentration of burning particles. As shown in Fig. 4 (a), it is hard to locate the edge of the flame cone using conventional photograph techniques while the flame can be easily identified in the shadowgraph as shown in Fig. 4 (b). For each dust concentration and gaseous fuel equivalence ratio, a minimum of 15 images are processed by an image process algorithm programmed in Matlab and the corresponding average cone angle is used to estimate the burning velocity. A sample of the processed image is shown in Fig. 4 (c). The algorithm converts the shadowgraph into a grey-scale image and detects the cone edge where a significant change in the normalized intensity (a value from 0 to 1) occurs on each row within the preselected boundary that encloses the flame cone. The detected cone edge is shown as two clusters of red or green dots in Fig 4. (c). Slopes that connect each dot on one side of the cone is

calculated. Then a best-fit line for all the detected dots, shown as black solid line in Fig. 4 (c), is used to obtain the cone half angle α where slope of the black solid line is the mean of all slopes. The standard deviation of the angle experimental measurement is within $\pm 1.5^\circ$.

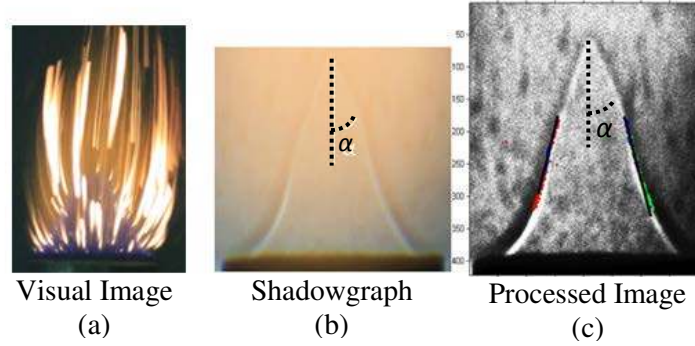


Fig. 4: Example of flame images

The laminar burning velocity is obtained by using angle method where

$$S_u = U \cdot \sin(\alpha) , \quad (1)$$

where S_u represents the laminar burning velocity, U is the average flow velocity, and α is the cone half-angle as shown in Fig. 4.

3. MATHEMATICAL MODEL

A mathematical model is developed to explain the observation made in the experiment and predict S_u with particles whose sizes are not included in the experiment. Fig. 5 illustrates the interaction of the particles with the premixed flame and is used as a basis to develop a model to estimate the change in S_u .

The path of a coal particle, assumed to be along a flow streamline, is shown in Fig. 5. The particle absorbs the heat from the flame while it travels through the devolatilization zone as illustrated by \dot{q}'' in the inset to Fig. 5. The temperature of the particle is assumed to be equal to the gas temperature and once it reaches T_v , the devolatilization is initiated thereby

releasing gaseous volatiles as shown by \dot{m}_v''' . This additional fuel released from coal particle can increase the equivalence ratio locally in the flame. For a lean mixture flame, increased equivalence ratio can promote S_u . In Fig. 5, T_f is the temperature of the flame and T_v represents the approximate temperature at which devolatilization initiates. The thickness of the zone between T_f and T_v is denoted by δ . It is assumed that the particle will pyrolyze and release volatiles when it traverses the distance δ . The height and the width of the flame cone are represented by h and b respectively. The cone half angle is designated as α . In addition, the particle also acts as a heat sink thereby reducing the flame temperature and thus S_u . These two effects are competing in nature and affect the flame simultaneously.

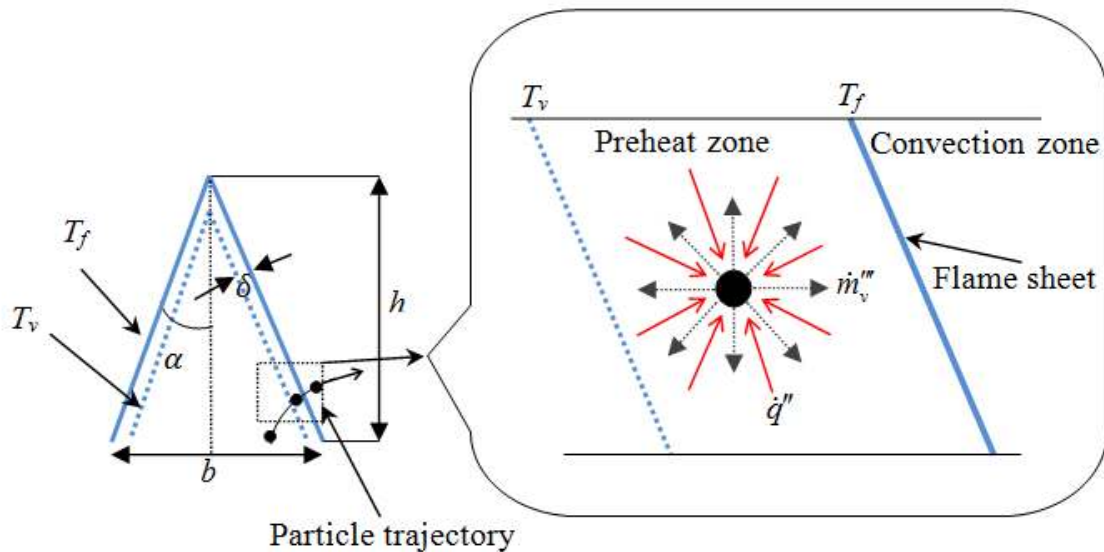


Fig. 5: Illustration of parameters involved (\dot{q}'' is the heat flux from flame to the particle; \dot{m}_v''' is volatile release rate per unit volume of the mixture; T_f is fame temperature; T_v is coal devolatilization initiation temperature; δ is the thickness of devolatilization zone; α is the cone half angle; b is the burner diameter; h is the cone height.)

To simplify the analysis, the two processes are decoupled into separate and parallel process in the model. The change in the flame temperature due to each effect is calculated separately and then superimposed to obtain the estimated true flame temperature.

3.1 Effect of equivalence ratio promotion

Coal particles can release volatiles into the gaseous mixture as the result of the elevated particle temperature. The volatiles are the additional gaseous fuel which increases the equivalence ratio locally. In order to estimate the amount of volatiles present in the gaseous mixture, it is necessary to explore the rate of the devolatilization process and quantify such rate.

There are four possible methods to estimate the devolatilization. The first method is based on the assumption that all volatiles are released when particle reach a given temperature. However, such method excludes the fact that devolatilization as it is also a time depended process. The second method is to treat the particles as liquid droplets where the vaporization can be estimated as discussed by Suard et al. [2]. This method, however, does not capture the non-linear behavior of devolatilization of coal while the droplet evaporation is fairly linear. The devolatilization can be solved by a set of equations which is based on the Arrhenius law as described by Solomon and Colket [7]. Or devolatilization rate can be estimated based on a temperature depended power-law relation as proposed by Seshadri et al [8]. Since the method based on Arrhenius law requires high computational cost, the model uses a temperature depended power law is used in this study.

Seshadri et al. [8] used the expression below to predict devolatilization rate of coal particles,

$$\dot{m}_v''' = A n_s 4\pi r^2 T_s^n, \quad (2)$$

where the unit of \dot{m}_v''' is mass of gaseous fuel vaporized per unit volume per second. The quantities A and n are constants which are presumed to be known and will be discussed in a later section. The particle temperature is denoted as T_s and it is assumed that

$T_s = \frac{T_b + T_v}{2}$, where T_b is the adiabatic flame temperature based on the methane-air

equivalence ratio and T_v devolatilization initiation time. For coal particles,

devolatilization initiates at about $T_v = 600\text{K}$ [9]. The value of T_b is calculated using an

equilibrium solver based on the minimization of free energy [10]. The total volume of particles per unit volume of mixture is estimated by dividing the dust concentration c_s (g/m^3) by the particle density ρ_s (g/m^3). The number of particles per unit volume (n_s) is then equal to $n_s = (c_s / \rho_s) / V_s$, where V_s is the volume of a single particle.

The duration of devolatilization needs to be determined to use Eq. 2 to estimate the total amount of vaporized fuel. Devolatilization is limited to a narrow band with thickness of δ which is the region close to the reaction zone on the unburned side where temperature increases from T_v to T_b as shown in Fig. 5. The thickness of this zone is estimated by applying an energy balance.

$$k \frac{d^2T}{dx^2} - \rho U C_{total} \frac{dT}{dx} = 0, \quad (3)$$

with boundary condition that $x=0, T=T_v$, and $x=\delta, T=T_b$. The specific heat of the mixture

$$C_{total} = C_p + \frac{4\pi r^3 C_s \rho_s n_s}{3\rho},$$

U is the averaged flow velocity, ρ is the density of the mixture,

and thermal conductivity is assumed to be as same as air of $k = 0.052 \text{ W} / \text{K} \cdot \text{m}$ at 400°C which is approximately equal to the average temperature in the devolatilization zone.

Integrating Eq. 3, the thickness of the devolatilization zone can be obtained as

$$\delta = \frac{k(T_b - T_v)}{\rho U C_{total} (T_b - T_u)}, \quad (4)$$

where the density of the mixture $\rho = \frac{\rho_{air} \dot{V}_{air} + \rho_{CH_4} \dot{V}_{CH_4}}{\dot{V}_{air} + \dot{V}_{CH_4}} + c_s$, and the averaged flow

$$\text{velocity } U = (\dot{V}_{air} + \dot{V}_{CH_4}) / \left(\frac{\pi b^2}{4} \right).$$

The time of devolatilization or the residence time of particles is then given by:

$$t_r = \left[\frac{\delta}{\sin(\alpha)} \right] / U. \quad (5)$$

The devolatilization time is used to estimate the total mass of released volatiles per unit volume during the passage of dust particles through δ and is given by:

$$m_v''' = \dot{m}_v''' t_r. \quad (6)$$

This additional fuel is assumed to be CH_4 for simplicity as suggested by Seshadri et al. [8] and added to the original gaseous mixture to obtain a new equivalence ratio. The new amount of gaseous fuel per unit volume in the mixture per unit volume is denoted as m_{fuel}''' and can be estimated as $m_{fuel}''' = m_{CH_4}''' + m_v'''$ where m_{CH_4}''' is the mass of the original methane per unit volume of the mixture. Accordingly the new equivalence ratio can be calculated as $\phi = 9.52 \cdot \left(\frac{m_{fuel}'''}{M_{CH_4}} / \frac{m_{air}'''}{M_{air}} \right)$ where the coefficient 9.52 is the ratio of numbers of moles of methane to air when ϕ equals to 1.

For the original mixture, the mass of methane and air present per unit volume are given by:

$$m_{CH_4}''' = \frac{\left(\frac{\dot{V}_{CH_4} P}{RT_u} \right)}{(\dot{V}_{air} + \dot{V}_{CH_4})} M_{CH_4}, \quad (7)$$

$$m_{air}''' = \frac{\left(\frac{\dot{V}_{air} P}{RT_u} \right)}{(\dot{V}_{air} + \dot{V}_{CH_4})} M_{air}, \quad (8)$$

where $P = 101,354 \text{ Pa}$, $T_u = 293 \text{ K}$, and $R = 8.314 \text{ J/K} \cdot \text{mole}$. The molecular weights of air and methane are $M_{air} = 28.97 \text{ g/mole}$ and $M_{CH_4} = 16.04 \text{ g/mole}$. \dot{V}_{air} and \dot{V}_{CH_4} are the volumetric flow rates of air and methane obtained experimentally using the mass flow controllers.

With this new equivalence ratio, a new flame temperature T_f' is estimated by an equilibrium solver [10]. The calculated results are present in Fig. 6 for coal particles at size of 75-90 μm with original methane-air equivalence ratio of 0.75, 0.80, and 0.85. In

Fig. 6, ϕ_s represents the equivalence ratio in terms of coal dust and air. As shown in Fig. 6, the flame temperature increases with increased dust concentration. This is because the increased dust concentration causes more volatiles to be released and a higher equivalence ratio can be obtained. Consequently, the flame temperature and the laminar burning velocity are promoted.

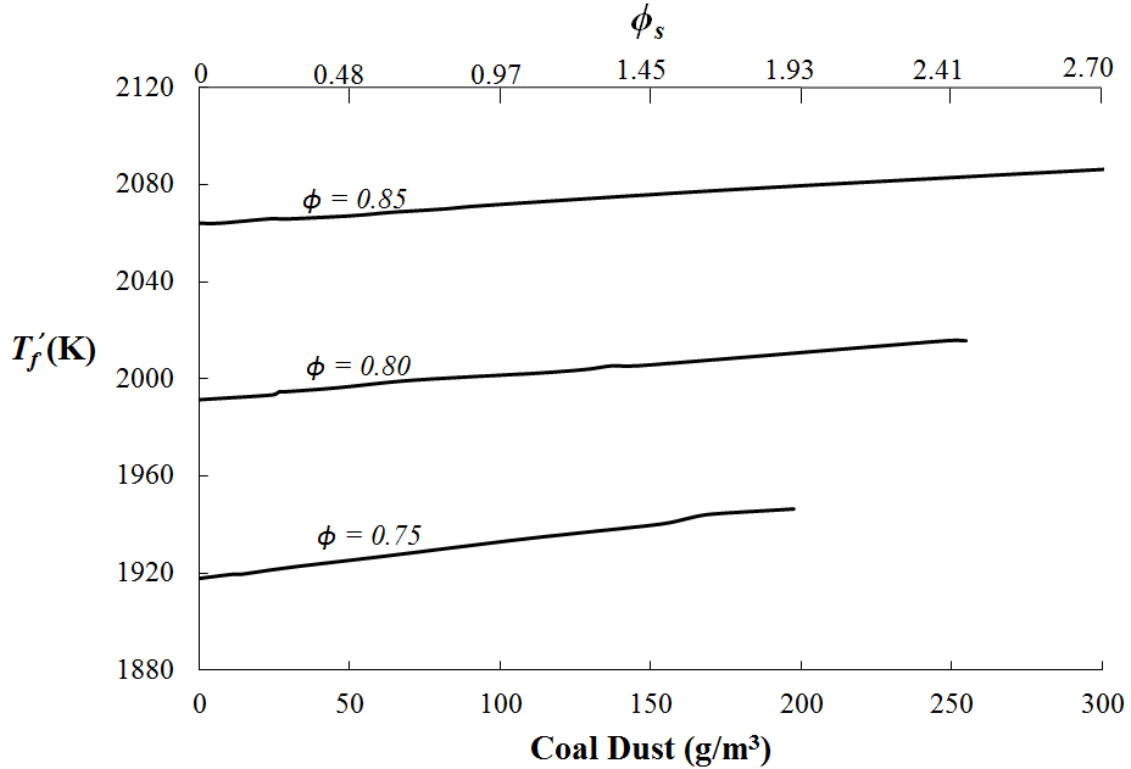


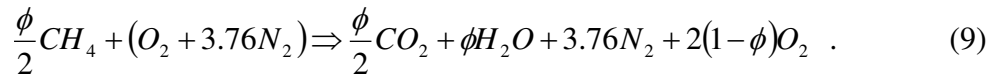
Fig. 6: Adiabatic flame temperature based on ϕ with additional gaseous fuel released from coal particles in the size range of 75-90 μm .

3.2 Heat sink effect of coal particles

In addition to a local increase in equivalence ratio, a coal particle will also act as a heat sink as it absorbs the heat from flame to raise its temperature for devolatilization. Two aspects are considered for the heat sink effect: 1. the heat used to raise the temperature of coal particles from ambient condition to the flame temperature; 2. the heat used as devolatilization heat for the coal particles. In order to model these two aspects, three assumptions have been made: 1. the heat release rate of the flame is assumed to remain

constant; 2. coal particles simply act as an inert particle which is also able to devolatilize to absorb additional energy from the flame; and 3. coal particles reach the flame temperature when they reach the flame sheet. Based on these three assumptions, the heat released to raise the gas temperature per unit time for flame without dust equals the sum of heat release to raise the temperature of gas and particles and heat of gasification per unit time. Therefore, each term should be determined to estimate the flame temperature that accounts for heat sink effect. It should be noted that the radiation is ignored from the analysis.

First, the heat released for flame without dust needs to be calculated. For a lean or stoichiometric methane-air mixture, the chemical reaction for the combustion with equivalence equal to ϕ is given by



The total heat released for the combustion shown in Eq. 9 is solved by energy balance:

$[(T_b - T_u) \sum C_p \cdot n_{product}]$ for $\frac{\phi}{2}$ mole of methane or 4.76 mole of air where T_b is the adiabatic flame temperature which is estimated using an equilibrium solver [10]. Thus, the heat release rate of the premixed flame without presence of coal dust for a given flow of air and ϕ can be calculated as

$$\dot{Q} = [(T_b - T_u) \sum C_p \cdot n_{product}] \frac{\dot{n}_{air}}{4.76}, \quad (10)$$

where \dot{n}_{air} is the number of moles of air supplied per unit time.

Based on the first assumption, the flame with particles releases the same amount of heat while it is also affected by the volatile gasification and temperature rise of particles.

Therefore the flame temperature T_f'' can be estimated using energy conservation as shown in Eq. 11

$$\dot{Q} = [(T_f'' - T_u) \sum C_p \cdot n_{product}] \frac{\dot{n}_{air}}{4.76} + \dot{n}_s C_s (T_f'' - T_u) + L_v / t, \quad (11)$$

where \dot{n}_s represents the local number of particles per unit volume per unit time that are passing through the flame

$$\dot{n}_s = (\dot{V}_{air} + \dot{V}_{CH_4}) n_s \rho_s V_{particle} / M_c, \quad (12)$$

where M_c is the molecular weight of carbon (12g/mole).

Similarly L_v in Eq.11 represents the heat of gasification which is assumed to be a fraction of the heat produced and given by

$$L_v = \chi(m_v''' \cdot V_d \cdot \Delta h_{CH_4}), \quad (13)$$

where χ is assumed to be 0.01 as suggested by Seshadri et al. [8], Δh_{CH_4} is the heat of combustion of methane, and the volume of the devolatilization zone is the conical space with a thickness of δ as shown in Fig. 5 given by

$$V_d = \frac{1}{3} \pi h \frac{b^2}{4} - \frac{1}{3} \pi \left(h - \frac{\delta}{\sin(\alpha)} \right) \left(\frac{b}{2} - \frac{\delta}{\cos(\alpha)} \right)^2. \quad (14)$$

The height of the flame cone is denoted as h , the diameter of the burner is represented by b , and α is assigned for the cone half-angle. L_v / t represents the heat consumed by gasification process where t denotes the time the particle spends in the devolatilization zone and is estimated by Eq. 5. Re-arranging Eq. 11, the new flame temperature T_f'' can be obtained as

$$T_f'' = \frac{\dot{Q} - L_v / t}{\frac{\dot{n}_{air}}{4.76} \sum C_p \cdot n_{product} + \dot{n}_s C_s} + T_u. \quad (15)$$

Using Eq. 15, the calculated results of T_f'' is plotted in Fig. 7 for coal particle with size range between 75 to 90 μm and equivalence ratio of the gaseous mixture of 0.75, 0.80 and 0.85. As observed in Fig. 7, the flame temperature reduces as the concentration of dust increases for all three equivalence ratios.

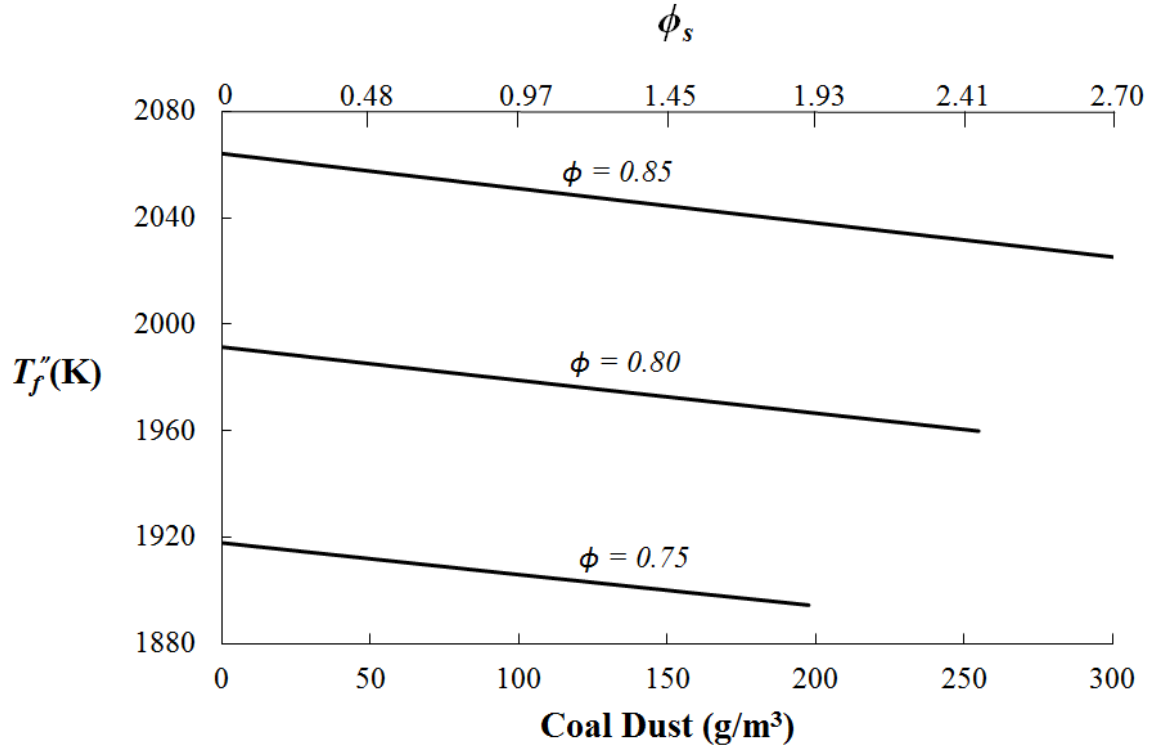


Fig. 7: The flame temperature based on the heat sink effect of coal particles at 75-90 μm

3.3 Combined effects

The combined effect of particle devolatilization and corresponding equivalence ratio promotion and heat sink effect as they interact with a premixed flame are accounted for by calculating an average flame temperature $T_f = (T_f' + T_f'')/2$. The corresponding flame temperature is then used to estimate S_u using the model developed by Seshadri et al. [8]:

$$S_u = \sqrt{\frac{2Bk\varepsilon^2}{\rho C_{total}} \exp\left(-\frac{E}{RT_f}\right)}, \quad (16)$$

where $\varepsilon = 1/Z_e$, $Z_e = \frac{E(T_f - T_u)}{RT_f^2}$. $B = 3.5 \times 10^6$ /mole \cdot s and $E = 88800$ kJ/mole are

chosen to match the calculated burning velocity with burning velocity obtained by experiment for flames without dust injection. ρ is the density of the mixture. The

constants $A = 0.034 \text{ g/m}^2 \text{ K} \cdot \text{s}$ and $n = 1.1$ are introduced in Eq. 2 to obtain the calculated burning velocities of dust-gas mixtures to match with the experiment measurements. The calculated burning velocities and experiment data are presented in Fig. 8. Due to the strong cohesive force, the dust entrainment rate is very unsteady for smaller particles. Therefore only one data point is obtained for 0 to 25 μm coal particles, and no data is obtained for 53 to 63 μm at $\phi=0.75$.

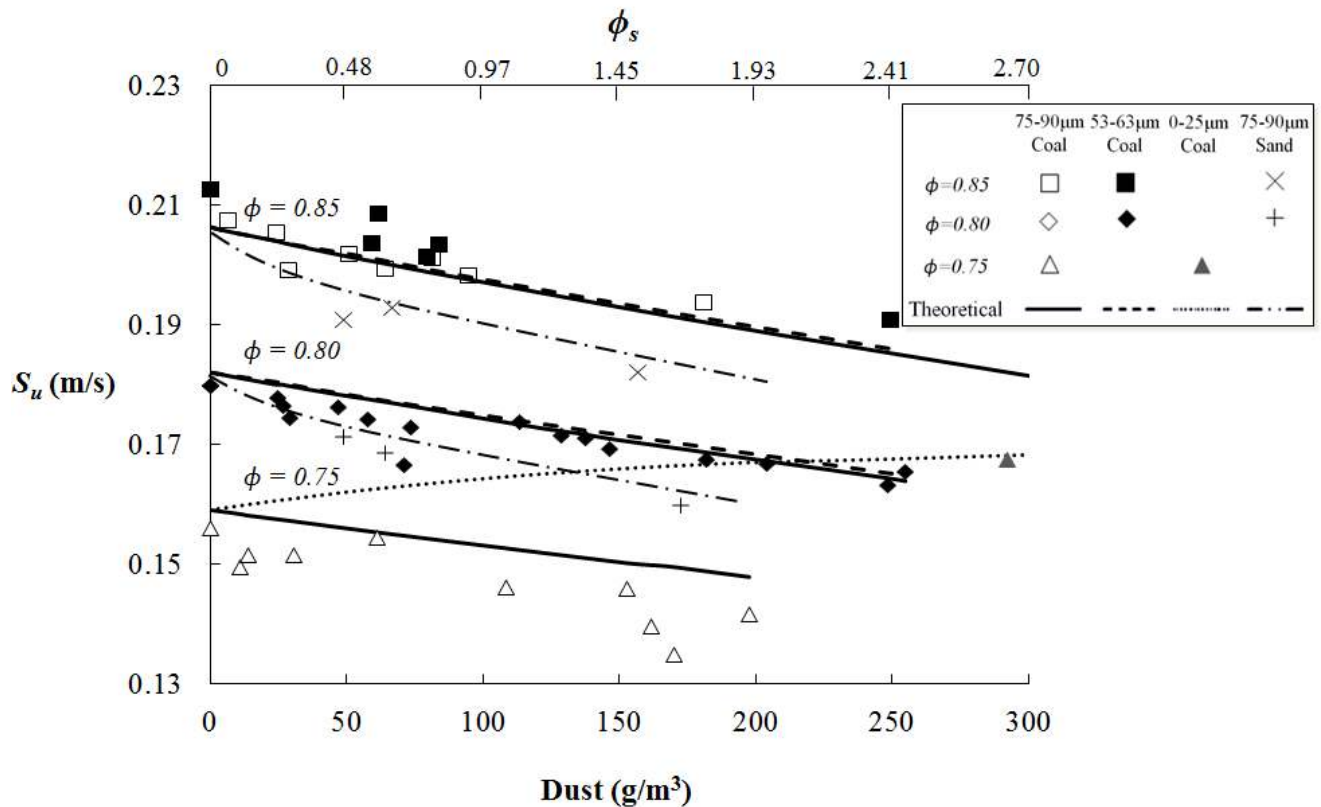


Fig. 8: Burning velocity methane-air premixed flame with injected coal particles and sand particles at lean conditions (Experimental data are represented in different shape of points and theoretical prediction is shown in lines.)

As shown in Fig. 8, the interaction of the coal particles with a laminar premixed methane-air flame reduces S_u when the particle size is larger than 25 μm . However, for 0 to 25 μm coal particles, S_u is promoted as shown by the solid grey triangular symbol in Fig. 8. It should be noted that at the same size range of 75 to 95 μm , the reduction in S_u for coal particles is less than that of sand. This observation demonstrates that the vaporized fuel is acting against the heat sink effect to maintain S_u as compared to the sand particles only

the heat sink effect plays a role. It is shown in the figure that the slope of S_u decreasing trend of S_u of 53 to 63 μm coal particles is less than the ones with size of 75 to 95 μm . It indicates that as the size of coal particle reduces, the increased equivalence ratio increases its significance compared with the heat sink effect. When the size of coal particles are as small as 0 to 25 μm , the influence of heat sink plays a minor role while the increased equivalence ratio affects S_u such that it increases.

The model is also used to calculate S_u with different dust concentrations at various equivalence ratios of methane-air mixture and coal particle sizes. The results are plotted in Fig. 9 where each color represents one original gaseous fuel equivalence ratio and different line type stands for a different particle size.

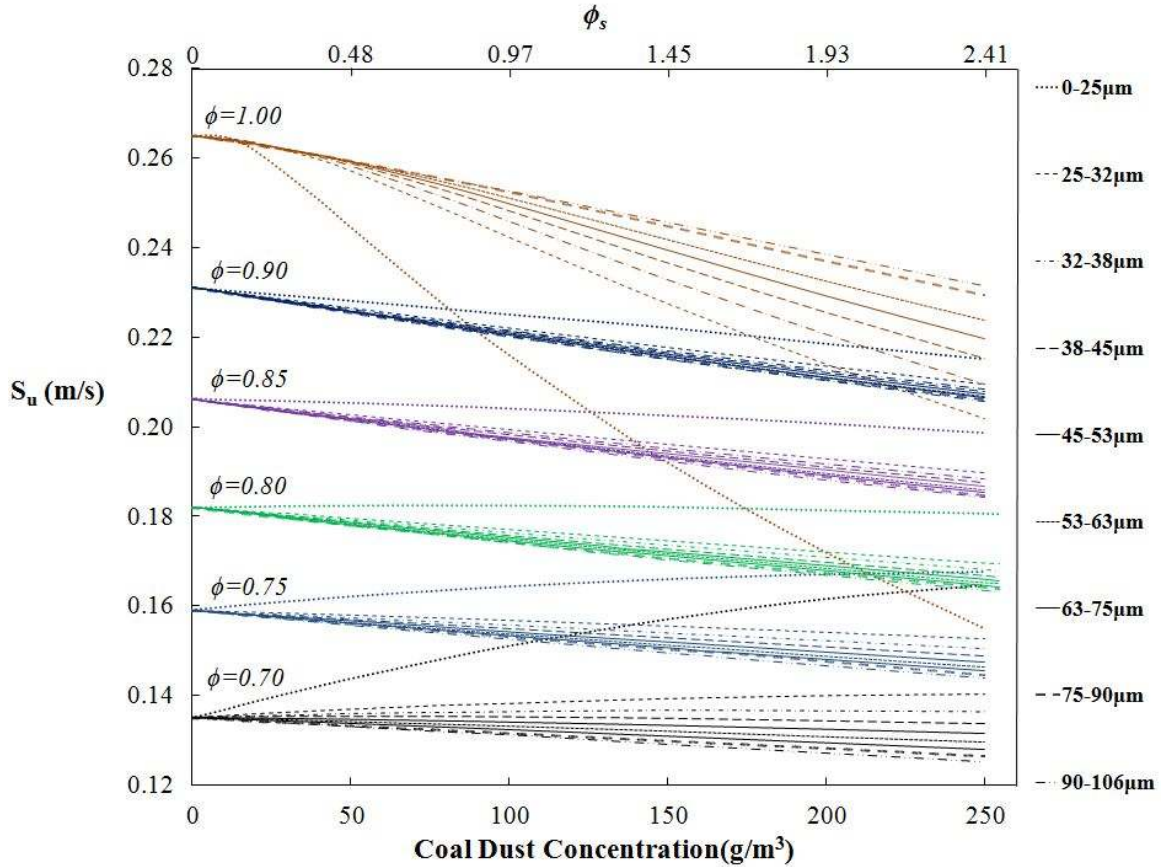


Fig. 9: Burning velocity for coal particle with different sizes at lean conditions

As shown in Fig. 9, the slope of the curve of S_u vs. dust concentration is negative but it gets flatter as the particle size decreases at a lean condition. However opposite trend is

shown in Fig. 9 when the ϕ equals 1 where the curve has a steeper slope with smaller particles. This can be explained by the increased specific surface area for smaller particles; and thereby the amount of released fuel is increased to promote the equivalence ratio locally. Therefore S_u increases as ϕ increases locally for a lean mixture while it decreases as ϕ increases locally as the stoichiometric mixture becomes fuel rich. It is also observed that the curve flatters as the mixture gets leaner while the particle size is kept the same; and the slopes become positive for 0 to 25 μm particles where ϕ ranges from 0.70 to 0.80 and particles with size range of 25 to 32 μm at $\phi = 0.70$. This can be explained by the fact that a lower flow rate is supplied for a leaner mixture in order to anchor the flame in the experiment. The flow velocity U is slower as flow rate gets smaller. Then the devolatilization zone thickness δ and residence time t_r as defined by Eq. 4 and Eq. 5 both get larger since U is the denominator in both equations. Therefore more vapors can be released due to a longer residence time t_r . Therefore the slope is flatter as the mixture gets leaner. Due to the larger specific surface area and longer residence time t_r , the slopes for the particles with size ranges from 0 to 25 μm and 25 to 32 μm become positive at range of 0.70 to 0.80 and 0.70 respectively.

4. DISCUSSION

The explosion in coal mine tunnels evolves through three stages: laminar flame, turbulent flame and deflagration. The Bunsen burner type experiment set-up in this study facilitates a better understanding of interaction of coal particles and flame at the first stage of the explosion. As shown in this study, small coal particles (0 to 32 μm) have the ability to enhance the laminar burning velocity S_u of methane-air mixture under certain conditions. It is also found that larger size coal particles reduce S_u .

In a coal mine explosion, the initial pressure blast of methane-air explosion (fire-damp) can shake off the dust deposited on various surfaces. Small particles can easily suspend in air as compare to the larger ones. Therefore, the laminar methane-air flame will first interact with fine particles. This study shows that if the laminar flame is at lean condition, the flame velocity will be enhanced by small particles. As the flame develops to a

turbulent condition, more dust at various sizes are drawn in the flame by the turbulence eddies formed in front of the flame front. In a turbulent flame, eddies will greatly increase the heat and mass transfer within the devolatilization zone which enhances the fuel vaporization process. This also increases the residence time of particles leading to more vaporized fuel. Therefore, it is expected that in a lean turbulent flame the increased amount of vaporized fuel will counteract the heat sink effect for the particle sizes larger than 32 μm . As a result, the flame velocity will be promoted by the presence of significant larger particles (as compared to the laminar cases). As the flame front is accelerated by the cumulated combustion products, a deflagration to detonation transition is likely.

5. CONCLUSION

In this study, a lab scale experiment has been conducted to understand the effects of the coal dust injected through a lean methane-air premixed flame. The laminar burning velocity S_u of the coal dust-methane-air mixture is determined by taking a shadowgraph of the resulting flame and using the cone-angle method. Experiment results show that the presence of coal dust at 53 to 63 μm and 75 to 90 μm reduces S_u at equivalence ratio of 0.75, 0.80, and 0.85 with dust concentration varies from 10 g/m^3 to 300 g/m^3 . However, particles with size at 0 to 25 μm promotes S_u at $\phi=0.80$. It is assumed that the coal particle acts as gaseous fuel contributor to increasing the equivalence ratio while it is also acting as heat sink to quench the flame. Both effects have been investigated mathematically based on such assumption. A model has been developed to predict the burning velocity of premixed gas-methane flame with coal dust at various dust concentration. It is observed that under certain conditions the laminar burning velocity increases mainly due to the released volatiles which locally increase the mixture equivalence ratio and thus the burning velocity. The amount of released volatiles is governed by the surface area per unit mass of dust and the residence time. However, under certain conditions, the heat sink effect of the coal particles reduces the flame temperature and thus the burning velocity as well.

6. ACKNOWLEDGEMENT

This work is funded by National Science Foundation (NSF) Award #0846764 and the authors like to give our special thanks to NSF.

References

- [1] J. B. Greenberg, A.C. McIntosh, and J. Brind, *Proceedings of the Royal Society*, 457 (2001) 1-31.
- [2] S. Suard, P. Haldenwang, and C. Nicoli, *Comptes Rendus Mecanique*, 332 (2004) 387-396.
- [3] P. Goral, R. Klemens, and P. Wolanski, *AIAA Progress in Astronautics and Aeronautics*, 113(1988), pp. 325-335.
- [4] D.B. Graves, and J.O.L. Wendt, *Symposium (International) on Combustion* (1982), Vol. 19, pp. 1189-1196.
- [5] Y. Xie, V. Raghavan, and A. S. Rangwala, *Powder Technology*, (2011) Vol. 213, Issue 1-3, pp. 199-201.
- [6] J.T. Botz, C. Loudon, J.B. Barger, J.S. Olafsen, and D.W. Steeples, *Journal of The Kansas Entomological Society*, 76(2003) 426-435.
- [7] P.R. Solomon, and M.B. Colket, *Symposium (International) on Combustion* (1979), Vol. 17, pp. 131-143.
- [8] K. Seshadri, A.L. Berlad, and V. Tangirala, *Combustion and Flame*, (1992) 89: 333-342.
- [9] L. D. Smoot, and P. J. Smith, *Coal Combustion and Gasification* (1985).
- [10] C. Morley, Gaseq (Ver 0.79), <<http://www.c.morley.dsl.pipex.com/>> (2005).

Chapter 4

Conclusions and Future Work

This thesis consists of two parts of studies. The first study on a novel dust injector facilitates the second study where the interaction of premixed laminar methane-air flame with coal dust particles is investigated.

In the first study, design, development, and calibration of a novel solid particle injector have been reported. The injector uses the pressure drop in the air flow across an orifice plate fitted in a circular pipe (venturi effect), to naturally entrain micron-sized solid particles such as coal dust. Coal dust is continuously fed from a feeder located outside the pipe into the orifice plate through peripheral openings in the pipe. Three types of designs for the peripheral openings, in terms of the shape, size and number are evaluated by testing which one of them results in maximum particle entrainment, especially at lower air flow-rates. Calibration of the device is carried out by precisely recording the mass loss rate of the coal dust as a function of volumetric flow-rate of air. The results show that there is an optimum area for the side openings, at which the injector performance will be the best for the given pipe and orifice-hole sizes. The entrainment rate is found to be a non-linear function of the flow-rate for low air flow-rates (till around 9 grams per minute) and dependent on the net area of the openings. For higher air flow-rates, the entrainment becomes almost independent of the opening area and also it becomes an almost linear function.

In the second study, a lab scale experiment has been conducted to understand the effects of the coal dust injected through a lean methane-air premixed flame. The laminar burning velocity S_u of the coal dust-methane-air mixture is determined by taking a shadowgraph of the resulting flame and using the cone-angle method. Experiment results show that the presence of coal dust at 53 to 63 μm and 75 to 90 μm reduces S_u at equivalence ratio of 0.75, 0.80, and 0.85 with dust concentration varies from 10 g/m^3 to 300 g/m^3 . However, particles with size at 0 to 25 μm promotes S_u at $\phi=0.80$. It is assumed that the coal particle acts as gaseous fuel contributor to increasing the equivalence ratio while it is also acting as heat sink to quench the flame. Both effects have been investigated mathematically based on such assumption. A model has been developed to predict the burning velocity of premixed gas-methane flame with coal dust at various dust

concentration. It is observed that under certain conditions the laminar burning velocity increases mainly due to the released volatiles which locally increase the mixture equivalence ratio and thus the burning velocity. The amount of released volatiles is governed by the surface area per unit mass of dust and the residence time. However, under certain conditions, the heat sink effect of the coal particles reduces the flame temperature and thus the burning velocity as well.

During the tests, it is found that it is difficult to obtain good data for particles that are extremely small, such as 0-25 μm particles. Similarly there is no good experiment data for the tests with the 53-63 μm particles at $\phi=0.75$ where the flow rate is smallest. This is mainly due to the high cohesive forces that exist between the particles which cause difficulty in entrainment with the current design. A higher flow rate is required to entrain the smaller particles where a stronger cohesive force exists. However, the lean flame blows off under such high flow rate. Furthermore, it is noted that the agglomeration is more obvious for the particles that are smaller than 45 μm . Although the agglomeration is prevented by the orifice jet in the burner tube, it is difficult to prevent agglomeration during the entrainment from the side openings which ultimately stop the dust entrainment. At end of the study, a motorized cylindrical metal mesh was installed vertically, annularly around the burner tube inside the cone feeder. Four fan-like blades were installed horizontally on the mesh. This provided sufficient agitation to the dust particles and improved the dust entrainment. A better dust feeding system can be investigated in the future if smaller particles ($<25 \mu\text{m}$) need to be studied further.

It is found that the measured burning velocity of pure gas flame where the equivalence ratio is close to 1 is less than the published data by about 10%. It is believed that the cause of such discrepancy is the velocity profile at burner opening which is not uniform. A Mach Hebra nozzle can be used as an improvement for the existing burner.

As discussed in Chapter 3, the current study is valid for laminar flames. Therefore the study on the interaction of coal particles with turbulent flame is the logical next step. Moreover, such study is directly related to dust explosions in industry since the deflagration is turbulent in nature.

Appendices

Appendix A: Experimental Apparatus Details

This section of appendix is supplemental information for the Experimental Apparatus section in the paper titled as *Naturally Entraining Solid Particle Injector*, and paper titled as *Study of Interaction of Entrained Coal Dust Particles in Lean Methane – Air Premixed Flames*.

A.1 Experimental Equipment

In this section, each experiment is presented and a short description each equipment is also provided

I. Sieving Dust

The coal dusts are the ones used for power generation and are sieved to different sizes for experimental purposes. *Retsch* AS300 Sieve Shaker was used. This machine is able to sieve the dust particles with multiple different sizes (particle diameter): 0-25 μm , 25-32 μm , 32-38 μm , 38-45 μm , 45-53 μm , 53-63 μm , 63-75 μm , 75-90 μm , 90-106 μm , and 106-125 μm . Besides coal dust, sand was also sieved at size of 75-90 μm for a control experiment set as mentioned in the paper. It is important to maintain the purity while sieving different materials at each time. Therefore, whenever a different material will be sieved, all sieving steel pans are cleaned by the ultrasonic cleaner prior to sieving. It is worth being mentioned that the sieving should be ran for multiple times (at least 3 times) for one batch of dust. It is because that some small particles tend to stay in the pans with larger sieving size since some sieving openings are blocked by the larger particles and the sieving time is not sufficient. In order to fix this problem after each sieving period (maximum setting for the machine is 99 min), paper towel can be used to gently wipe the bottom side of the sieving pan and then start another sieving period. All sieved particles are kept in different containers according to their sizes for future uses.



AS300 Sieve Shaker



VR 1 Ultrasonic Cleaner

Fig. A.1-1: Sieve Shaker and Ultrasonic Cleaner

II. Novel Dust Injector



Fig.A.1-2: Middle Sections of the Novel Dust Injector



Bottom pipe section with
orifice plate



Dust Injector
Assembly

Fig.A.1-3: Dust Injector

III. Load Cell



Fig. A-1.3: Cole-Parmer Symmetry PR 4200 with Precision of 0.01g

The load cell has a capacity of 4200g with precision of 0.01g. A RS-232 interface is built-in this device. The RS-232 connection is connect to computer by a RS-232 to USB cable. The load cell transfers the instantaneous weight every 0.2 sec to the computer. The data is recorded by a free computer software called *Terminal 1.9* which can be obtained online.

IV. Mass Flow Controller



Fig. A-1-4: Sierra Smart-Trak 2 Model 100 Mass Flow Controller with Manual Control Panel

Two mass flow controllers were used in the tests: 1. a Methane Mass Flow Controller with capacity up to 500 SCCM with precision of 5SCCM; 2. an Air Mass Flow Controller with capacity up to 5 SLPM with precision of 0.05 SLPM. The flow rate is controlled by the manual control panel. During the experiment, it is found that the two Mass Flow Controllers need to be re-zeroed if it has not been used for a while. It should be noted that this equipment is very sensitive to solid impurities in the gas. Therefore, a filter was installed for each controller. This action is recommended by the manufacturer. Furthermore, the device should be set to "Close" position and unplugged when it was not in use otherwise it will heat up and damage may be made to the controllers.

V. Dust Burner Assembly

The dust burner is the dust injector with few minor modifications: 1. slot side openings that can be partially or totally covered by the brass jacket tube; 2. the thickness of the burner tube is reduced to 1mm for a better flame stability, and minimize the friction between tube wall and dust at the openings. Fig. A-1.5 and A-1.6 illustrate the details of the burner.



Fig. A-1.5: Burner with 60° Cone Feeder

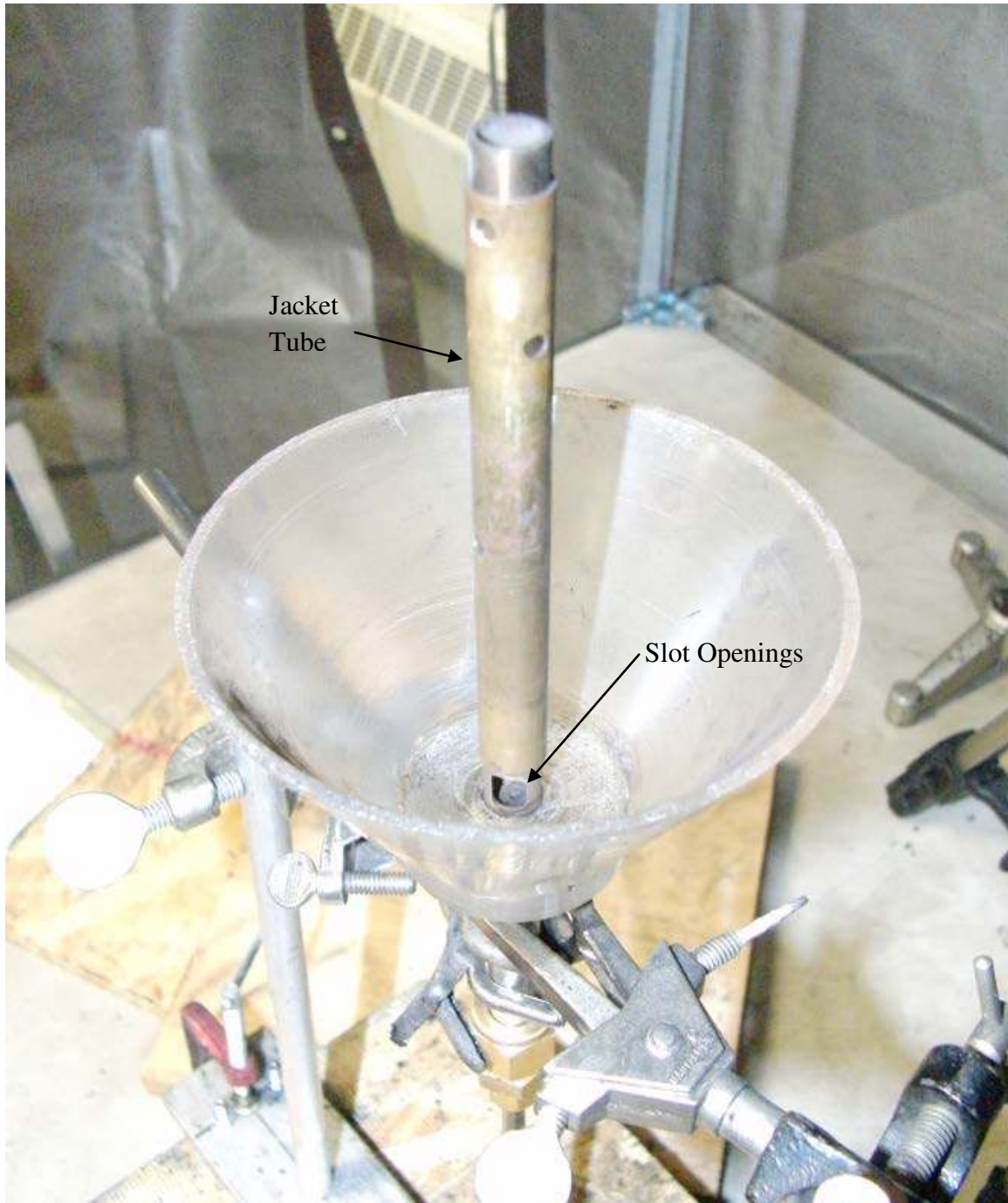


Fig. A-1.6: Burner Assembly

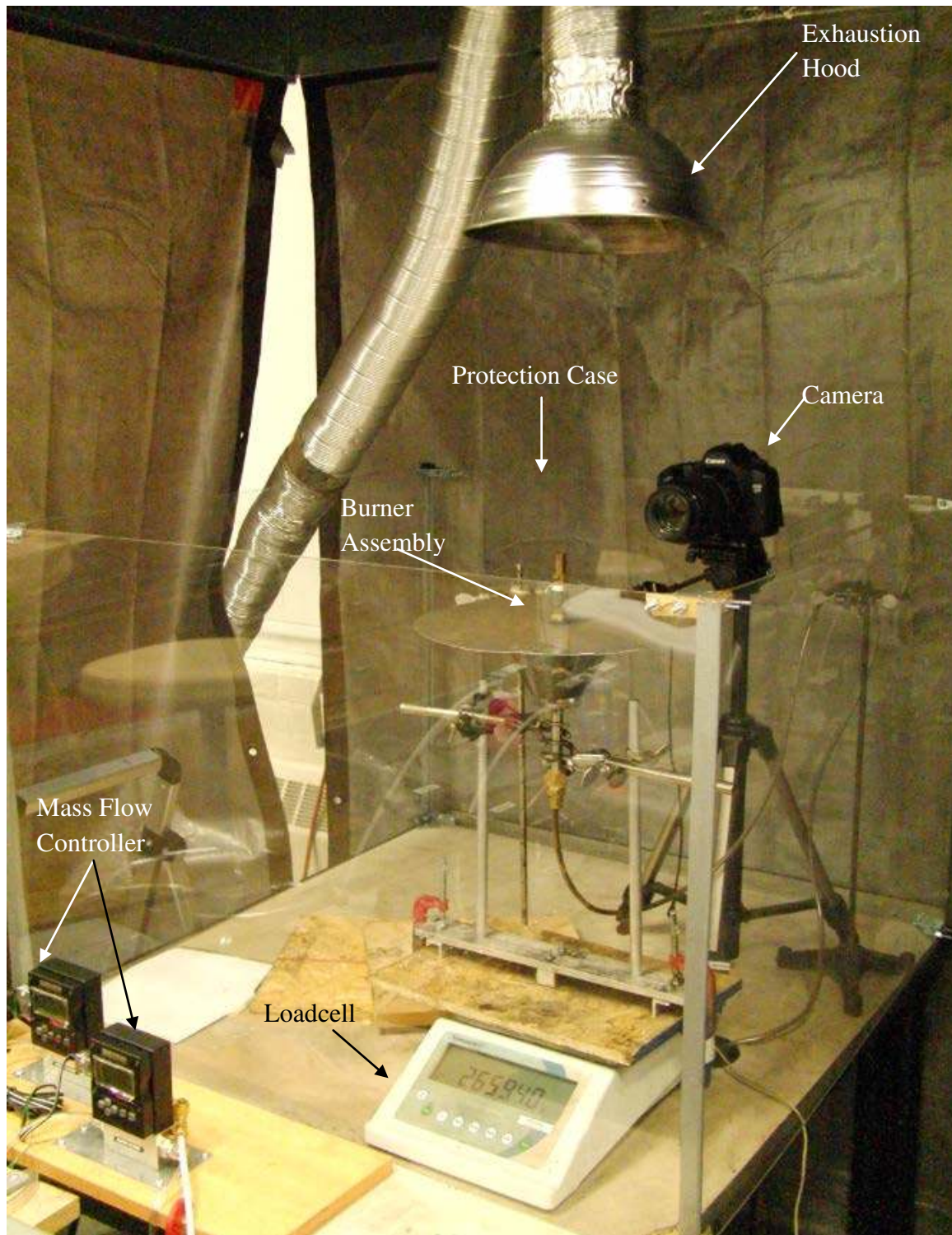


Fig. A-1.7: Experiment Setup

Fig. A-1.7 is the image shows the experiment setup (exclude the light source and double convex lens for shadowgraph but they are presented in next section). As shown, a transparent protection case is built and incased the apparatus. This is used to minimize

the draft that can impact the flame. Furthermore, an addition exhaustion hood is installed on the top of the burner which runs at a much lower flow rate compare to the lab hood. This hood is powered by the fan and duct work is made that all smoke is exhausted to a enclosed hood in the lab. The small hood was proved to be sufficient to extract the smoke produced during each tests.

VI. Shadowgraph Set-up

The *Shadowgraph* (also called as *Shadowgrams*) is a fairly simple and less expensive visualization technique as compared to a similar technique called *Schlieren photography*. The details of Shadowgraph and Schlieren photography can be found in *Schlieren and Shadowgraph Techniques: Visualizing Phenomena in Transparent Media* by G.S. Settles. In short words, the Schlieren images are based on the first derivative of density while it is the second derivative of density for Shadowgraph. It should be noted that Shadowgraph used in in this study is Direct Shadowgraph in parallel light. This method essentially eliminate the distortion/magnification of shadowgraph with diverge light. The locations of visualized flame cone using these techniques are different from the visible flame cone as illustrated in the figure below. However, these techniques do not make a difference in flame cone angle.

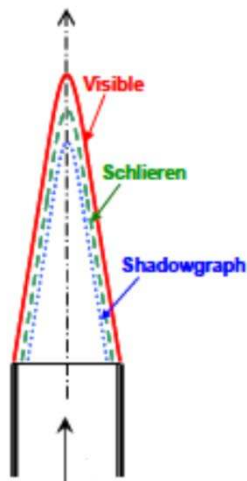


Fig. A-1.8: Location of Visible Flame, Schlieren Image, and Shadowgraph in a Flame Cone

In this study, a simple shadowgraph set-up was constructed using the project lamp assembly from an old-fashion projector, a double convex lens with focus length of 20cm, and Canon SLR camera with a macro-lens as shown in the figure below. The light from the project lamp (420W) is converted into a point light source by covering the lamp with a steel plate with a pin-hole. Extra caution needs to be taken since the lamp produces extensive heat that will turn the steel plate into red-hot. It is recommended that the lamp

should not be kept on for more than 15min and cool-down time of around 5min is needed for each run.

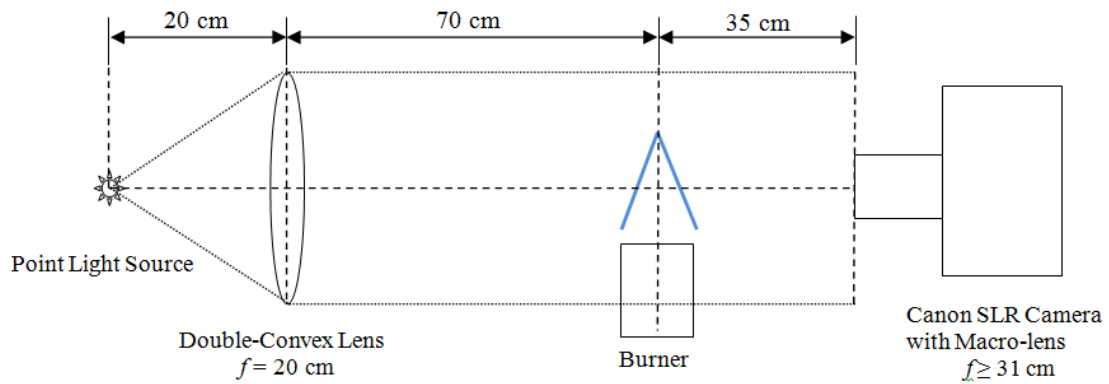


Fig. A-1.9: Shadowgraph Setup

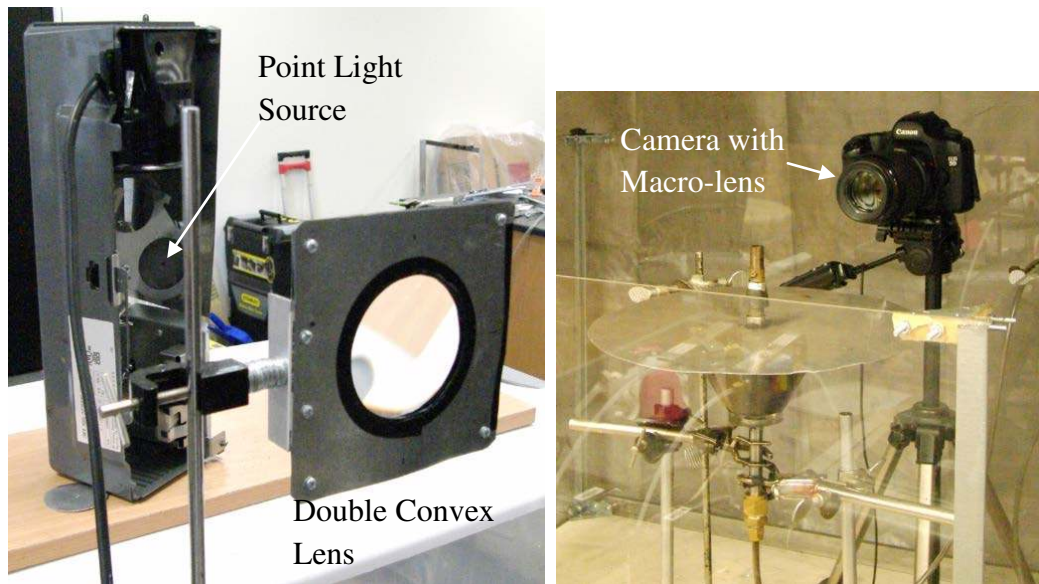


Fig. A-1.9: Shadowgraph Apparatus

A.2 Procedures of Conducting Experiment for Study

The experiment is conducted as follows:

1. Check the apparatus and fix any abnormal conditions.
2. Place the burner assembly on the load cell.
3. Lower the jacket brass tube completely and thus close the side openings

4. Fill the cone feeder with coal dust with desired size.
5. Install the dust collection pan and ensure that it is free of contact from the burner.
6. Place camera at the right position and take sample picture with lamp on and without flame to ensure the position of burner, light source and camera are on a same axis.
Note: Camera was configured as all manual where the focus is at the maximum (to the nearest point), shutter speed at 4000, and aperture is maximized at 2.8.
7. Set up the load cell connection, and camera remote shooting connection with a PC.
8. Turn on the exhaust hood.
9. Open the valve and adjust the pressure of methane and air pressurized gas cylinder.
10. Plug in the power chord for the Mass Flow Controller (MFC).
11. Ensure that the MFC is at *Closed* mode to prevent unwanted gas leak or accumulation
12. Turn on the valves at gas distribution piping systems for both air and methane.
13. Adjust the flow rate to the desired value at the manual control panel of MFC.
14. Set the MFC mod at *Automatic* for both air and methane at the same time.
15. Ignite the flame with a torch.
16. Adjust the jacket tube to enable dust injection at a desired level.
17. Start the load cell recording.
18. Take Shadowgraph pictures using remote control.
19. Stop the flow by change the MFC mod to *Closed* after 5min or more if more pictures need to be taken. For high unstable flame with very high dust concentration, stop the flow once the flame is extinguished.
20. Close the side opening completely.
21. Close the main valves at the gas cylinders.
22. Set MFC mod as *Purge* at the same time and ignite the burner.
23. Shut off all valves once all gases have been bled out.
24. Set MFC mod as *Close* and unplug the MFC.
25. Turn off the exhaust hood.

Appendix B: Algorithm for Angle Measurement

B.1 Description of the Algorithm using Matlab

The Matlab subscript has been developed for the flame cone measurements. There are two parts of this code: 1. The main code handles the image cropping, edge detection, angle measuring, and finally image saving; 2. The automatic supplement code enable Matlab automatically process multiple pictures.

The concepts detecting the cone edge and effectively make the angle measurement are the most important part of this code.

1. Edge Detection: First each image has been converted into binary image with enhanced contrast. And each image has been cropped with around 420 pixels on the x-axis for the sake of processing number of images. Then each row within the scan boundary which is manual defined is scanned to find out most dramatic change of the pixel value change (0 for black and 1 for white) for both sides of the cone, but processed separately. This method can successfully detect the edges of the cone. However, it will also pick up areas other than on the edge since the maximum change of pixel value may also occurs at the burning particles. Nevertheless, the majority of identified pixels are on the cone edge.
2. Effective Angle Measurement: Many other methods have been tried to make the most effective or accurate angle measurement. However, the one present here is the most effective one. As mentioned in last paragraph, the edge detection is essentially picking up the pixel or point on the image where the maximum value changes occurs. Therefore, a line fit is a best method to get the angle based on these detected points. However, it is problematic to get a line fit with many outliers as the detected pixels. Therefore, the slope of a line between each detected point has been measured and the media of all the values of the slopes is chosen to be the slope of the line for line fit. It should be not that at the right side of the cone, slopes should be positive and thus all slopes with a negative sign are excluded. The same process was taken for the left side of the cone. Once the slope of the line for line fit is determined, a line-fit is drawn on the image to enable to make the final check. If the line-fit does not match the cone edge, this image or data is excluded. However, such line-fit very rarely occurs.

The actual code can be reviewed in section B.2.

B.2 Developed Algorithm (Matlab Code)

I. Main Algorithm – Angle_Function_02

```
function [Angle] = angle_function_02(file_drill) %% start operating on folder
file=strcat(file_drill); % define image file
im1 = imread(file); % read image file
% bc1 = imread(file); % read image file
bc1=im1(:,:,3); % change to blue channel only
% bc1=im1(:,:,:); % change to blue channel only
imgcrop1=imcrop(bc1,[1370.5 1138.5 1213 750]); % crop image file MANUALLY
A=histeq(imgcrop1); % increase contrast of image
I=imresize(A,[259.7,420.01]); % reduce resolution of image MANUALLY, 1/4 of the
original; NOTE:[number of rows(vercticle pix number), number of columns(horizontal pix
number)
[row,column] = size(I); % find size of image % setting edge scan area in y direction; And
moving step in y direction
y_max = 200 ;
y_min = 110 ;
del_y = 1 ; % setting edge scan areas for left and right cone edges
x_min_left = 53 ;
x_max_left = 200 ;
x_min_right = 220 ;
x_max_right = 367 ; % other edge scan constant
test_loop = 1 ;
aa = 1 ;
y=0 ;
x1_store=0;
k_store = 0 ;% edge detection
y(1) = y_min ;
while y(end) <= y_max
test_loop = test_loop + 1 ;
% Left side bottom line
i = y(aa); % y1 value
count_01 = 1 ;
for k = x_min_left:x_max_left; % limiting x to the center of the cone (214)
k_store(count_01) = k ;
P(k) = I(i,k);
count_01 = count_01+1 ;
end;
```

```

[v1,x1]= max(P);
x1_store(aa) = x1 ;
P_store(y(aa),:) = P ;
PP = double(P) ;%smooth PP
for hh=x_min_left+6:(x_max_left-6);
PP_smooth(hh) = mean(PP(hh-5:hh+5)) ;
end
ee = 1 ;
for dd = x_min_left:x_max_left-10;
dd_store(dd) = dd ;
del_P(dd) = PP_smooth(dd+1) - PP_smooth(dd) ;
ee=ee+1 ;
end
[test(aa) max_del_P(aa)] = max(del_P(x_min_left+10:x_max_left-10)) ;
max_del_P(aa) = max_del_P(aa) + x_min_left + 10; %offset
%% Right Side Bottom Line
count_02 = 1 ;
for j = x_min_right:x_max_right;
j_store(count_02) = j ;
Q(j)= I(i,j);
count_02 = count_02 + 1 ;
end;
[v3,x3]= max(Q);
x3_store(aa) = x3 ;
Q_store(y(aa),:) = Q ;
QQ = double(Q) ;
%smooth QQ
for ll=x_min_right+6:(x_max_right-6) ;
QQ_smooth(ll) = mean(QQ(ll-5:ll+5)) ;
end
mm = 1 ;
for nn = x_min_right:x_max_right-10 ;
nn_store(mm) = nn ;
del_Q(nn) = QQ_smooth(nn+1) - QQ_smooth(nn) ;
mm=mm+1 ;
end
[test(aa) min_del_Q(aa)] = min(del_Q(x_min_right+10:x_max_right-10)) ;
min_del_Q(aa) = min_del_Q(aa) + x_min_right + 10 ; %offset
y(aa+1) = y(aa) + del_y ;
aa = aa + 1 ;

```

```

end
ff = 1 ;
for gg = min(x3_store):max(x3_store)-1 ;
gg_store(ff) = gg ;
del_Q(gg) = Q(gg)-Q(gg+1) ;
ff=ff+1 ;
end

figure
clf
imshow(I) % show image
hold on
%Slopes calculation and selection
% % compute all slopes on left side
totpoints_l=y_max-y_min;
numslopes_l=(totpoints_l^2-totpoints_l)/2;
slopes_l=zeros(numslopes_l,1);
T=0;
for i=1:totpoints_l
for j=i+1:totpoints_l;
T=T+1;
slopes_l(T)=(y(i)-y(j))/(max_del_P(i)-max_del_P(j));
end
end
%taking only negative slope for left side
slopes_l(slopes_l>0) =[];
% find median of slopes
slope_left = median(slopes_l)
% % compute all slopes on right side
totpoints_r=y_max-y_min;
numslopes_r=(totpoints_r^2-totpoints_r)/2;
slopes_r=zeros(numslopes_r,1);
U=0;
for i=1:totpoints_r
for j=i+1:totpoints_r;
U=U+1;
slopes_r(U)=(y(i)-y(j))/(min_del_Q(i)-min_del_Q(j));
end
end
%taking only positive slope for right side

```

```

slopes_r(slopes_r<0) =[];
% find median of slopes
slope_right=median(slopes_r)
%% plot the slope and detected points
% plot original data with best guess at slope
plot(max_del_P,y(1:length(max_del_P)),'*',sort(max_del_P),slope_left*sort(max_del_P)
+(((y_max+y_min)/2-median(slope_left*sort(max_del_P))))),'g-')
% plot original data with best guess at slope
plot(min_del_Q,y(1:length(min_del_Q)),'+',sort(min_del_Q),slope_right*sort(min_del_Q)
)-(median(slope_right*sort(min_del_Q))-((y_max+y_min)/2)),'r-')

%Calculating Angle based on slope
Angle_a = 90 -(-180/pi*atan(slope_left));
Angle_b = 90 -(-180/pi*atan(slope_right));

Angle = (Angle_a + Angle_b)/2;
Angle

hold off
axis on

pause(0.5)

```

II. Automatic Process Algorithm

```

clear all
close all
clc

dname = ('G:\Combustion Lab\experiment\Burning velocity\images\gas flames with low
flow rate\phi=0.7--1.1_0.081\selected');%Default Directory To be Opened

%% Set up basic file name path to read
top_file = [dname '\'] ; %Set up main database to
open and look inside
ls_top_file = ls(top_file) ; %List Files inside main
folder
c = cellstr(ls_top_file) ; %Turn cells from ls
function into strings

```

```

cc_drill          = c(3:length(c))          ; %Set up a matrix
without the . and .. produces by the ls function
S                = size(cc_drill)          ; %Find the size of matrix
containing names of files inside of main database
a                = 1                      ; %This counter is set to 3 to
account for the . and .. at the beggining of each matrix created by ls

while a <= S(1)
close all
file_drill       = char(cellstr([top_file char(cc_drill(a))])) ; %File to be
operated on
data_n           = char(cc_drill(a))
file_name        = char(cc_drill(a))      ;

% Operations on files in folder

[Angle(a)] = angle_function_02(file_drill) ;

set(gcf, 'PaperPositionMode', 'auto');
h = gcf ;
saveas(h, [dname '\z_' file_name ], 'jpg');

a                = a+1                    ;

end

```

Appendix C: Experimental Data

C.1 Pressure Drop Calculation for Dust Injector

Table C.1-1 (calculation is based on *Introduction to Fluid Mechanics* (2003), by Robert W. Fox et al.)

D=	12	12	12	12	12	12	mm
	0.012	0.012	0.012	0.012	0.012	0.012	m
dt(orifice dia.)=	1	1	1	1	1	1	mm
	0.001	0.001	0.001	0.001	0.001	0.001	m
m(mass flow rate)=	1000	1500	2000	2500	3000	3500	cc/min
	1.13E-05	0.000017	2.27E-05	2.83E-05	0.000034	3.97E-05	kg/s
miu(viscosity)=	1.03E-05	1.03E-05	1.03E-05	1.03E-05	1.03E-05	1.03E-05	kg/m.s
roh(density)=	0.68	0.68	0.68	0.68	0.68	0.68	kg/m ³
A=	0.000113	0.000113	0.000113	0.000113	0.000113	0.000113	m ²
At(orifice area)=	7.85E-07	7.85E-07	7.85E-07	7.85E-07	7.85E-07	7.85E-07	m ²
Re=	117.089	175.6335	234.178	292.7225	351.267	409.8115	
beta(=At/A)=	0.006944	0.006944	0.006944	0.006944	0.006944	0.006944	
C(discharge coeff.)=	0.595911	0.595909	0.595907	0.595906	0.595905	0.595905	corner tap config.
K(flow ceoff.)=	0.595911	0.595909	0.595907	0.595906	0.595905	0.595905	
V=	0.147366	0.221049	0.294731	0.368414	0.442097	0.51578	m/s
Vt=	21.22066	31.83099	42.44132	53.05165	63.66198	74.27231	m/s
p1-p2=	431.155	970.1077	1724.644	2694.765	3880.471	5281.761	Pa
	0.004312	0.009701	0.017246	0.026948	0.038805	0.052818	bar
D=	0.012	0.012	0.012	0.012	0.012	0.012	m
	1	1	1	1	1	1	mm
dt(orifice dia.)=	0.001	0.001	0.001	0.001	0.001	0.001	m
	4000	4500	5000	5500	6000	6500	cc/min
m(mass flow rate)=	4.53E-05	0.000051	5.67E-05	6.23E-05	0.000068	7.37E-05	kg/s
	1.03E-05	1.03E-05	1.03E-05	1.03E-05	1.03E-05	1.03E-05	kg/m.s
miu(viscosity)=	0.68	0.68	0.68	0.68	0.68	0.68	kg/m ³
roh(density)=	0.000113	0.000113	0.000113	0.000113	0.000113	0.000113	m ²
A=	7.85E-07	7.85E-07	7.85E-07	7.85E-07	7.85E-07	7.85E-07	m ²
At(orifice area)=	468.356	526.9005	585.445	643.9895	702.534	761.0785	
Re=	0.006944	0.006944	0.006944	0.006944	0.006944	0.006944	
beta(=At/A)=	0.595905	0.595904	0.595904	0.595904	0.595904	0.595903	corner tap config.
C(discharge coeff.)=	0.595905	0.595904	0.595904	0.595904	0.595904	0.595903	
K(flow ceoff.)=	0.589463	0.663146	0.736828	0.810511	0.884194	0.957877	m/s
V=	84.88264	95.49297	106.1033	116.7136	127.324	137.9343	m/s
Vt=	6898.635	8731.095	10779.14	13042.77	15521.98	18216.78	Pa
p1-p2=	0.068986	0.087311	0.107791	0.130428	0.15522	0.182168	bar

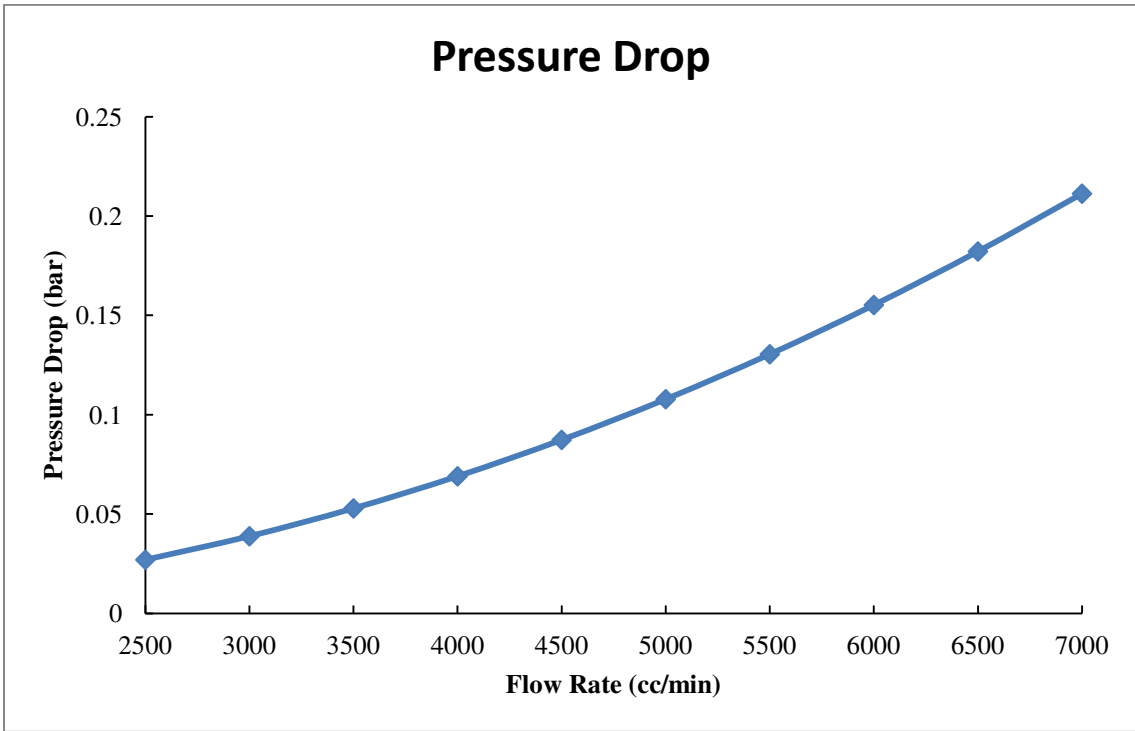


Fig. C.1-1

C.2 Dust Entrainment Data for Dust Injector

Table C.2-1

Three 2.70 cm² Openings	
Flow Rate (L/min)	Averaged Entrainment Rate (g/min)
1	0
1.5	0.634
2	2.118
3	8.08
4	16.912
5	28.34
6	41.874
7	58.558
8	84.964
9	113.744
10	154.126

Table C.2-2

Three 1.51 cm² Openings	
Flow Rate (L/min)	Averaged Entrainment Rate (g/min)
1	0
1.5	0.566
2	1.564
3	6.124
4	13.42
5	24.576
6	37.8
7	58.73
8	85.746
9	118.222
10	150.14

Table C.2-3

Six 1.18 cm² Openings	
Flow Rate (L/min)	Averaged Entrainment Rate (g/min)
1.5	0
2	1.116
3	4.47
4	9.744
5	18.822
6	37.534
7	58.686
8	82.67
9	122.62
10	152.846

Entrainment Rate for Different Dust Entrain Sections

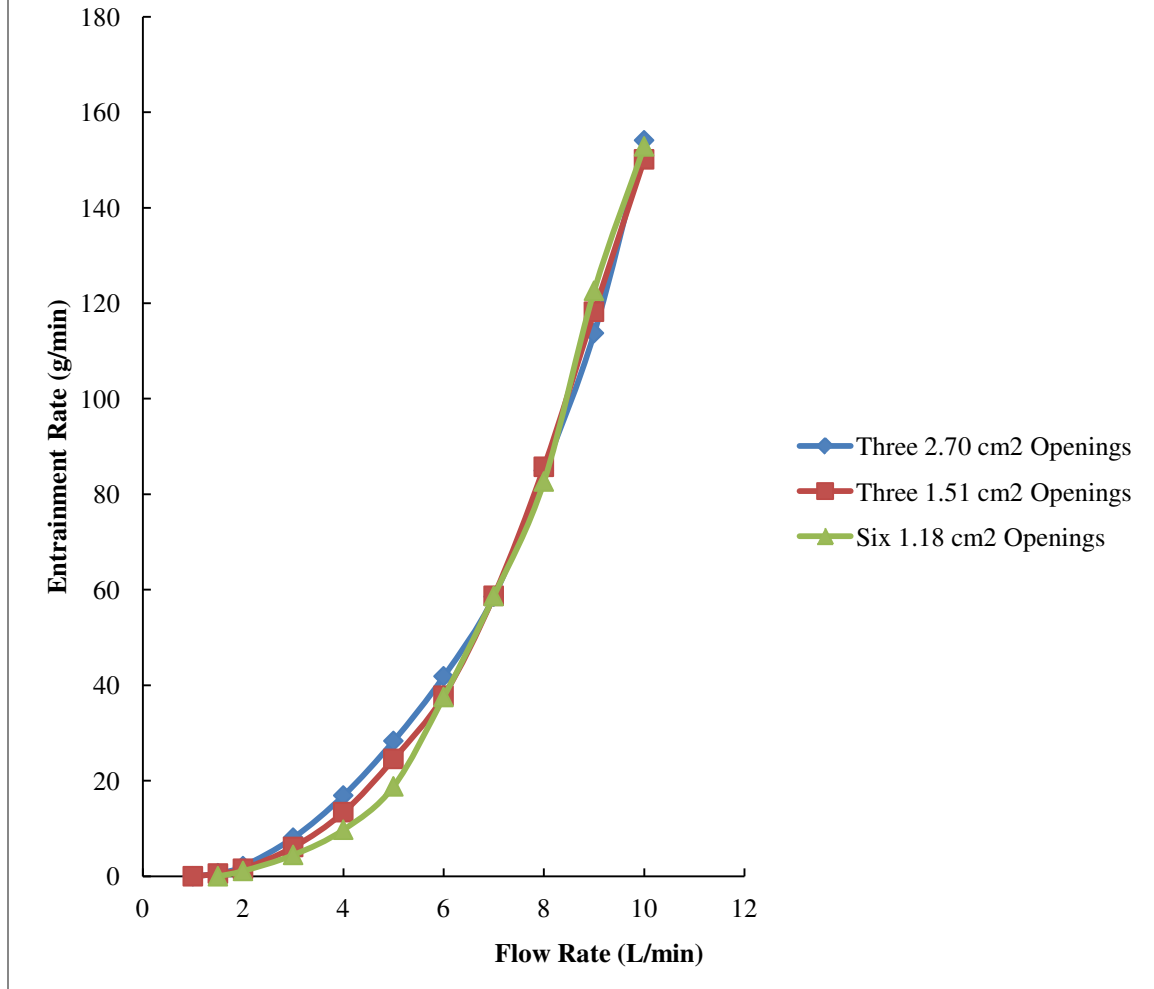


Fig. C.2-1

C.3 Summary Sheet of Flame Cone Angle for Experiment.

1. Dust Free Flame

1.1 $\phi=0.75$ (Flow Rate: Air 2.0 SLPM; Methane: 0.158 SLPM)

Average Cone Angle: 46.386

1.2 $\phi=0.80$ (Flow Rate: Air 2.5 SLPM; Methane: 0.21 SLPM)

Average Cone Angle: 42.344

1.3 $\phi=0.85$ (Flow Rate: Air 2.5 SLPM; Methane: 0.223 SLPM)

Average Cone Angle: 50.351

2. Sand at 75-90 μm

2.1 $\phi=0.80$ (Flow Rate: Air 2.5 SLPM; Methane: 0.21 SLPM)

Experiment NO. 1: Dust Concentration: 48.74; Average Cone Angle: 40.272

Experiment NO. 2: Dust Concentration: 64.24; Average Cone Angle: 39.586

Experiment NO. 3: Dust Concentration: 178.28; Average Cone Angle: 37.488

2.2 $\phi=0.85$ (Flow Rate: Air 2.5 SLPM; Methane: 0.223 SLPM)

Experiment NO. 1: Dust Concentration: 66.14; Average Cone Angle: 45.379

Experiment NO. 3: Dust Concentration: 48.60; Average Cone Angle: 44.583

Experiment NO. 4: Dust Concentration: 48.50; Average Cone Angle: 45.179

Experiment NO. 5: Dust Concentration: 156.54; Average Cone Angle: 40.701

3. Coal Particles at 75-90 μm

3.1 $\phi=0.75$ (Flow Rate: Air 2.0 SLPM; Methane: 0.158 SLPM)

Experiment NO. 1: Dust Concentration: 108.50; Average Cone Angle: 43.287
Experiment NO. 2: Dust Concentration: 11.07; Average Cone Angle: 44.333
Experiment NO. 3: Dust Concentration: 161.36; Average Cone Angle: 41.212
Experiment NO. 4: Dust Concentration: 169.71; Average Cone Angle: 39.764
Experiment NO. 5: Dust Concentration: 153.01; Average Cone Angle: 43.222
Experiment NO. 6: Dust Concentration: 13.91; Average Cone Angle: 44.960
Experiment NO. 7: Dust Concentration: 197.53; Average Cone Angle: 41.862
Experiment NO. 8: Dust Concentration: 61.20; Average Cone Angle: 45.907
Experiment NO. 9: Dust Concentration: 30.60; Average Cone Angle: 44.945

2.2 $\phi=0.80$ (Flow Rate: Air 2.5 SLPM; Methane: 0.21 SLPM)

Experiment NO. 1: Dust Concentration: 26.58; Average Cone Angle: 41.532
Experiment NO. 2: Dust Concentration: 70.89; Average Cone Angle: 39.156
Experiment NO. 4: Dust Concentration: 248.13; Average Cone Angle: 38.250
Experiment NO. 5: Dust Concentration: 24.371; Average Cone Angle: 41.900
Experiment NO. 6: Dust Concentration: 146.22; Average Cone Angle: 39.781
Experiment NO. 8: Dust Concentration: 254.77; Average Cone Angle: 38.848
Experiment NO. 11: Dust Concentration: 128.49; Average Cone Angle: 40.314
Experiment NO. 12: Dust Concentration: 112.98; Average Cone Angle: 40.873
Experiment NO. 13: Dust Concentration: 28.801; Average Cone Angle: 41.021
Experiment NO. 14: Dust Concentration: 137.35; Average Cone Angle: 40.165
Experiment NO. 15: Dust Concentration: 46.52; Average Cone Angle: 41.495

2.3 $\phi=0.85$ (Flow Rate: Air 2.5 SLPM; Methane: 0.223 SLPM)

Experiment NO. 1: Dust Concentration: 28.66; Average Cone Angle: 46.909

Experiment NO. 2: Dust Concentration: 6.614; Average Cone Angle: 49.024
Experiment NO. 4: Dust Concentration: 50.71; Average Cone Angle: 47.622
Experiment NO. 5: Dust Concentration: 180.80; Average Cone Angle: 45.595
Experiment NO. 6: Dust Concentration: 24.25; Average Cone Angle: 48.530
Experiment NO. 7: Dust Concentration: 81.58; Average Cone Angle: 47.418
Experiment NO. 8: Dust Concentration: 302.06; Average Cone Angle: 43.973
Experiment NO. 9: Dust Concentration: 94.816; Average Cone Angle: 46.714
Experiment NO. 10: Dust Concentration: 6.61; Average Cone Angle: 48.7619
Experiment NO. 11: Dust Concentration: 63.94; Average Cone Angle: 47.001

4. Coal Particles at 53-63 μm

4.1 $\phi=0.80$ (Flow Rate: Air 2.5 SLPM; Methane: 0.21 SLPM)

Experiment NO. 3: Dust Concentration: 57.60; Average Cone Angle: 40.953
Experiment NO. 5: Dust Concentration: 181.66; Average Cone Angle: 39.308
Experiment NO. 6: Dust Concentration: 203.82; Average Cone Angle: 39.161
Experiment NO. 8: Dust Concentration: 73.11; Average Cone Angle: 40.641

4.2 $\phi=0.85$ (Flow Rate: Air 2.5 SLPM; Methane: 0.223 SLPM)

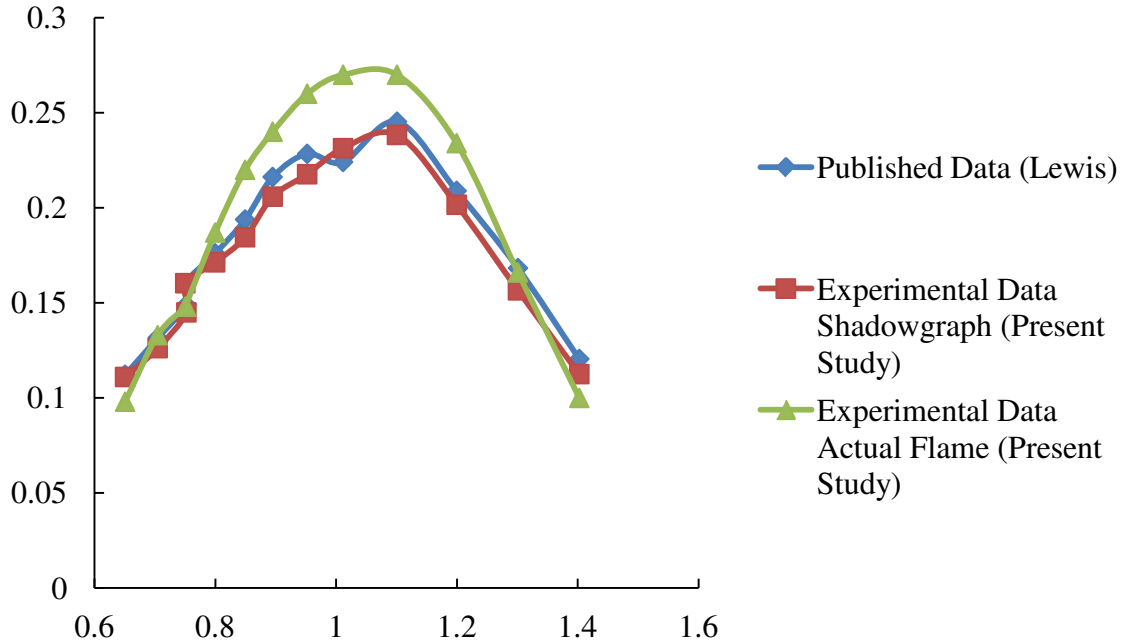
Experiment NO. 3: Dust Concentration: 61.73; Average Cone Angle 49.312
Experiment NO. 5: Dust Concentration: 59.53; Average Cone Angle: 48.0801
Experiment NO. 10: Dust Concentration: 79.37; Average Cone Angle: 47.543
Experiment NO. 11: Dust Concentration: 83.78; Average Cone Angle: 47.973
Experiment NO. 17: Dust Concentration: 249.15; Average Cone Angle: 44.883

5. Coal Particles at 0-25 μm

5.1 $\phi=0.75$ (Flow Rate: Air 2.0 SLPM; Methane: 0.158 SLPM)

Experiment NO. 3: Dust Concentration: 292.12 g/m³; Average Cone Angle: 50.008

6. S_u (gas only) with Equivalence Ratio Ranges from 0.7 to 1.4

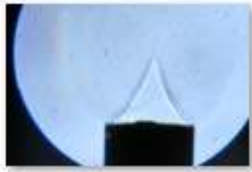


The laminar burning velocity of premixed methane-air flame without dust is experimentally determined and compared with the published data which is presented in *Combustion, Flames and Explosions of Gases* (1987) by Bernard Lewis and Guenther von Elbe. The plot above concludes the results obtained in this set of tests. As shown in this plot, the burning velocity measured based on shadowgraph and actual flame image is very small. The differences between them are believed to be caused by errors that associated with the test. However, it is noted that the burning velocity where the equivalence ratio is close to 1 is lower than the published data. It is believed that the flow velocity profile is very uneven. It should be noted that the published data are selected from previous study that is mainly due to similar experimental set-up is used. However, experimental data in other studies which uses different experimental set-up may have different value than that presented here. The further action can be done related to this issue is discussed in the Conclusions and Future Work section.

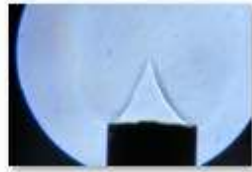
C. 4 Pictures and Entrainment Data

1. Dust Free

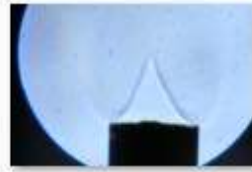
1.1 $\phi=0.75$; Flow Rate: Air 2 SLPM; Methane 0.158 SLPM



IMG_9999_158.JPG



IMG_9999_161.JPG



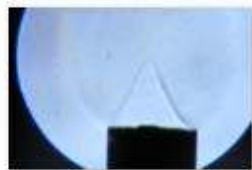
IMG_9999_163.JPG



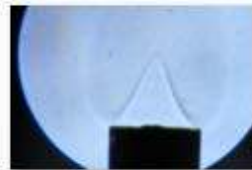
IMG_9999_164.JPG



IMG_9999_170.JPG



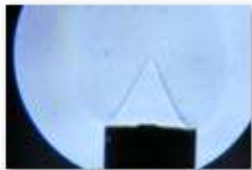
IMG_9999_171.JPG



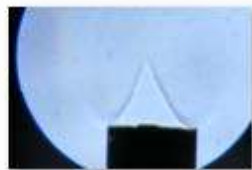
IMG_9999_172.JPG



IMG_9999_174.JPG



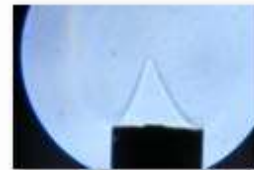
IMG_9999_178.JPG



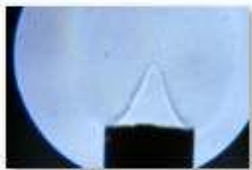
IMG_9999_180.JPG



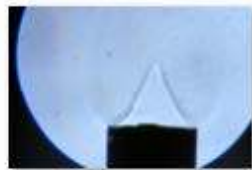
IMG_9999_181.JPG



IMG_9999_182.JPG



IMG_9999_185.JPG



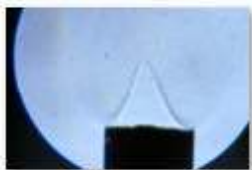
IMG_9999_186.JPG



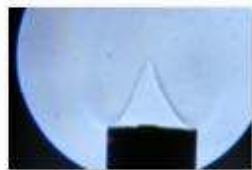
IMG_9999_192.JPG



IMG_9999_197.JPG



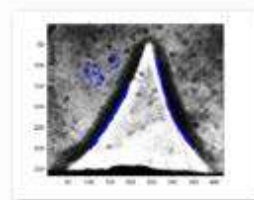
IMG_9999_198.JPG



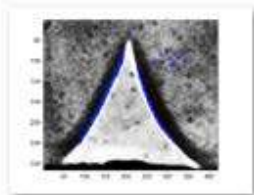
IMG_9999_200.JPG



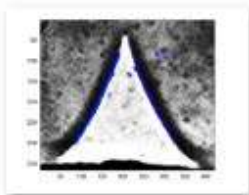
IMG_9999_201.JPG



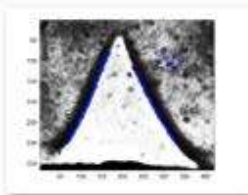
z_IMG_9999_158.JPG



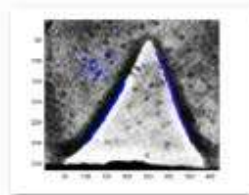
z_IMG_9999_161.JPG



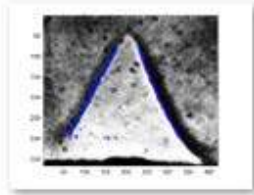
z_IMG_9999_163.JPG



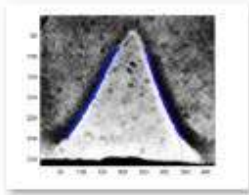
z_IMG_9999_164.JPG



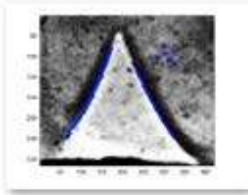
z_IMG_9999_170.JPG



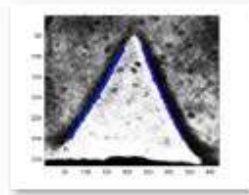
z_IMG_9999_171.JPG



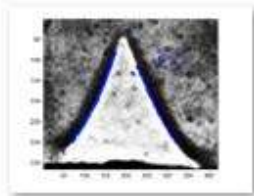
z_IMG_9999_172.JPG



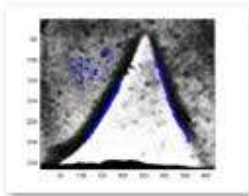
z_IMG_9999_174.JPG



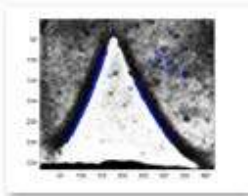
z_IMG_9999_178.JPG



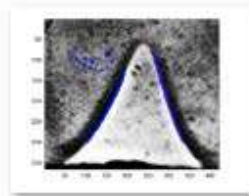
z_IMG_9999_180.JPG



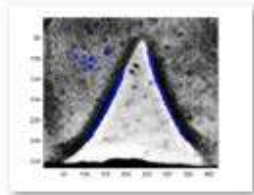
z_IMG_9999_181.JPG



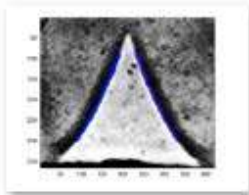
z_IMG_9999_182.JPG



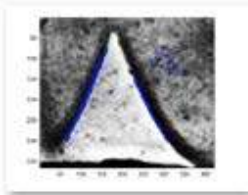
z_IMG_9999_185.JPG



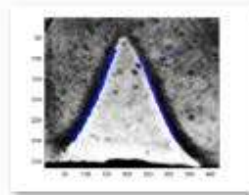
z_IMG_9999_186.JPG



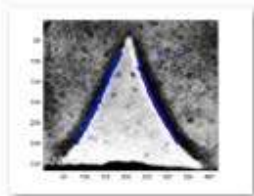
z_IMG_9999_192.JPG



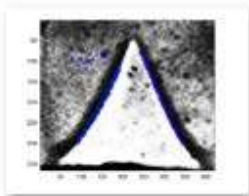
z_IMG_9999_197.JPG



z_IMG_9999_198.JPG

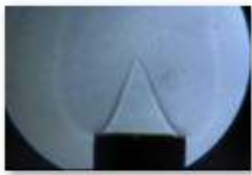


z_IMG_9999_200.JPG

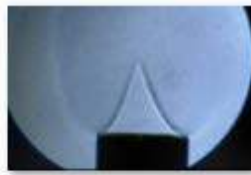


z_IMG_9999_201.JPG

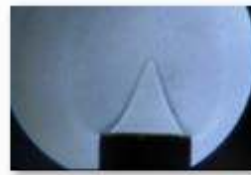
1.2 $\phi=0.80$; Flow Rate: Air 2.5 SLPM; Methane 0.21 SLPM



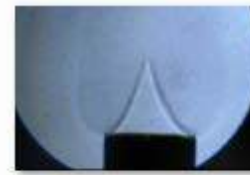
IMG_9999_795.JPG



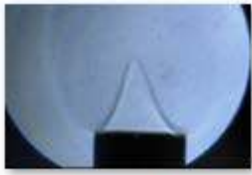
IMG_9999_808.JPG



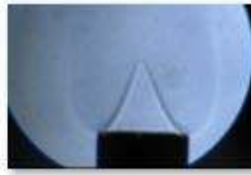
IMG_9999_811.JPG



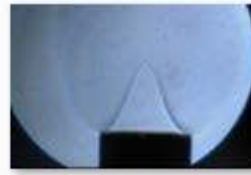
IMG_9999_818.JPG



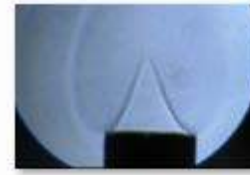
IMG_9999_831.JPG



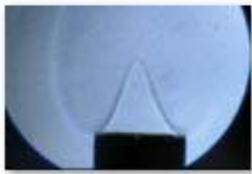
IMG_9999_834.JPG



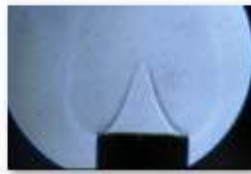
IMG_9999_835.JPG



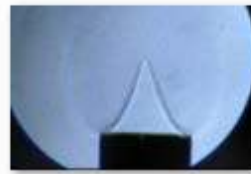
IMG_9999_837.JPG



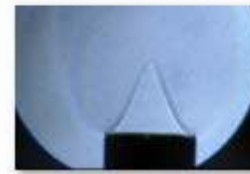
IMG_9999_838.JPG



IMG_9999_840.JPG



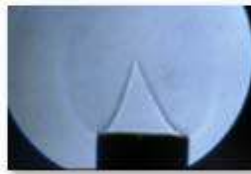
IMG_9999_842.JPG



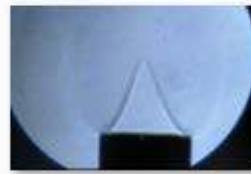
IMG_9999_844.JPG



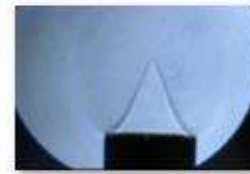
IMG_9999_845.JPG



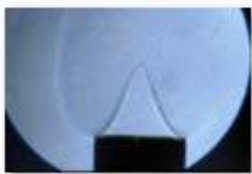
IMG_9999_846.JPG



IMG_9999_852.JPG



IMG_9999_853.JPG



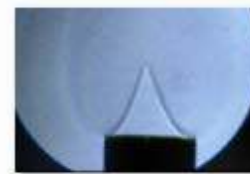
IMG_9999_854.JPG



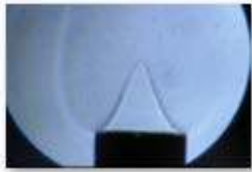
IMG_9999_857.JPG



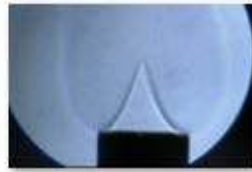
IMG_9999_858.JPG



IMG_9999_861.JPG



IMG_9999_854.JPG



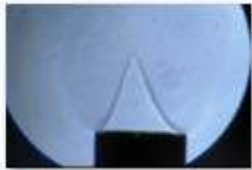
IMG_9999_857.JPG



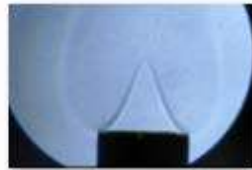
IMG_9999_858.JPG



IMG_9999_861.JPG



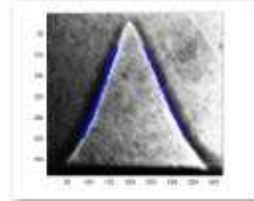
IMG_9999_865.JPG



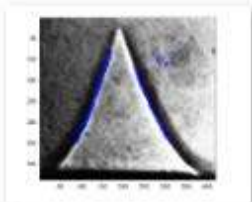
IMG_9999_866.JPG



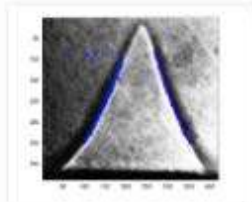
IMG_9999_867.JPG



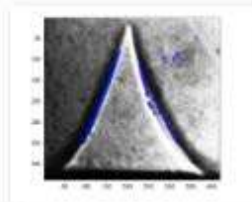
z_IMG_9999_795.JPG



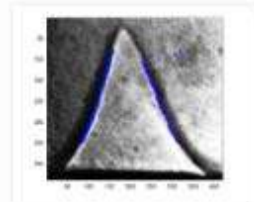
z_IMG_9999_808.JPG



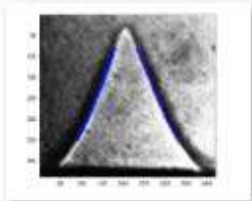
z_IMG_9999_811.JPG



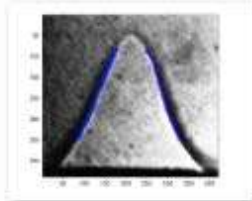
z_IMG_9999_818.JPG



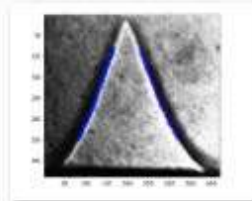
z_IMG_9999_831.JPG



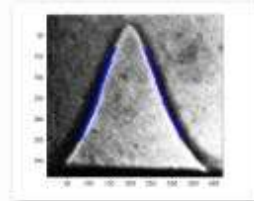
z_IMG_9999_834.JPG



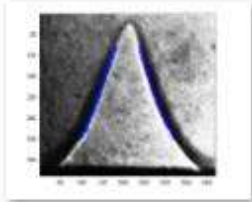
z_IMG_9999_835.JPG



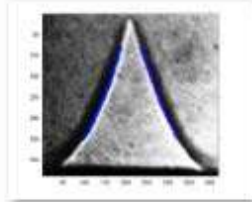
z_IMG_9999_837.JPG



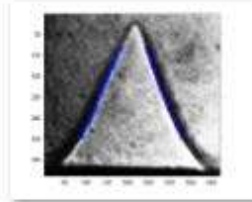
z_IMG_9999_838.JPG



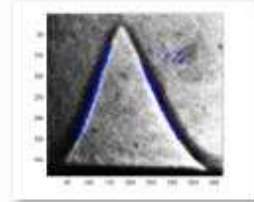
z_IMG_9999_840.JPG



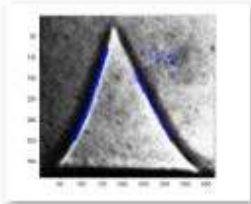
z_IMG_9999_842.JPG



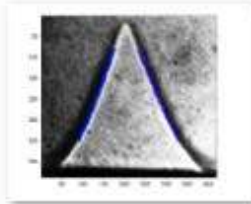
z_IMG_9999_844.JPG



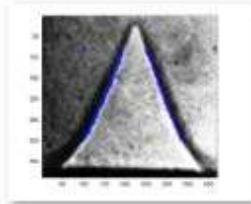
z_IMG_9999_845.JPG



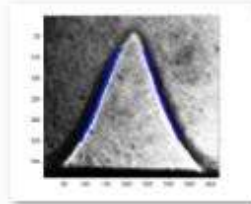
z_IMG_9999_846.JPG



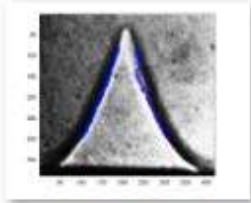
z_IMG_9999_852.JPG



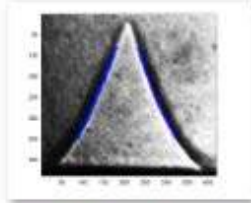
z_IMG_9999_853.JPG



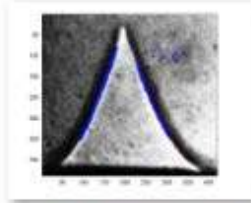
z_IMG_9999_854.JPG



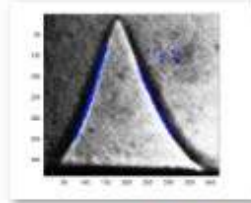
z_IMG_9999_857.JPG



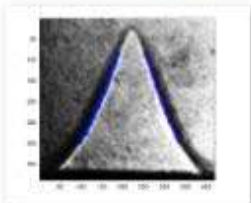
z_IMG_9999_858.JPG



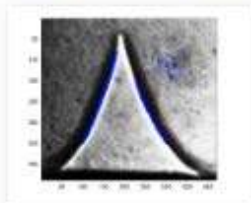
z_IMG_9999_861.JPG



z_IMG_9999_865.JPG



z_IMG_9999_866.JPG



z_IMG_9999_867.JPG

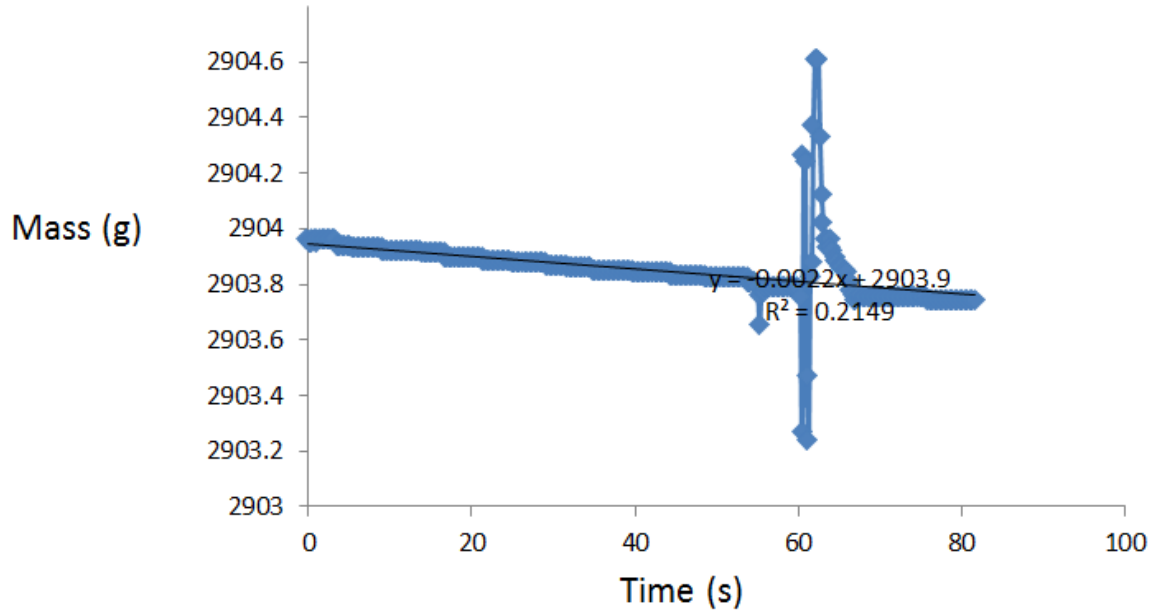
1.3 $\phi=0.85$; Flow Rate: Air 2.5 SLPM; Methane 0.223 SLPM



2. Sand Particles (75-90 μm)

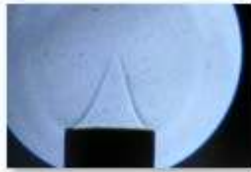
2.1 $\phi=0.80$; Flow Rate: Air 2.5 SLPM; Methane 0.21 SLPM

Experiment NO. 1.



Air Flow Rate		Fuel Flow rate		Volume flow rate	nozzle width	U	Phi
SLPM	mole/sec	SLPM	mole/sec	m ³ /s	m	m/sec	
2.5	0.001732	0.21	0.000145	4.51E-05	0.010744	0.497869	0.79968

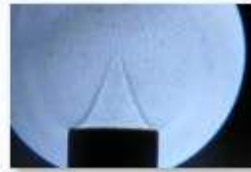
Entrainment Rate
 0.0022 g/sec
 Concentration
 48.74 g/m³



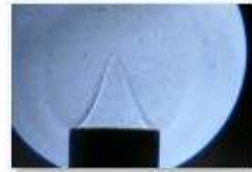
IMG_9999_795.JPG



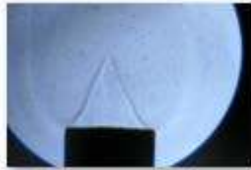
IMG_9999_799.JPG



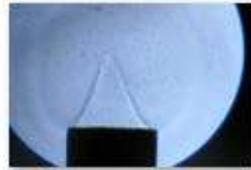
IMG_9999_801.JPG



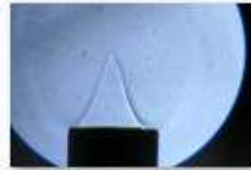
IMG_9999_803.JPG



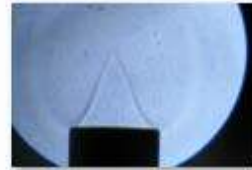
IMG_9999_805.JPG



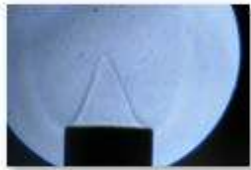
IMG_9999_806.JPG



IMG_9999_808.JPG



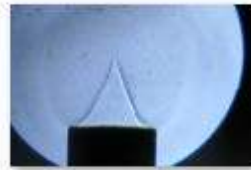
IMG_9999_818.JPG



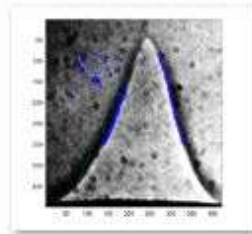
IMG_9999_823.JPG



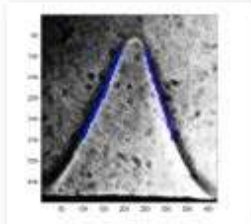
IMG_9999_824.JPG



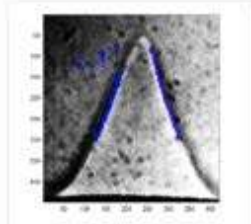
IMG_9999_825.JPG



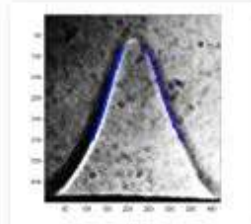
z_IMG_9999_795.JPG



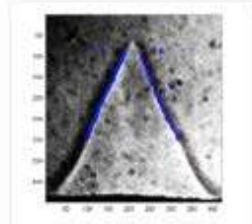
z_IMG_9999_799.JPG



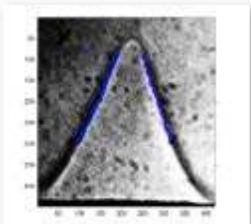
z_IMG_9999_801.JPG



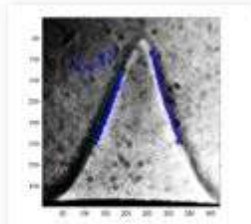
z_IMG_9999_803.JPG



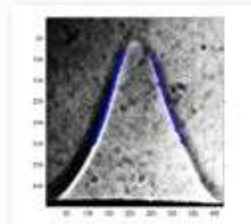
z_IMG_9999_805.JPG



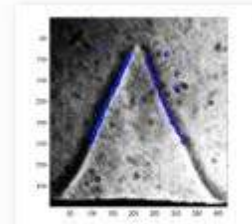
z_IMG_9999_799.JPG



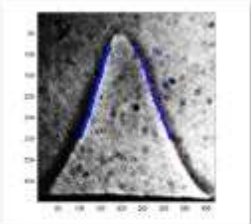
z_IMG_9999_801.JPG



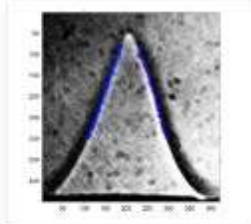
z_IMG_9999_803.JPG



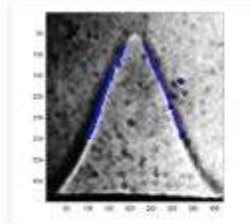
z_IMG_9999_805.JPG



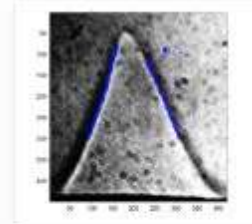
z_IMG_9999_806.JPG



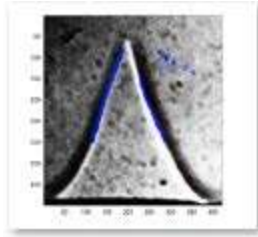
z_IMG_9999_808.JPG



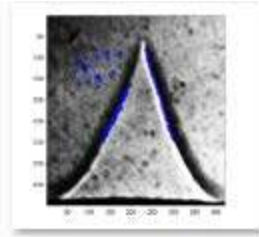
z_IMG_9999_818.JPG



z_IMG_9999_823.JPG

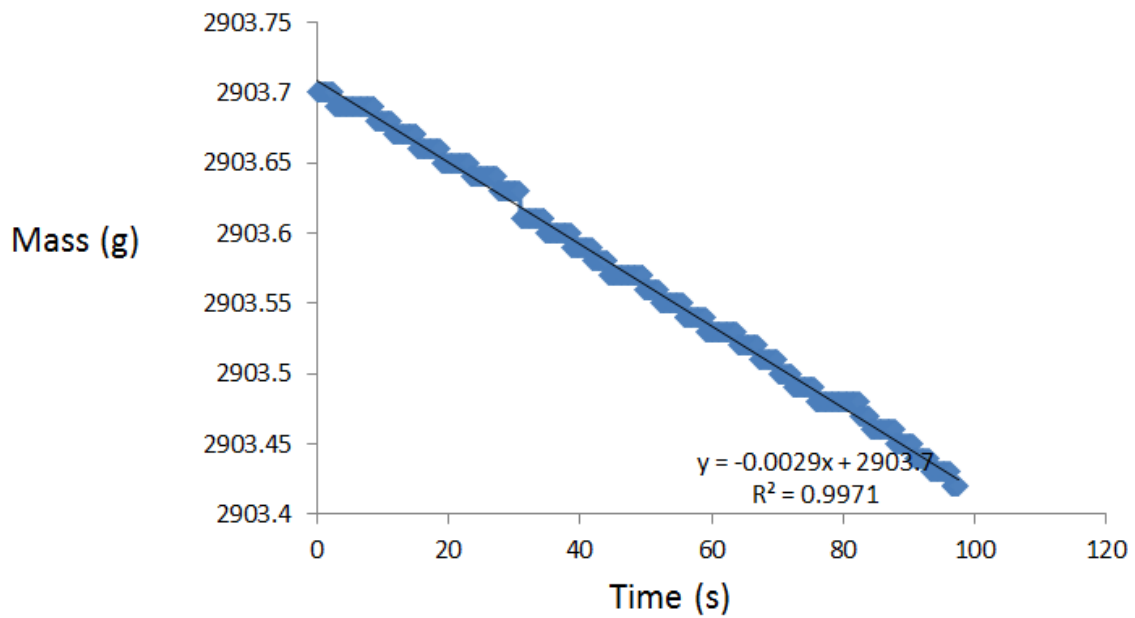


z_IMG_9999_824.JPG



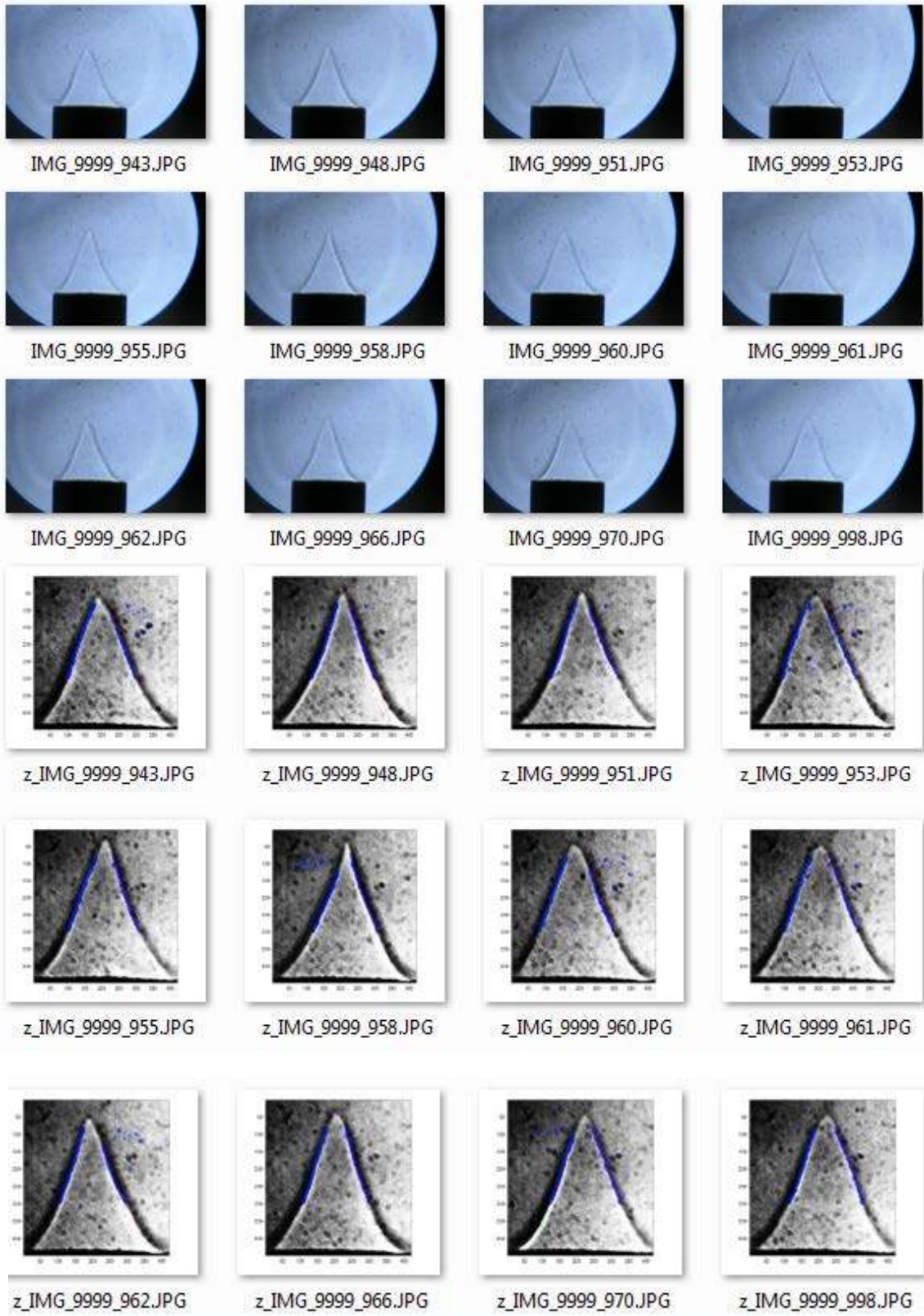
z_IMG_9999_825.JPG

Experiment NO. 2.

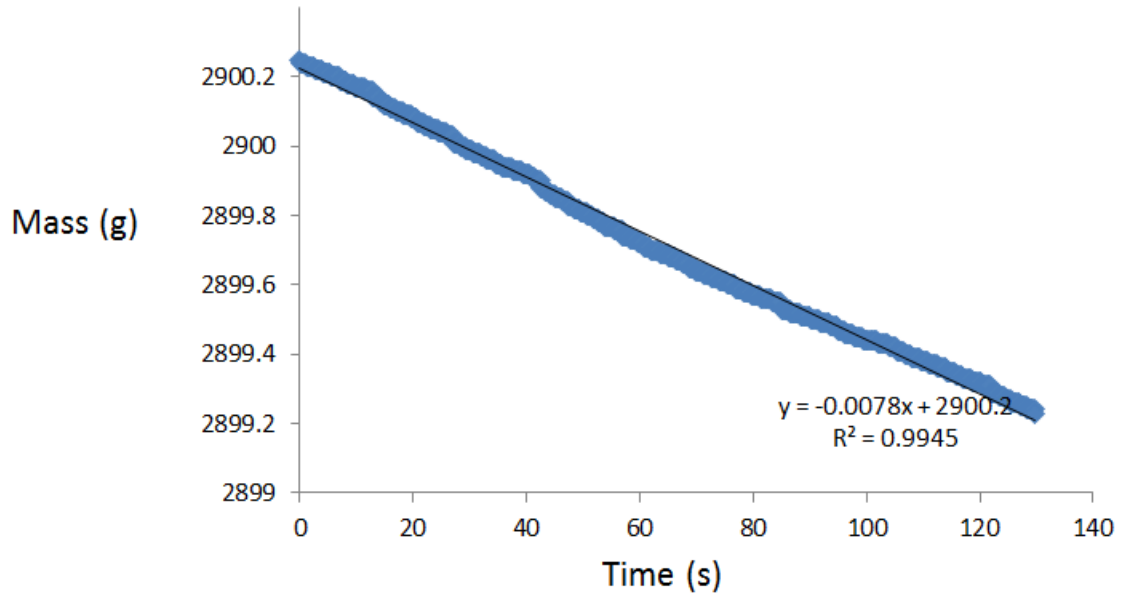


Air Flow Rate		Fuel Flow rate		Volume flow rate	nozzle width	U	Phi
SLPM	mole/sec	SLPM	mole/sec	m ³ /s	m	m/sec	
2.5	0.001732	0.21	0.000145	4.51E-05	0.010744	0.497869	0.79968

Entrainment Rate
 0.0029 g/sec
 Concentration
 64.24819 g/m³

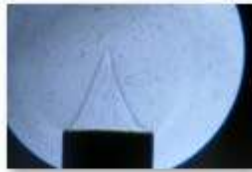


Experiment NO. 3.

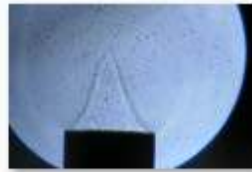


Air Flow Rate		Fuel Flow rate		Volume flow rate	nozzle width	U	Phi
SLPM	mole/sec	SLPM	mole/sec	m ³ /s	m	m/sec	
2.5	0.001732	0.21	0.000145	4.51E-05	0.010744	0.497869	0.79968

Entrainment Rate
0.0078 g/sec
Concentration
172.8055 g/m³



IMG_9999_1325.JPG



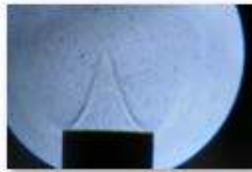
IMG_9999_1353.JPG



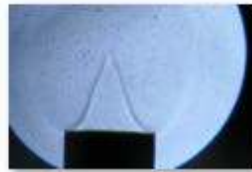
IMG_9999_1355.JPG



IMG_9999_1361.JPG



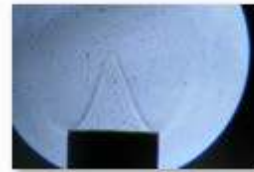
IMG_9999_1367.JPG



IMG_9999_1373.JPG



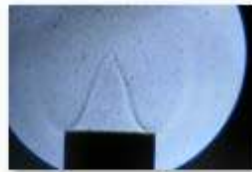
IMG_9999_1411.JPG



IMG_9999_1414.JPG



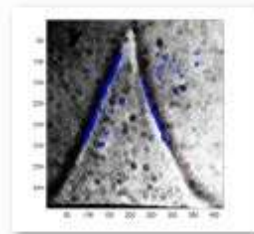
IMG_9999_1415.JPG



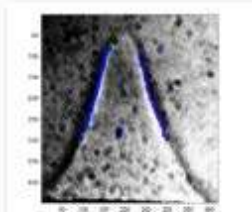
IMG_9999_1417.JPG



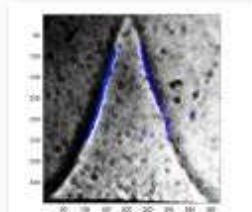
IMG_9999_1423.JPG



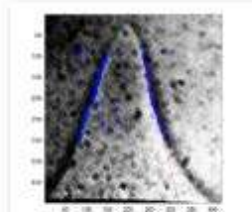
z_IMG_9999_1325.JPG



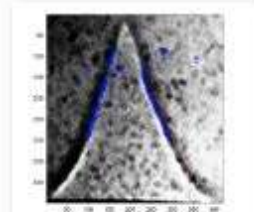
z_IMG_9999_1353.JPG



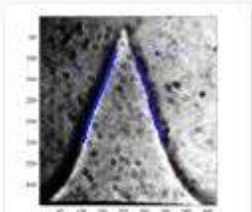
z_IMG_9999_1355.JPG



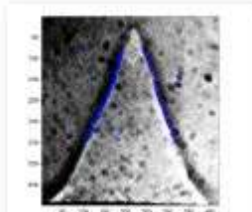
z_IMG_9999_1361.JPG



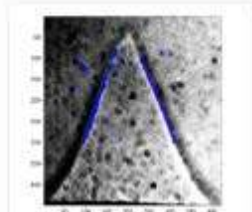
z_IMG_9999_1367.JPG



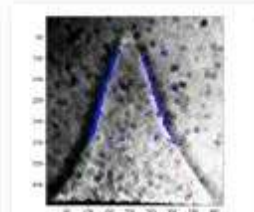
z_IMG_9999_1373.JPG



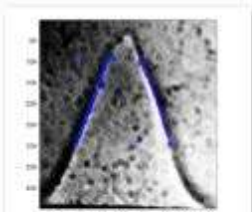
z_IMG_9999_1411.JPG



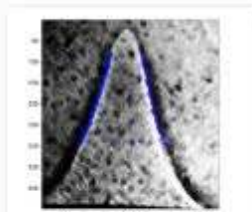
z_IMG_9999_1414.JPG



z_IMG_9999_1415.JPG



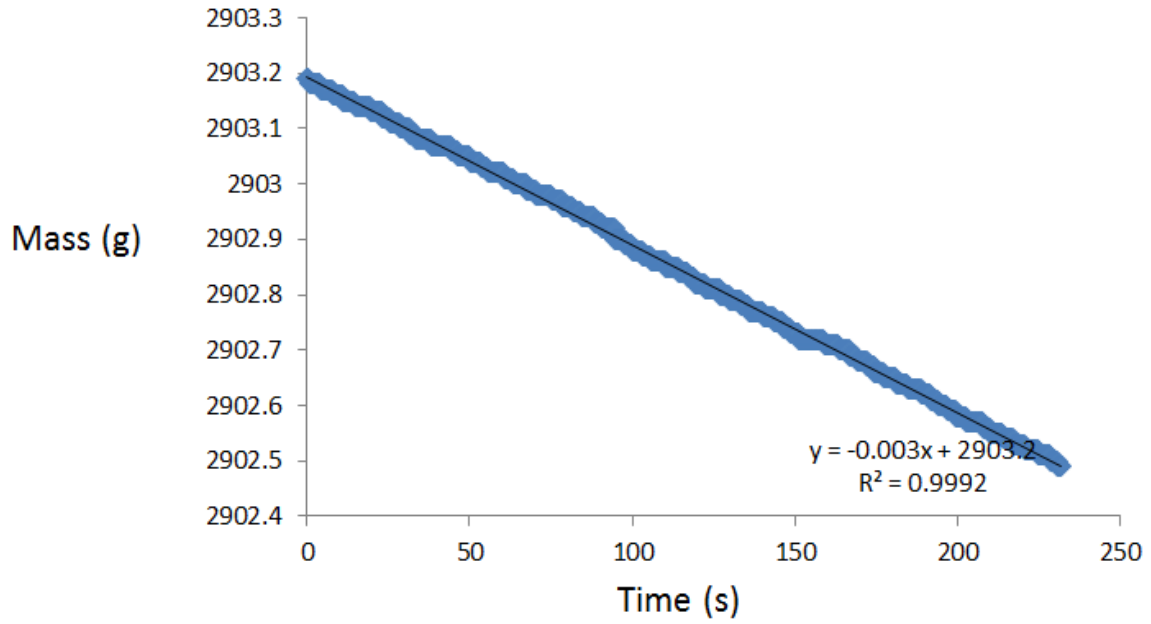
z_IMG_9999_1417.JPG



z_IMG_9999_1423.JPG

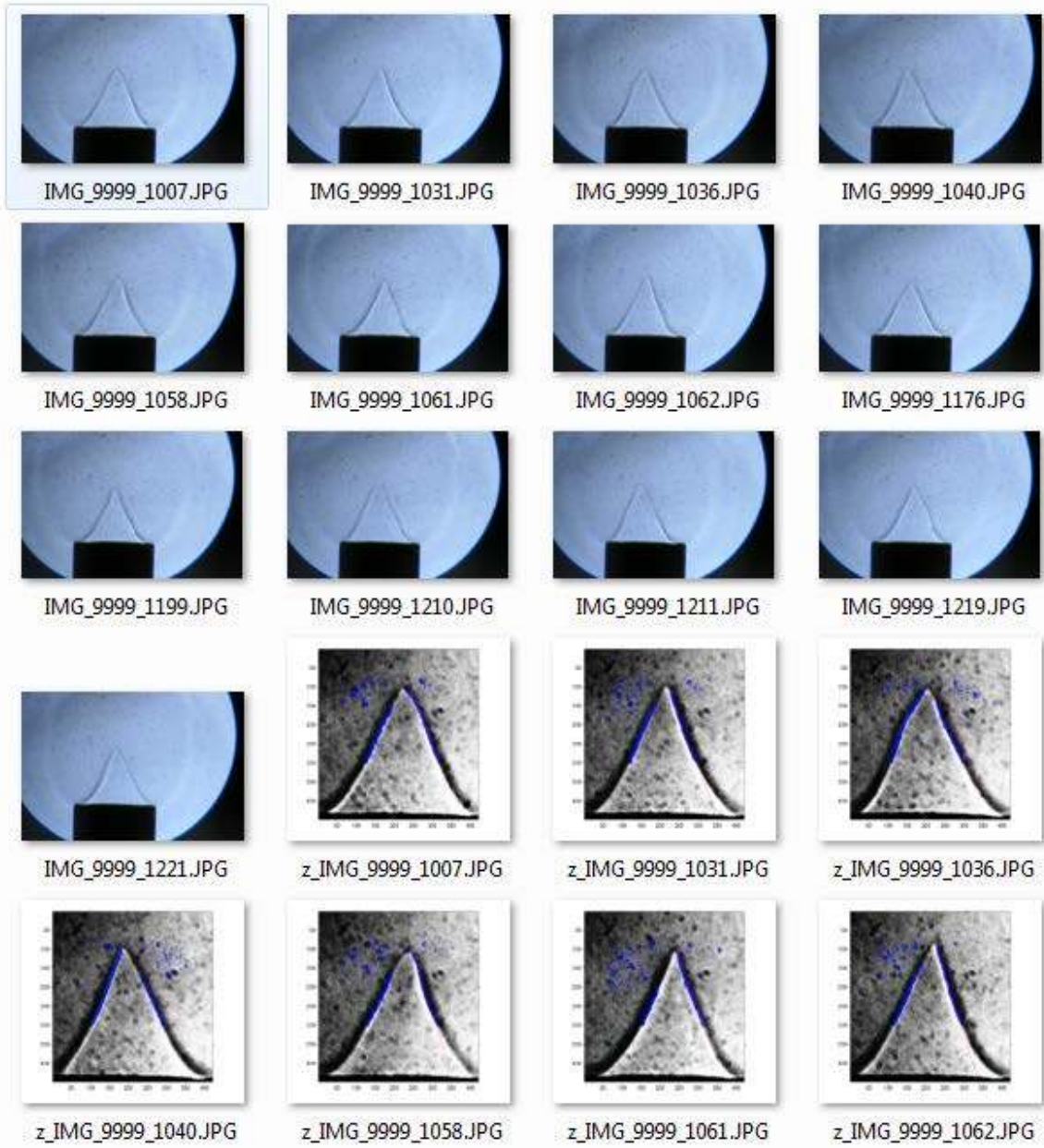
2.2 $\phi=0.85$; Flow Rate: Air 2.5 SLPM; Methane 0.223 SLPM

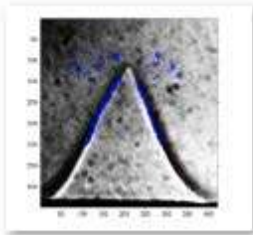
Experiment NO. 1.



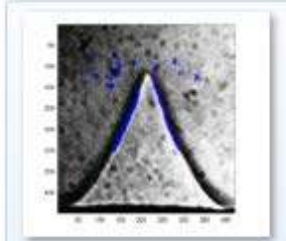
Air Flow Rate		Fuel Flow rate		Volume flow rate	nozzle width	U	Phi
SLPM	mole/sec	SLPM	mole/sec	m ³ /s	m	m/sec	
2.5	0.001732	0.223	0.000155	4.54E-05	0.010744	0.500255	0.849184

Entrainment Rate
0.003 g/sec
Concentration
66.14662 g/m³

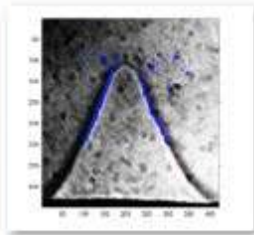




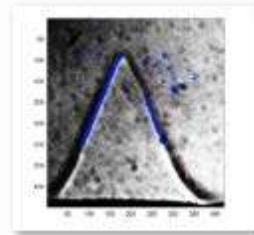
z_IMG_9999_1176.JPG



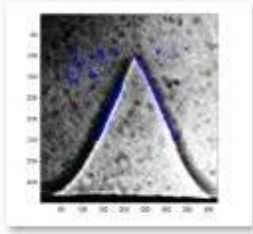
z_IMG_9999_1199.JPG



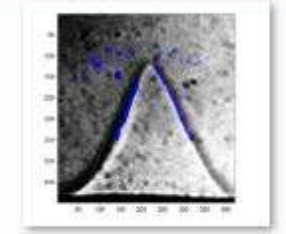
z_IMG_9999_1210.JPG



z_IMG_9999_1211.JPG

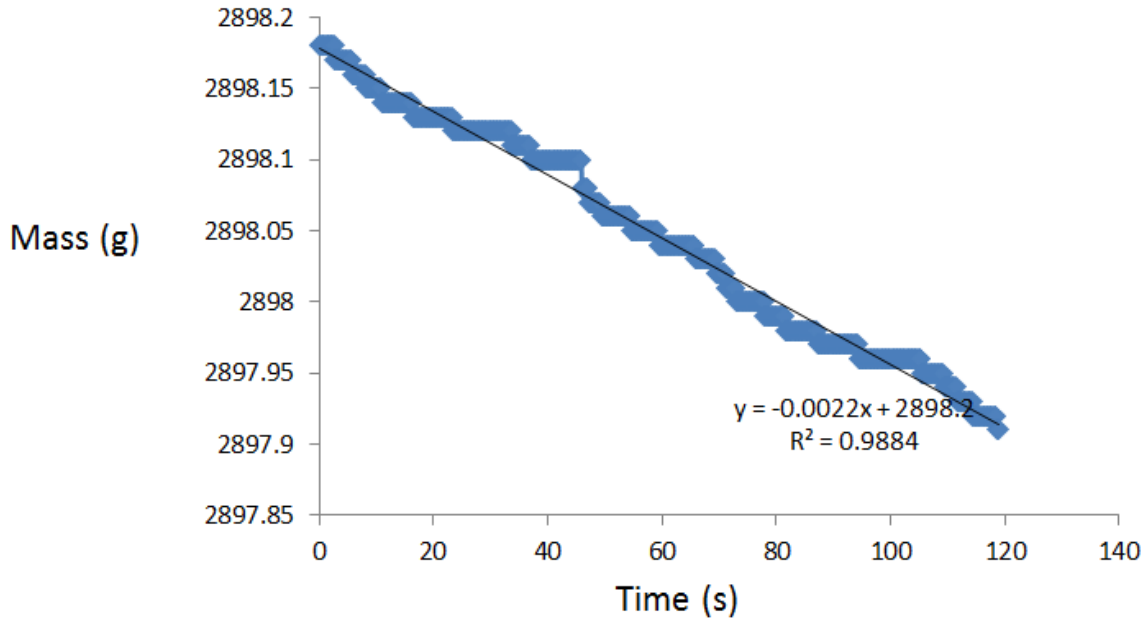


z_IMG_9999_1219.JPG



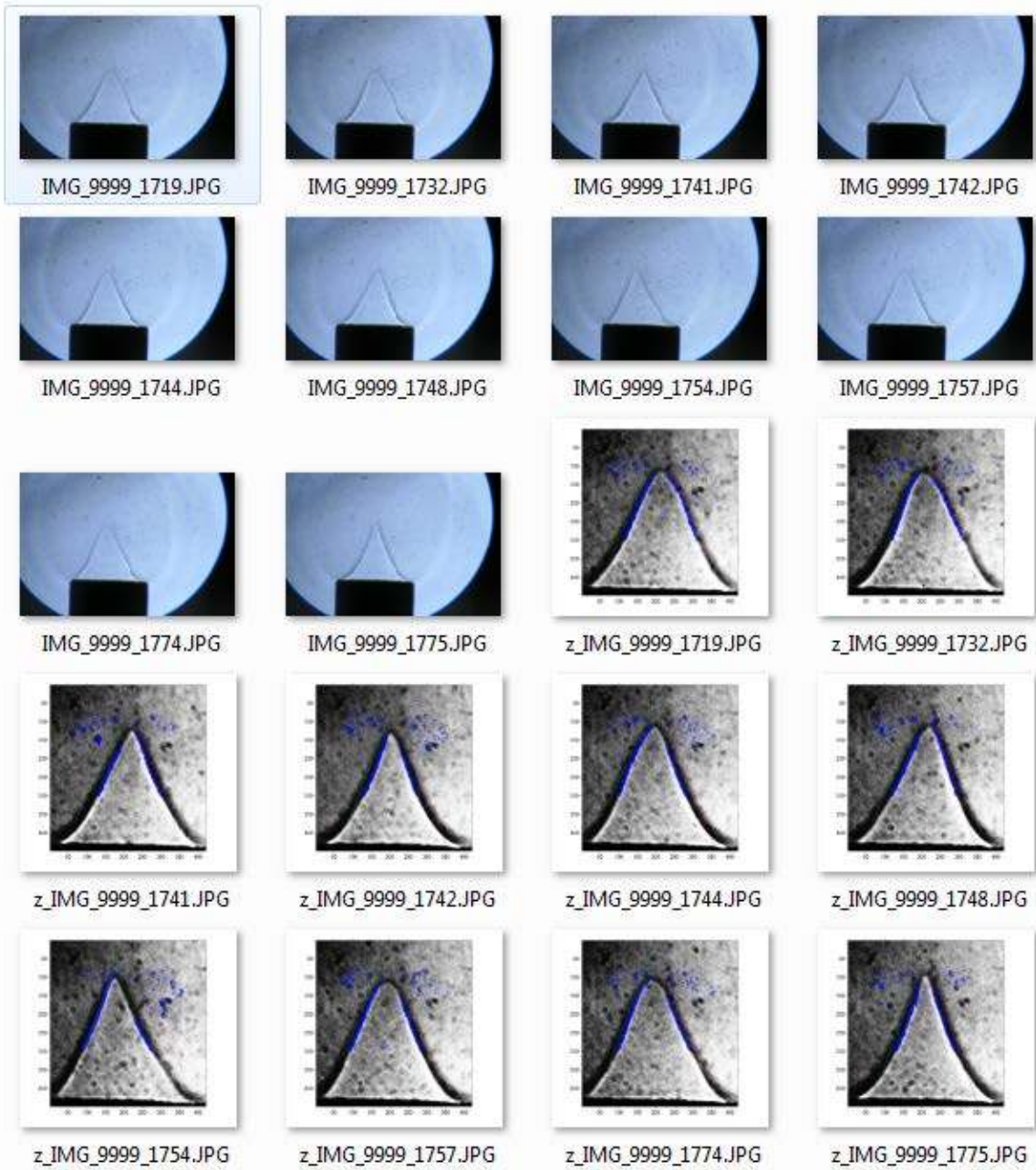
z_IMG_9999_1221.JPG

Experiment NO. 3.

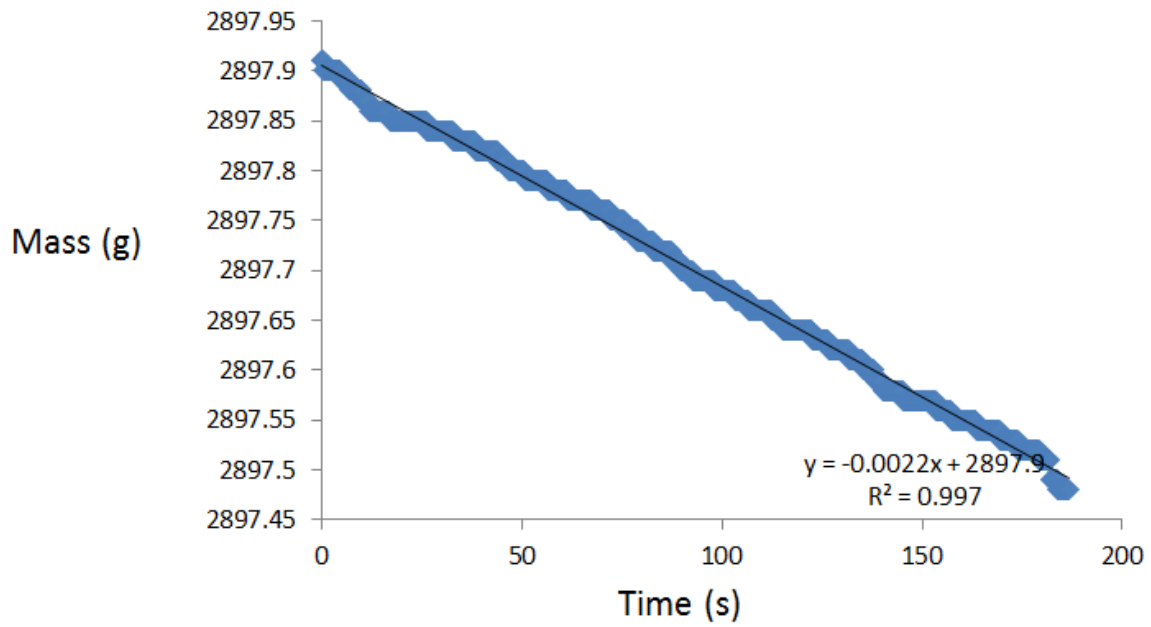


Air Flow Rate		Fuel Flow rate		Volume flow rate	nozzle width	U	Phi
SLPM	mole/sec	SLPM	mole/sec	m ³ /s	m	m/sec	
2.5	0.001732	0.223	0.000155	4.54E-05	0.010744	0.500255	0.849184

Entrainment Rate
0.0022 g/sec
Concentration
48.50752 g/m³



Experiment NO. 4.

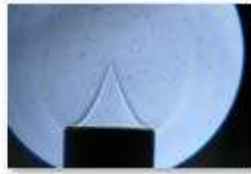


Air Flow Rate		Fuel Flow rate		Volume flow rate	nozzle width	U	Phi
SLPM	mole/sec	SLPM	mole/sec	m ³ /s	m	m/sec	
2.5	0.001732	0.223	0.000155	4.54E-05	0.010744	0.500255	0.849184

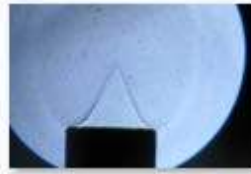
Entrainment Rate
0.0022 g/sec
Concentration
48.50752 g/m³



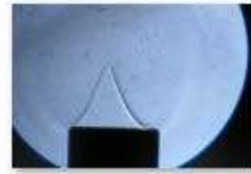
IMG_9999_1794.JPG



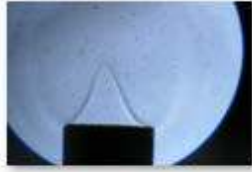
IMG_9999_1799.JPG



IMG_9999_1803.JPG



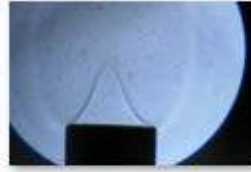
IMG_9999_1804.JPG



IMG_9999_1815.JPG



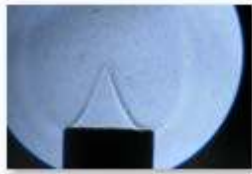
IMG_9999_1817.JPG



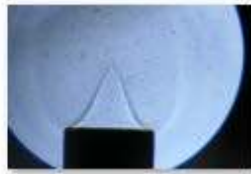
IMG_9999_1826.JPG



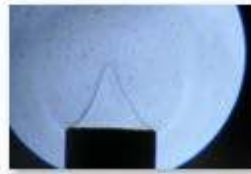
IMG_9999_1827.JPG



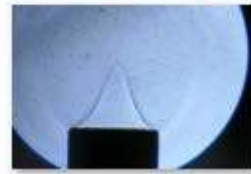
IMG_9999_1848.JPG



IMG_9999_1866.JPG



IMG_9999_1874.JPG



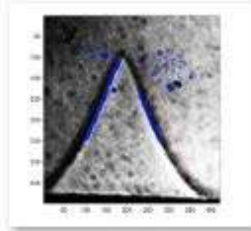
IMG_9999_1876.JPG



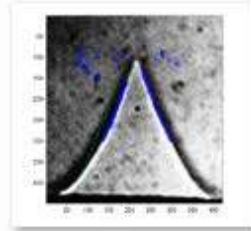
IMG_9999_1878.JPG



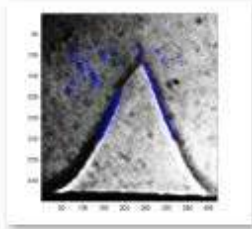
IMG_9999_1881.JPG



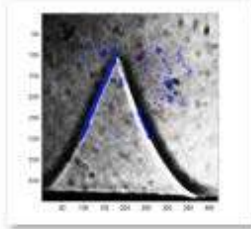
z_IMG_9999_1794.JPG



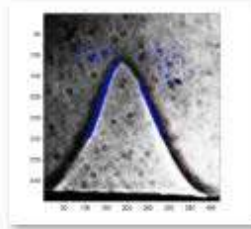
z_IMG_9999_1799.JPG



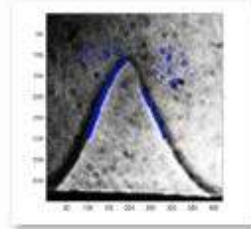
z_IMG_9999_1803.JPG



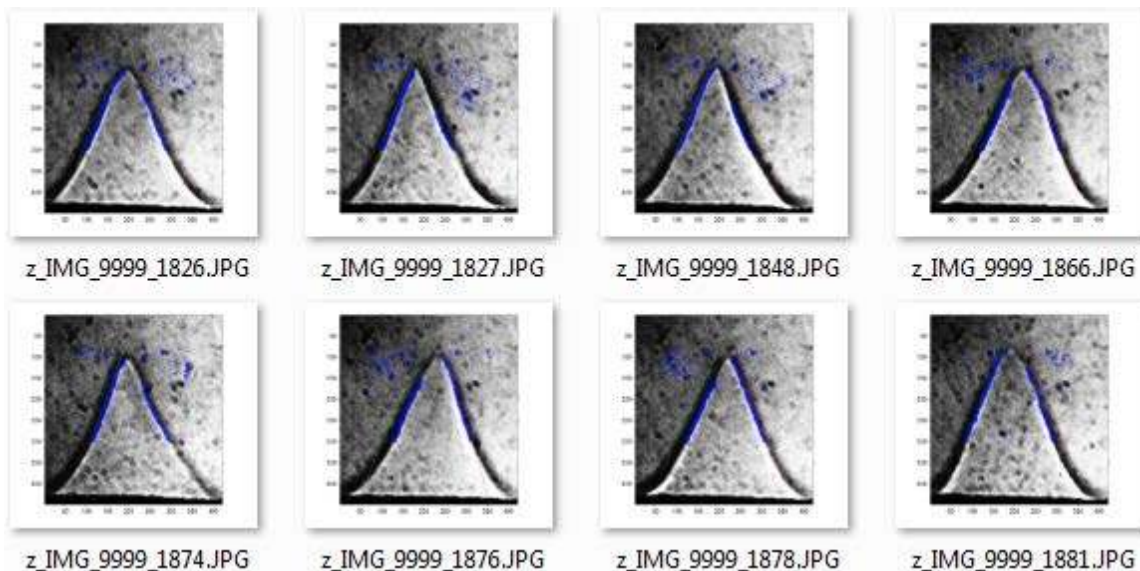
z_IMG_9999_1804.JPG



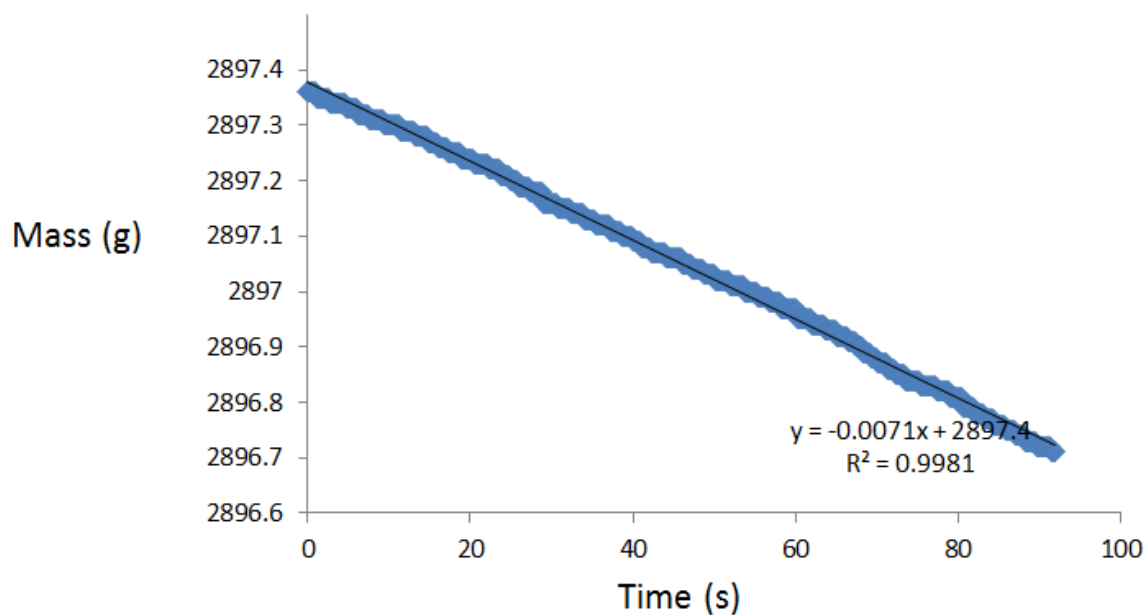
z_IMG_9999_1815.JPG



z_IMG_9999_1817.JPG



Experiment NO. 5.



Air Flow Rate		Fuel Flow rate		Volume flow rate	nozzle width	U	Phi
SLPM	mole/sec	SLPM	mole/sec	m ³ /s	m	m/sec	
2.5	0.001732	0.223	0.000155	4.54E-05	0.010744	0.500255	0.849184

Entrainment Rate

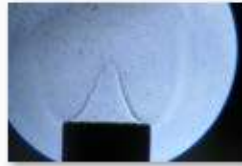
0.0071 g/sec

Concentration

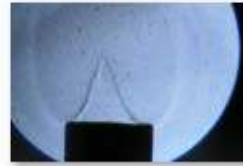
156.547 g/m³



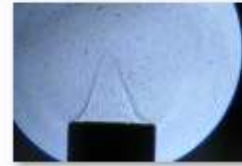
IMG_9999_1885.JPG



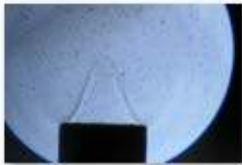
IMG_9999_1886.JPG



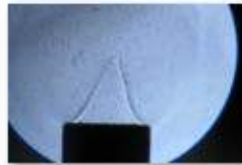
IMG_9999_1891.JPG



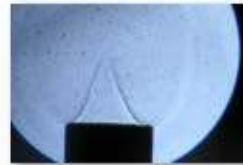
IMG_9999_1902.JPG



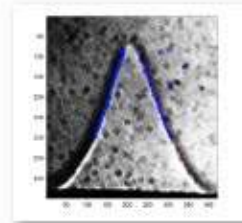
IMG_9999_1905.JPG



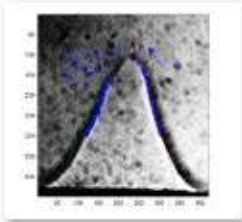
IMG_9999_1908.JPG



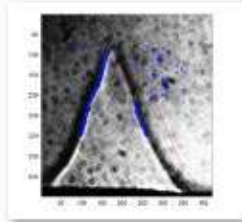
IMG_9999_1916.JPG



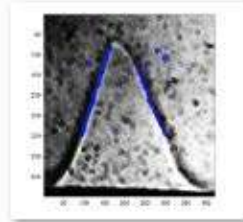
z_IMG_9999_1885.JPG



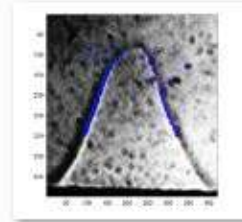
z_IMG_9999_1886.JPG



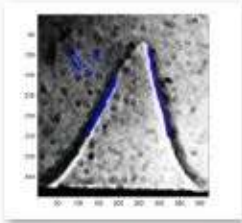
z_IMG_9999_1891.JPG



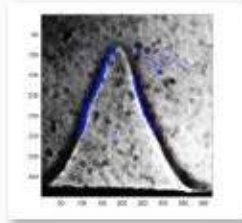
z_IMG_9999_1902.JPG



z_IMG_9999_1905.JPG



z_IMG_9999_1908.JPG

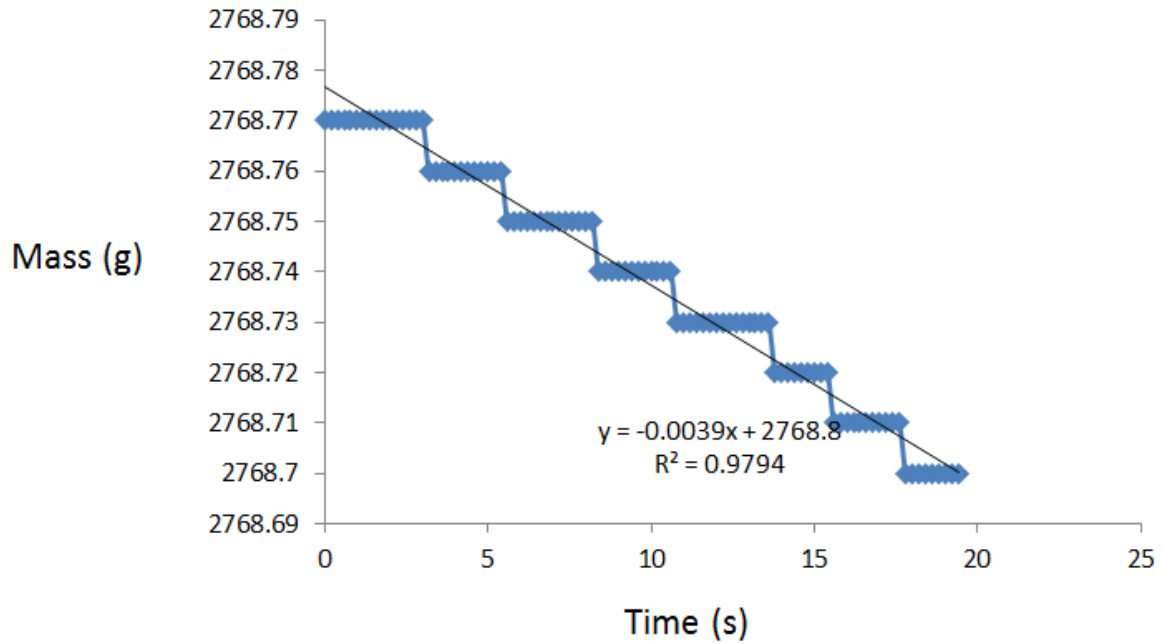


z_IMG_9999_1916.JPG

3. Coal Particles (75-90 μm)

3.1 $\phi=0.75$; Flow Rate: Air 2.0 SLPM; Methane 0.158 SLPM

Experiment NO. 1.



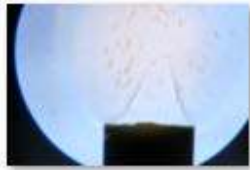
Air Flow Rate		Fuel Flow rate		Volume flow rate	nozzle width	U	Phi
SLPM	mole/sec	SLPM	mole/sec	m ³ /s	m	m/sec	
2	0.001386	0.158	0.000109	3.59E-05	0.010744	0.39646	0.75208

Entrainment Rate

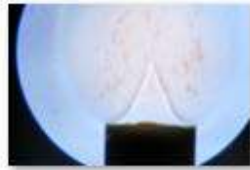
0.0039 g/sec

Concentration

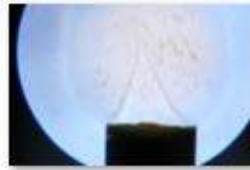
108.5034 g/m³



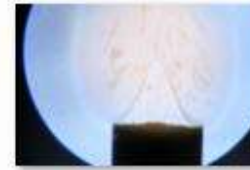
IMG_9999_206.JPG



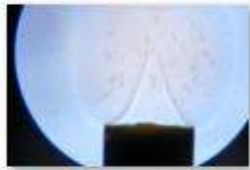
IMG_9999_207.JPG



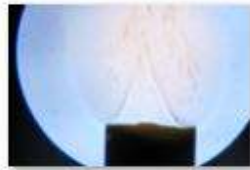
IMG_9999_208.JPG



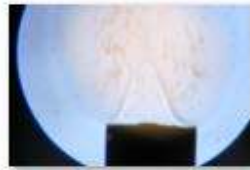
IMG_9999_209.JPG



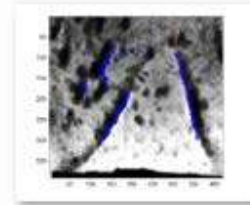
IMG_9999_210.JPG



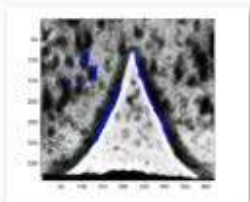
IMG_9999_211.JPG



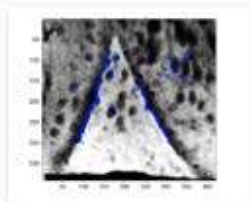
IMG_9999_215.JPG



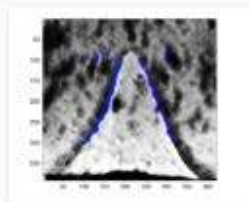
z_IMG_9999_206.JPG



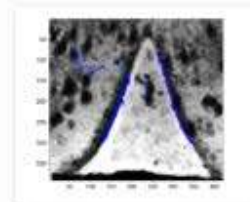
z_IMG_9999_207.JPG



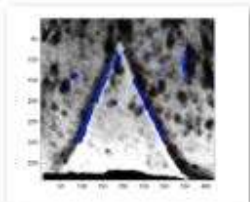
z_IMG_9999_208.JPG



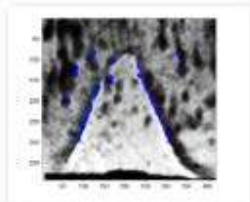
z_IMG_9999_209.JPG



z_IMG_9999_210.JPG

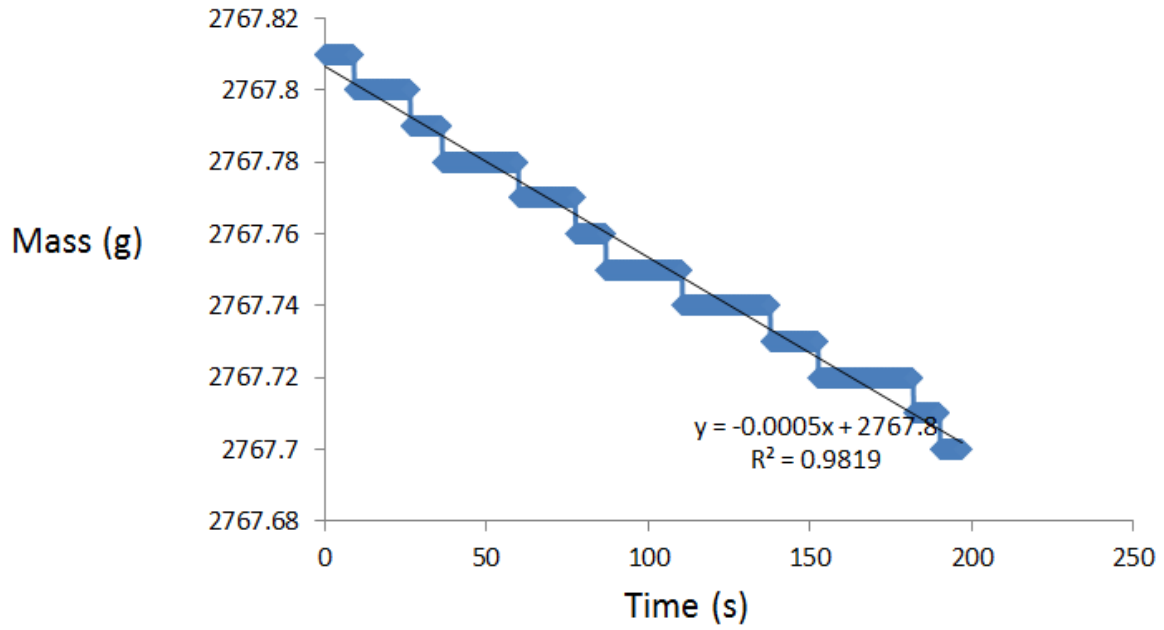


z_IMG_9999_211.JPG



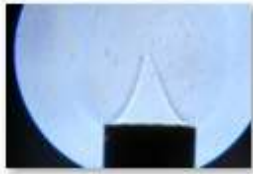
z_IMG_9999_215.JPG

Experiment NO. 2

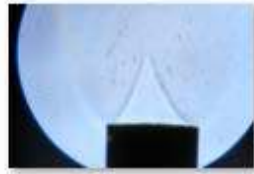


Air Flow Rate		Fuel Flow rate		Volume flow rate	nozzle width	U	Phi
SLPM	mole/sec	SLPM	mole/sec	m ³ /s	m	m/sec	
2.5	0.001732	0.21	0.000145	4.51E-05	0.010744	0.497869	0.79968

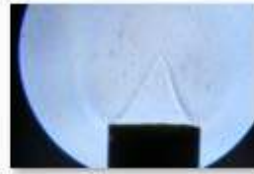
Entrainment Rate
 0.0005 g/sec
 Concentration
 11.07727 g/m³



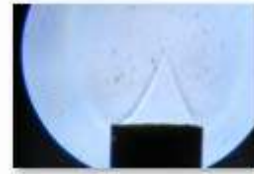
IMG_9999_218.JPG



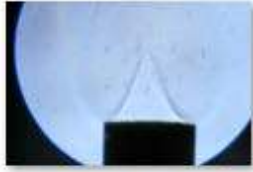
IMG_9999_220.JPG



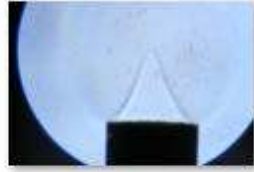
IMG_9999_221.JPG



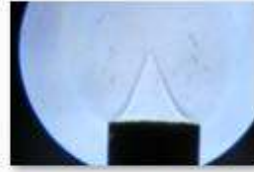
IMG_9999_226.JPG



IMG_9999_229.JPG



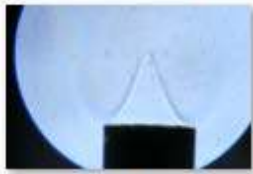
IMG_9999_230.JPG



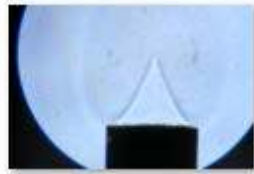
IMG_9999_232.JPG



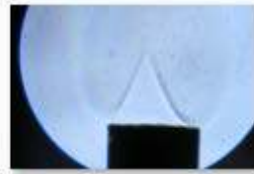
IMG_9999_272.JPG



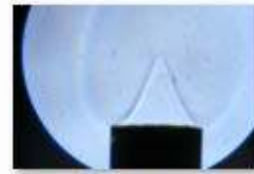
IMG_9999_274.JPG



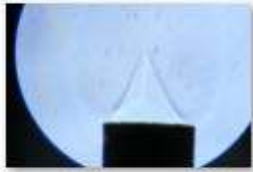
IMG_9999_281.JPG



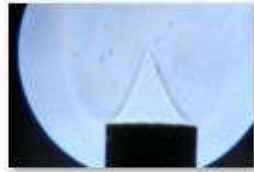
IMG_9999_285.JPG



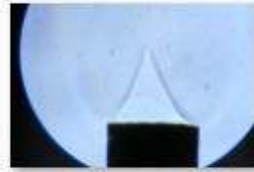
IMG_9999_288.JPG



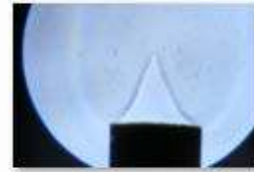
IMG_9999_321.JPG



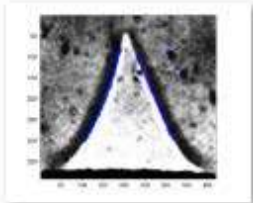
IMG_9999_327.JPG



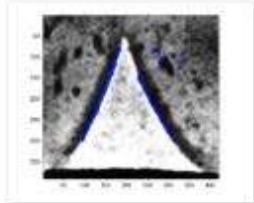
IMG_9999_328.JPG



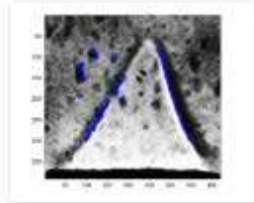
IMG_9999_329.JPG



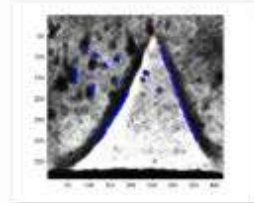
z_IMG_9999_218.JPG



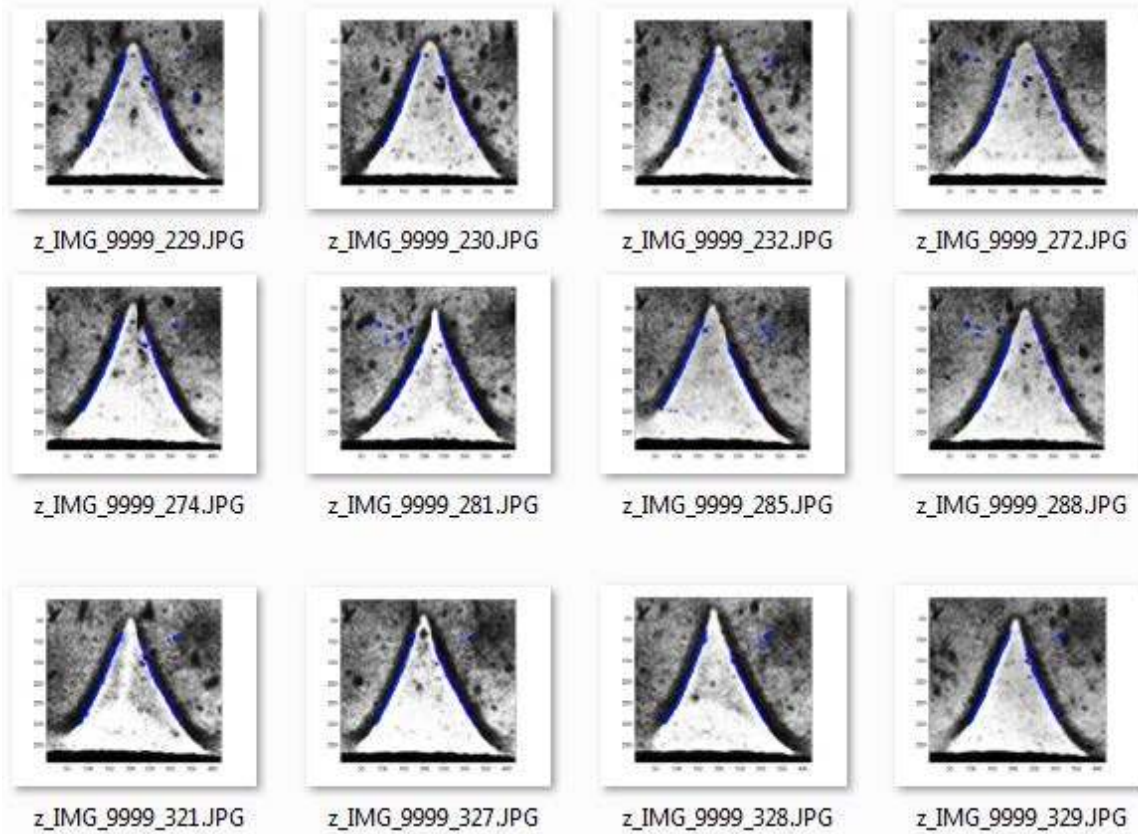
z_IMG_9999_220.JPG



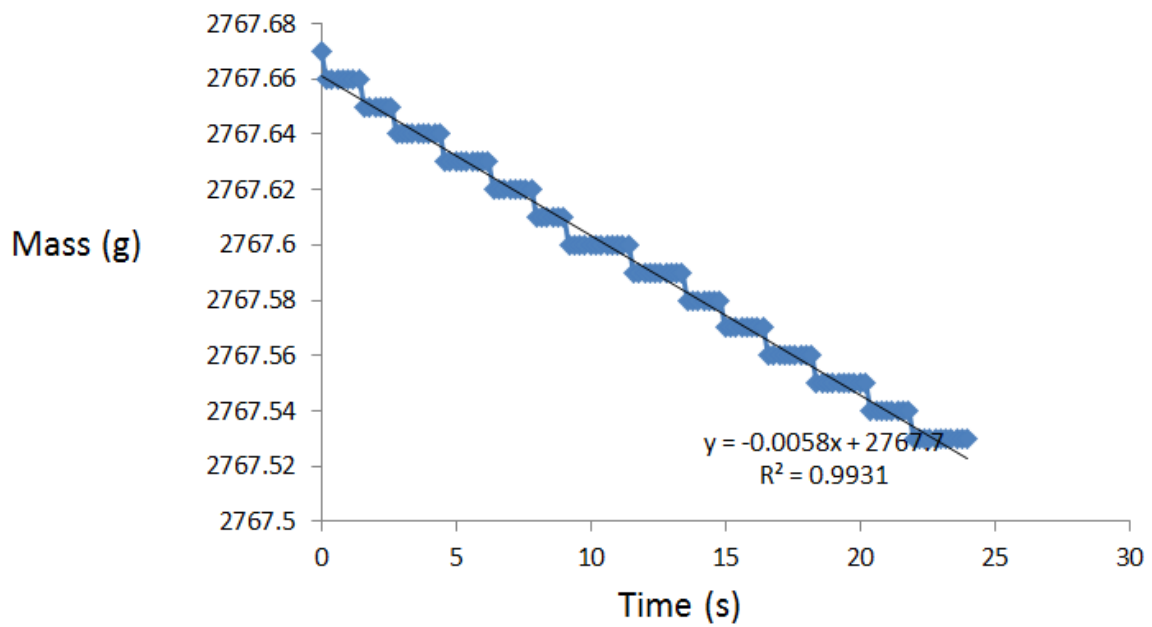
z_IMG_9999_221.JPG



z_IMG_9999_226.JPG

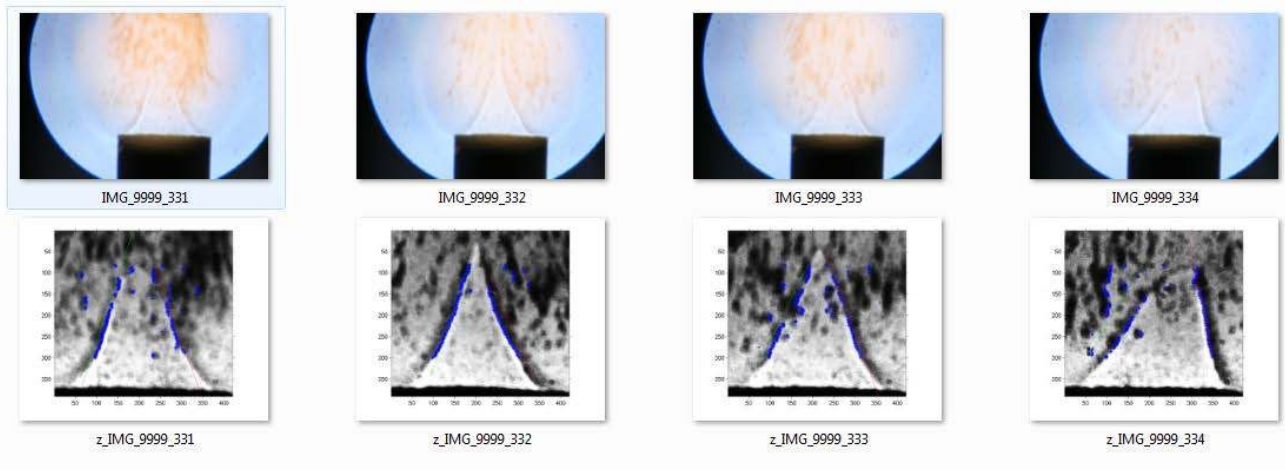


Experiment NO. 3

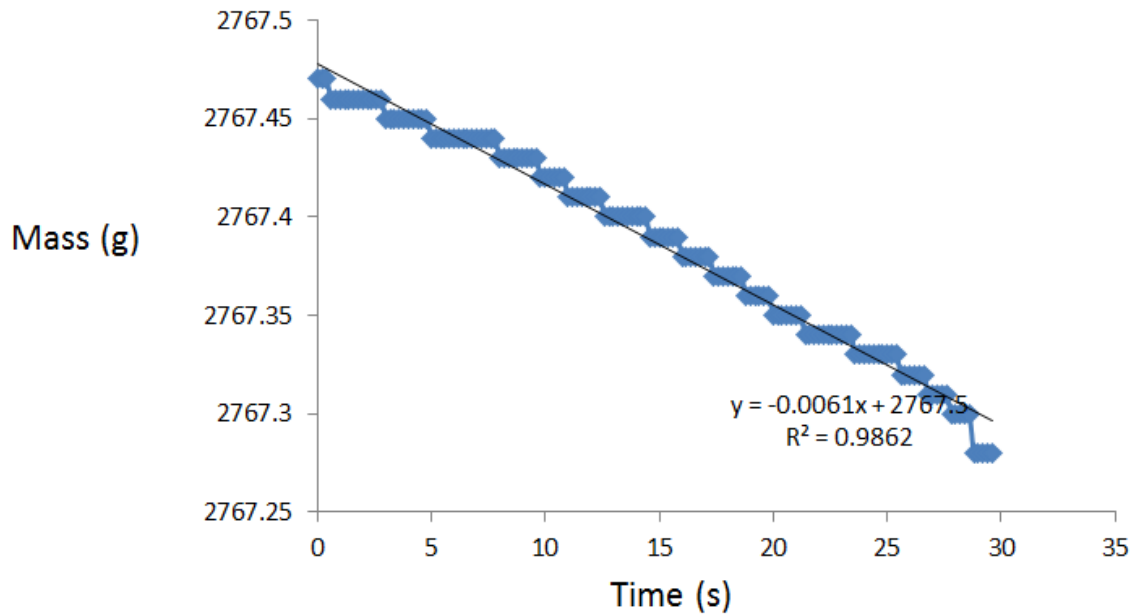


Air Flow Rate		Fuel Flow rate		Volume flow rate	nozzle width	U	Phi
SLPM	mole/sec	SLPM	mole/sec	m3/s	m	m/sec	
2	0.001386	0.158	0.000109	3.59E-05	0.010744	0.39646	0.75208

Entrainment Rate
0.0058 g/sec
Concentration
161.3641 g/m³

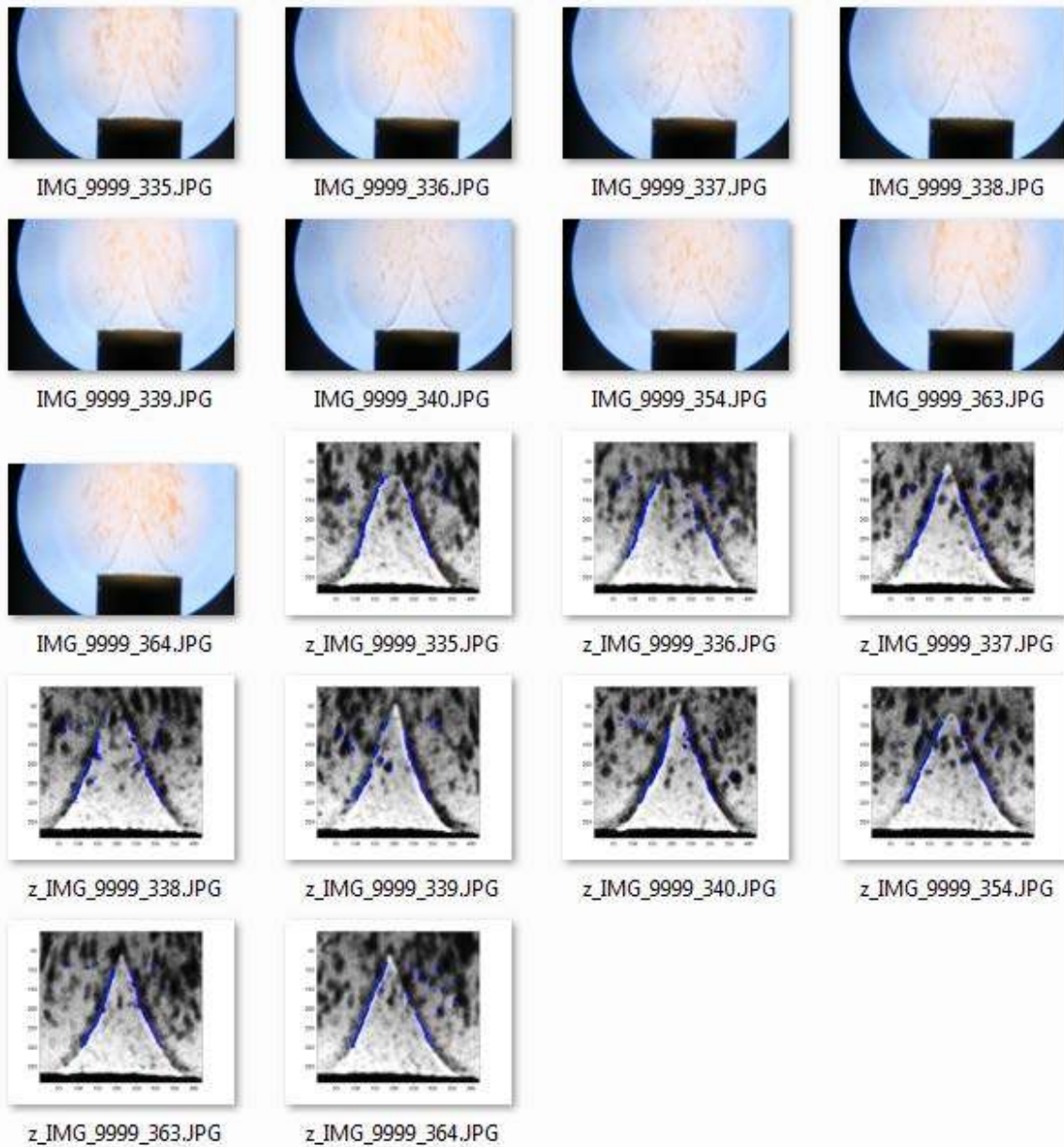


Experiment NO. 4.

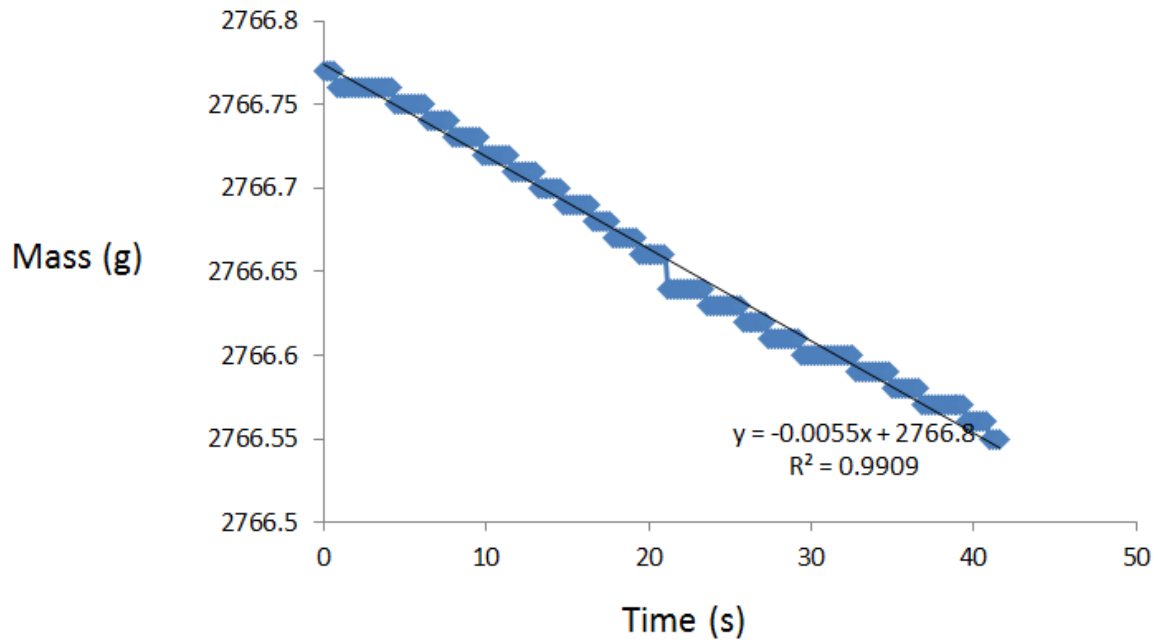


Air Flow Rate		Fuel Flow rate		Volume flow rate	nozzle width	U	Phi
SLPM	mole/sec	SLPM	mole/sec	m3/s	m	m/sec	
2	0.001386	0.158	0.000109	3.59E-05	0.010744	0.39646	0.75208

Entrainment Rate
0.0061 g/sec
Concentration
169.7105 g/m³

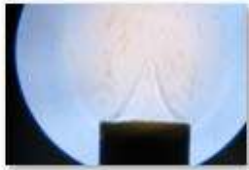


Experiment NO. 5

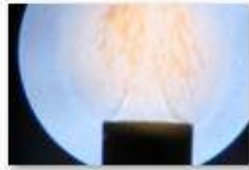


Air Flow Rate		Fuel Flow rate		Volume flow rate	nozzle width	U	Phi
SLPM	mole/sec	SLPM	mole/sec	m ³ /s	m	m/sec	
2	0.001386	0.158	0.000109	3.59E-05	0.010744	0.39646	0.75208

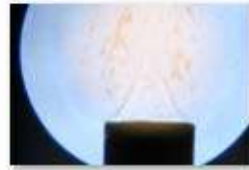
Entrainment Rate
0.0055 g/sec
Concentration
153.0177 g/m³



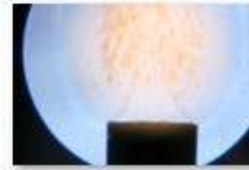
IMG_9999_373.JPG



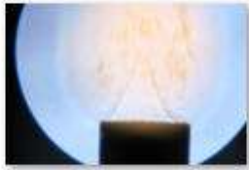
IMG_9999_375.JPG



IMG_9999_376.JPG



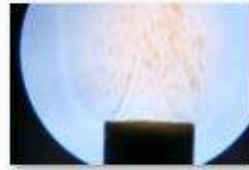
IMG_9999_378.JPG



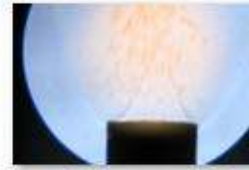
IMG_9999_380.JPG



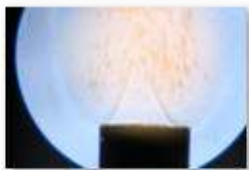
IMG_9999_383.JPG



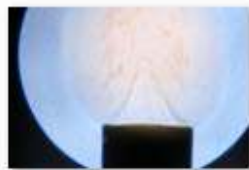
IMG_9999_384.JPG



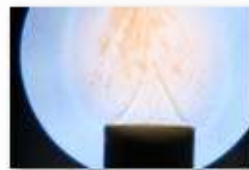
IMG_9999_385.JPG



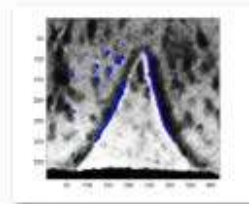
IMG_9999_386.JPG



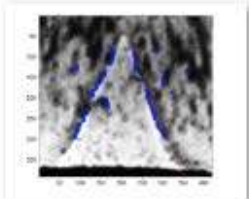
IMG_9999_393.JPG



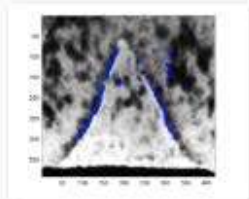
IMG_9999_394.JPG



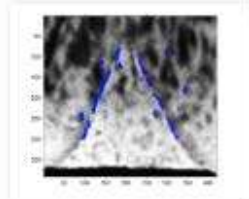
z_IMG_9999_373.JPG



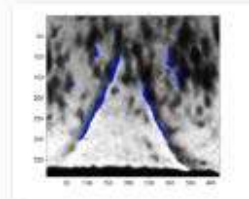
z_IMG_9999_375.JPG



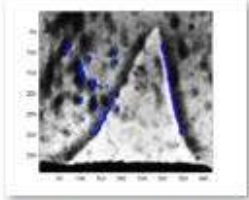
z_IMG_9999_376.JPG



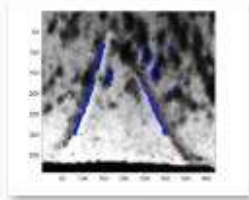
z_IMG_9999_378.JPG



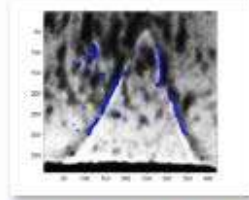
z_IMG_9999_380.JPG



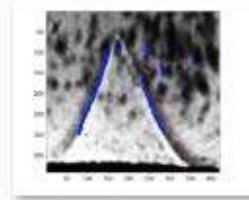
z_IMG_9999_383.JPG



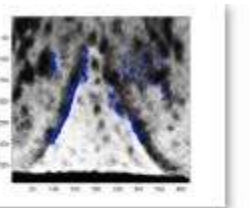
z_IMG_9999_384.JPG



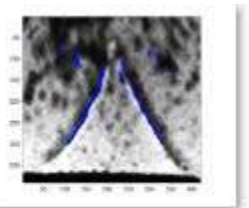
z_IMG_9999_385.JPG



z_IMG_9999_386.JPG

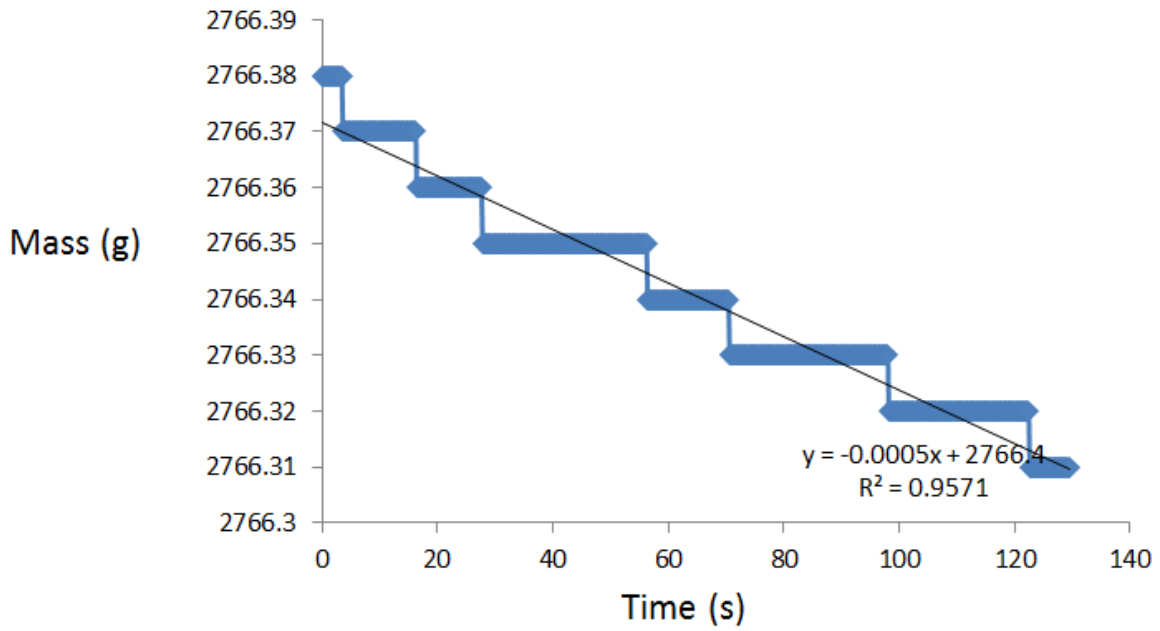


z_IMG_9999_393.JPG



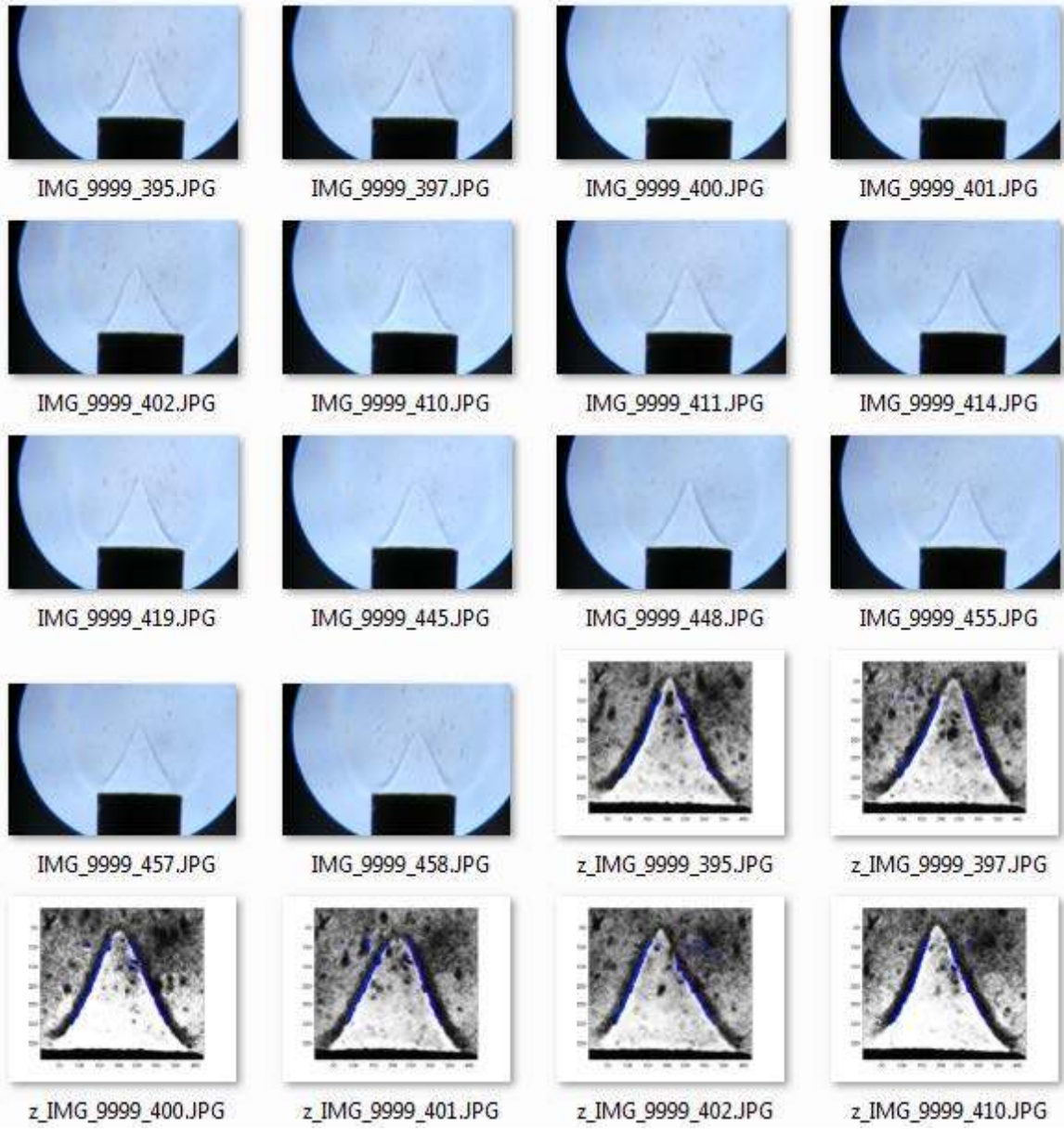
z_IMG_9999_394.JPG

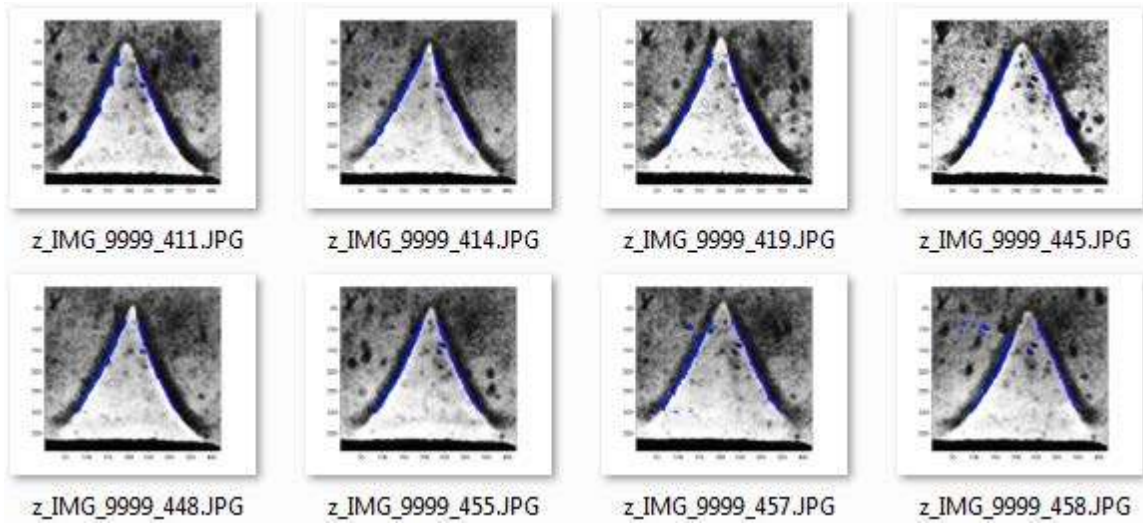
Experiment NO. 6



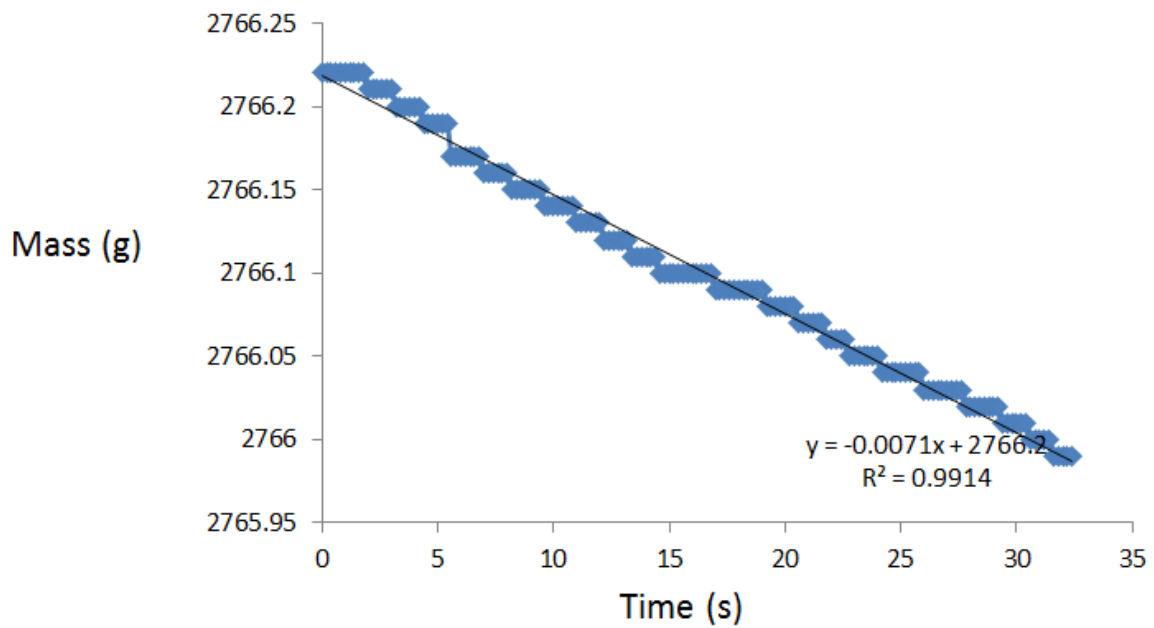
Air Flow Rate		Fuel Flow rate		Volume flow rate	nozzle width	U	Phi
SLPM	mole/sec	SLPM	mole/sec	m ³ /s	m	m/sec	
2	0.001386	0.158	0.000109	3.59E-05	0.010744	0.39646	0.75208

Entrainment Rate
 0.0005 g/sec
 Concentration
 13.9107 g/m³



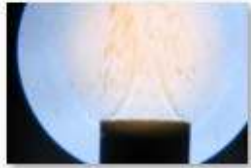


Experiment NO. 7

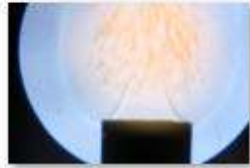


Air Flow Rate		Fuel Flow rate		Volume flow rate	nozzle width	U	Phi
SLPM	mole/sec	SLPM	mole/sec	m ³ /s	m	m/sec	
2	0.001386	0.158	0.000109	3.59E-05	0.010744	0.39646	0.75208

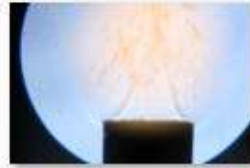
Entrainment Rate
0.0071 g/sec
Concentration
197.5319 g/m³



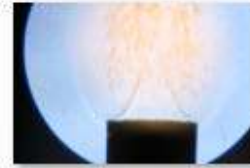
IMG_9999_460.JPG



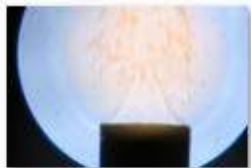
IMG_9999_461.JPG



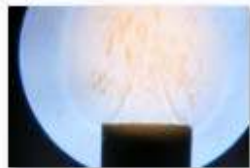
IMG_9999_462.JPG



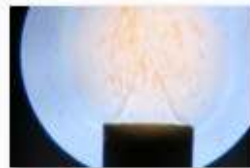
IMG_9999_463.JPG



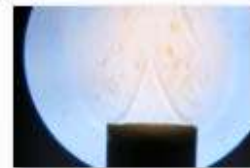
IMG_9999_464.JPG



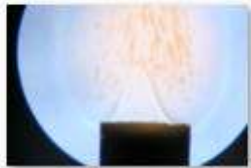
IMG_9999_465.JPG



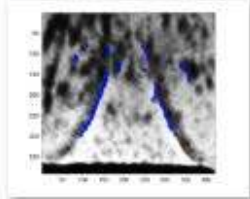
IMG_9999_467.JPG



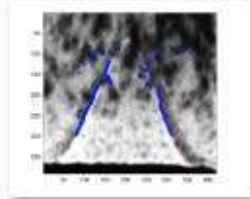
IMG_9999_468.JPG



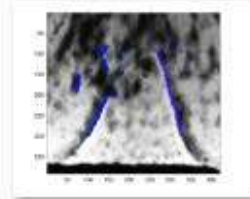
IMG_9999_469.JPG



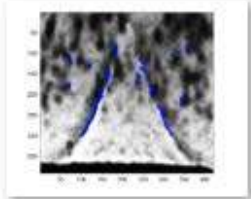
z_IMG_9999_460.JPG



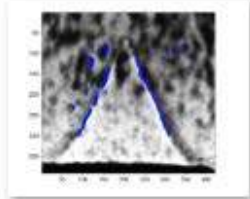
z_IMG_9999_461.JPG



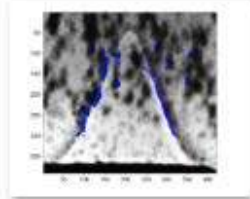
z_IMG_9999_462.JPG



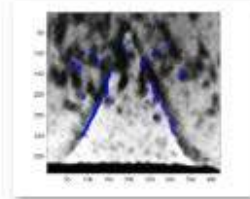
z_IMG_9999_463.JPG



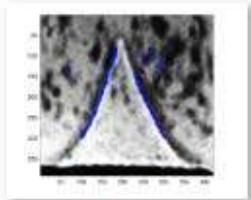
z_IMG_9999_464.JPG



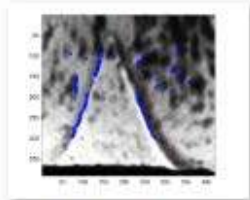
z_IMG_9999_465.JPG



z_IMG_9999_467.JPG

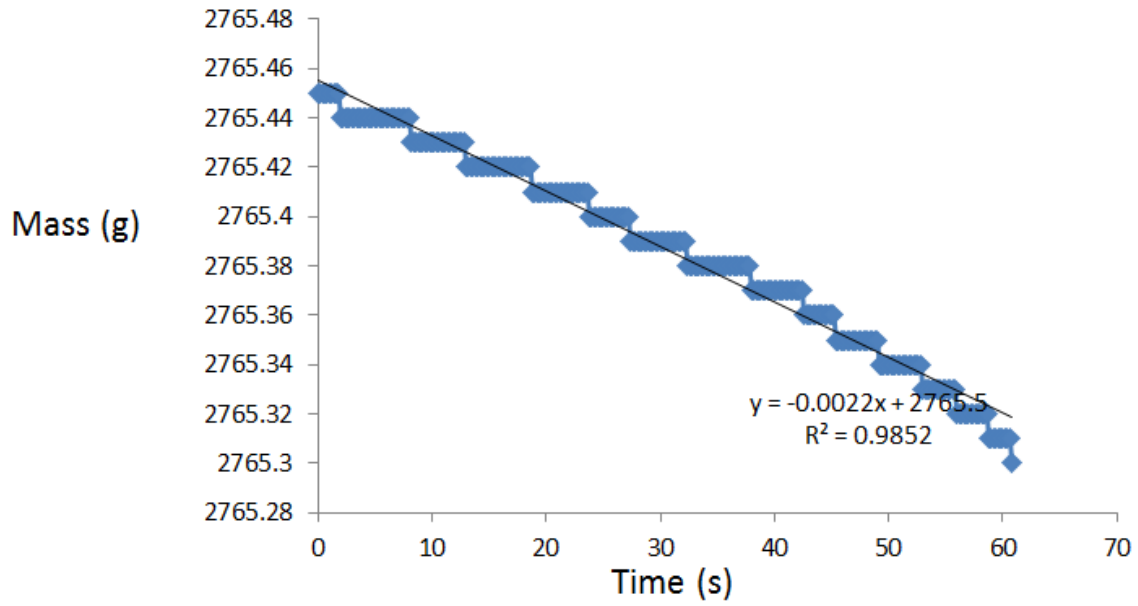


z_IMG_9999_468.JPG



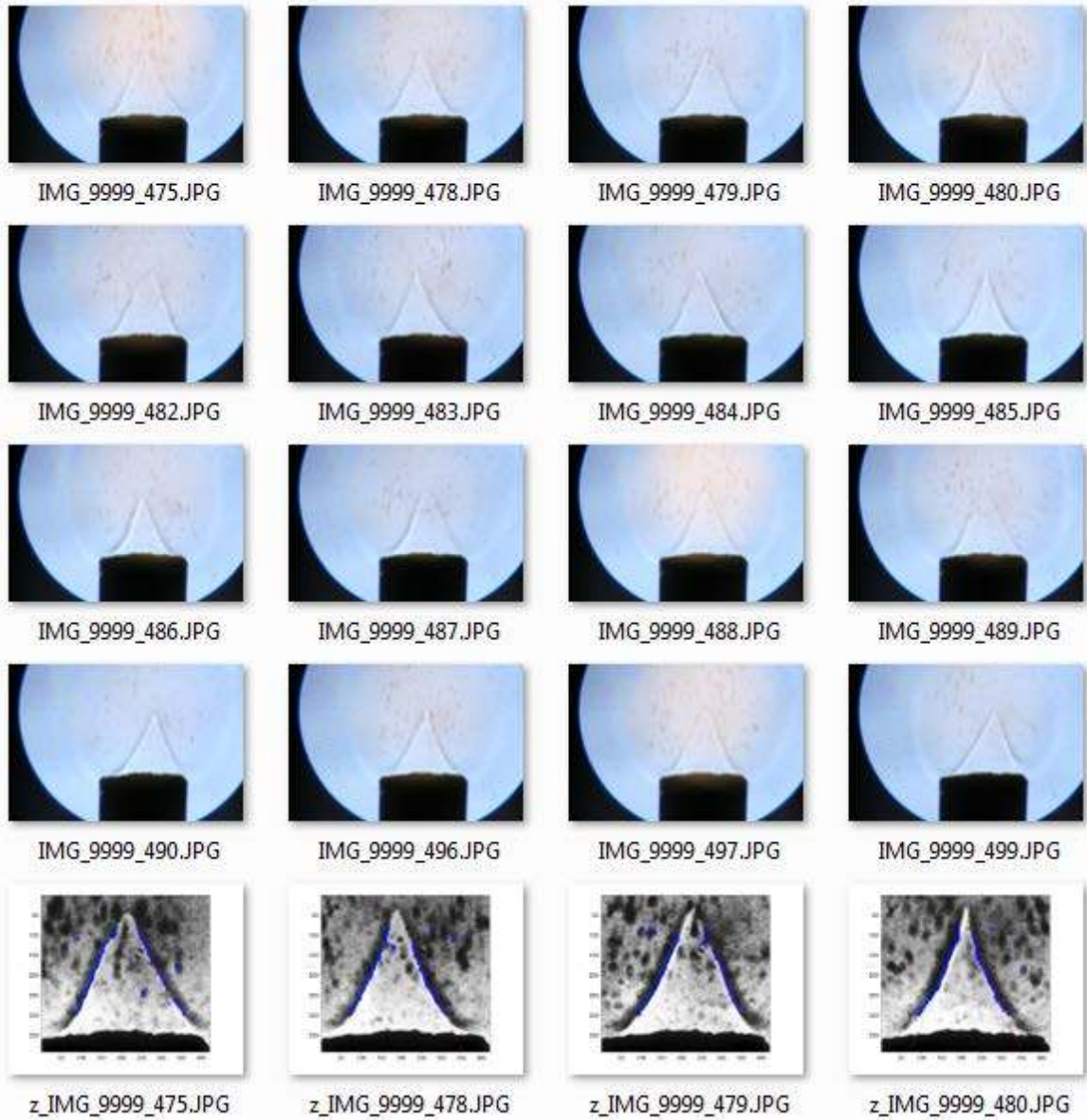
z_IMG_9999_469.JPG

Experiment NO. 8

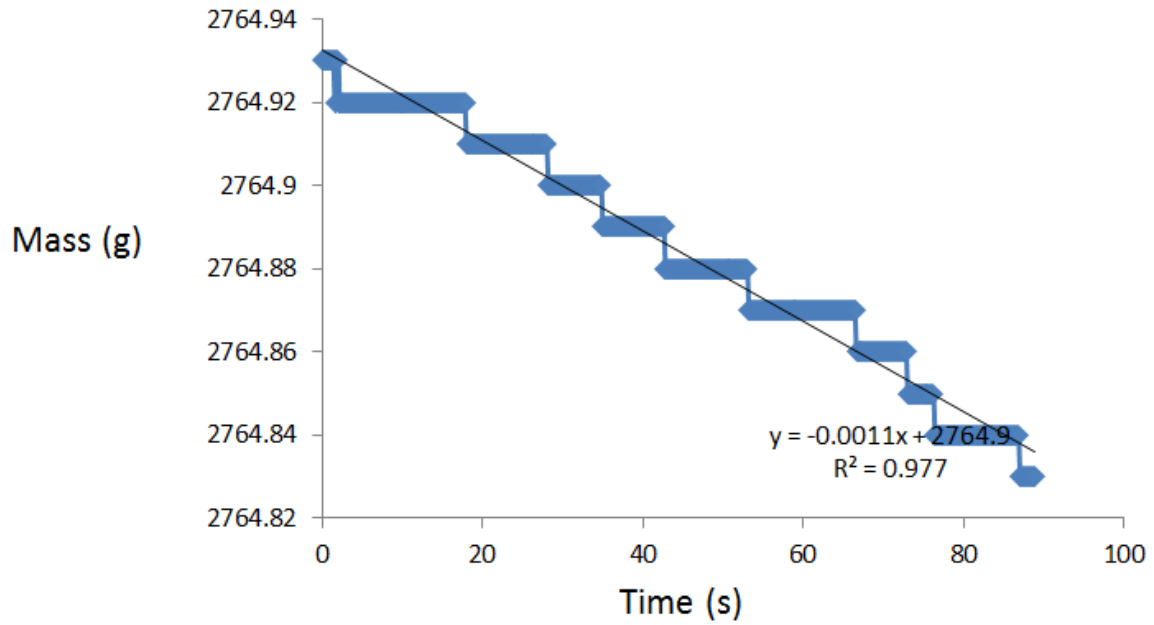


Air Flow Rate		Fuel Flow rate		Volume flow rate	nozzle width	U	Phi
SLPM	mole/sec	SLPM	mole/sec	m ³ /s	m	m/sec	
2	0.001386	0.158	0.000109	3.59E-05	0.010744	0.39646	0.75208

Entrainment Rate
0.0022 g/sec
Concentration
61.20707 g/m³

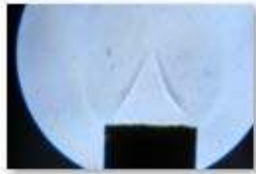


9.

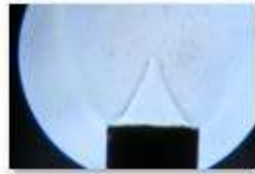


Air Flow Rate		Fuel Flow rate		Volume flow rate	nozzle width	U	Phi
SLPM	mole/sec	SLPM	mole/sec	m ³ /s	m	m/sec	
2	0.001386	0.158	0.000109	3.59E-05	0.010744	0.39646	0.75208

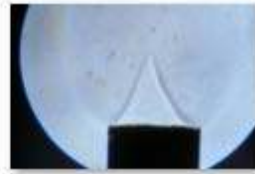
Entrainment Rate
0.0011 g/sec
Concentration
30.60353 g/m³



IMG_9999_517.JPG



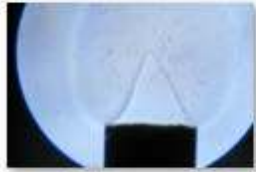
IMG_9999_518.JPG



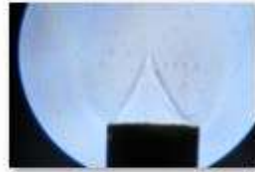
IMG_9999_519.JPG



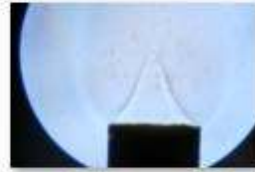
IMG_9999_520.JPG



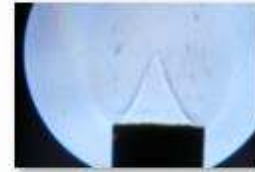
IMG_9999_521.JPG



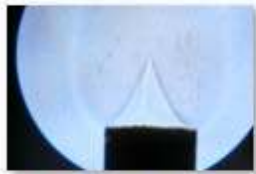
IMG_9999_524.JPG



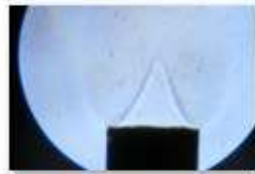
IMG_9999_533.JPG



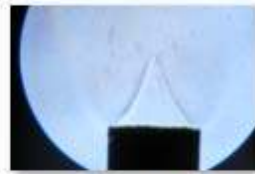
IMG_9999_537.JPG



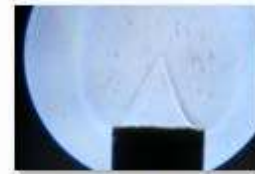
IMG_9999_588.JPG



IMG_9999_589.JPG



IMG_9999_590.JPG



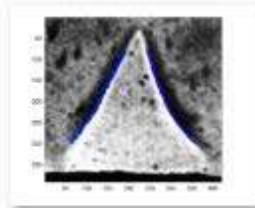
IMG_9999_591.JPG



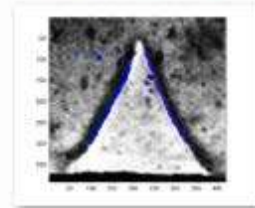
IMG_9999_594.JPG



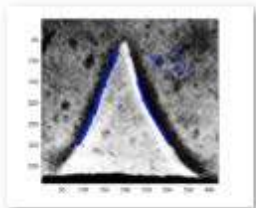
IMG_9999_598.JPG



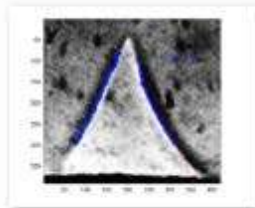
z_IMG_9999_517.JPG



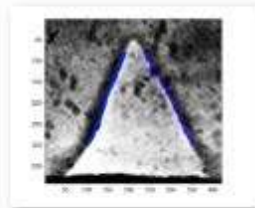
z_IMG_9999_518.JPG



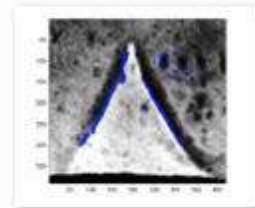
z_IMG_9999_519.JPG



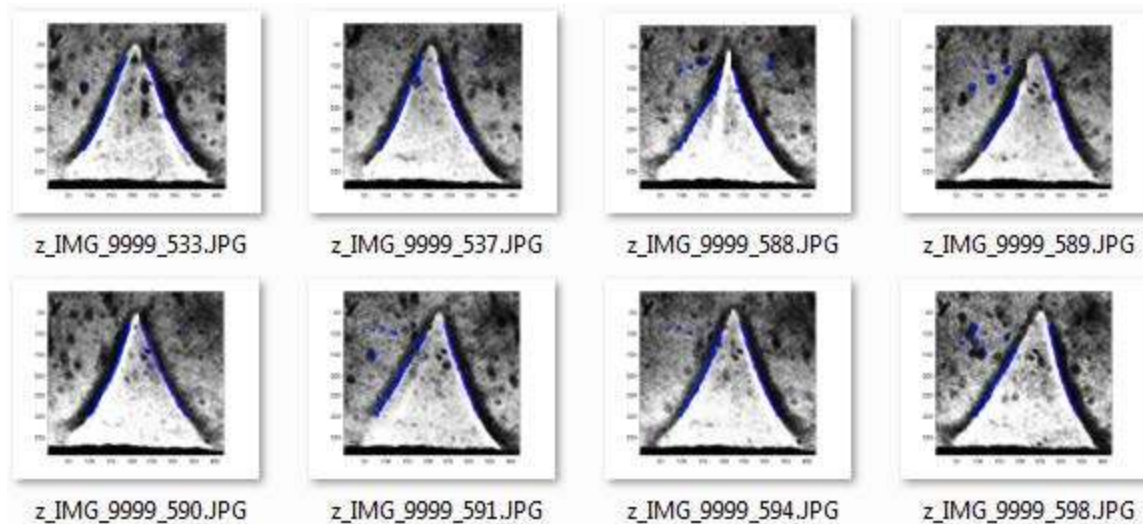
z_IMG_9999_520.JPG



z_IMG_9999_521.JPG

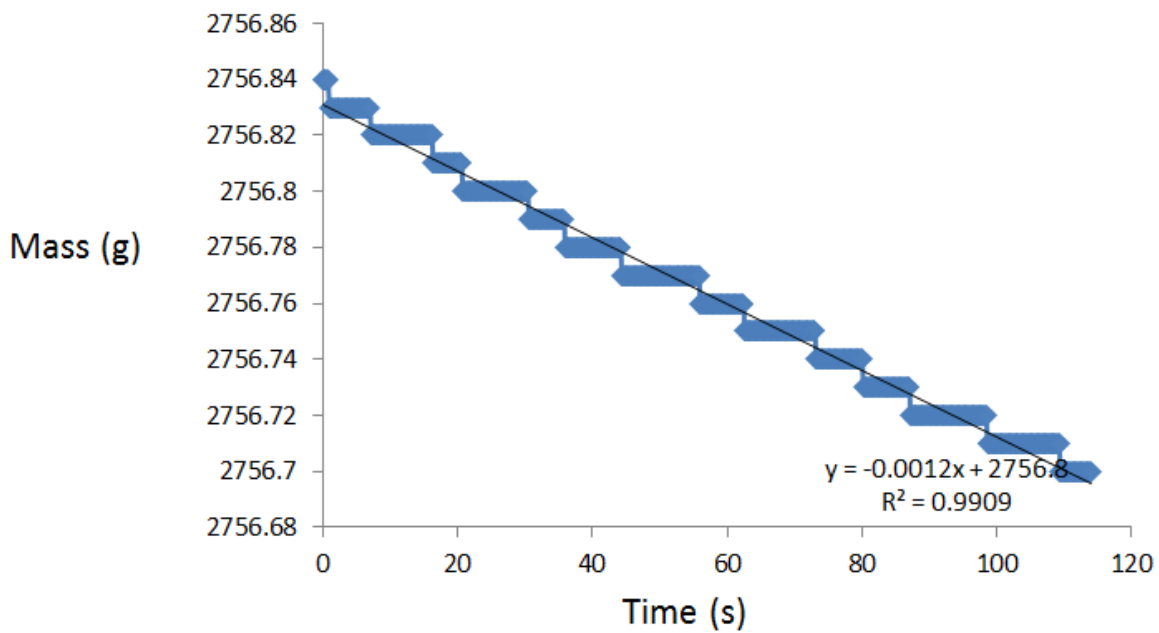


z_IMG_9999_524.JPG



3.2 $\phi=0.80$; Flow Rate: Air 2.5 SLPM; Methane 0.21 SLPM

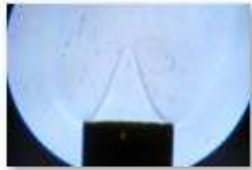
Experiment NO. 1



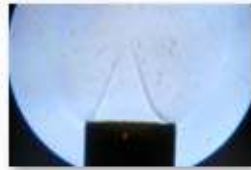
Air Flow Rate		Fuel Flow rate		Volume flow rate	nozzle width	U
SLPM	mole/sec	SLPM	mole/sec	m ³ /s	m	m/sec
2.5	0.001732	0.21	0.000145	4.51E-05	0.010744	0.497869

Entrainment Rate
0.0012 g/sec
Concentration
26.58546 g/m³

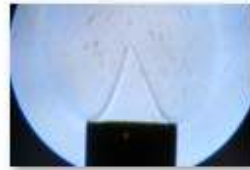




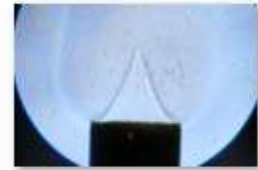
IMG_9999_1041.JPG



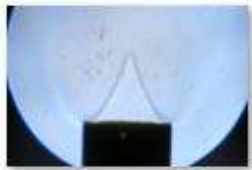
IMG_9999_1042.JPG



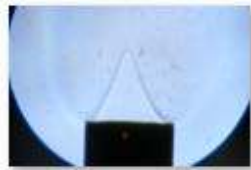
IMG_9999_1043.JPG



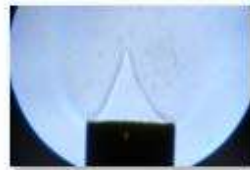
IMG_9999_1045.JPG



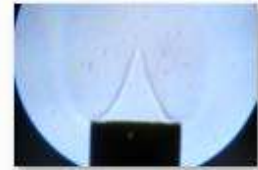
IMG_9999_1046.JPG



IMG_9999_1047.JPG



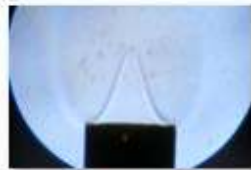
IMG_9999_1048.JPG



IMG_9999_1049.JPG



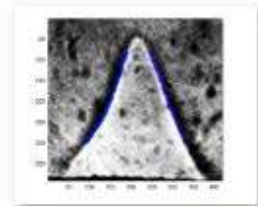
IMG_9999_1050.JPG



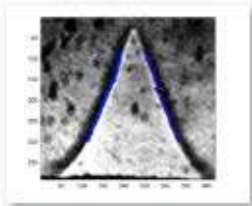
IMG_9999_1052.JPG



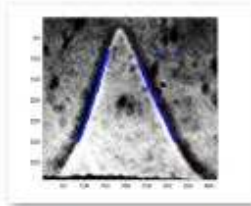
IMG_9999_1053.JPG



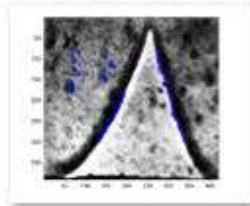
z_IMG_9999_999.JPG



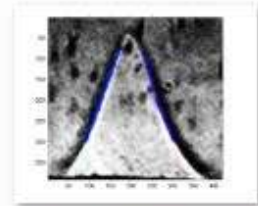
z_IMG_9999_1001.JPG



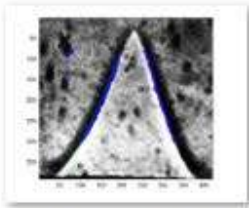
z_IMG_9999_1002.JPG



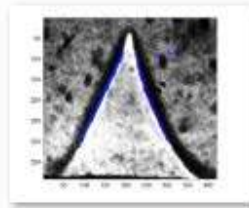
z_IMG_9999_1003.JPG



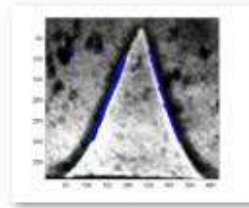
z_IMG_9999_1005.JPG



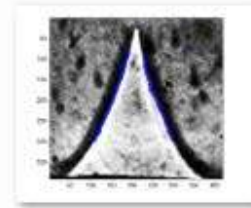
z_IMG_9999_1027.JPG



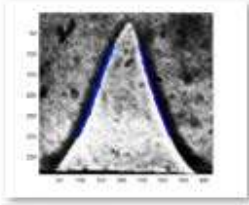
z_IMG_9999_1028.JPG



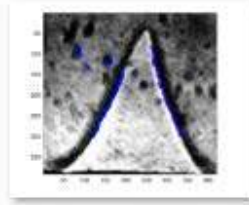
z_IMG_9999_1029.JPG



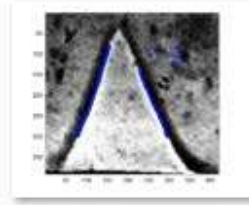
z_IMG_9999_1033.JPG



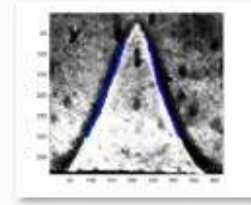
z_IMG_9999_1036.JPG



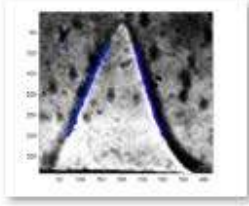
z_IMG_9999_1037.JPG



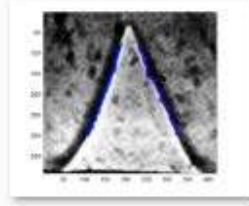
z_IMG_9999_1039.JPG



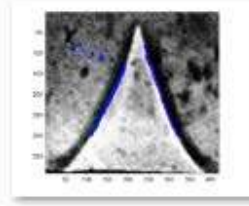
z_IMG_9999_1041.JPG



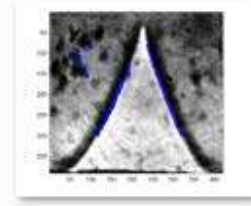
z_IMG_9999_1042.JPG



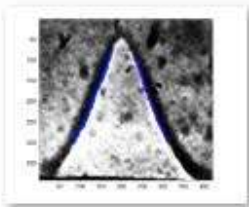
z_IMG_9999_1043.JPG



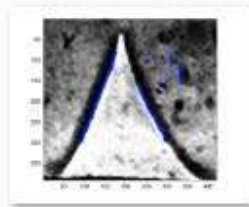
z_IMG_9999_1045.JPG



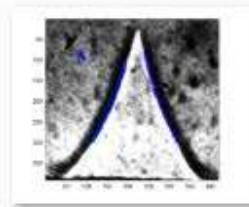
z_IMG_9999_1046.JPG



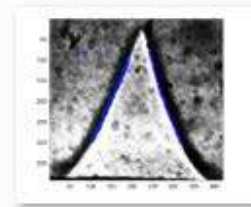
z_IMG_9999_1047.JPG



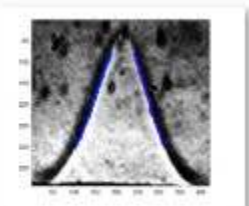
z_IMG_9999_1048.JPG



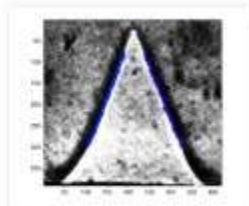
z_IMG_9999_1049.JPG



z_IMG_9999_1050.JPG

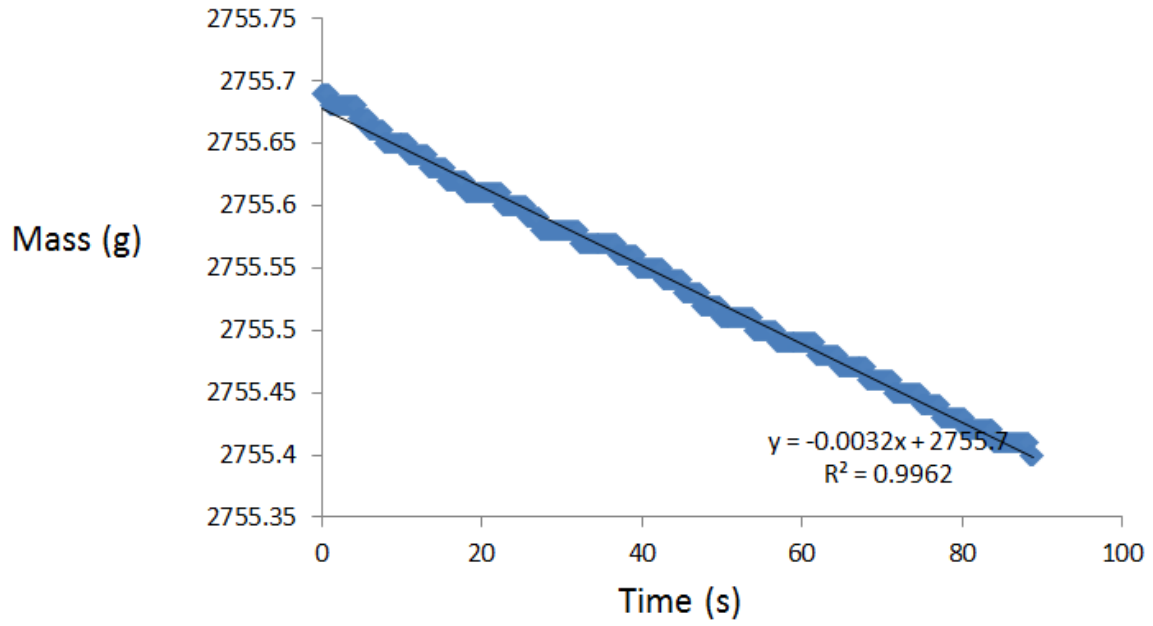


z_IMG_9999_1052.JPG



z_IMG_9999_1053.JPG

Experiment NO. 2

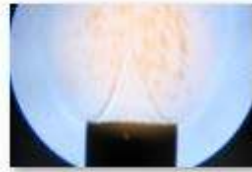


Air Flow Rate		Fuel Flow rate		Volume flow rate	nozzle width	U	Phi
SLPM	mole/sec	SLPM	mole/sec	m ³ /s	m	m/sec	
2.5	0.00173 2	0.21	0.00014 5	4.51E-05	0.010744	0.49786 9	0.7996 8

Entrainment Rate
 0.0032 g/sec
 Concentration
 70.89455 g/m³



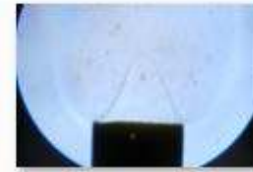
IMG_9999_1057.JPG



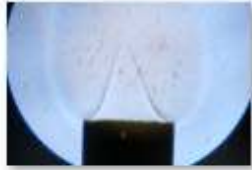
IMG_9999_1058.JPG



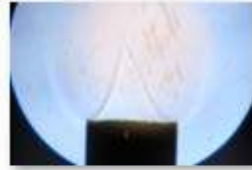
IMG_9999_1059.JPG



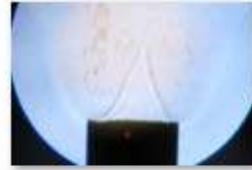
IMG_9999_1060.JPG



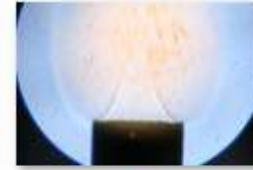
IMG_9999_1061.JPG



IMG_9999_1062.JPG



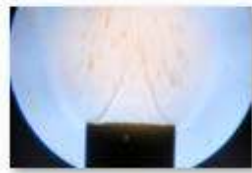
IMG_9999_1063.JPG



IMG_9999_1064.JPG



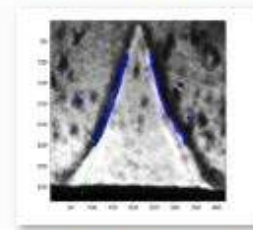
IMG_9999_1065.JPG



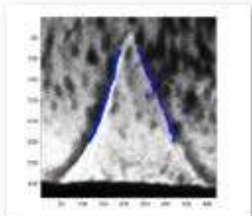
IMG_9999_1066.JPG



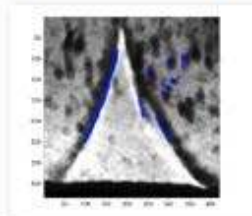
IMG_9999_1067.JPG



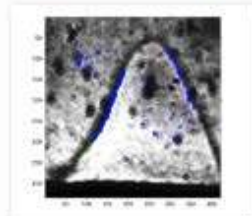
z_IMG_9999_1057.JPG



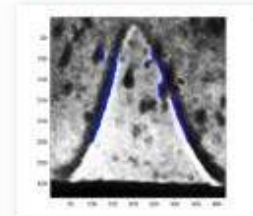
z_IMG_9999_1058.JPG



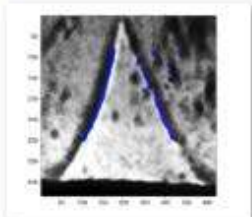
z_IMG_9999_1059.JPG



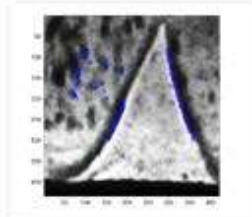
z_IMG_9999_1060.JPG



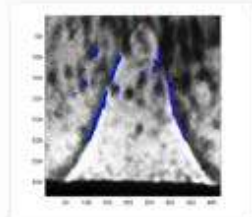
z_IMG_9999_1061.JPG



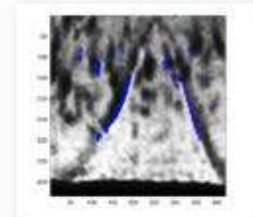
z_IMG_9999_1062.JPG



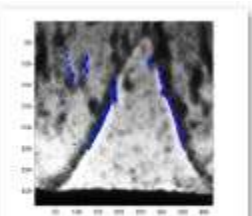
z_IMG_9999_1063.JPG



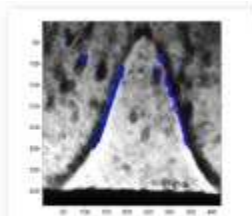
z_IMG_9999_1064.JPG



z_IMG_9999_1065.JPG

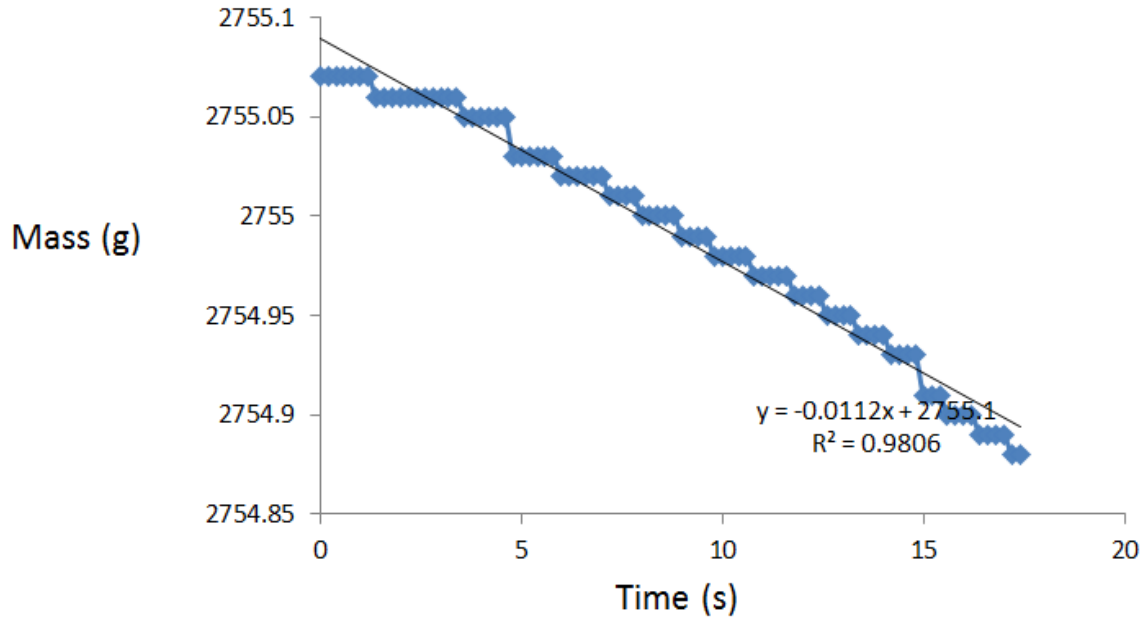


z_IMG_9999_1066.JPG



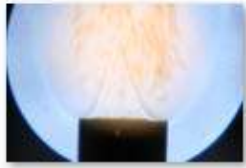
z_IMG_9999_1067.JPG

Experiment NO. 4

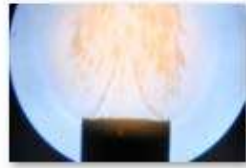


Air Flow Rate		Fuel Flow rate		Volume flow rate	nozzle width	U	Phi
SLPM	mole/sec	SLPM	mole/sec	m ³ /s	m	m/sec	
2.5	0.001732	0.21	0.000145	4.51E-05	0.010744	0.497869	0.79968

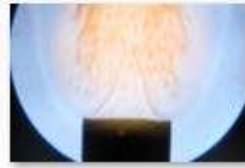
Entrainment Rate
0.0112 g/sec
Concentration
248.1309 g/m³



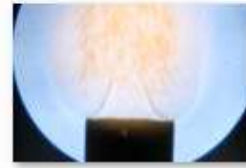
IMG_9999_1172.JPG



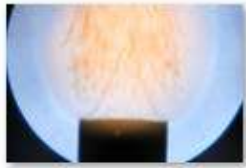
IMG_9999_1173.JPG



IMG_9999_1174.JPG



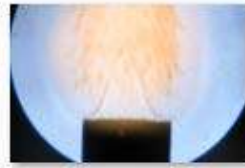
IMG_9999_1175.JPG



IMG_9999_1176.JPG



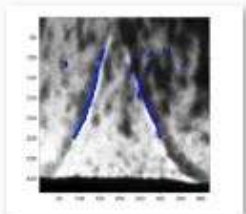
IMG_9999_1177.JPG



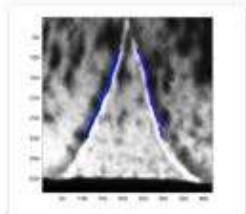
IMG_9999_1178.JPG



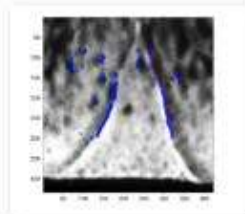
IMG_9999_1179.JPG



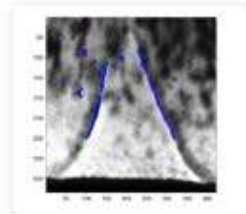
z_IMG_9999_1172.JPG



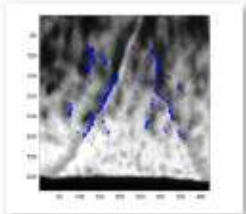
z_IMG_9999_1173.JPG



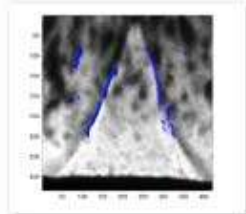
z_IMG_9999_1174.JPG



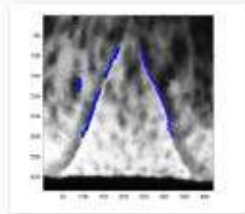
z_IMG_9999_1175.JPG



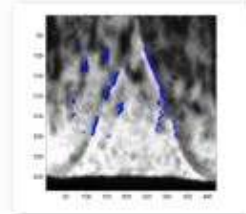
z_IMG_9999_1176.JPG



z_IMG_9999_1177.JPG

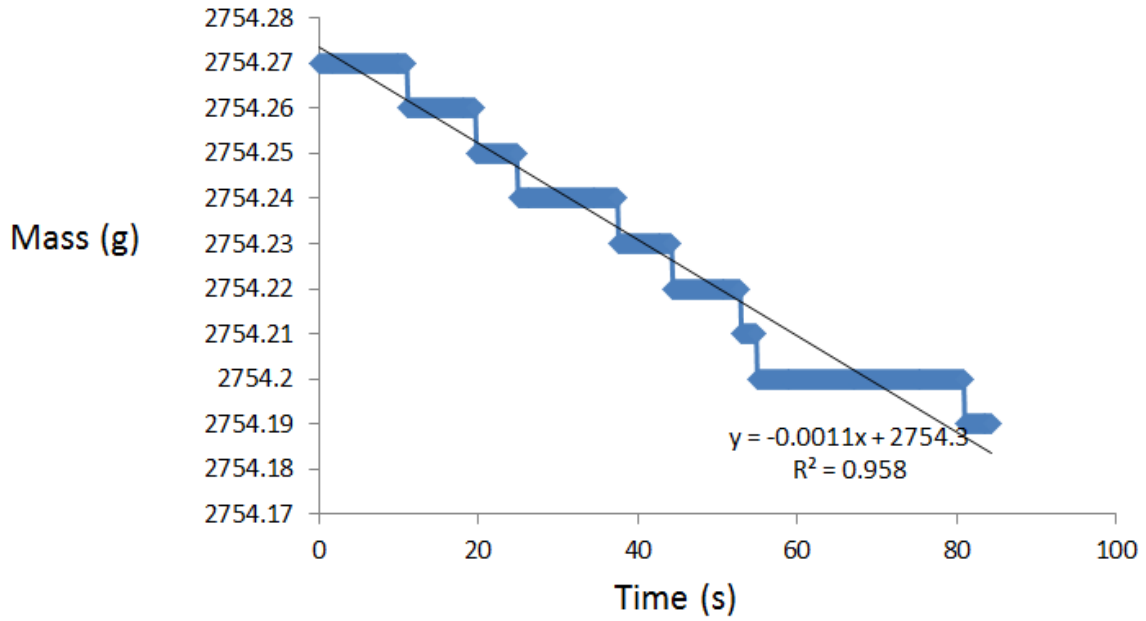


z_IMG_9999_1178.JPG



z_IMG_9999_1179.JPG

Experiment NO. 5

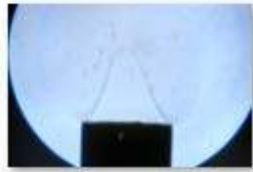


Air Flow Rate		Fuel Flow rate		Volume flow rate	nozzle width	U	Phi
SLPM	mole/sec	SLPM	mole/sec	m ³ /s	m	m/sec	
2.5	0.001732	0.21	0.000145	4.51E-05	0.010744	0.497869	0.79968

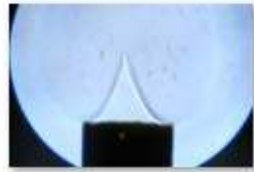
Entrainment Rate
0.0011 g/sec
Concentration
24.37 g/m³



IMG_9999_1189.JPG



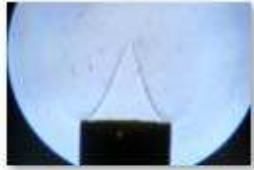
IMG_9999_1190.JPG



IMG_9999_1191.JPG



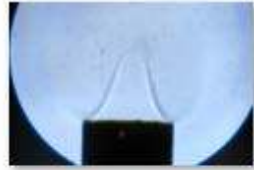
IMG_9999_1192.JPG



IMG_9999_1193.JPG



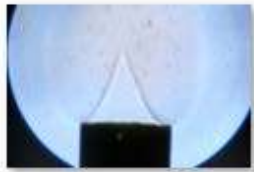
IMG_9999_1194.JPG



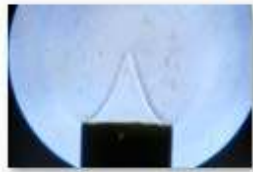
IMG_9999_1195.JPG



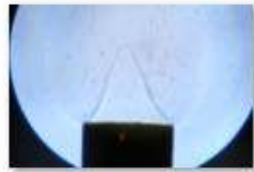
IMG_9999_1196.JPG



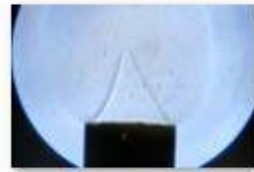
IMG_9999_1197.JPG



IMG_9999_1198.JPG



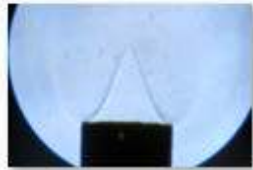
IMG_9999_1199.JPG



IMG_9999_1200.JPG



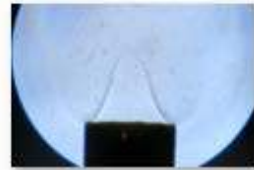
IMG_9999_1201.JPG



IMG_9999_1202.JPG



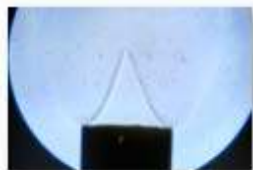
IMG_9999_1203.JPG



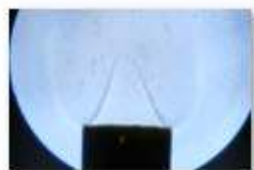
IMG_9999_1204.JPG



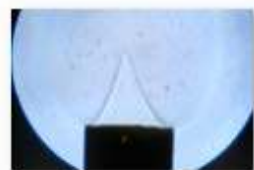
IMG_9999_1205.JPG



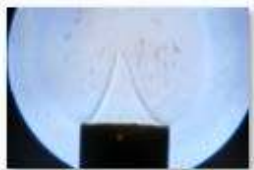
IMG_9999_1206.JPG



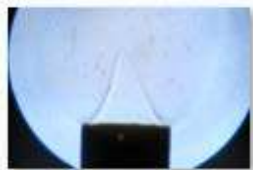
IMG_9999_1207.JPG



IMG_9999_1208.JPG



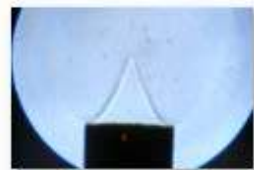
IMG_9999_1209.JPG



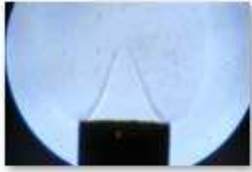
IMG_9999_1210.JPG



IMG_9999_1211.JPG



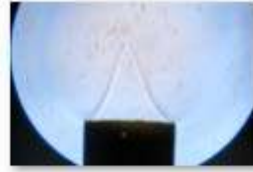
IMG_9999_1212.JPG



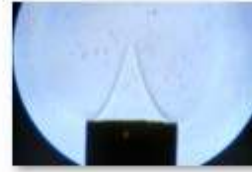
IMG_9999_1213.JPG



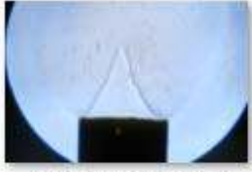
IMG_9999_1214.JPG



IMG_9999_1215.JPG



IMG_9999_1216.JPG



IMG_9999_1217.JPG



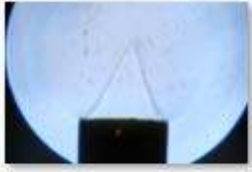
IMG_9999_1218.JPG



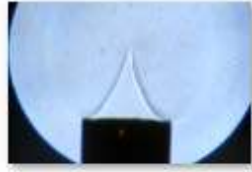
IMG_9999_1219.JPG



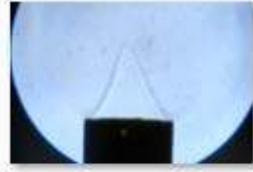
IMG_9999_1220.JPG



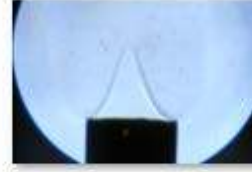
IMG_9999_1221.JPG



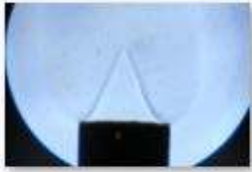
IMG_9999_1222.JPG



IMG_9999_1223.JPG



IMG_9999_1224.JPG



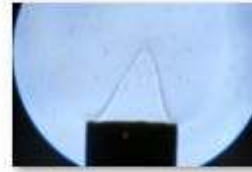
IMG_9999_1225.JPG



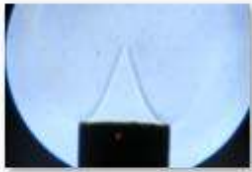
IMG_9999_1226.JPG



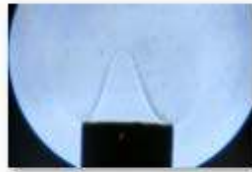
IMG_9999_1227.JPG



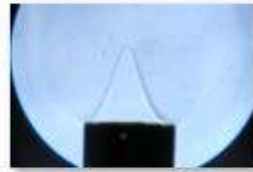
IMG_9999_1228.JPG



IMG_9999_1229.JPG



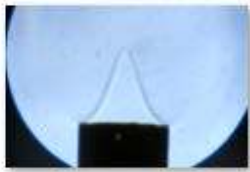
IMG_9999_1230.JPG



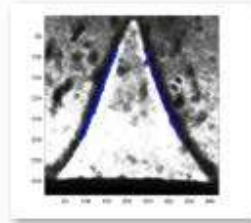
IMG_9999_1231.JPG



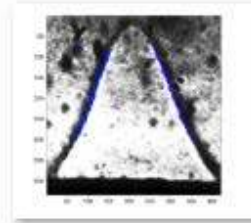
IMG_9999_1232.JPG



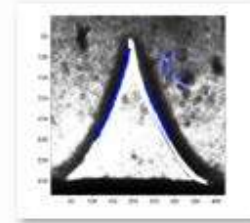
IMG_9999_1233.JPG



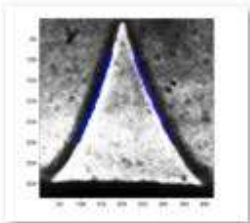
z_IMG_9999_1189.JPG



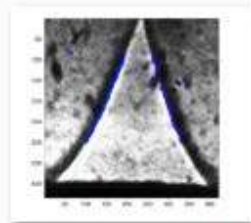
z_IMG_9999_1190.JPG



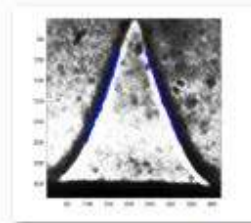
z_IMG_9999_1191.JPG



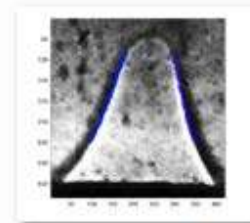
z_IMG_9999_1192.JPG



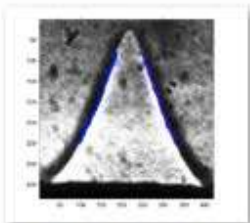
z_IMG_9999_1193.JPG



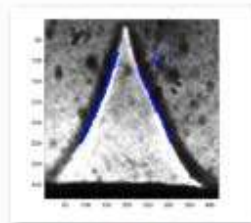
z_IMG_9999_1194.JPG



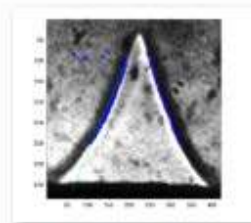
z_IMG_9999_1195.JPG



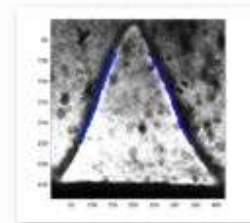
z_IMG_9999_1196.JPG



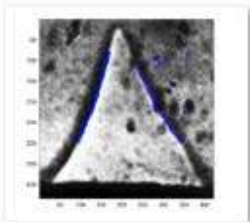
z_IMG_9999_1197.JPG



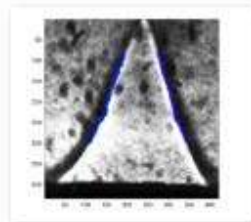
z_IMG_9999_1198.JPG



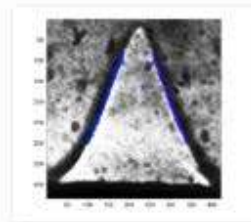
z_IMG_9999_1199.JPG



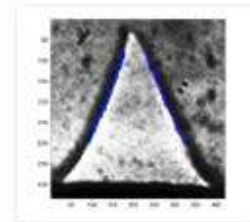
z_IMG_9999_1200.JPG



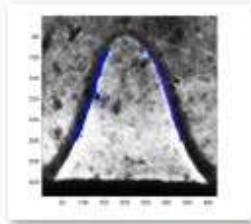
z_IMG_9999_1201.JPG



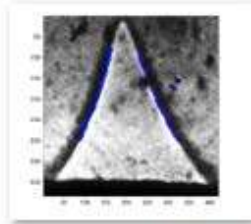
z_IMG_9999_1202.JPG



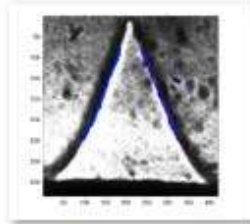
z_IMG_9999_1203.JPG



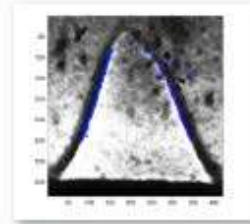
z_IMG_9999_1204.JPG



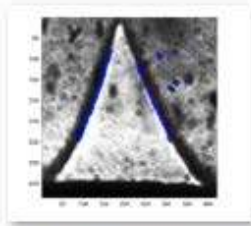
z_IMG_9999_1205.JPG



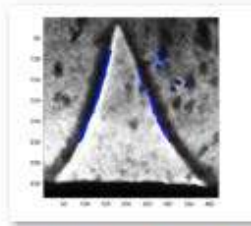
z_IMG_9999_1206.JPG



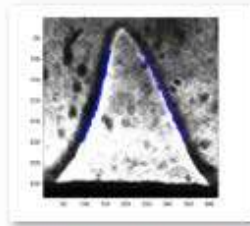
z_IMG_9999_1207.JPG



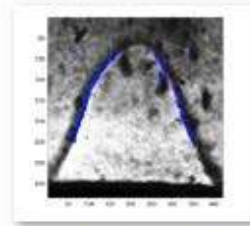
z_IMG_9999_1208.JPG



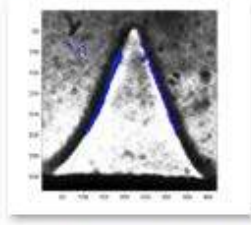
z_IMG_9999_1209.JPG



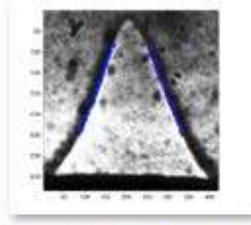
z_IMG_9999_1210.JPG



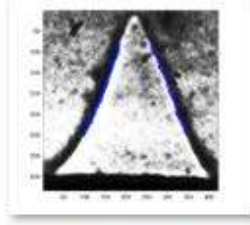
z_IMG_9999_1211.JPG



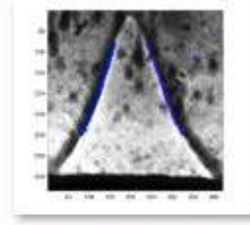
z_IMG_9999_1212.JPG



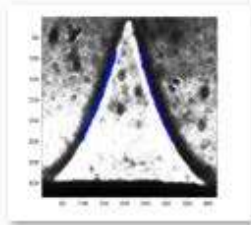
z_IMG_9999_1213.JPG



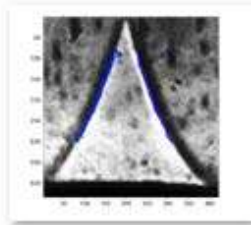
z_IMG_9999_1214.JPG



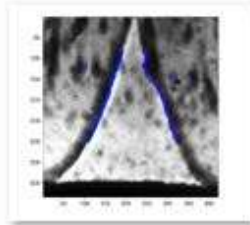
z_IMG_9999_1215.JPG



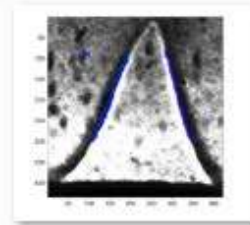
z_IMG_9999_1216.JPG



z_IMG_9999_1217.JPG



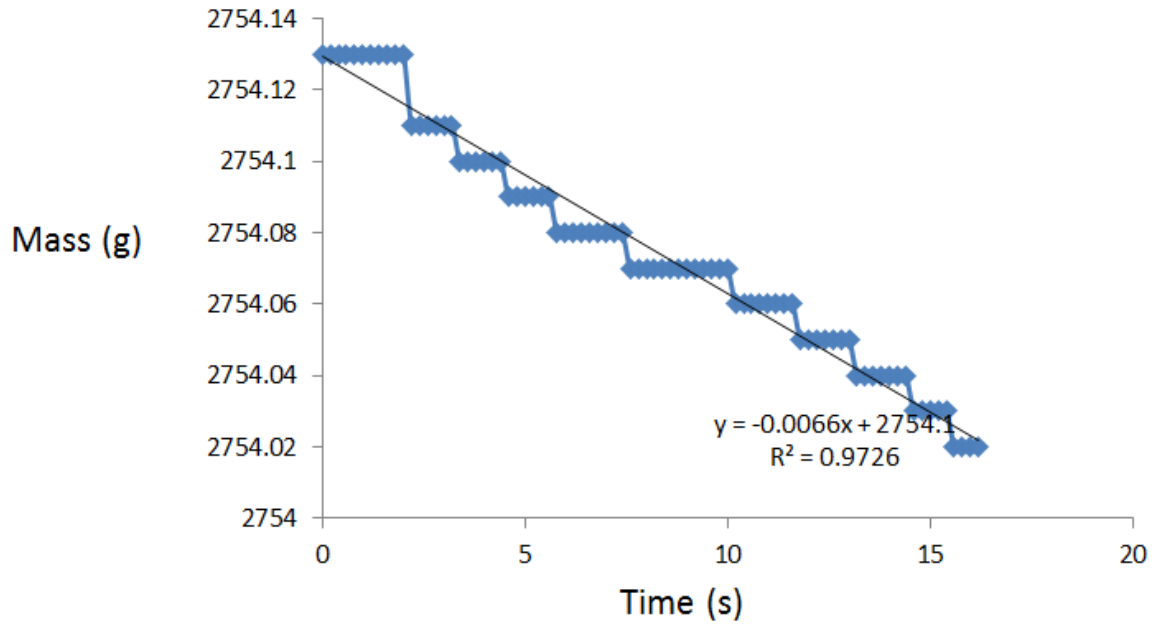
z_IMG_9999_1218.JPG



z_IMG_9999_1219.JPG



Experiment NO. 6



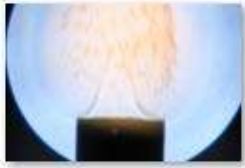
Air Flow Rate		Fuel Flow rate		Volume flow rate	nozzle width	U	Phi
SLPM	mole/sec	SLPM	mole/sec	m ³ /s	m	m/sec	
2.5	0.001732	0.21	0.000145	4.51E-05	0.010744	0.497869	0.79968

Entrainment Rate

0.0066 g/sec

Concentration

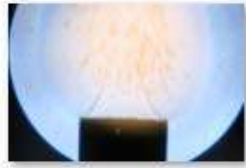
146.22 g/m³



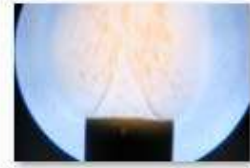
IMG_9999_1234.JPG



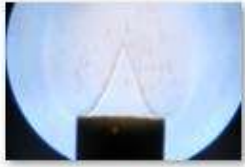
IMG_9999_1235.JPG



IMG_9999_1236.JPG



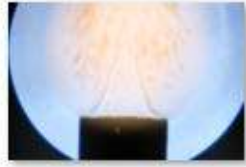
IMG_9999_1237.JPG



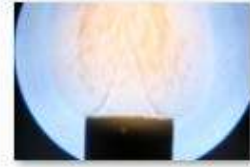
IMG_9999_1238.JPG



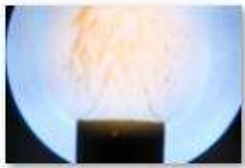
IMG_9999_1239.JPG



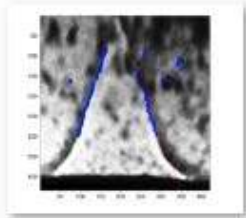
IMG_9999_1240.JPG



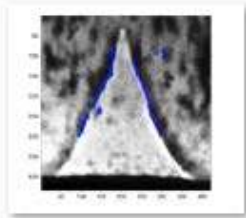
IMG_9999_1241.JPG



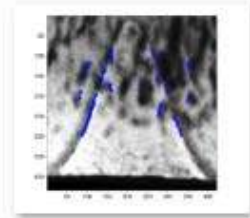
IMG_9999_1242.JPG



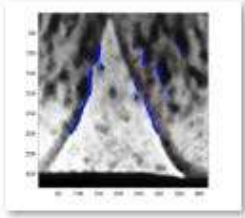
z_IMG_9999_1234.JPG



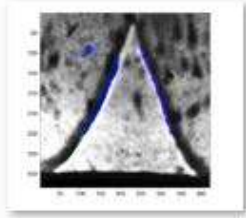
z_IMG_9999_1235.JPG



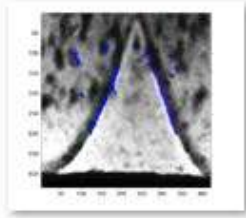
z_IMG_9999_1236.JPG



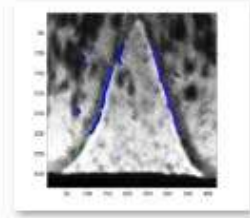
z_IMG_9999_1237.JPG



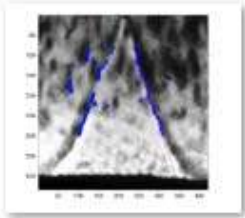
z_IMG_9999_1238.JPG



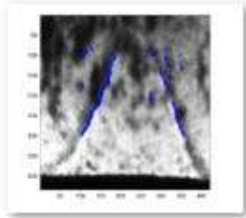
z_IMG_9999_1239.JPG



z_IMG_9999_1240.JPG

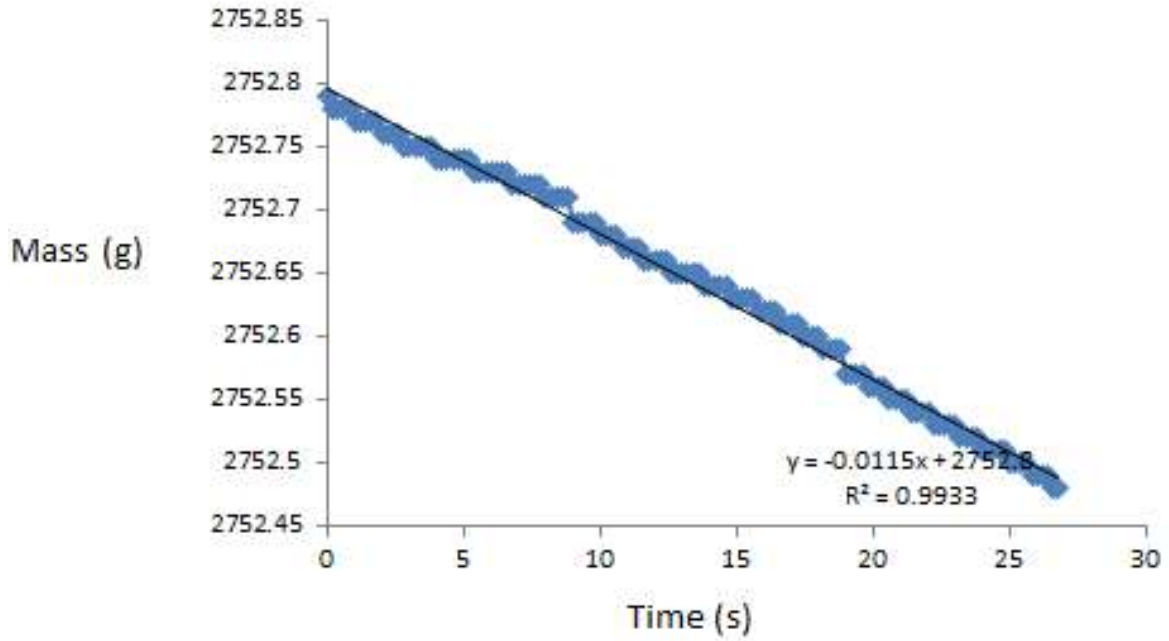


z_IMG_9999_1241.JPG



z_IMG_9999_1242.JPG

Experiment NO. 8

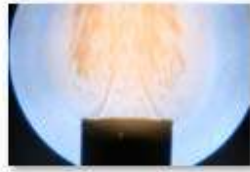


Air Flow Rate		Fuel Flow rate		Volume flow rate	nozzle width	U	Phi
SLPM	mole/sec	SLPM	mole/sec	m ³ /s	m	m/sec	
2.5	0.001732	0.21	0.000145	4.51E-05	0.010744	0.497869	0.79968

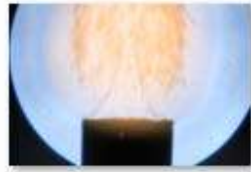
Entrainment Rate
0.0115 g/sec
Concentration
254.7773 g/m³



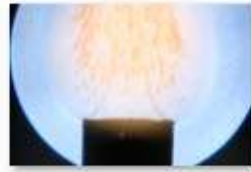
IMG_9999_1252.JPG



IMG_9999_1253.JPG



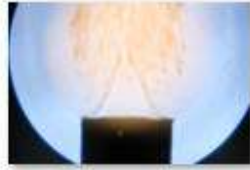
IMG_9999_1254.JPG



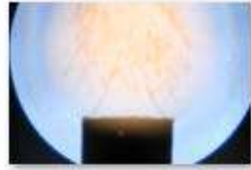
IMG_9999_1255.JPG



IMG_9999_1256.JPG



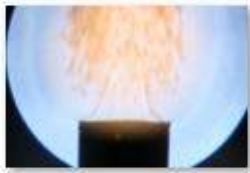
IMG_9999_1257.JPG



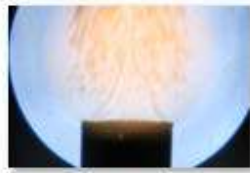
IMG_9999_1258.JPG



IMG_9999_1259.JPG



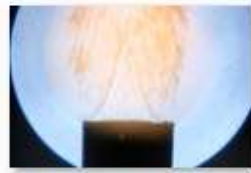
IMG_9999_1260.JPG



IMG_9999_1261.JPG



IMG_9999_1262.JPG



IMG_9999_1263.JPG



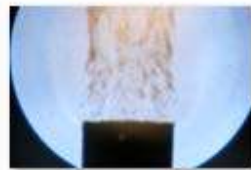
IMG_9999_1264.JPG



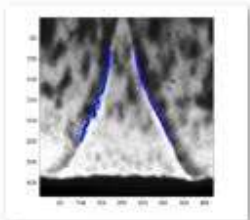
IMG_9999_1265.JPG



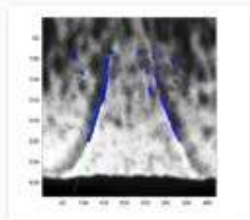
IMG_9999_1266.JPG



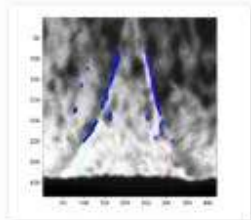
IMG_9999_1267.JPG



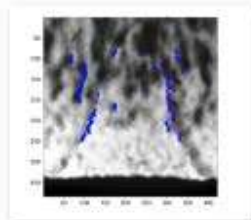
z_IMG_9999_1252.JPG



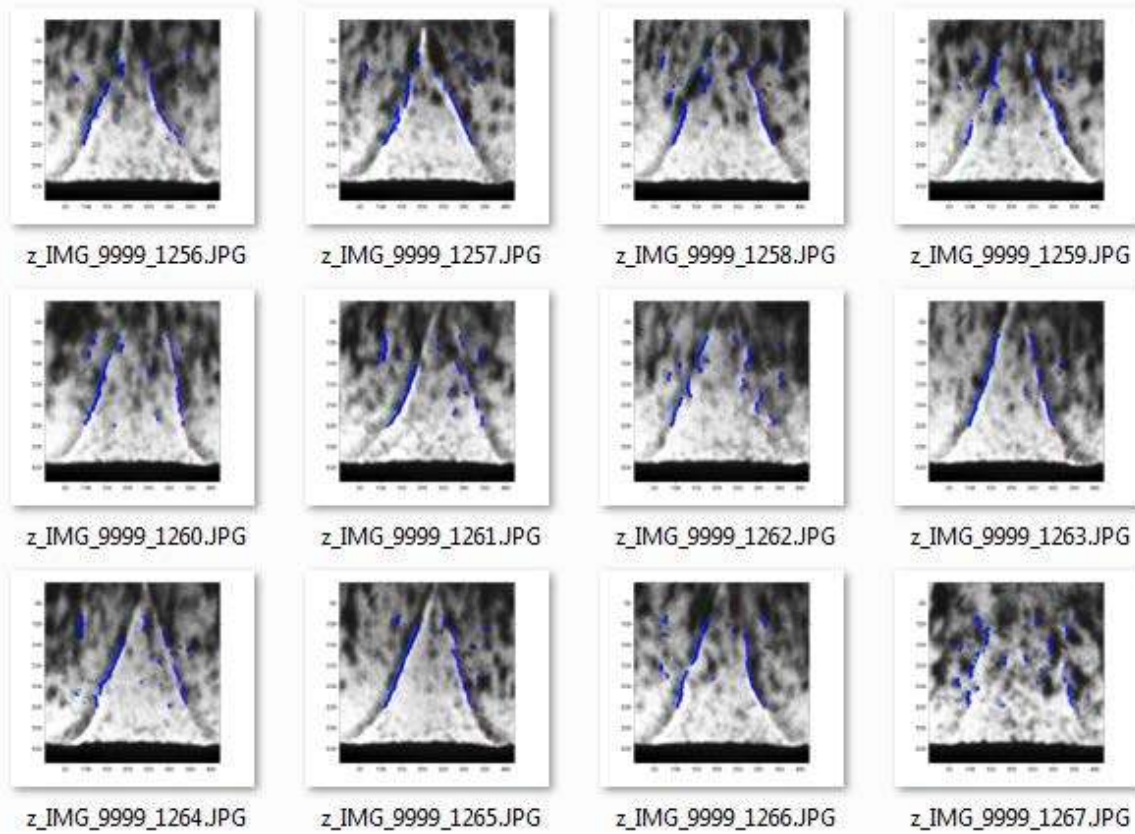
z_IMG_9999_1253.JPG



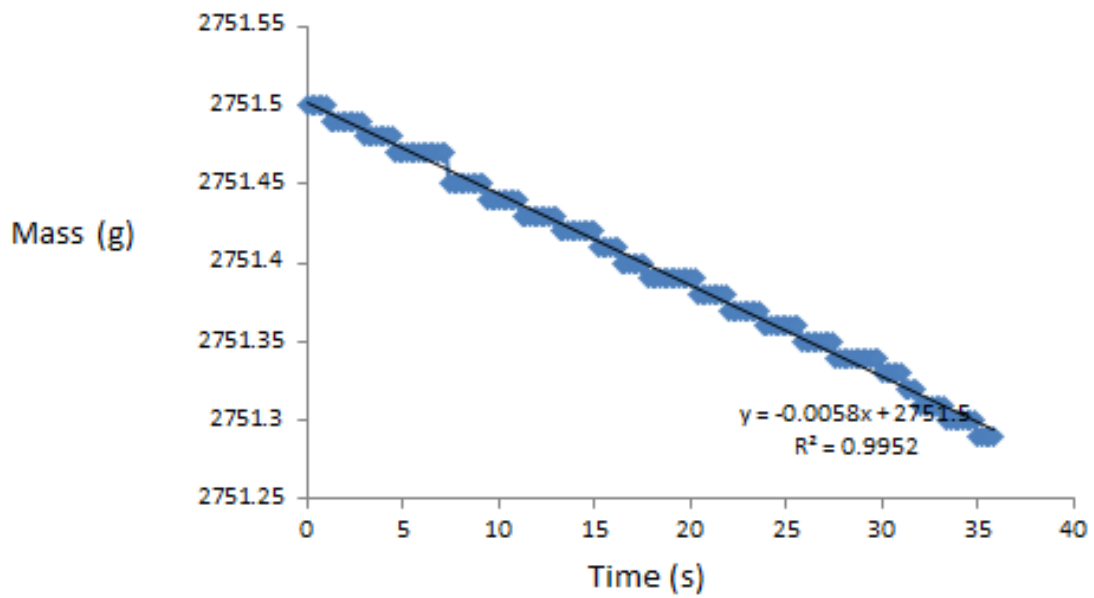
z_IMG_9999_1254.JPG



z_IMG_9999_1255.JPG

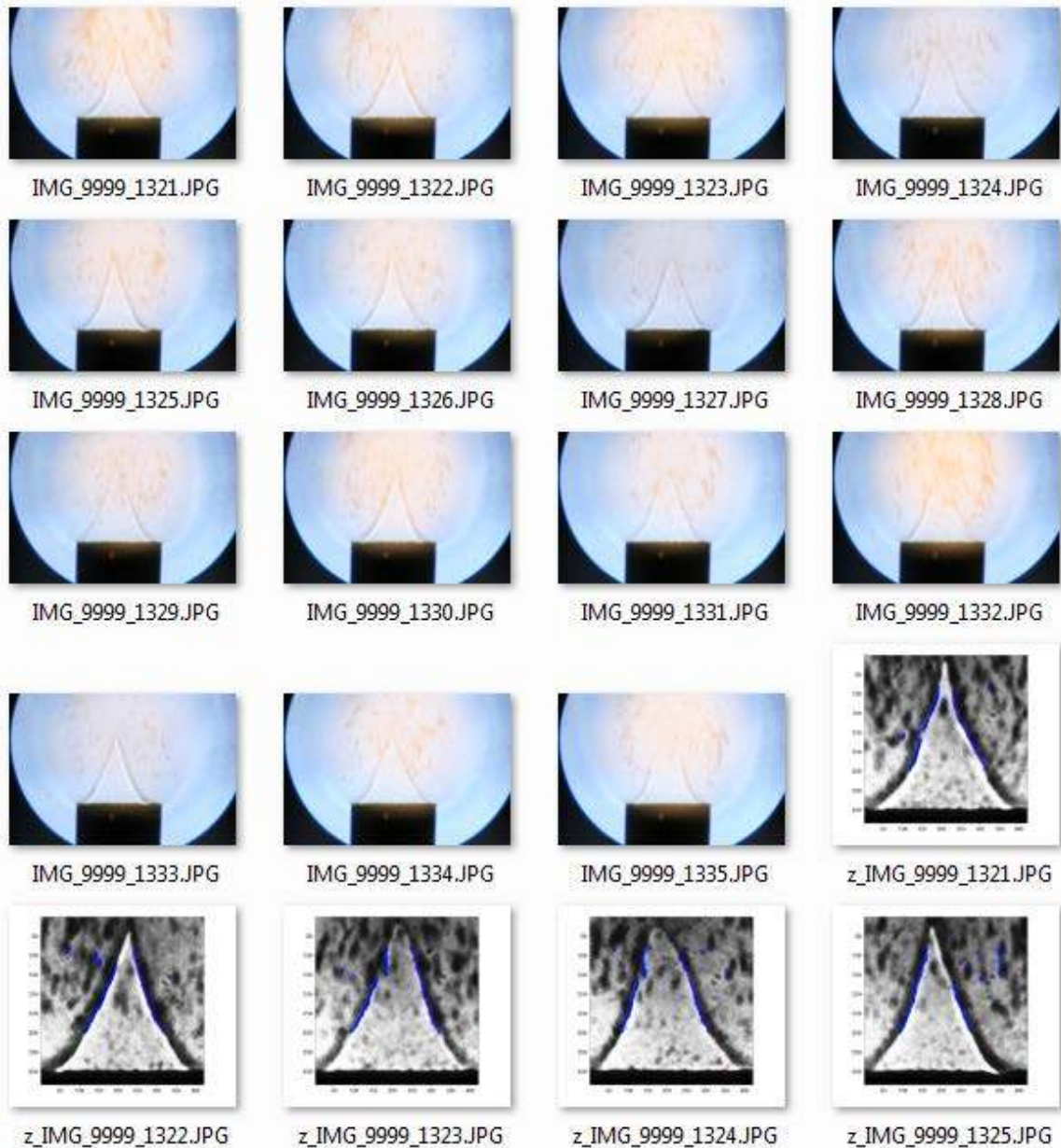


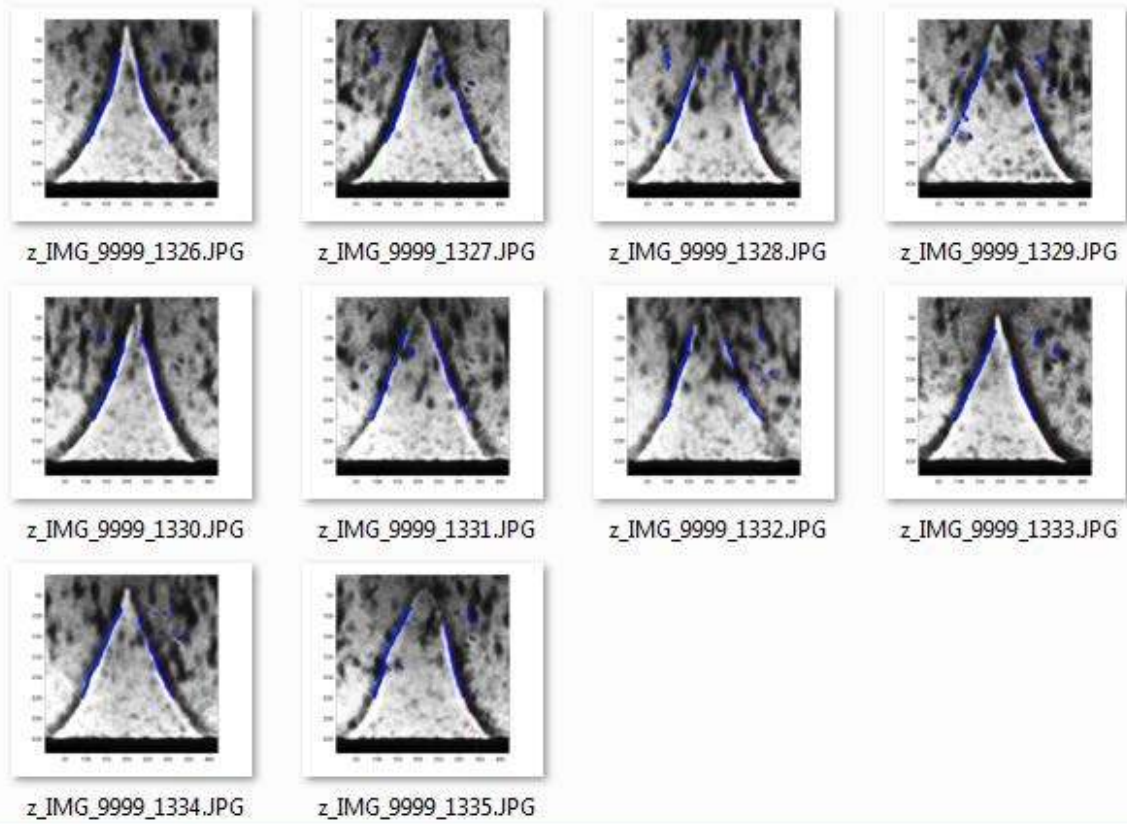
Experiment NO. 11



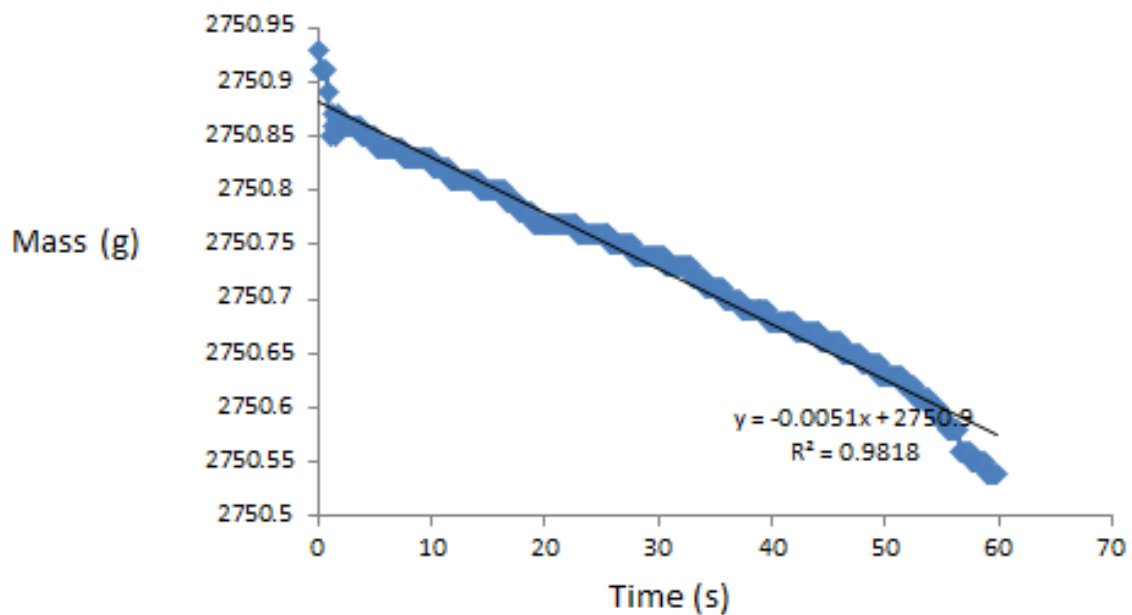
Air Flow Rate		Fuel Flow rate		Volume flow rate	nozzle width	U	Phi
SLPM	mole/sec	SLPM	mole/sec	m3/s	m	m/sec	
2.5	0.001732	0.21	0.000145	4.51E-05	0.010744	0.497869	0.79968

Entrainment Rate
0.0058 g/sec
Concentration
128.4964 g/m³



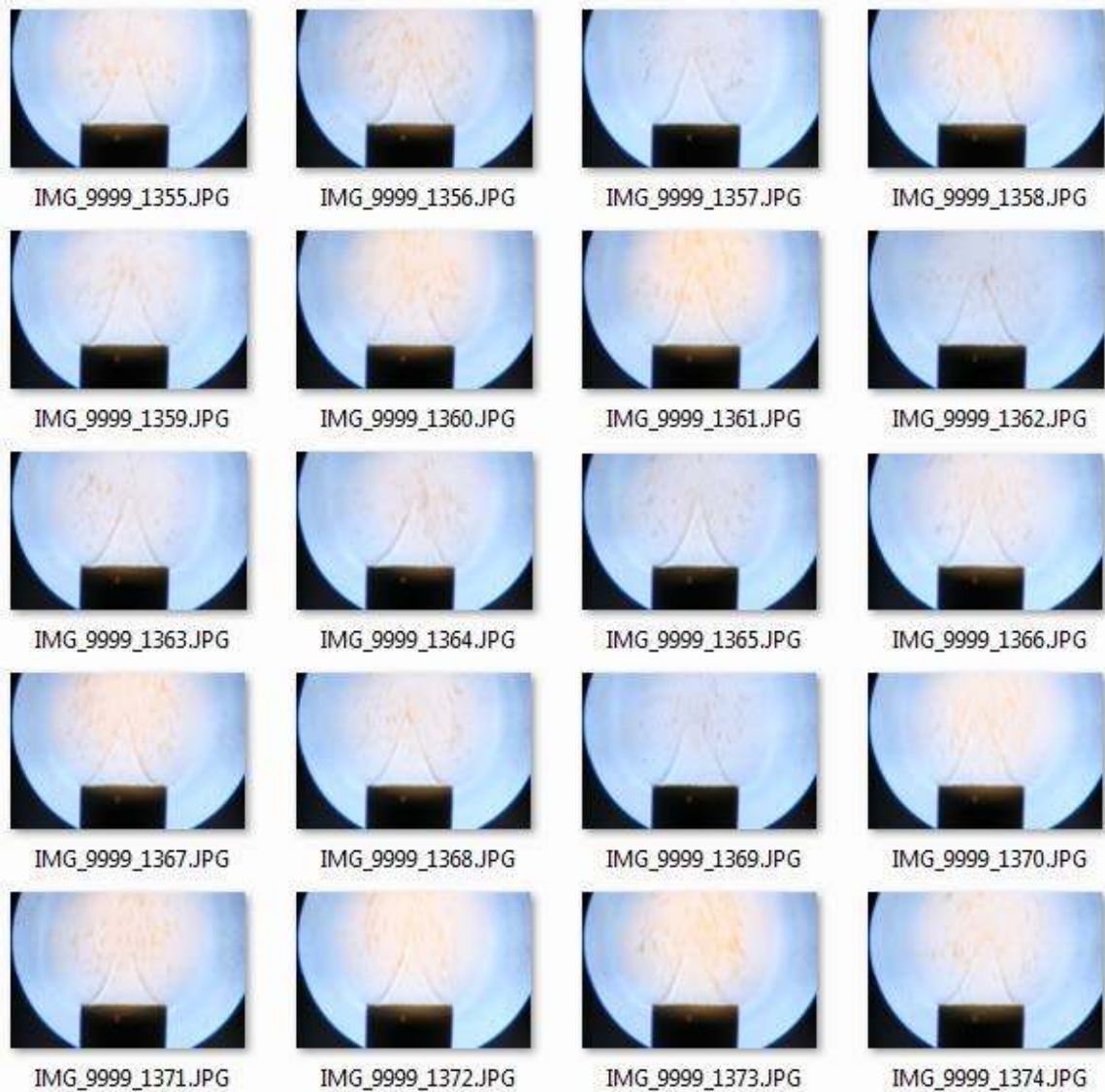


Experiment NO. 12



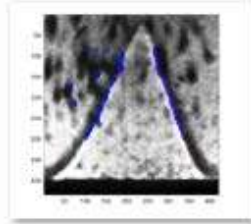
Air Flow Rate		Fuel Flow rate		Volume flow rate	nozzle width	U	Phi
SLPM	mole/sec	SLPM	mole/sec	m3/s	m	m/sec	
2.5	0.001732	0.21	0.000145	4.51E-05	0.010744	0.497869	0.79968

Entrainment Rate
0.0051 g/sec
Concentration
112.9882 g/m³

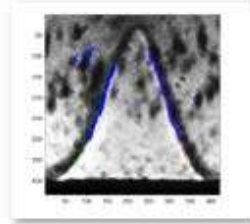




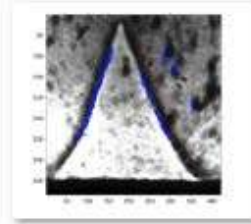
IMG_9999_1375.JPG



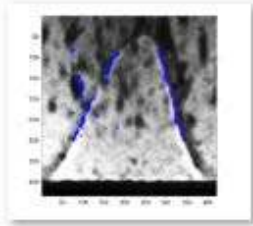
z_IMG_9999_1355.JPG



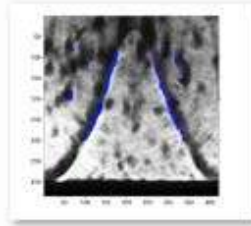
z_IMG_9999_1356.JPG



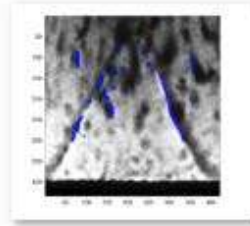
z_IMG_9999_1357.JPG



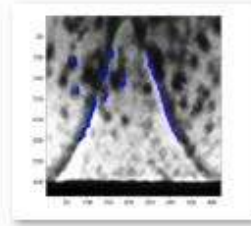
z_IMG_9999_1358.JPG



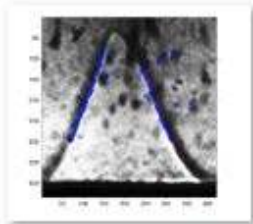
z_IMG_9999_1359.JPG



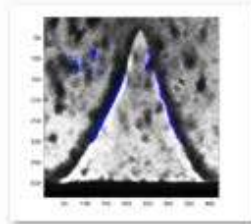
z_IMG_9999_1360.JPG



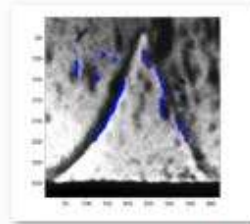
z_IMG_9999_1361.JPG



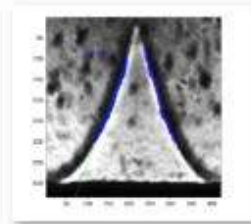
z_IMG_9999_1362.JPG



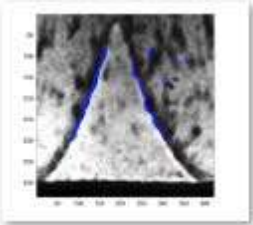
z_IMG_9999_1363.JPG



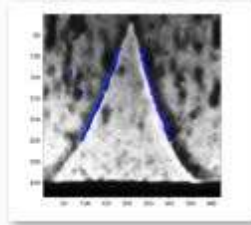
z_IMG_9999_1364.JPG



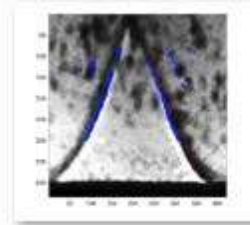
z_IMG_9999_1365.JPG



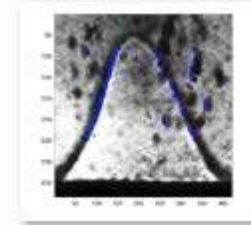
z_IMG_9999_1366.JPG



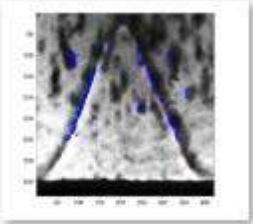
z_IMG_9999_1367.JPG



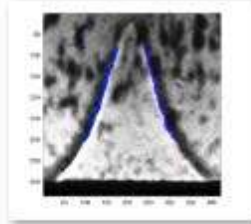
z_IMG_9999_1368.JPG



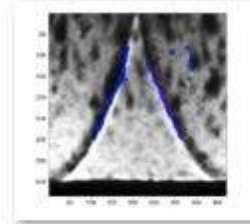
z_IMG_9999_1369.JPG



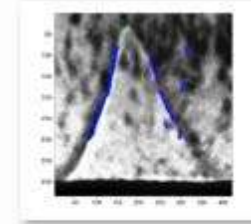
z_IMG_9999_1370.JPG



z_IMG_9999_1371.JPG

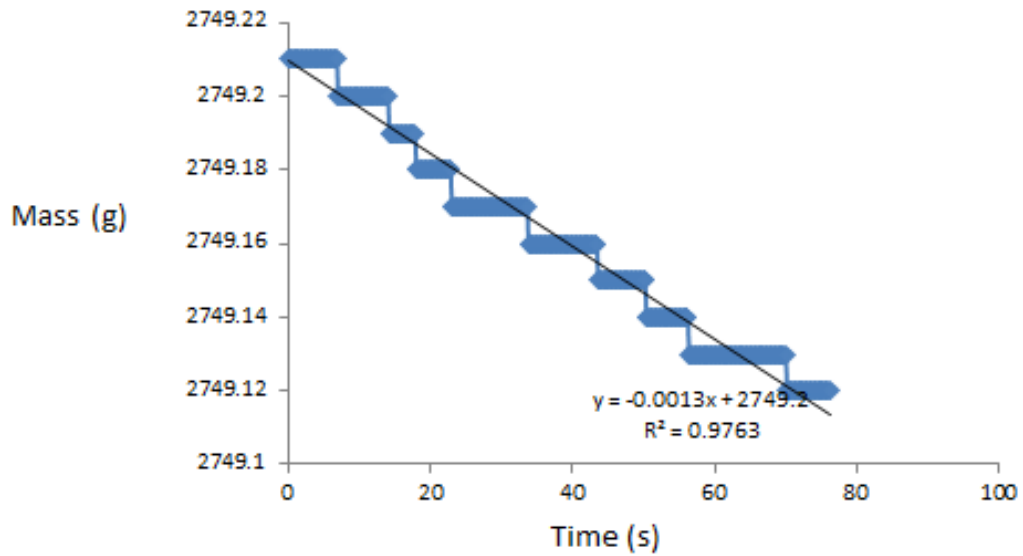


z_IMG_9999_1372.JPG



z_IMG_9999_1373.JPG

Experiment NO. 13

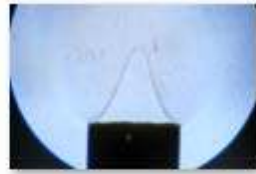


Air Flow Rate		Fuel Flow rate		Volume flow rate	nozzle width	U	Phi
SLP M	mole/sec	SLP M	mole/sec	m ³ /s	m	m/sec	
2.5	0.001732	0.21	0.000145	4.51E-05	0.010744	0.497869	0.79968

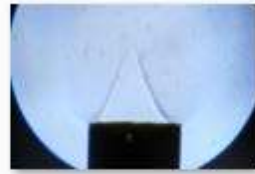
Entrainment Rate
0.0013 g/sec
Concentration
28.80091 g/m³



IMG_9999_1413.JPG



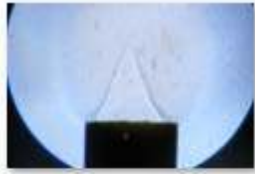
IMG_9999_1414.JPG



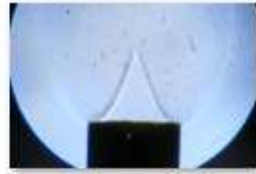
IMG_9999_1415.JPG



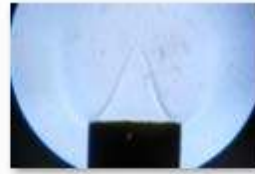
IMG_9999_1416.JPG



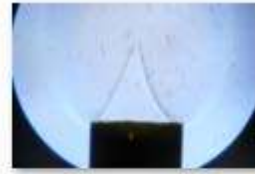
IMG_9999_1417.JPG



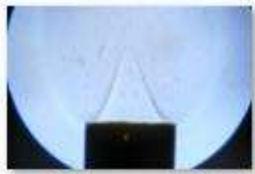
IMG_9999_1418.JPG



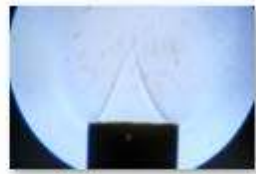
IMG_9999_1419.JPG



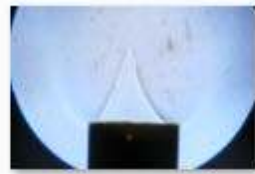
IMG_9999_1420.JPG



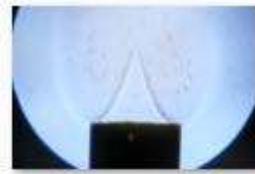
IMG_9999_1421.JPG



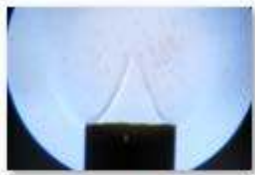
IMG_9999_1422.JPG



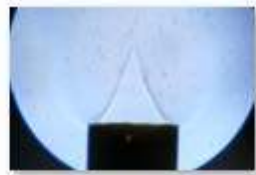
IMG_9999_1423.JPG



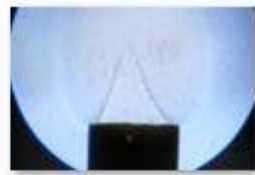
IMG_9999_1424.JPG



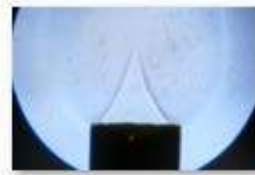
IMG_9999_1425.JPG



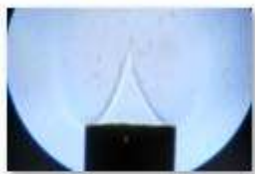
IMG_9999_1426.JPG



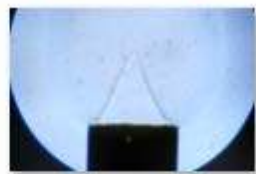
IMG_9999_1427.JPG



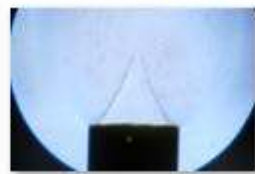
IMG_9999_1428.JPG



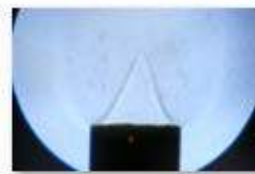
IMG_9999_1429.JPG



IMG_9999_1430.JPG



IMG_9999_1431.JPG



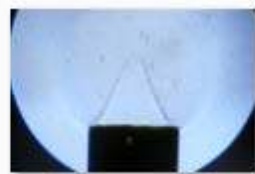
IMG_9999_1432.JPG



IMG_9999_1433.JPG



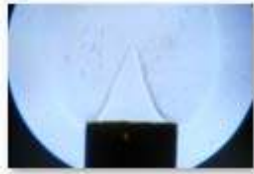
IMG_9999_1434.JPG



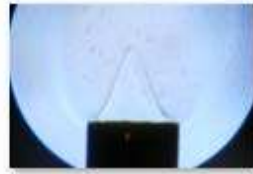
IMG_9999_1435.JPG



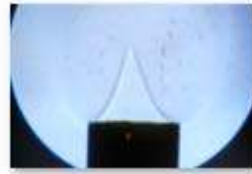
IMG_9999_1436.JPG



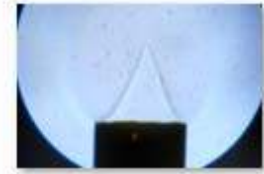
IMG_9999_1437.JPG



IMG_9999_1438.JPG



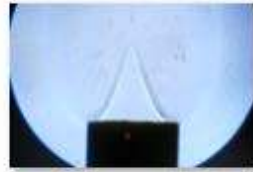
IMG_9999_1439.JPG



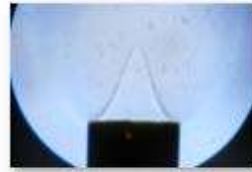
IMG_9999_1440.JPG



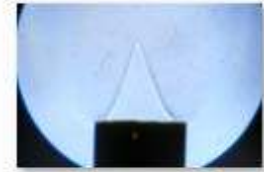
IMG_9999_1441.JPG



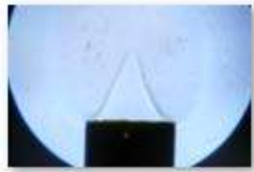
IMG_9999_1442.JPG



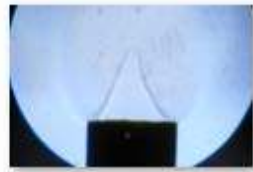
IMG_9999_1443.JPG



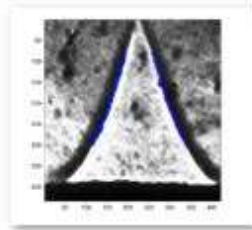
IMG_9999_1444.JPG



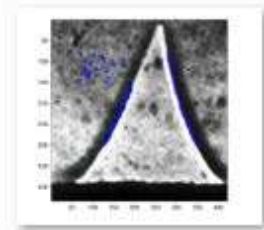
IMG_9999_1445.JPG



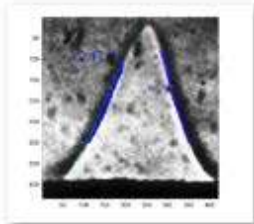
IMG_9999_1446.JPG



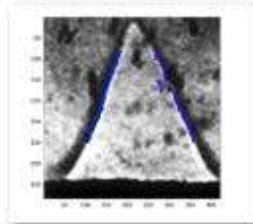
z_IMG_9999_1409.JPG



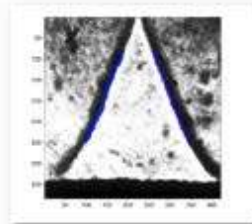
z_IMG_9999_1410.JPG



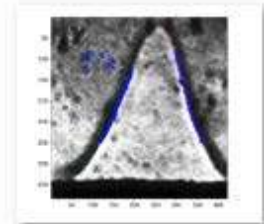
z_IMG_9999_1411.JPG



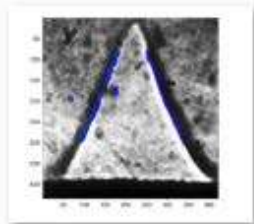
z_IMG_9999_1412.JPG



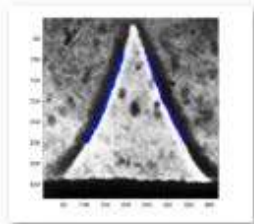
z_IMG_9999_1413.JPG



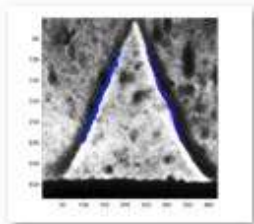
z_IMG_9999_1414.JPG



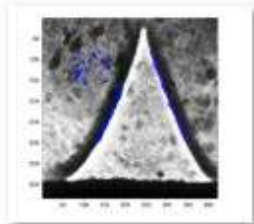
z_IMG_9999_1415.JPG



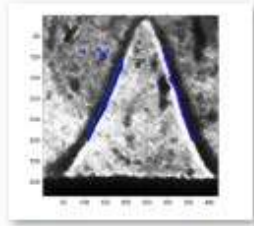
z_IMG_9999_1416.JPG



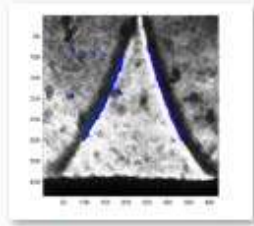
z_IMG_9999_1417.JPG



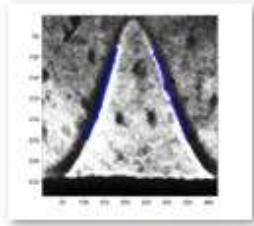
z_IMG_9999_1418.JPG



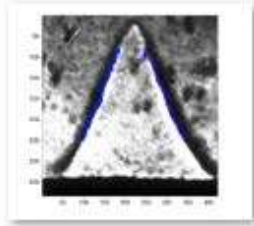
z_IMG_9999_1419.JPG



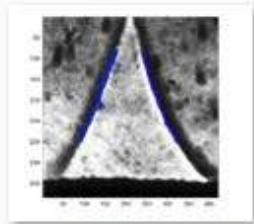
z_IMG_9999_1420.JPG



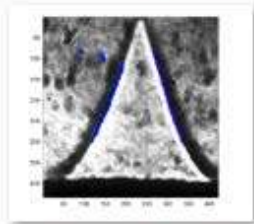
z_IMG_9999_1421.JPG



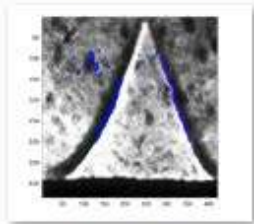
z_IMG_9999_1422.JPG



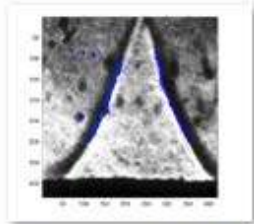
z_IMG_9999_1423.JPG



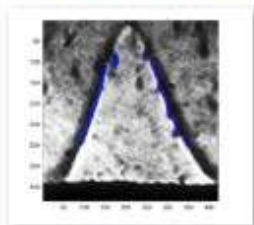
z_IMG_9999_1424.JPG



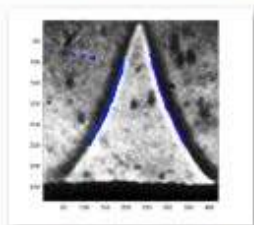
z_IMG_9999_1425.JPG



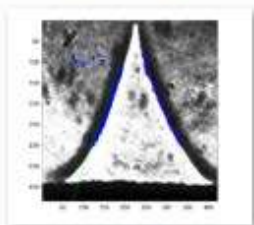
z_IMG_9999_1426.JPG



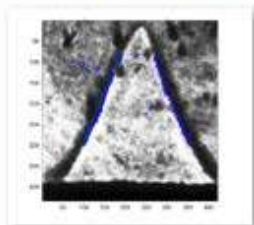
z_IMG_9999_1427.JPG



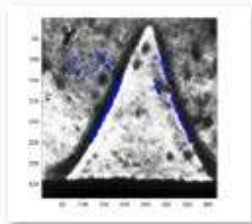
z_IMG_9999_1428.JPG



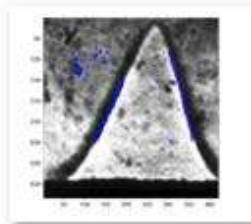
z_IMG_9999_1429.JPG



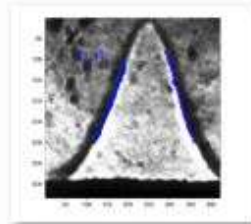
z_IMG_9999_1430.JPG



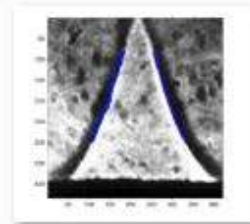
z_IMG_9999_1431.JPG



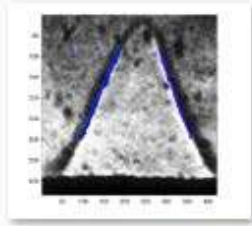
z_IMG_9999_1432.JPG



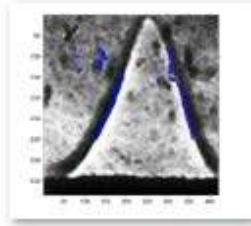
z_IMG_9999_1433.JPG



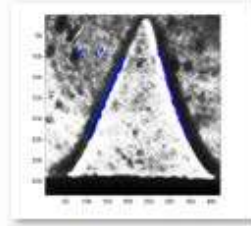
z_IMG_9999_1434.JPG



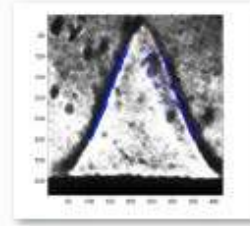
z_IMG_9999_1435.JPG



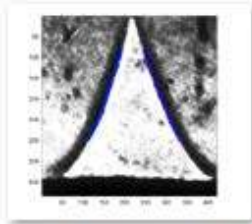
z_IMG_9999_1436.JPG



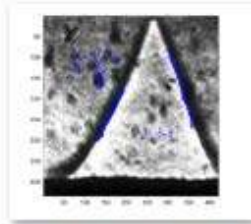
z_IMG_9999_1437.JPG



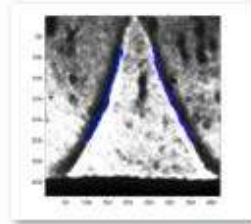
z_IMG_9999_1438.JPG



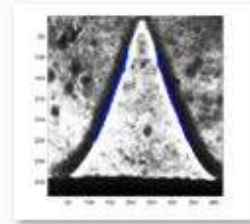
z_IMG_9999_1439.JPG



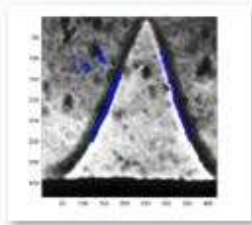
z_IMG_9999_1440.JPG



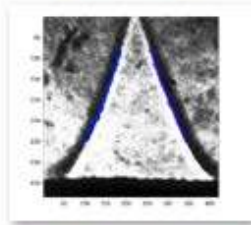
z_IMG_9999_1441.JPG



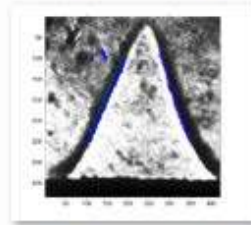
z_IMG_9999_1442.JPG



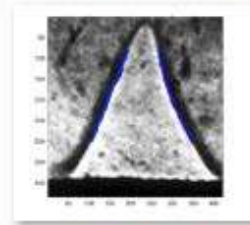
z_IMG_9999_1443.JPG



z_IMG_9999_1444.JPG

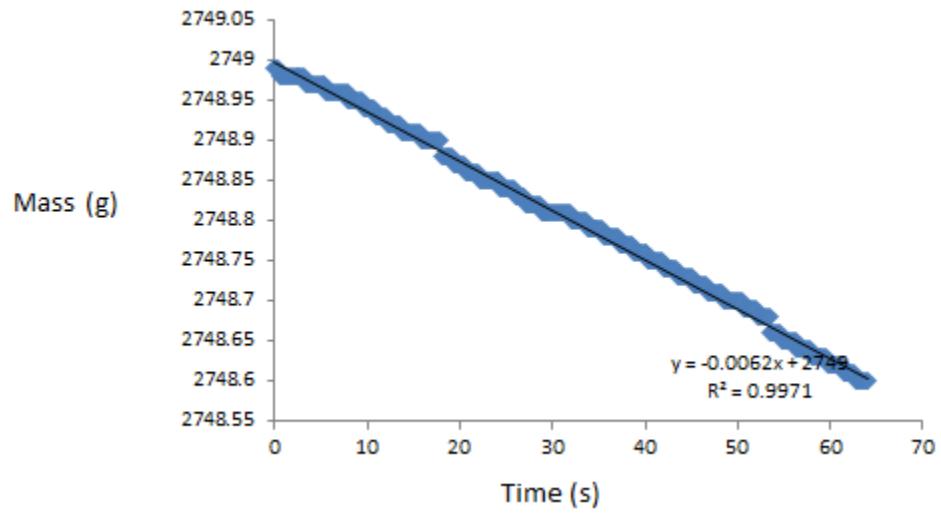


z_IMG_9999_1445.JPG



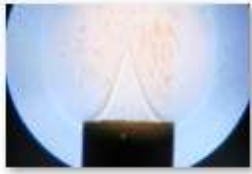
z_IMG_9999_1446.JPG

Experiment NO. 14

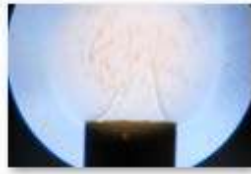


Air Flow Rate		Fuel Flow rate		Volume flow rate	nozzle width	U	Phi
SLPM	mole/sec	SLPM	mole/sec	m3/s	m	m/sec	
2.5	0.001732	0.21	0.000145	4.51E-05	0.010744	0.497869	0.79968

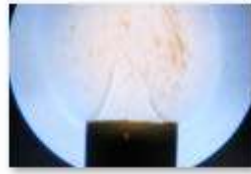
Entrainment Rate
 0.0062 g/sec
 Concentration
 137.3582 g/m³



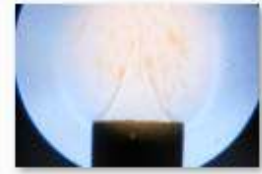
IMG_9999_1467.JPG



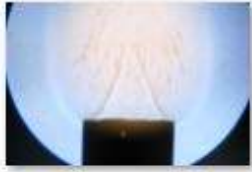
IMG_9999_1468.JPG



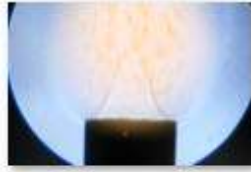
IMG_9999_1469.JPG



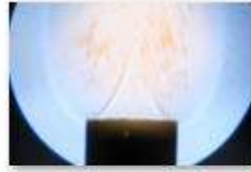
IMG_9999_1470.JPG



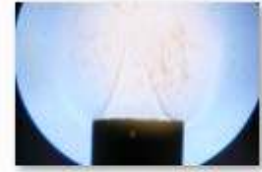
IMG_9999_1471.JPG



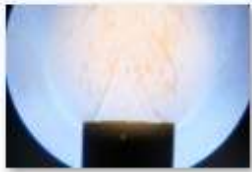
IMG_9999_1472.JPG



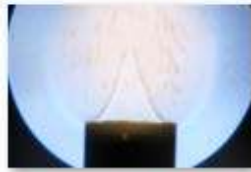
IMG_9999_1473.JPG



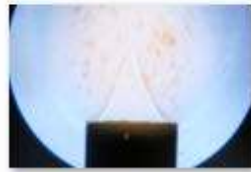
IMG_9999_1474.JPG



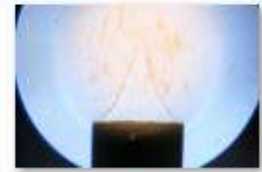
IMG_9999_1475.JPG



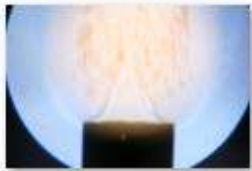
IMG_9999_1476.JPG



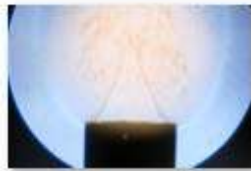
IMG_9999_1477.JPG



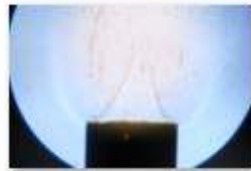
IMG_9999_1478.JPG



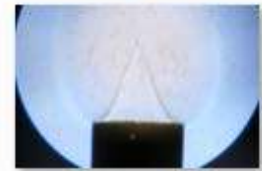
IMG_9999_1479.JPG



IMG_9999_1480.JPG



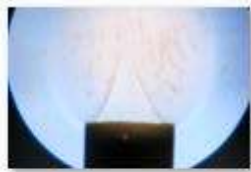
IMG_9999_1481.JPG



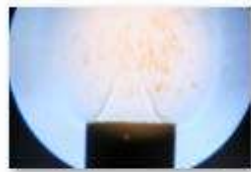
IMG_9999_1482.JPG



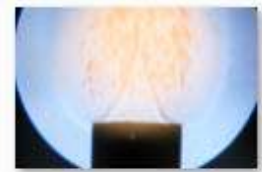
IMG_9999_1483.JPG



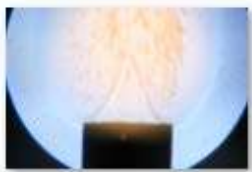
IMG_9999_1484.JPG



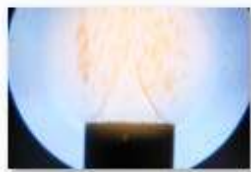
IMG_9999_1485.JPG



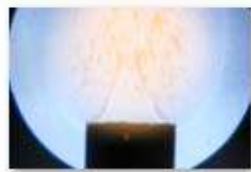
IMG_9999_1486.JPG



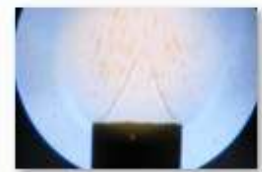
IMG_9999_1487.JPG



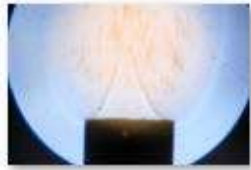
IMG_9999_1488.JPG



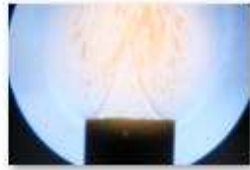
IMG_9999_1489.JPG



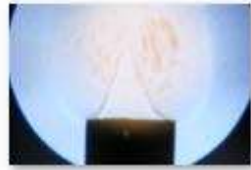
IMG_9999_1490.JPG



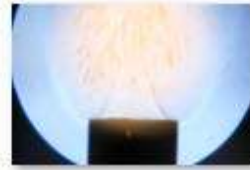
IMG_9999_1491.JPG



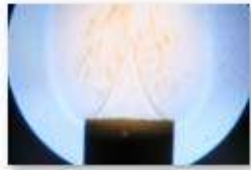
IMG_9999_1492.JPG



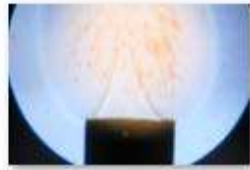
IMG_9999_1493.JPG



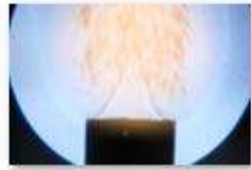
IMG_9999_1494.JPG



IMG_9999_1495.JPG



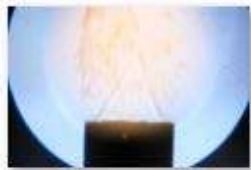
IMG_9999_1496.JPG



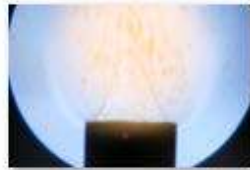
IMG_9999_1497.JPG



IMG_9999_1498.JPG



IMG_9999_1499.JPG



IMG_9999_1500.JPG



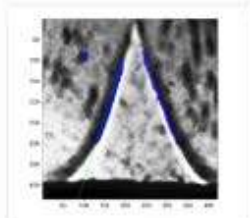
IMG_9999_1501.JPG



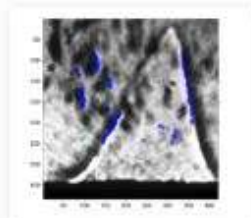
IMG_9999_1502.JPG



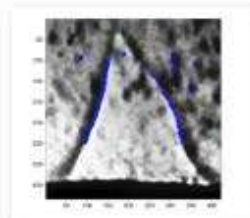
IMG_9999_1503.JPG



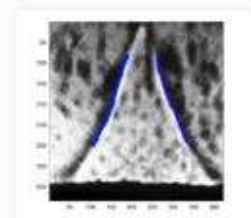
z_IMG_9999_1467.JPG



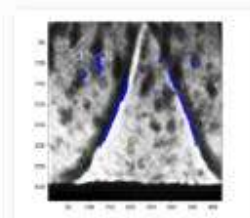
z_IMG_9999_1468.JPG



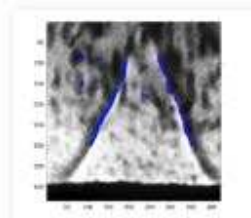
z_IMG_9999_1469.JPG



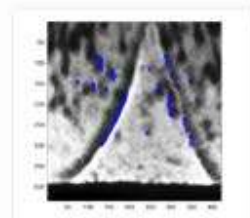
z_IMG_9999_1470.JPG



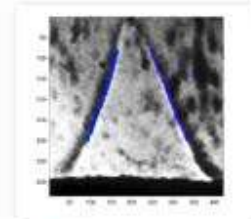
z_IMG_9999_1471.JPG



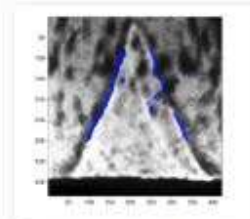
z_IMG_9999_1472.JPG



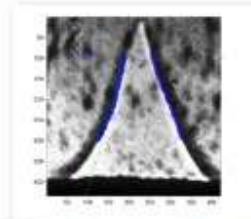
z_IMG_9999_1473.JPG



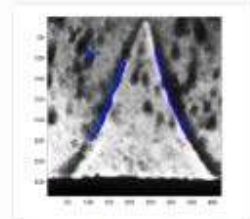
z_IMG_9999_1474.JPG



z_IMG_9999_1475.JPG

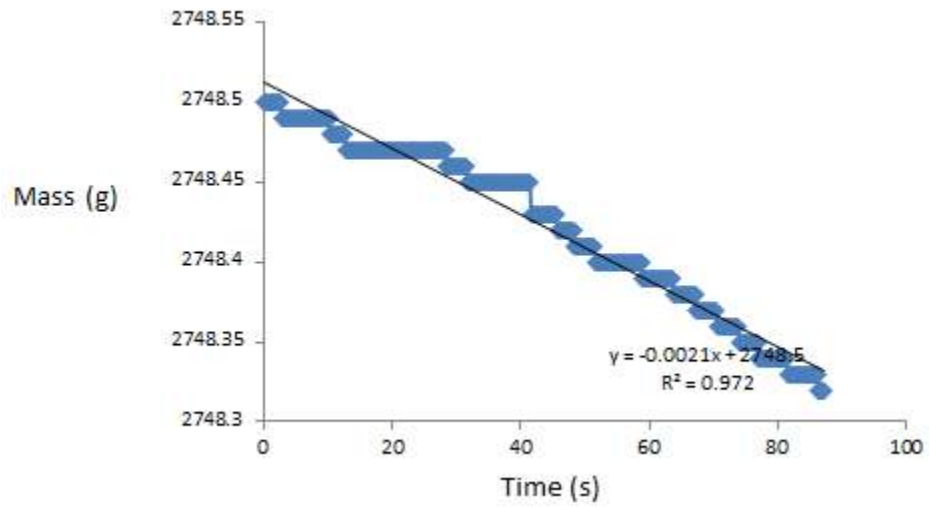


z_IMG_9999_1476.JPG



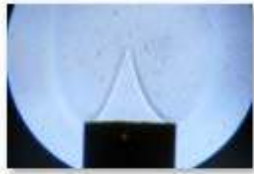
z_IMG_9999_1477.JPG

Experiment NO. 15

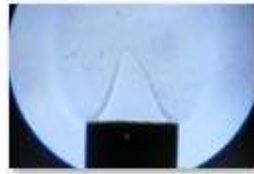


Air Flow Rate		Fuel Flow rate		Volume flow rate	nozzle width	U	Phi
SLP M	mole/sec	SLP M	mole/sec	m ³ /s	m	m/sec	
2.5	0.001732	0.21	0.00014 5	4.51E-05	0.01074 4	0.497869	0.7996 8

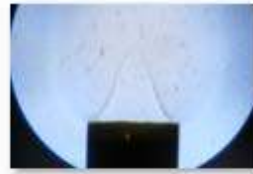
Entrainment Rate
 0.0021 g/sec
 Concentration
 46.5245
 5 g/m³



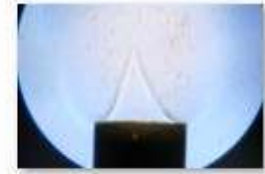
IMG_9999_1504.JPG



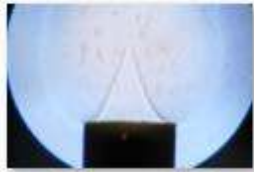
IMG_9999_1505.JPG



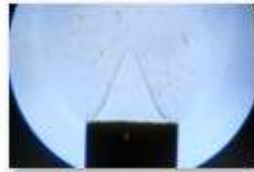
IMG_9999_1506.JPG



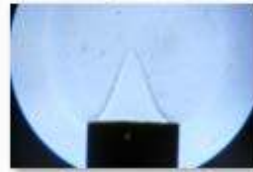
IMG_9999_1507.JPG



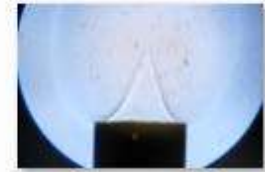
IMG_9999_1508.JPG



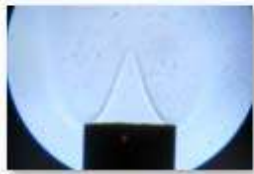
IMG_9999_1509.JPG



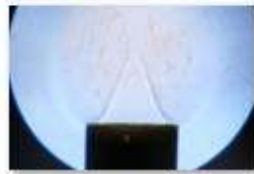
IMG_9999_1510.JPG



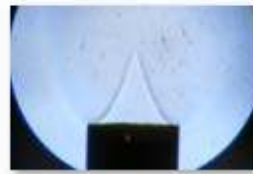
IMG_9999_1511.JPG



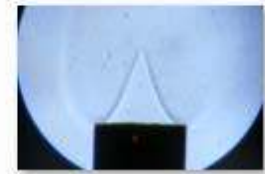
IMG_9999_1512.JPG



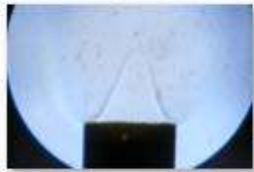
IMG_9999_1513.JPG



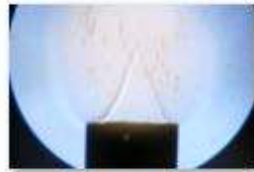
IMG_9999_1514.JPG



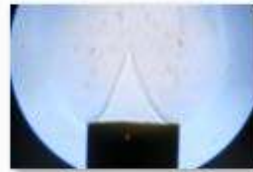
IMG_9999_1515.JPG



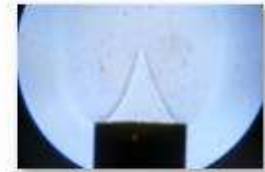
IMG_9999_1516.JPG



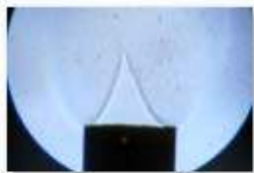
IMG_9999_1517.JPG



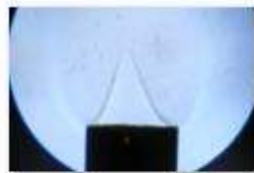
IMG_9999_1518.JPG



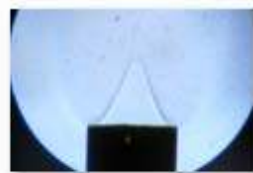
IMG_9999_1519.JPG



IMG_9999_1520.JPG



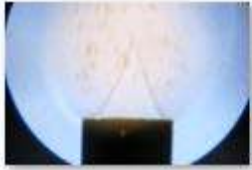
IMG_9999_1521.JPG



IMG_9999_1522.JPG



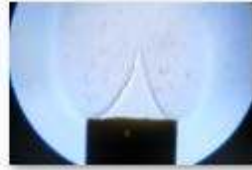
IMG_9999_1523.JPG



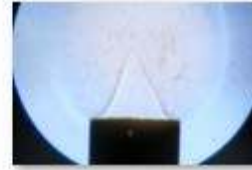
IMG_9999_1524.JPG



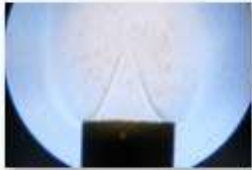
IMG_9999_1525.JPG



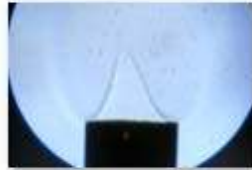
IMG_9999_1526.JPG



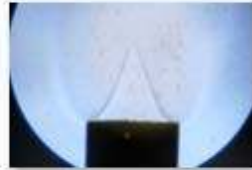
IMG_9999_1527.JPG



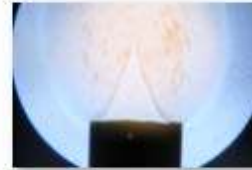
IMG_9999_1528.JPG



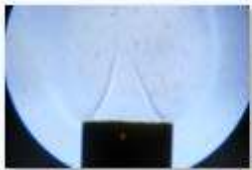
IMG_9999_1529.JPG



IMG_9999_1530.JPG



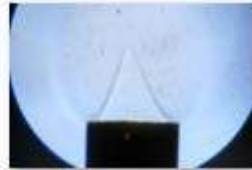
IMG_9999_1531.JPG



IMG_9999_1532.JPG



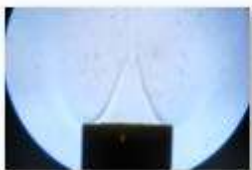
IMG_9999_1533.JPG



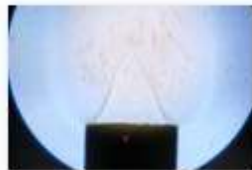
IMG_9999_1534.JPG



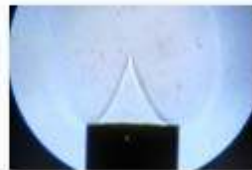
IMG_9999_1535.JPG



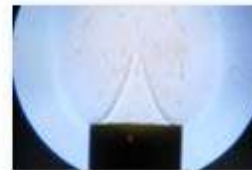
IMG_9999_1536.JPG



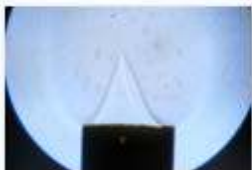
IMG_9999_1537.JPG



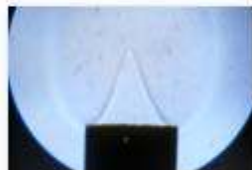
IMG_9999_1538.JPG



IMG_9999_1539.JPG



IMG_9999_1540.JPG



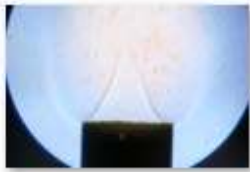
IMG_9999_1541.JPG



IMG_9999_1542.JPG



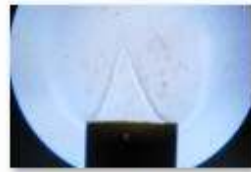
IMG_9999_1543.JPG



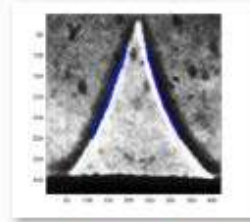
IMG_9999_1544.JPG



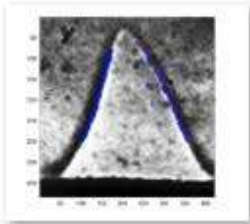
IMG_9999_1545.JPG



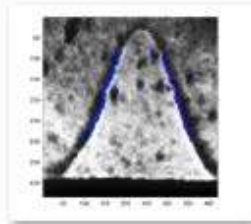
IMG_9999_1546.JPG



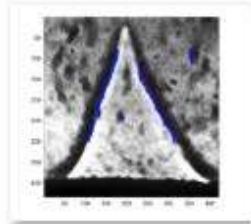
z_IMG_9999_1504.JPG



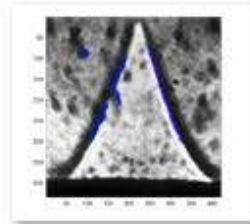
z_IMG_9999_1505.JPG



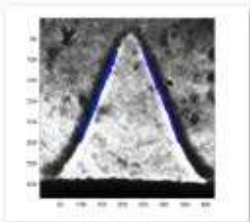
z_IMG_9999_1506.JPG



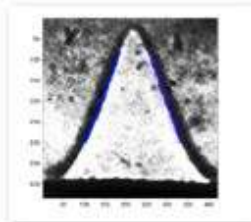
z_IMG_9999_1507.JPG



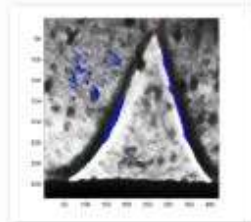
z_IMG_9999_1508.JPG



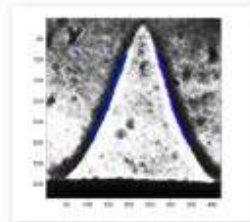
z_IMG_9999_1509.JPG



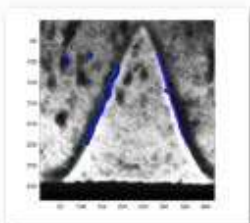
z_IMG_9999_1510.JPG



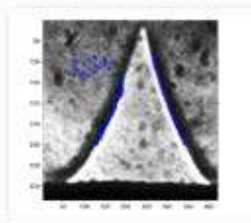
z_IMG_9999_1511.JPG



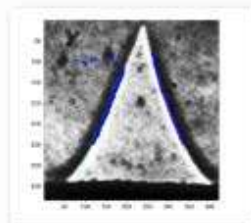
z_IMG_9999_1512.JPG



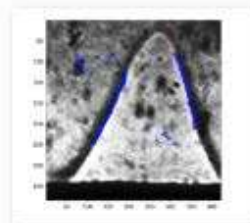
z_IMG_9999_1513.JPG



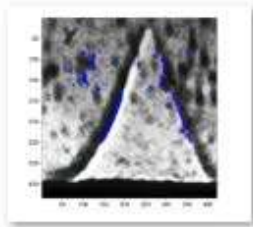
z_IMG_9999_1514.JPG



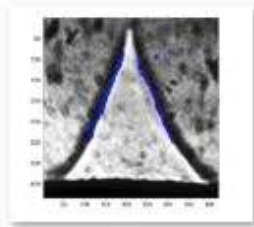
z_IMG_9999_1515.JPG



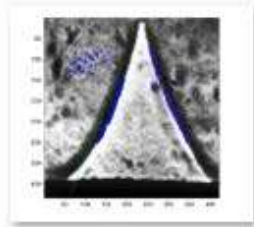
z_IMG_9999_1516.JPG



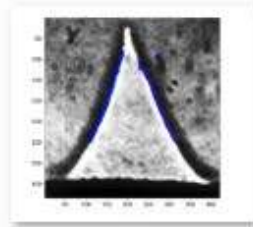
z_IMG_9999_1517.JPG



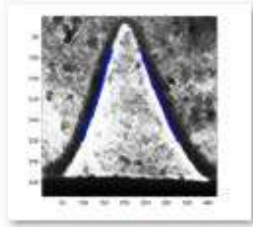
z_IMG_9999_1518.JPG



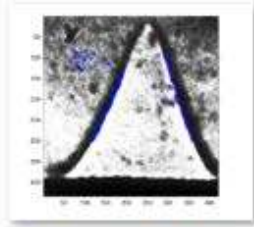
z_IMG_9999_1519.JPG



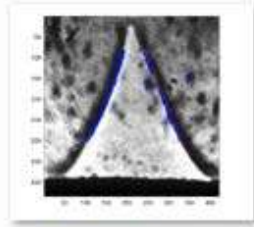
z_IMG_9999_1520.JPG



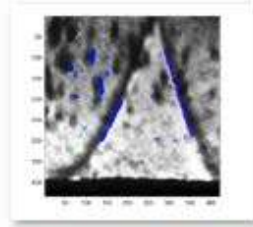
z_IMG_9999_1521.JPG



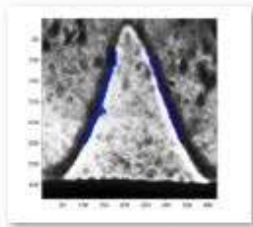
z_IMG_9999_1522.JPG



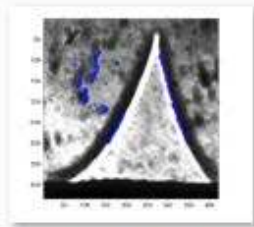
z_IMG_9999_1523.JPG



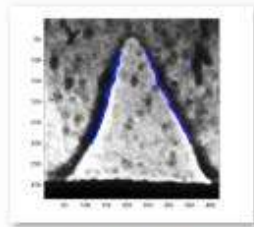
z_IMG_9999_1524.JPG



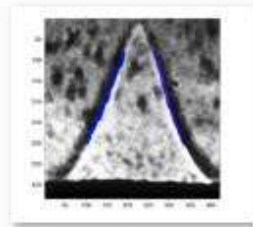
z_IMG_9999_1525.JPG



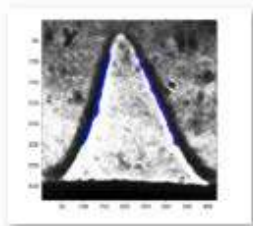
z_IMG_9999_1526.JPG



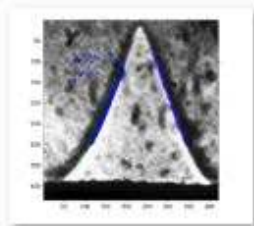
z_IMG_9999_1527.JPG



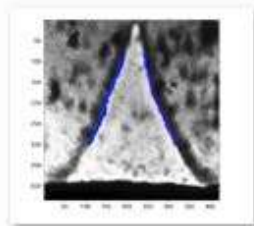
z_IMG_9999_1528.JPG



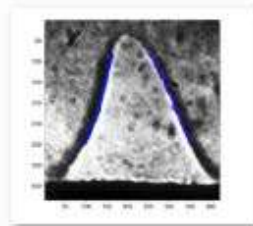
z_IMG_9999_1529.JPG



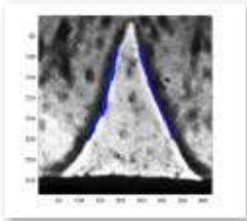
z_IMG_9999_1530.JPG



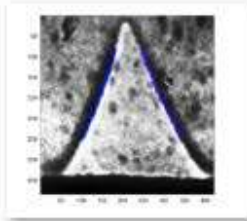
z_IMG_9999_1531.JPG



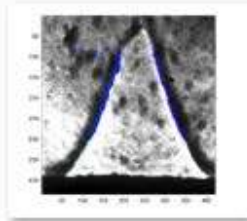
z_IMG_9999_1532.JPG



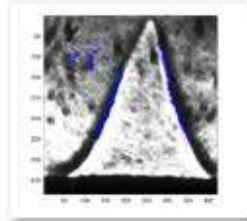
z_IMG_9999_1533.JPG



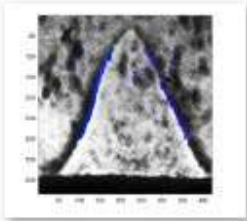
z_IMG_9999_1534.JPG



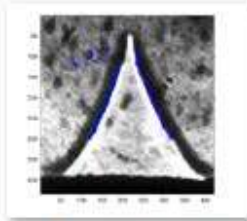
z_IMG_9999_1535.JPG



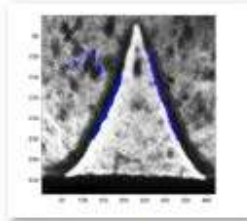
z_IMG_9999_1536.JPG



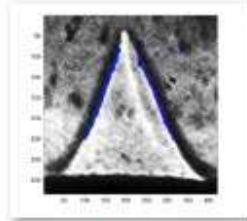
z_IMG_9999_1537.JPG



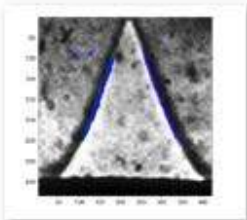
z_IMG_9999_1538.JPG



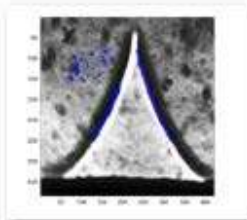
z_IMG_9999_1539.JPG



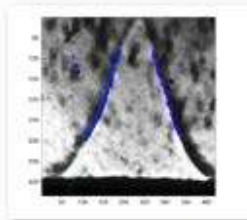
z_IMG_9999_1540.JPG



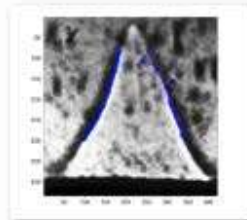
z_IMG_9999_1541.JPG



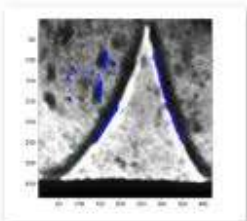
z_IMG_9999_1542.JPG



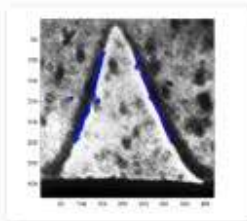
z_IMG_9999_1543.JPG



z_IMG_9999_1544.JPG



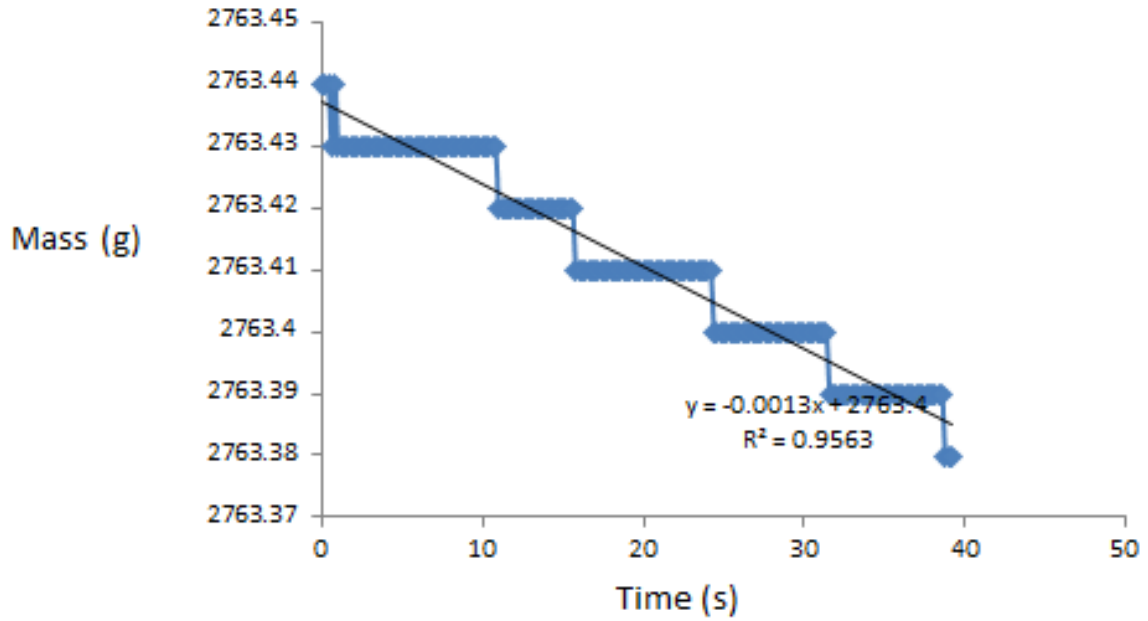
z_IMG_9999_1545.JPG



z_IMG_9999_1546.JPG

3.3 $\phi=0.85$; Flow Rate: Air 2.5 SLPM; Methane 0.223 SLPM

Experiment NO. 1

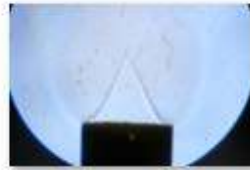


Air Flow Rate		Fuel Flow rate		Volume flow rate	nozzle width	U	Phi
SLPM	mole/sec	SLPM	mole/sec	m ³ /s	m	m/sec	
2.5	0.001732	0.223	0.000155	4.54E-05	0.010744	0.500255	0.849184

Entrainment Rate
 0.0013 g/sec
 Concentration
 28.66353 g/m³



IMG_9999_271.JPG



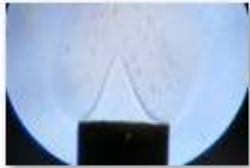
IMG_9999_273.JPG



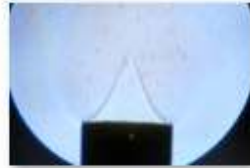
IMG_9999_275.JPG



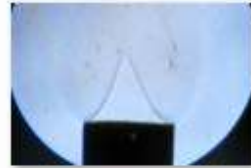
IMG_9999_280.JPG



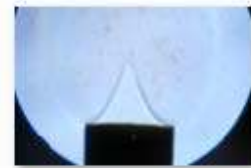
IMG_9999_282.JPG



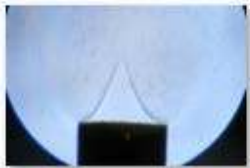
IMG_9999_287.JPG



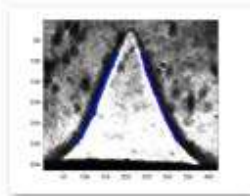
IMG_9999_288.JPG



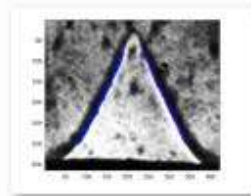
IMG_9999_290.JPG



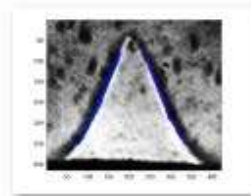
IMG_9999_291.JPG



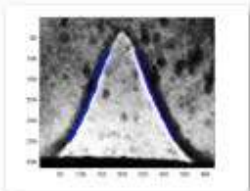
z_IMG_9999_271.JPG



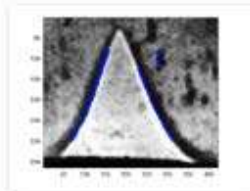
z_IMG_9999_273.JPG



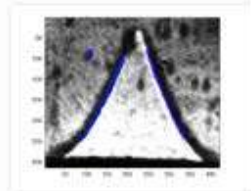
z_IMG_9999_275.JPG



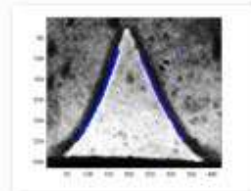
z_IMG_9999_280.JPG



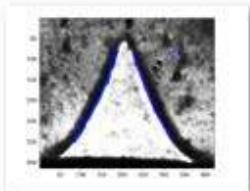
z_IMG_9999_282.JPG



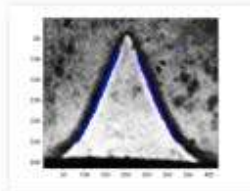
z_IMG_9999_287.JPG



z_IMG_9999_288.JPG

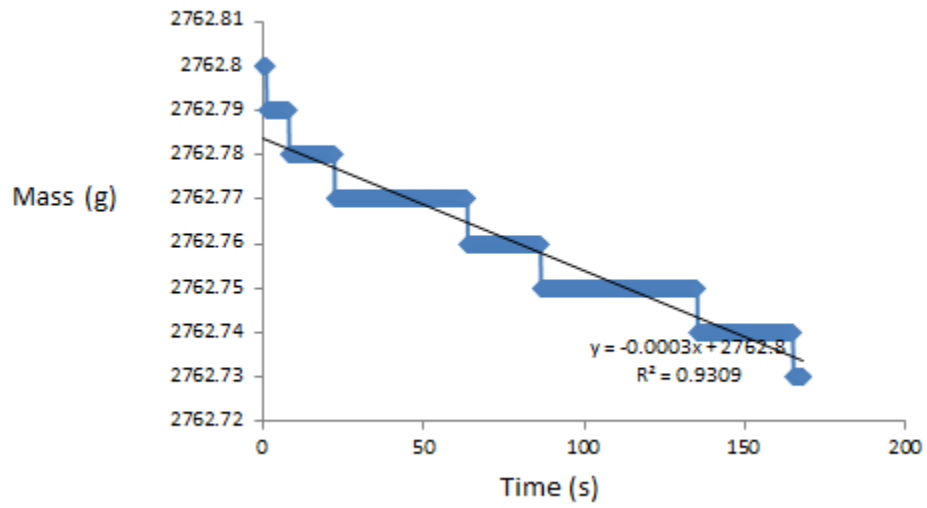


z_IMG_9999_290.JPG



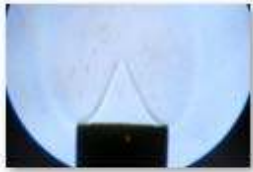
z_IMG_9999_291.JPG

Experiment NO. 2



Air Flow Rate		Fuel Flow rate		Volume flow rate	nozzle width	U	Phi
SLPM	mole/sec	SLPM	mole/sec	m ³ /s	m	m/sec	
2.5	0.001732	0.223	0.000155	4.54E-05	0.010744	0.500255	0.849184

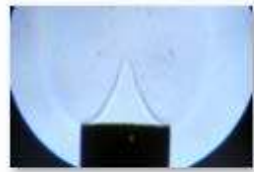
Entrainment Rate
 0.0003 g/sec
 Concentration
 6.614662 g/m³



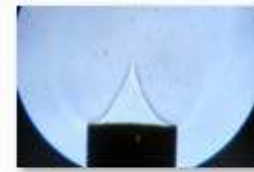
IMG_9999_300.JPG



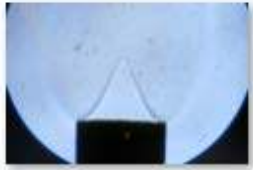
IMG_9999_307.JPG



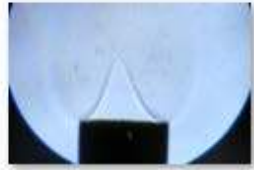
IMG_9999_311.JPG



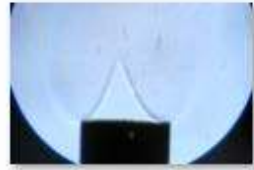
IMG_9999_312.JPG



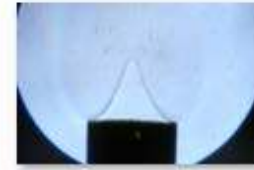
IMG_9999_314.JPG



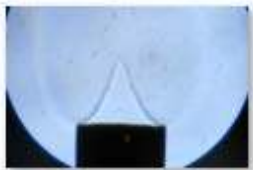
IMG_9999_315.JPG



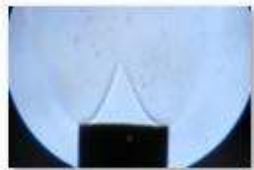
IMG_9999_316.JPG



IMG_9999_319.JPG



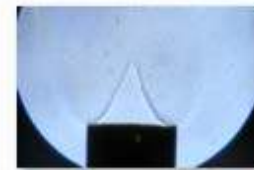
IMG_9999_323.JPG



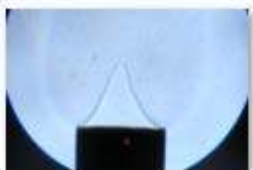
IMG_9999_326.JPG



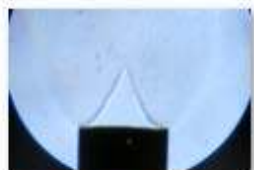
IMG_9999_331.JPG



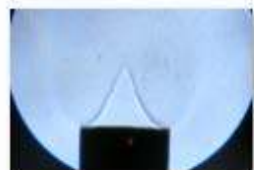
IMG_9999_339.JPG



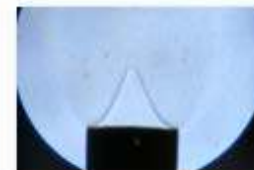
IMG_9999_343.JPG



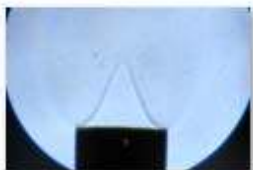
IMG_9999_362.JPG



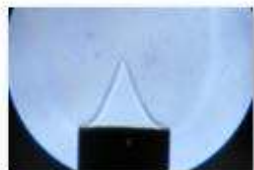
IMG_9999_382.JPG



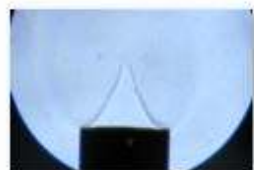
IMG_9999_383.JPG



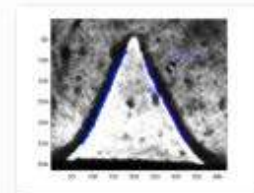
IMG_9999_385.JPG



IMG_9999_386.JPG

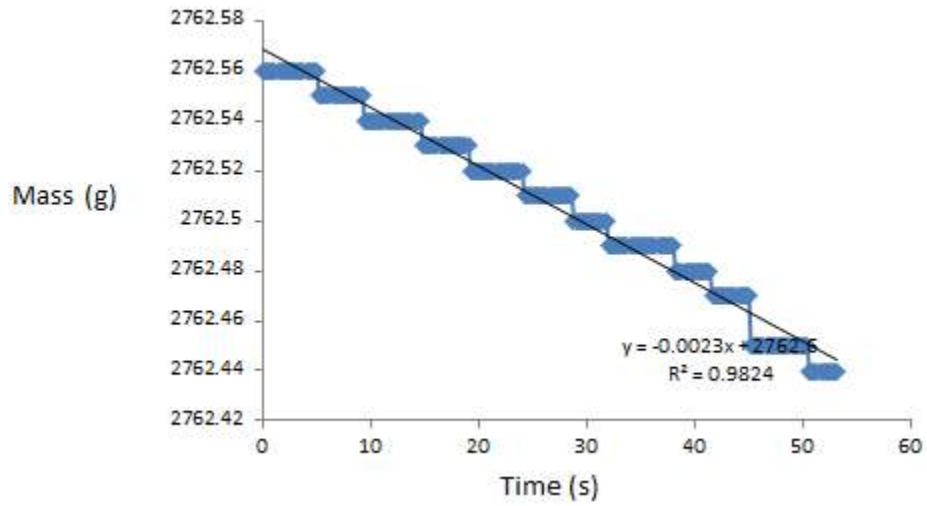


IMG_9999_388.JPG



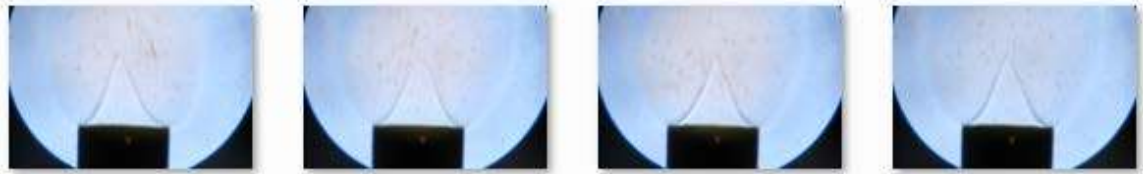
z_IMG_9999_300.JPG

Experiment NO. 4



Air Flow Rate		Fuel Flow rate		Volume flow rate	nozzle width	U	Phi
SLPM	mole/sec	SLPM	mole/sec	m ³ /s	m	m/sec	
2.5	0.001732	0.223	0.000155	4.54E-05	0.010744	0.500255	0.849184

Entrainment Rate
 0.0023 g/sec
 Concentration
 50.71241 g/m³

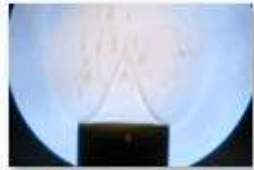


IMG_9999_440.JPG

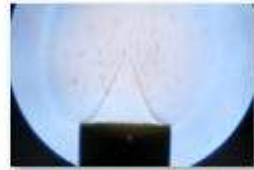
IMG_9999_441.JPG

IMG_9999_444.JPG

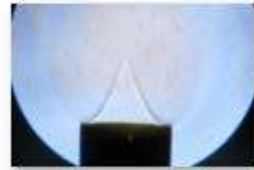
IMG_9999_446.JPG



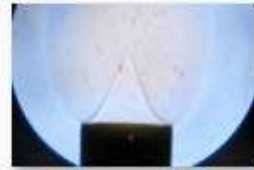
IMG_9999_452.JPG



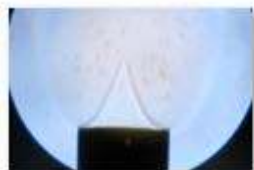
IMG_9999_459.JPG



IMG_9999_462.JPG



IMG_9999_463.JPG



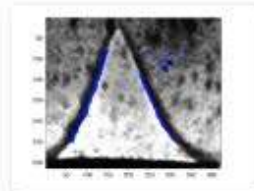
IMG_9999_464.JPG



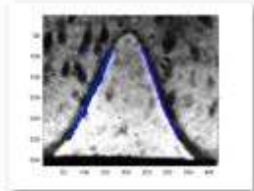
IMG_9999_466.JPG



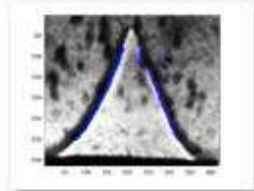
IMG_9999_470.JPG



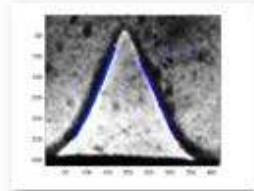
z_IMG_9999_440.JPG



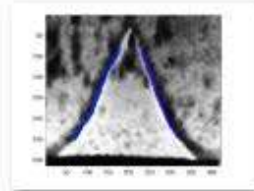
z_IMG_9999_441.JPG



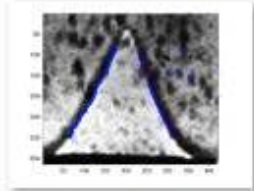
z_IMG_9999_444.JPG



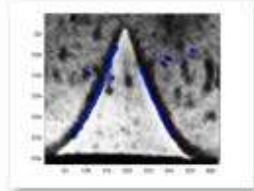
z_IMG_9999_446.JPG



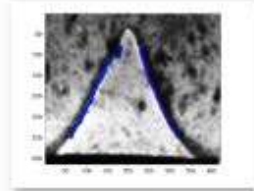
z_IMG_9999_452.JPG



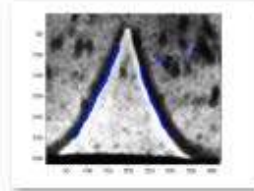
z_IMG_9999_459.JPG



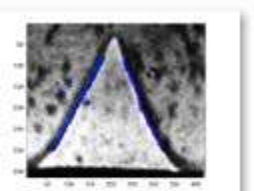
z_IMG_9999_462.JPG



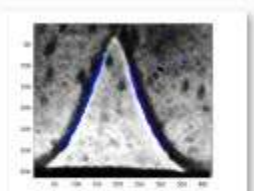
z_IMG_9999_463.JPG



z_IMG_9999_464.JPG

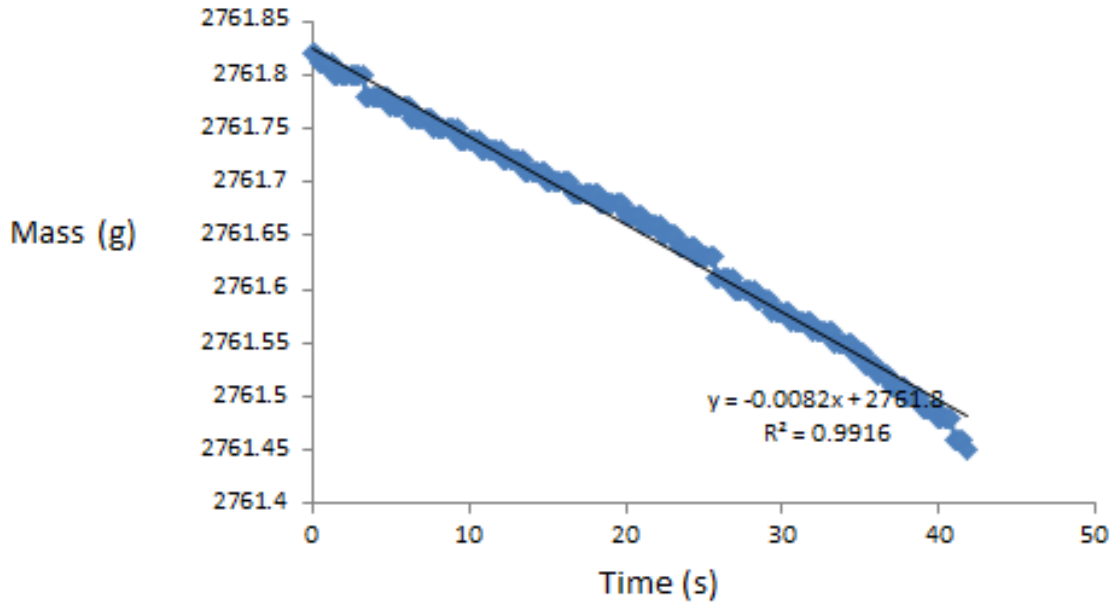


z_IMG_9999_466.JPG



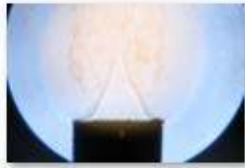
z_IMG_9999_470.JPG

Experiment NO. 5

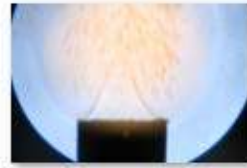


Air Flow Rate		Fuel Flow rate		Volume flow rate	nozzle width	U	Phi
SLPM	mole/sec	SLPM	mole/sec	m ³ /s	m	m/sec	
2.5	0.001732	0.223	0.000155	4.54E-05	0.010744	0.500255	0.849184

Entrainment Rate
 0.0082 g/sec
 Concentration
 180.8008 g/m³



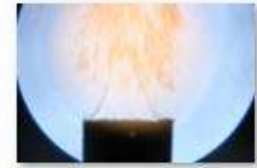
IMG_9999_475.JPG



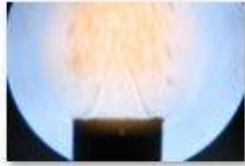
IMG_9999_482.JPG



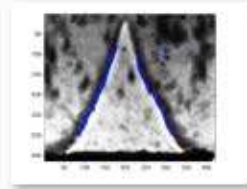
IMG_9999_483.JPG



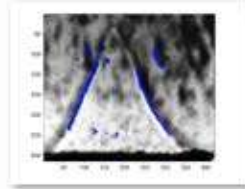
IMG_9999_486.JPG



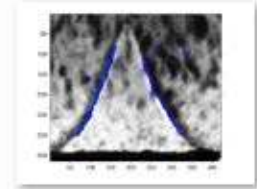
IMG_9999_488.JPG



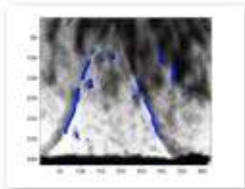
z_IMG_9999_475.JPG



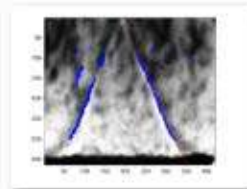
z_IMG_9999_482.JPG



z_IMG_9999_483.JPG

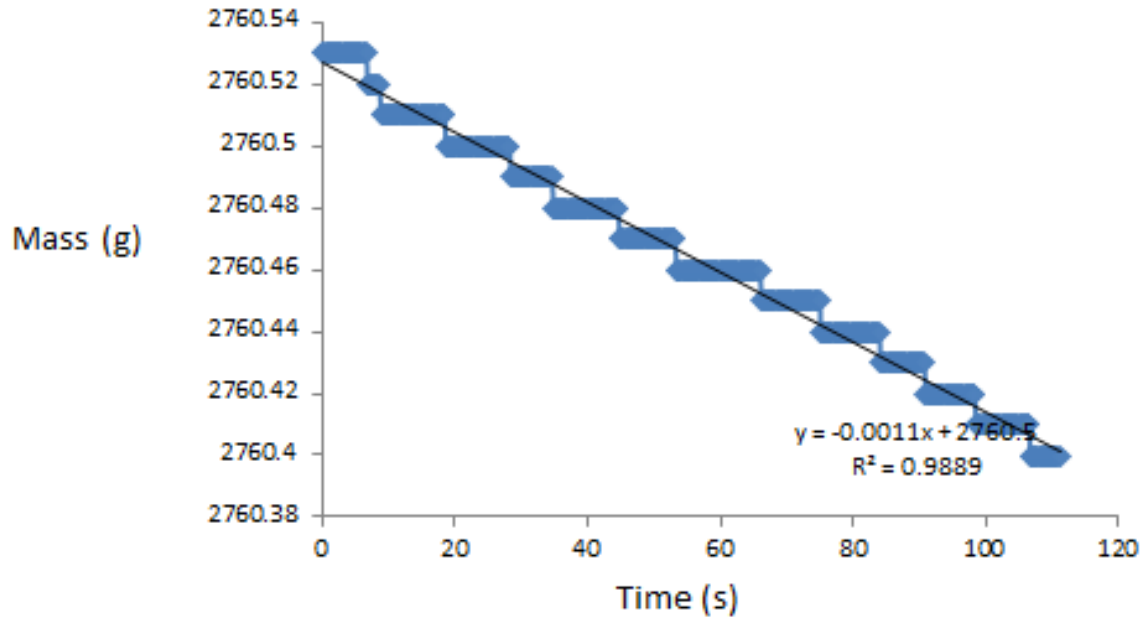


z_IMG_9999_486.JPG



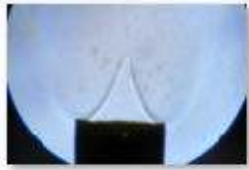
z_IMG_9999_488.JPG

Experiment NO. 6

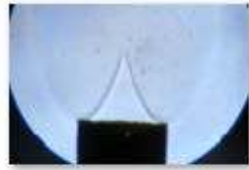


Air Flow Rate		Fuel Flow rate		Volume flow rate	nozzle width	U	Phi
SLPM	mole/sec	SLPM	mole/sec	m ³ /s	m	m/sec	
2.5	0.001732	0.223	0.000155	4.54E-05	0.010744	0.500255	0.849184

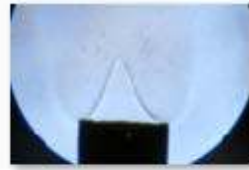
Entrainment Rate
0.0011 g/sec
Concentration
24.25376 g/m³



IMG_9999_504.JPG



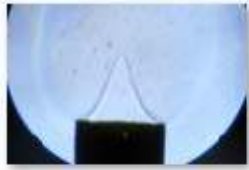
IMG_9999_506.JPG



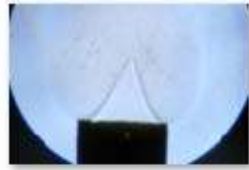
IMG_9999_513.JPG



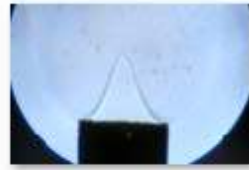
IMG_9999_528.JPG



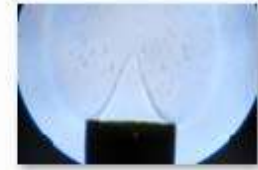
IMG_9999_537.JPG



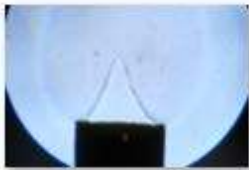
IMG_9999_542.JPG



IMG_9999_589.JPG



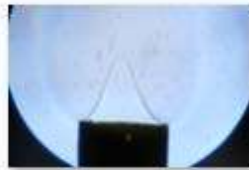
IMG_9999_595.JPG



IMG_9999_596.JPG



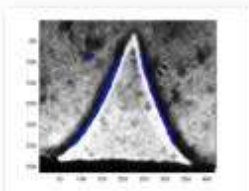
IMG_9999_597.JPG



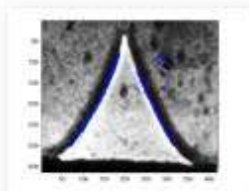
IMG_9999_598.JPG



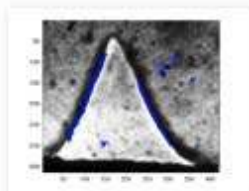
IMG_9999_599.JPG



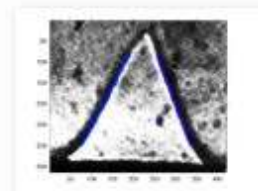
z_IMG_9999_504.JPG



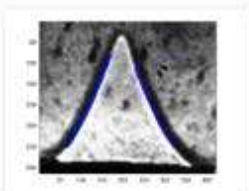
z_IMG_9999_506.JPG



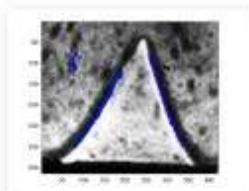
z_IMG_9999_513.JPG



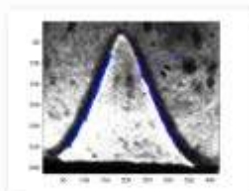
z_IMG_9999_528.JPG



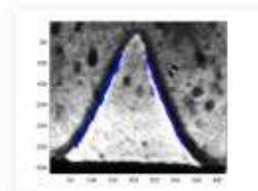
z_IMG_9999_537.JPG



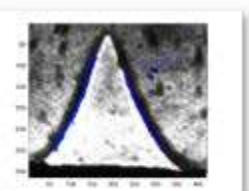
z_IMG_9999_542.JPG



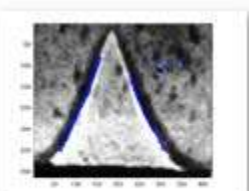
z_IMG_9999_589.JPG



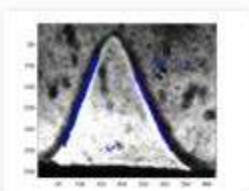
z_IMG_9999_595.JPG



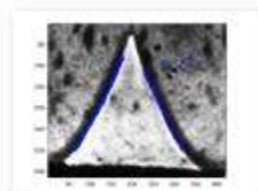
z_IMG_9999_596.JPG



z_IMG_9999_597.JPG

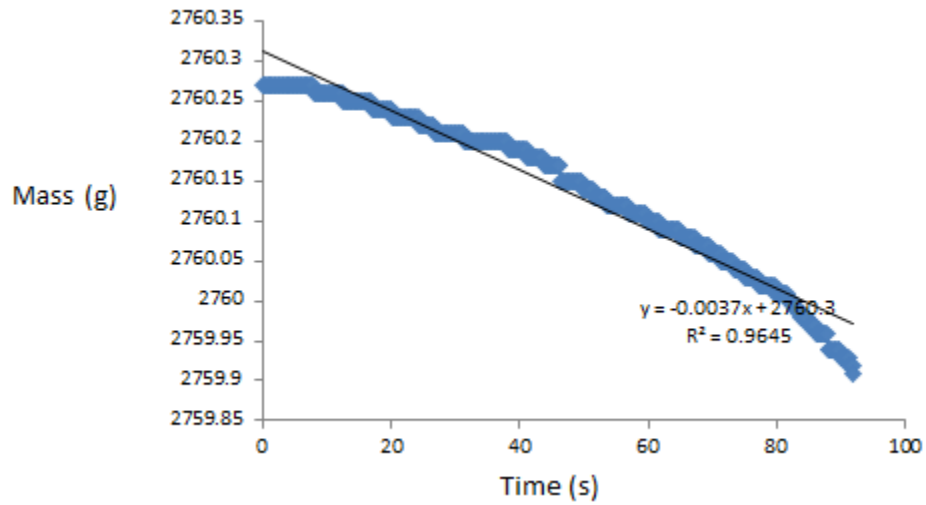


z_IMG_9999_598.JPG



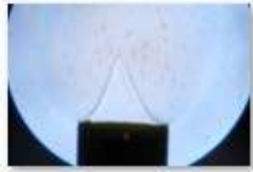
z_IMG_9999_599.JPG

Experiment NO. 7

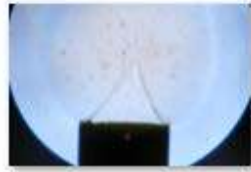


Air Flow Rate		Fuel Flow rate		Volume flow rate	nozzle width	U	Phi
SLPM	mole/sec	SLPM	mole/sec	m3/s	m	m/sec	
2.5	0.001732	0.223	0.000155	4.54E-05	0.010744	0.500255	0.849184

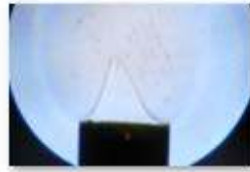
Entrainment Rate
 0.0037 g/sec
 Concentration
 81.58083 g/m³



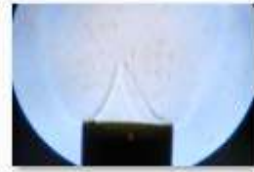
IMG_9999_604.JPG



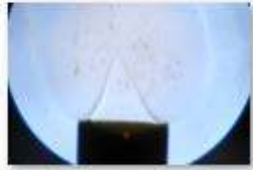
IMG_9999_605.JPG



IMG_9999_606.JPG



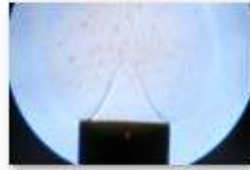
IMG_9999_607.JPG



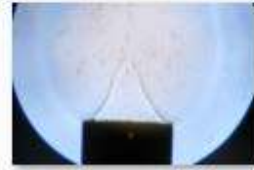
IMG_9999_608.JPG



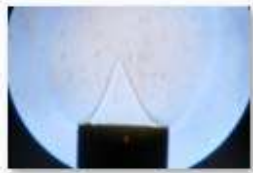
IMG_9999_609.JPG



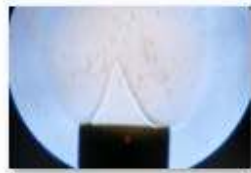
IMG_9999_610.JPG



IMG_9999_611.JPG



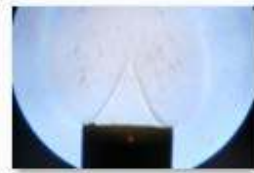
IMG_9999_612.JPG



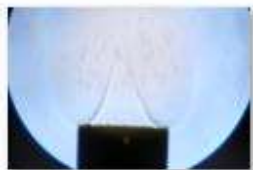
IMG_9999_613.JPG



IMG_9999_614.JPG



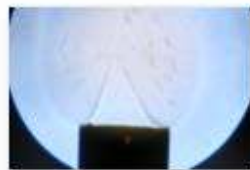
IMG_9999_615.JPG



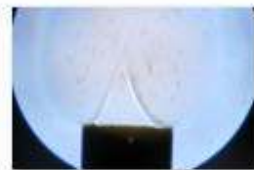
IMG_9999_616.JPG



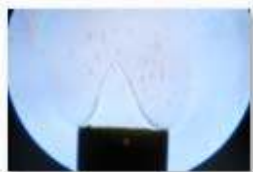
IMG_9999_617.JPG



IMG_9999_618.JPG



IMG_9999_619.JPG



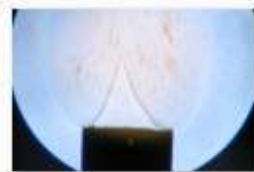
IMG_9999_620.JPG



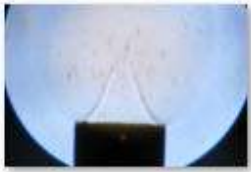
IMG_9999_621.JPG



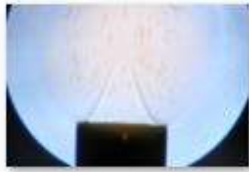
IMG_9999_622.JPG



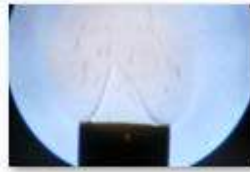
IMG_9999_623.JPG



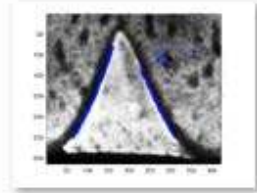
IMG_9999_624.JPG



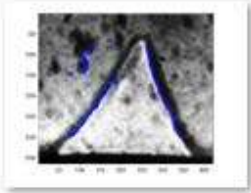
IMG_9999_625.JPG



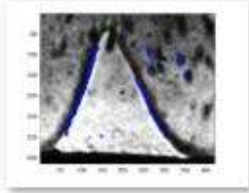
IMG_9999_626.JPG



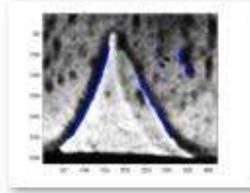
z_IMG_9999_604.JPG



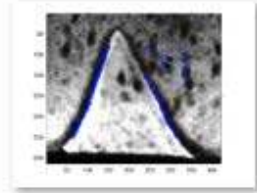
z_IMG_9999_605.JPG



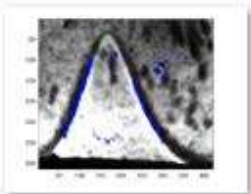
z_IMG_9999_606.JPG



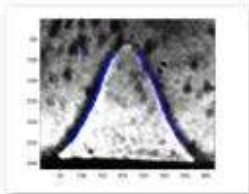
z_IMG_9999_607.JPG



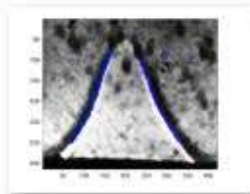
z_IMG_9999_608.JPG



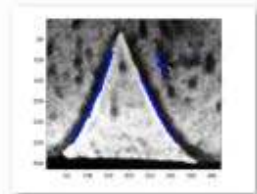
z_IMG_9999_609.JPG



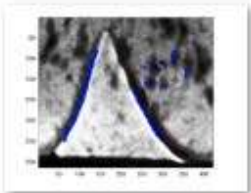
z_IMG_9999_610.JPG



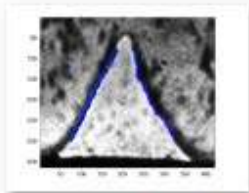
z_IMG_9999_611.JPG



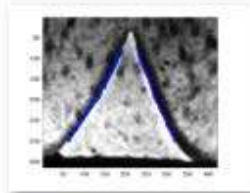
z_IMG_9999_612.JPG



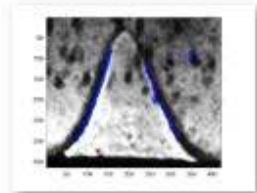
z_IMG_9999_613.JPG



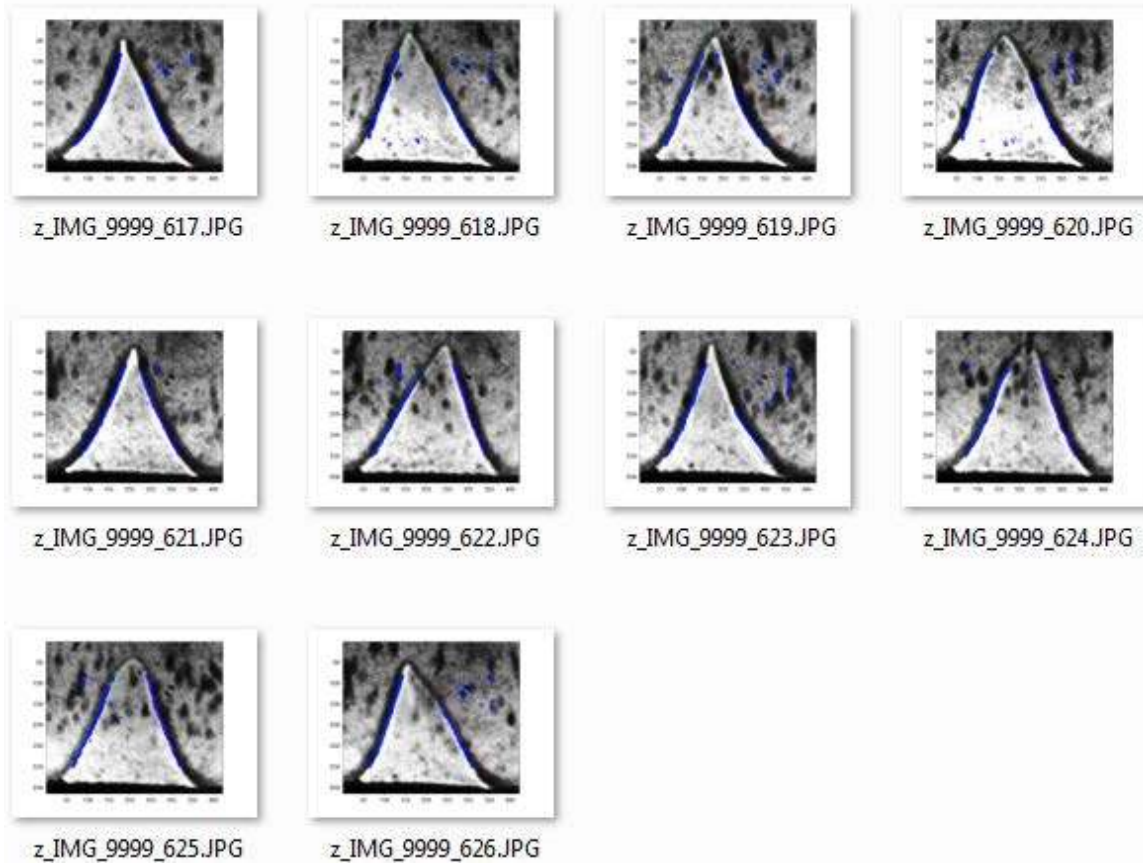
z_IMG_9999_614.JPG



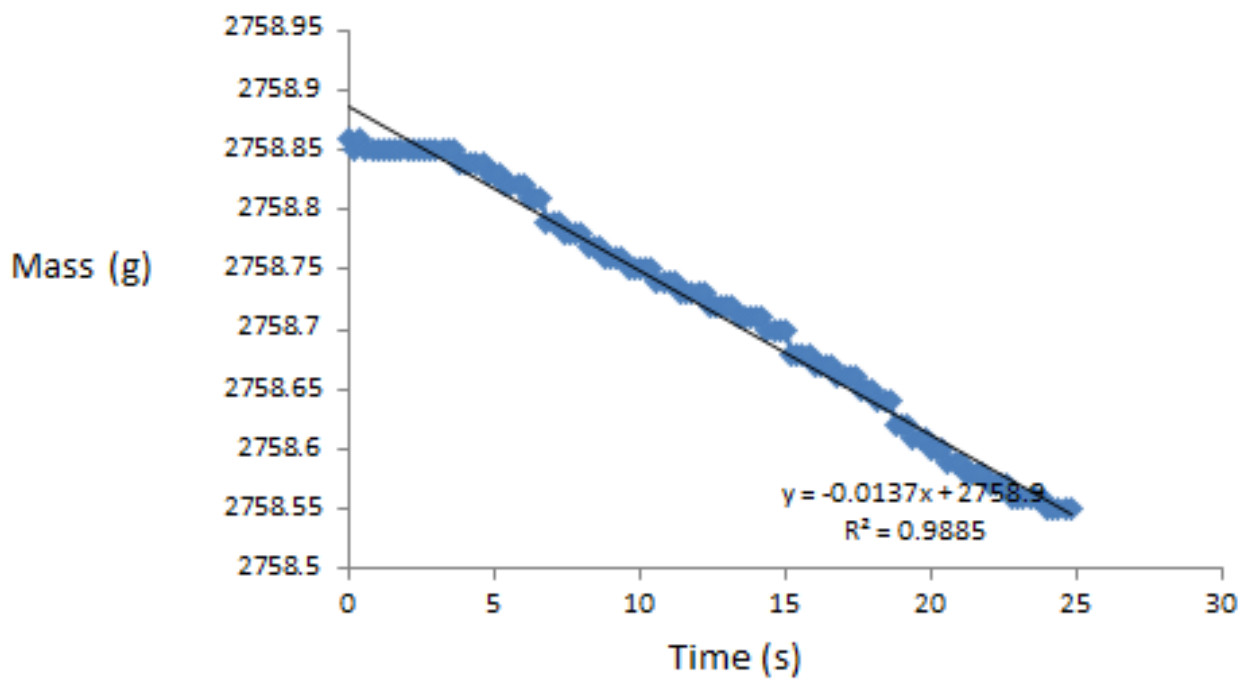
z_IMG_9999_615.JPG



z_IMG_9999_616.JPG

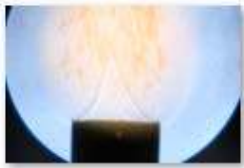


Experiment NO.8



Air Flow Rate		Fuel Flow rate		Volume flow rate	nozzle width	U	Phi
SLPM	mole/sec	SLPM	mole/sec	m3/s	m	m/sec	
2.5	0.001732	0.223	0.000155	4.54E-05	0.010744	0.500255	0.849184

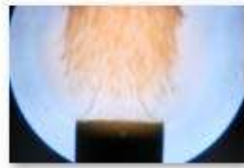
Entrainment Rate
0.0137 g/sec
Concentration
302.0696 g/m³



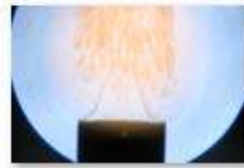
IMG_9999_740.JPG



IMG_9999_742.JPG



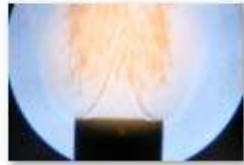
IMG_9999_743.JPG



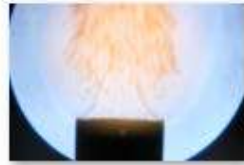
IMG_9999_744.JPG



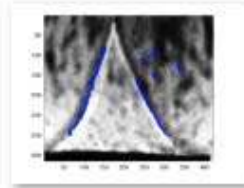
IMG_9999_745.JPG



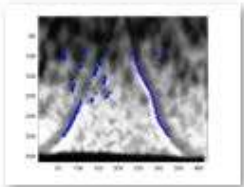
IMG_9999_746.JPG



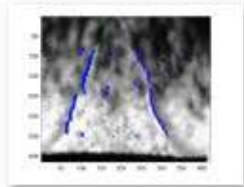
IMG_9999_749.JPG



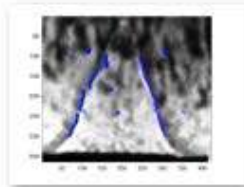
z_IMG_9999_740.JPG



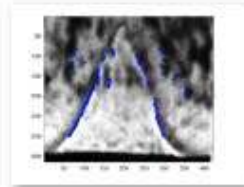
z_IMG_9999_742.JPG



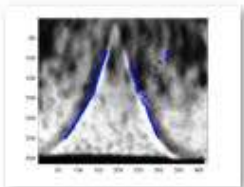
z_IMG_9999_743.JPG



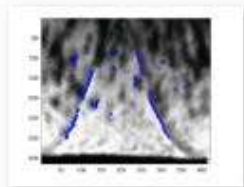
z_IMG_9999_744.JPG



z_IMG_9999_745.JPG

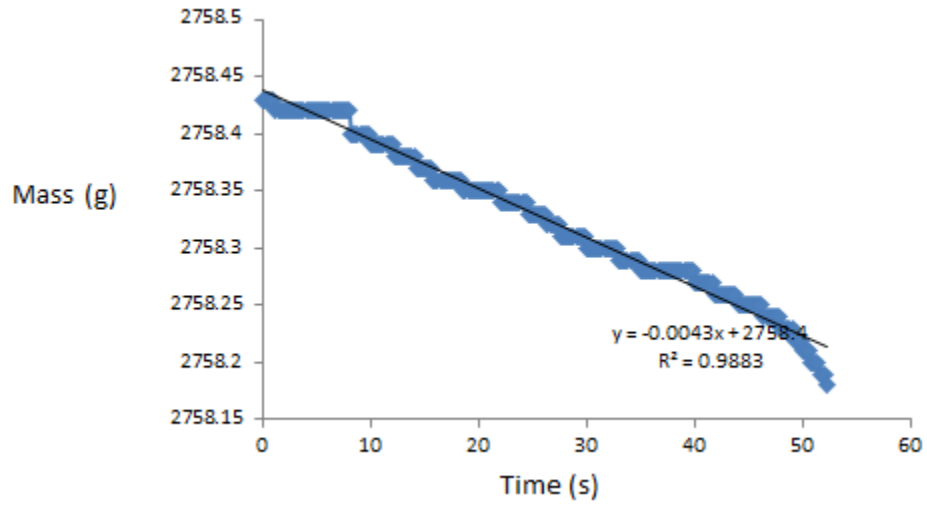


z_IMG_9999_746.JPG



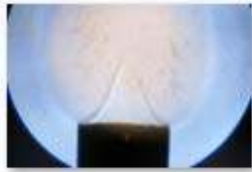
z_IMG_9999_749.JPG

Experiment NO. 9

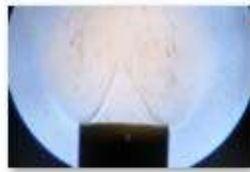


Air Flow Rate		Fuel Flow rate		Volume flow rate	nozzle width	U	Phi
SLPM	mole/sec	SLPM	mole/sec	m ³ /s	m	m/sec	
2.5	0.001732	0.223	0.000155	4.54E-05	0.010744	0.500255	0.849184

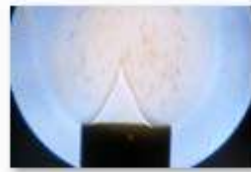
Entrainment Rate
 0.0043 g/sec
 Concentration
 94.81015 g/m³



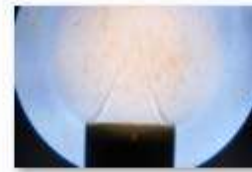
IMG_9999_753.JPG



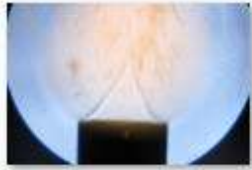
IMG_9999_754.JPG



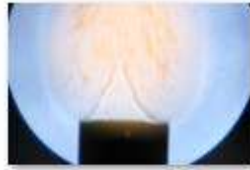
IMG_9999_755.JPG



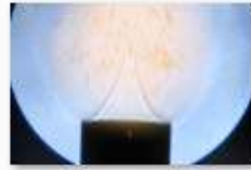
IMG_9999_756.JPG



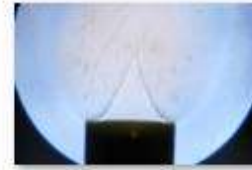
IMG_9999_757.JPG



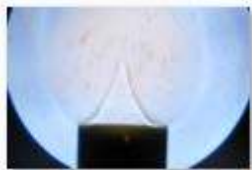
IMG_9999_758.JPG



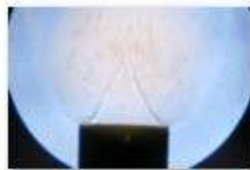
IMG_9999_759.JPG



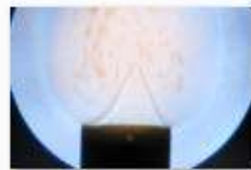
IMG_9999_760.JPG



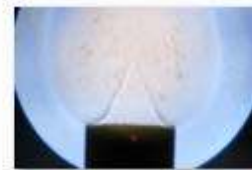
IMG_9999_761.JPG



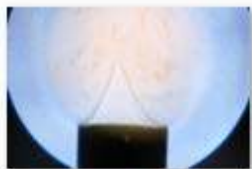
IMG_9999_762.JPG



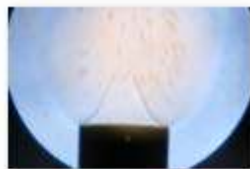
IMG_9999_763.JPG



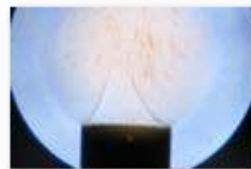
IMG_9999_764.JPG



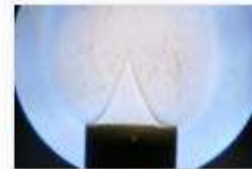
IMG_9999_765.JPG



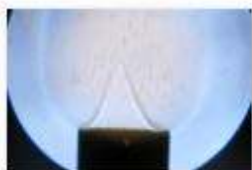
IMG_9999_766.JPG



IMG_9999_767.JPG



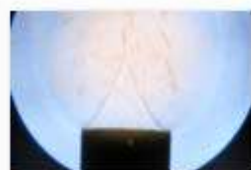
IMG_9999_768.JPG



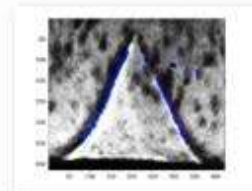
IMG_9999_769.JPG



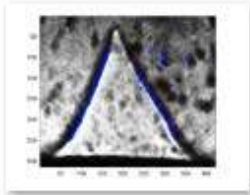
IMG_9999_770.JPG



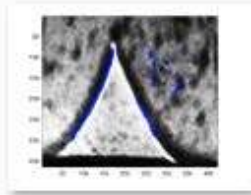
IMG_9999_771.JPG



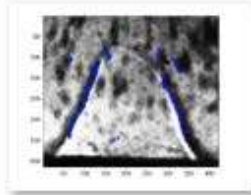
z_IMG_9999_753.JPG



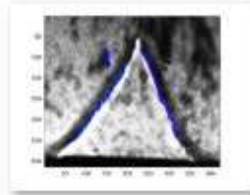
z_IMG_9999_754.JPG



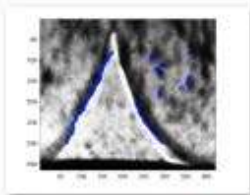
z_IMG_9999_755.JPG



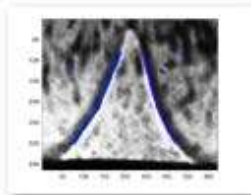
z_IMG_9999_756.JPG



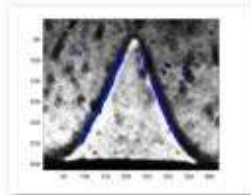
z_IMG_9999_757.JPG



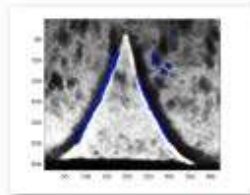
z_IMG_9999_758.JPG



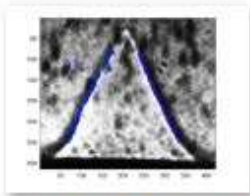
z_IMG_9999_759.JPG



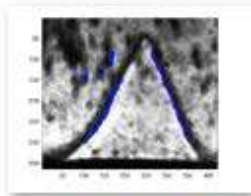
z_IMG_9999_760.JPG



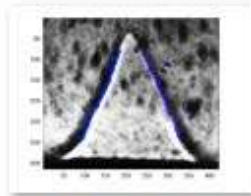
z_IMG_9999_761.JPG



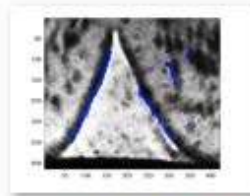
z_IMG_9999_762.JPG



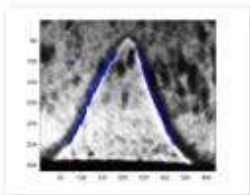
z_IMG_9999_763.JPG



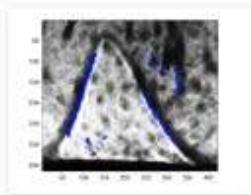
z_IMG_9999_764.JPG



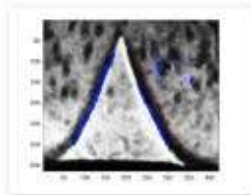
z_IMG_9999_765.JPG



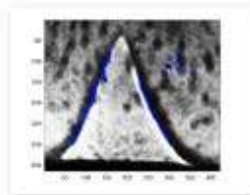
z_IMG_9999_766.JPG



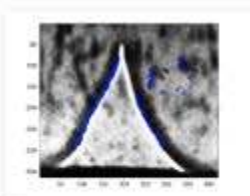
z_IMG_9999_767.JPG



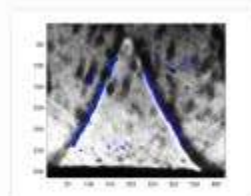
z_IMG_9999_768.JPG



z_IMG_9999_769.JPG

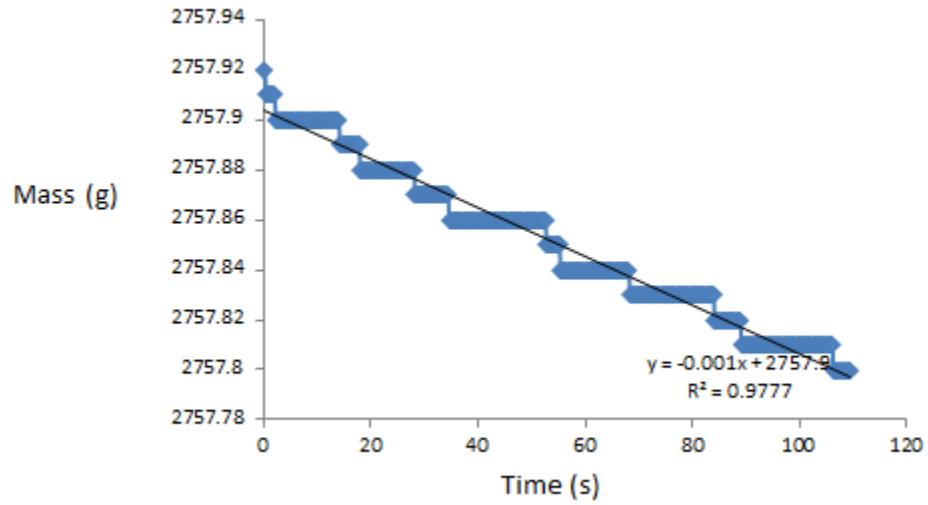


z_IMG_9999_770.JPG



z_IMG_9999_771.JPG

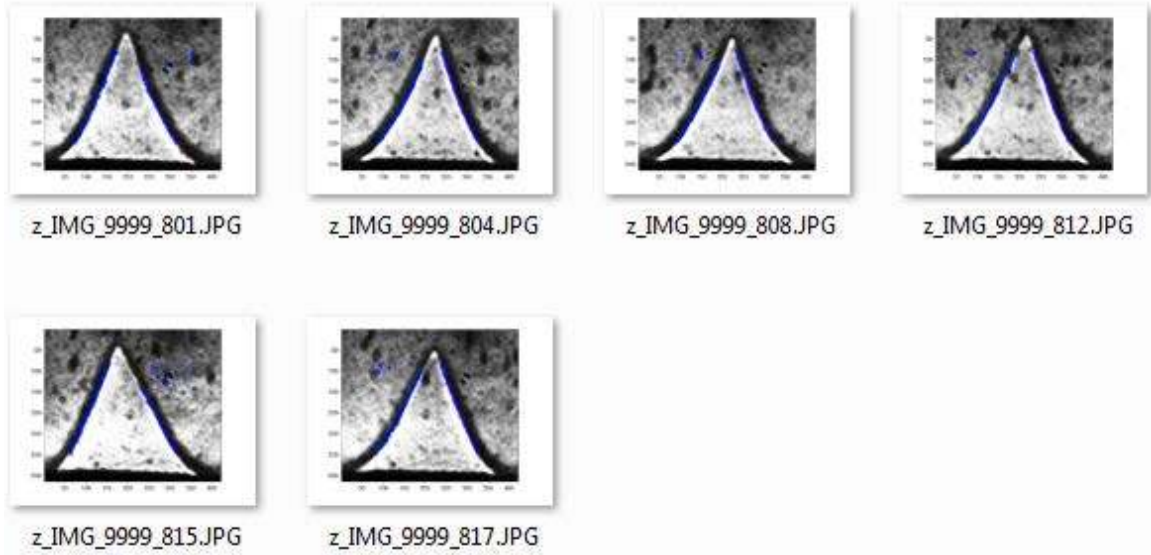
Experiment NO. 10



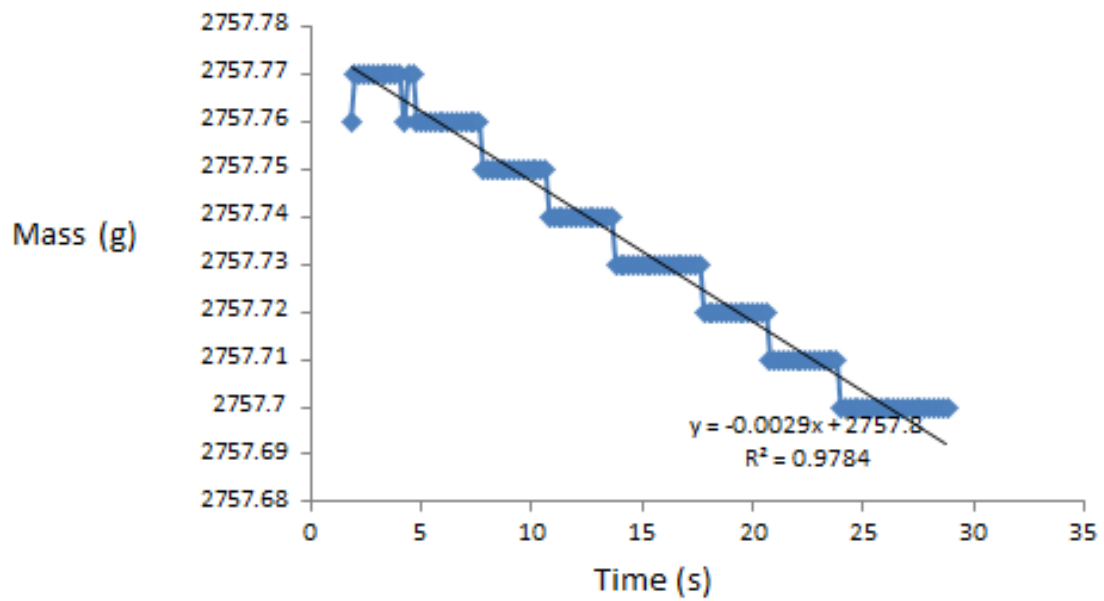
Air Flow Rate		Fuel Flow rate		Volume flow rate	nozzle width	U	Phi
SLPM	mole/sec	SLPM	mole/sec	m ³ /s	m	m/sec	
2.5	0.001732	0.223	0.000155	4.54E-05	0.010744	0.500255	0.849184

Entrainment Rate
 0.0003 g/sec
 Concentration
 6.614662 g/m³



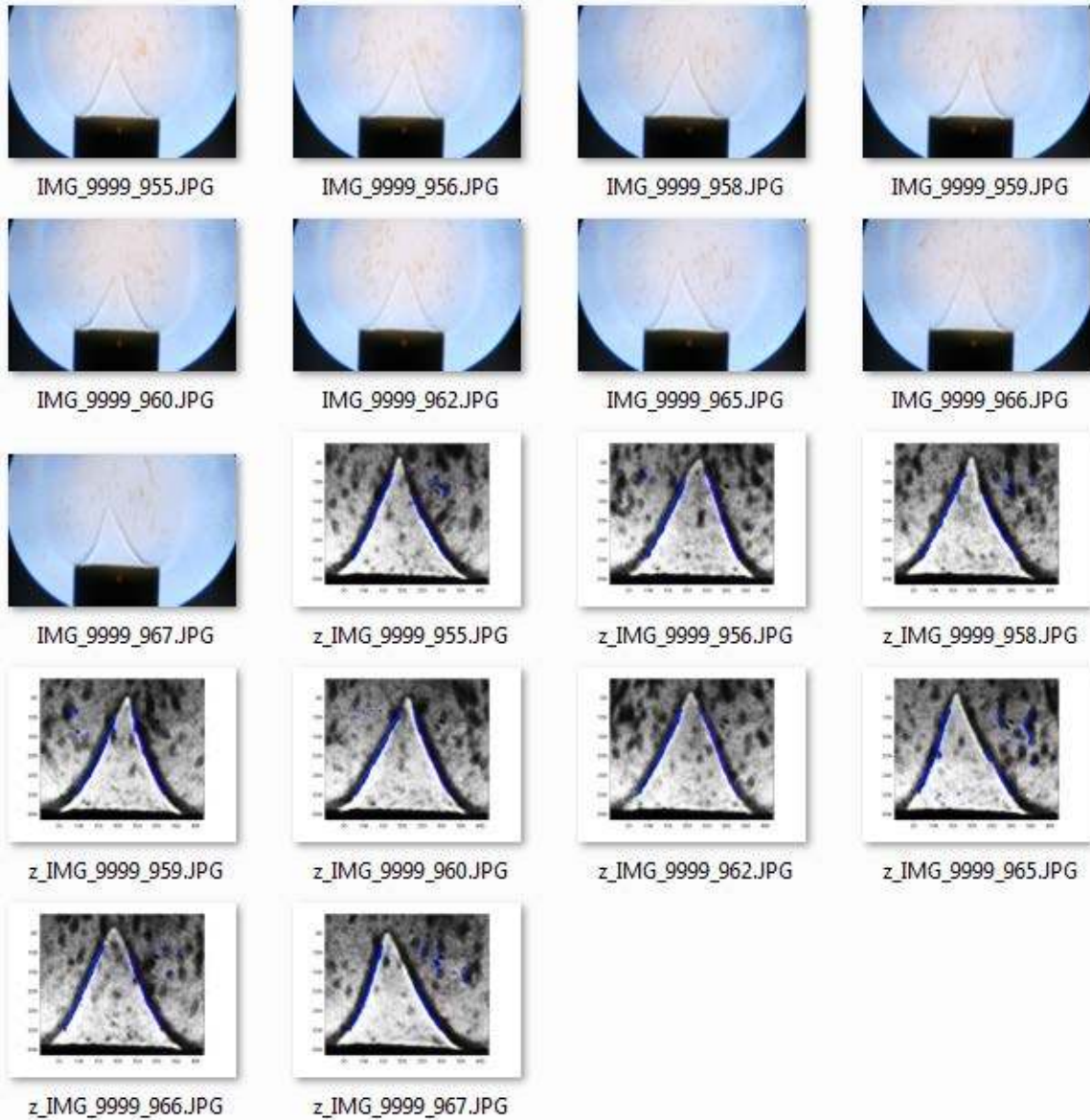


Experiment NO. 11



Air Flow Rate		Fuel Flow rate		Volume flow rate	nozzle width	U	Phi
SLPM	mole/sec	SLPM	mole/sec	m ³ /s	m	m/sec	
2.5	0.001732	0.223	0.000155	4.54E-05	0.010744	0.500255	0.849184

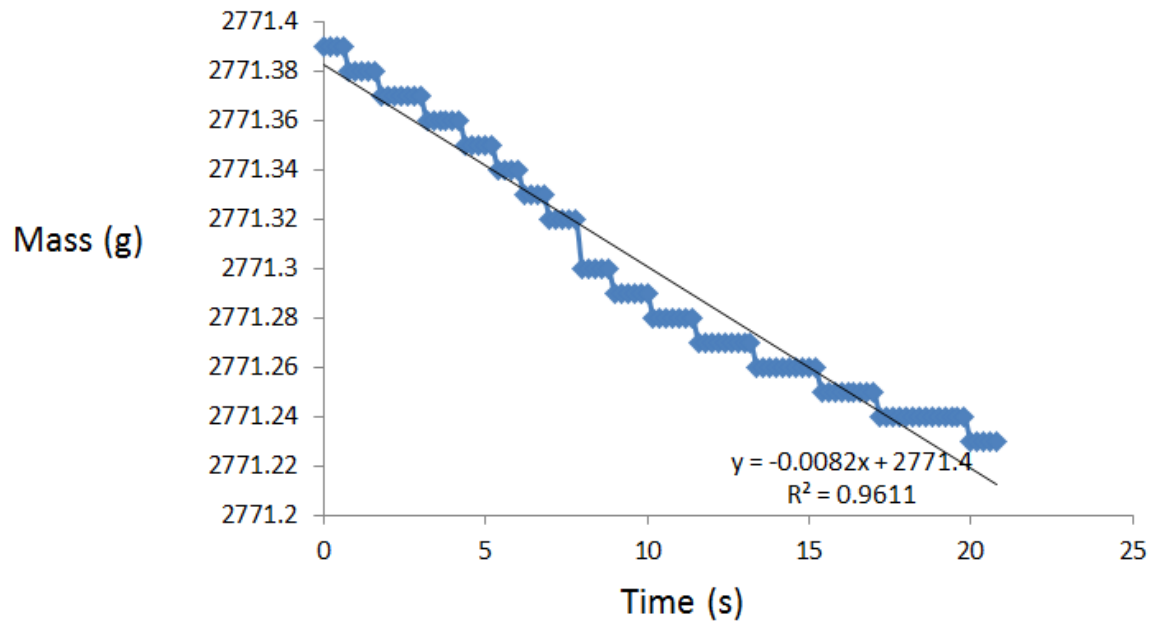
Entrainment Rate
0.0029 g/sec
Concentration
63.94173 g/m³



4. Coal Particles (53-63 μm)

4.1 $\phi=0.80$; Flow Rate: Air 2.5 SLPM; Methane 0.21 SLPM

Experiment NO. 5



Air Flow Rate		Fuel Flow rate		Volume flow rate	nozzle width	U	Phi
SLPM	mole/sec	SLPM	mole/sec	m ³ /s	m	m/sec	
2.5	0.001732	0.21	0.000145	4.51E-05	0.010744	0.497869	0.79968

Entrainment Rate
8.20E-03 g/sec
Concentration
181.6673 g/m³



IMG_1188.JPG



IMG_1189.JPG



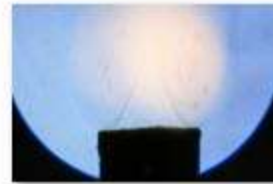
IMG_1190.JPG



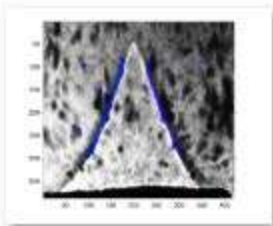
IMG_1192.JPG



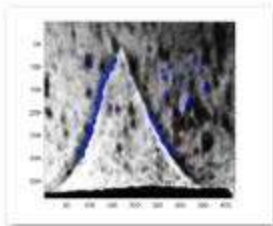
IMG_1194.JPG



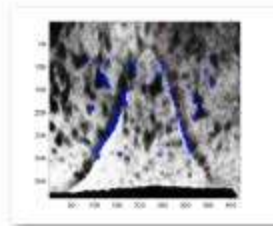
IMG_1195.JPG



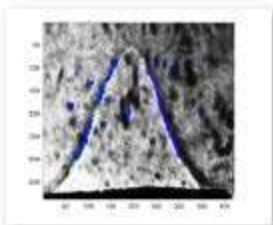
z_IMG_1188.JPG



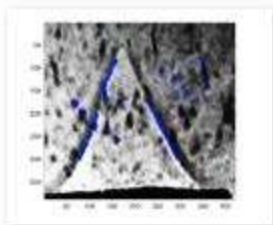
z_IMG_1189.JPG



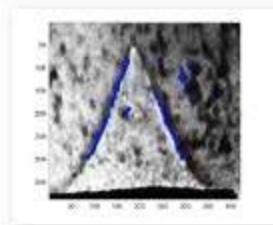
z_IMG_1190.JPG



z_IMG_1192.JPG

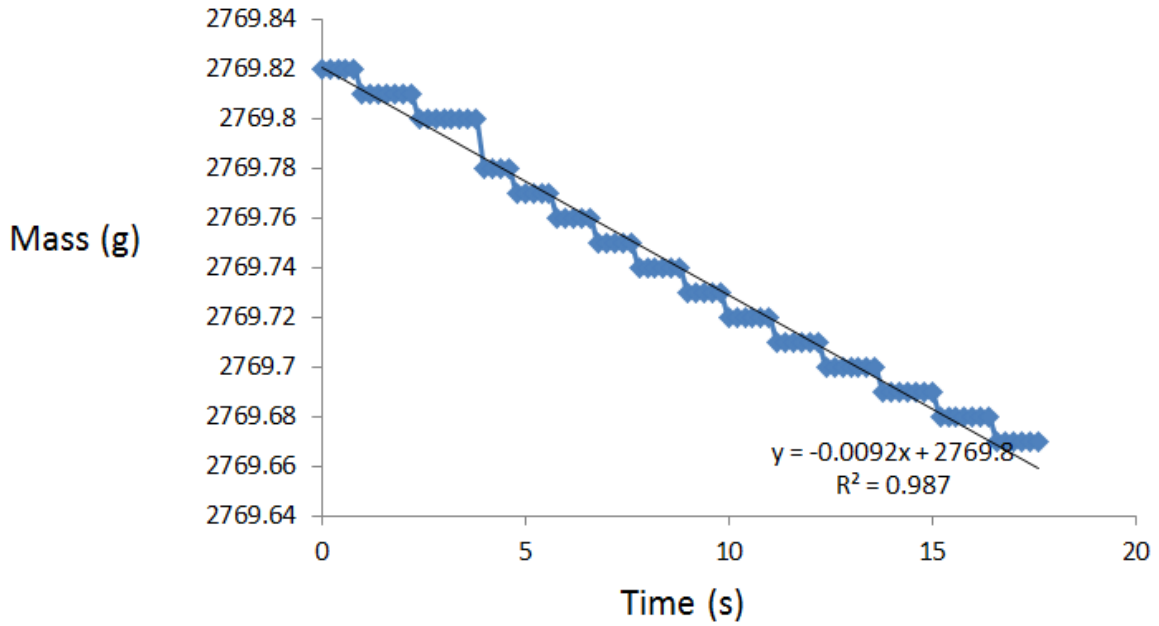


z_IMG_1194.JPG



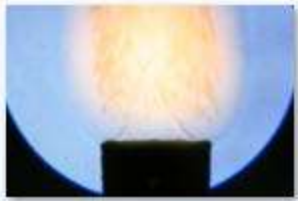
z_IMG_1195.JPG

Experiment NO. 6

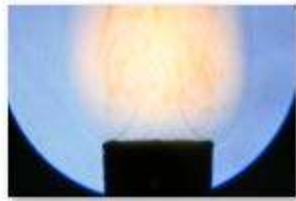


Air Flow Rate		Fuel Flow rate		Volume flow rate	nozzle width	U	Phi
SLPM	mole/sec	SLPM	mole/sec	m ³ /s	m	m/sec	
2.5	0.001732	0.21	0.000145	4.51E-05	0.010744	0.497869	0.79968

Entrainment Rate
 9.20E-03 g/sec
 Concentration
 203.8218 g/m³



IMG_1201.JPG



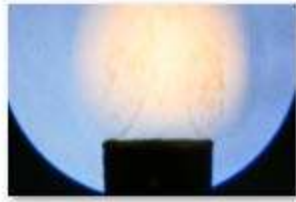
IMG_1202.JPG



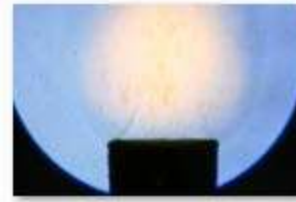
IMG_1203.JPG



IMG_1204.JPG



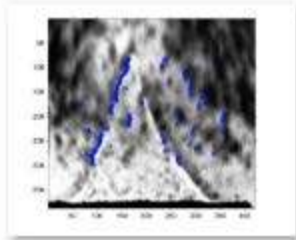
IMG_1205.JPG



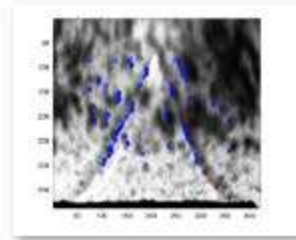
IMG_1206.JPG



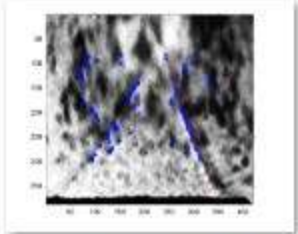
IMG_1207.JPG



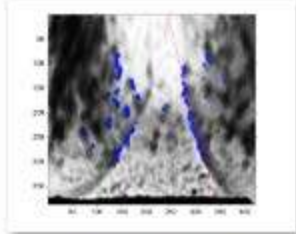
z_IMG_1201.JPG



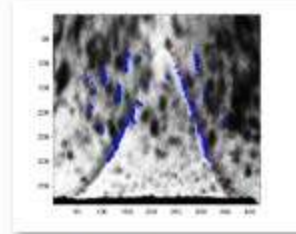
z_IMG_1202.JPG



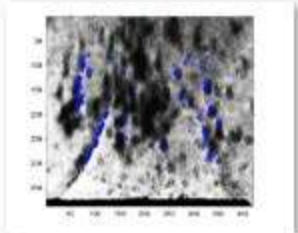
z_IMG_1203.JPG



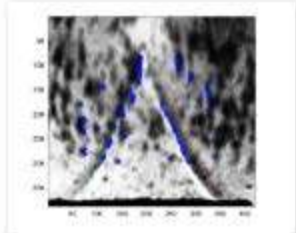
z_IMG_1204.JPG



z_IMG_1205.JPG

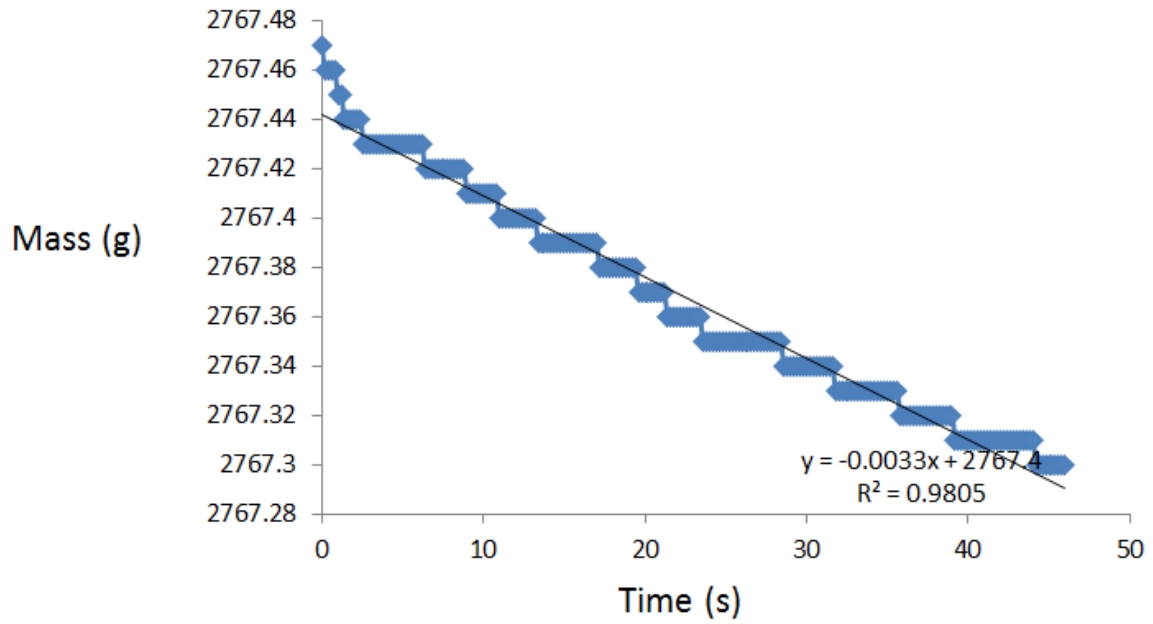


z_IMG_1206.JPG



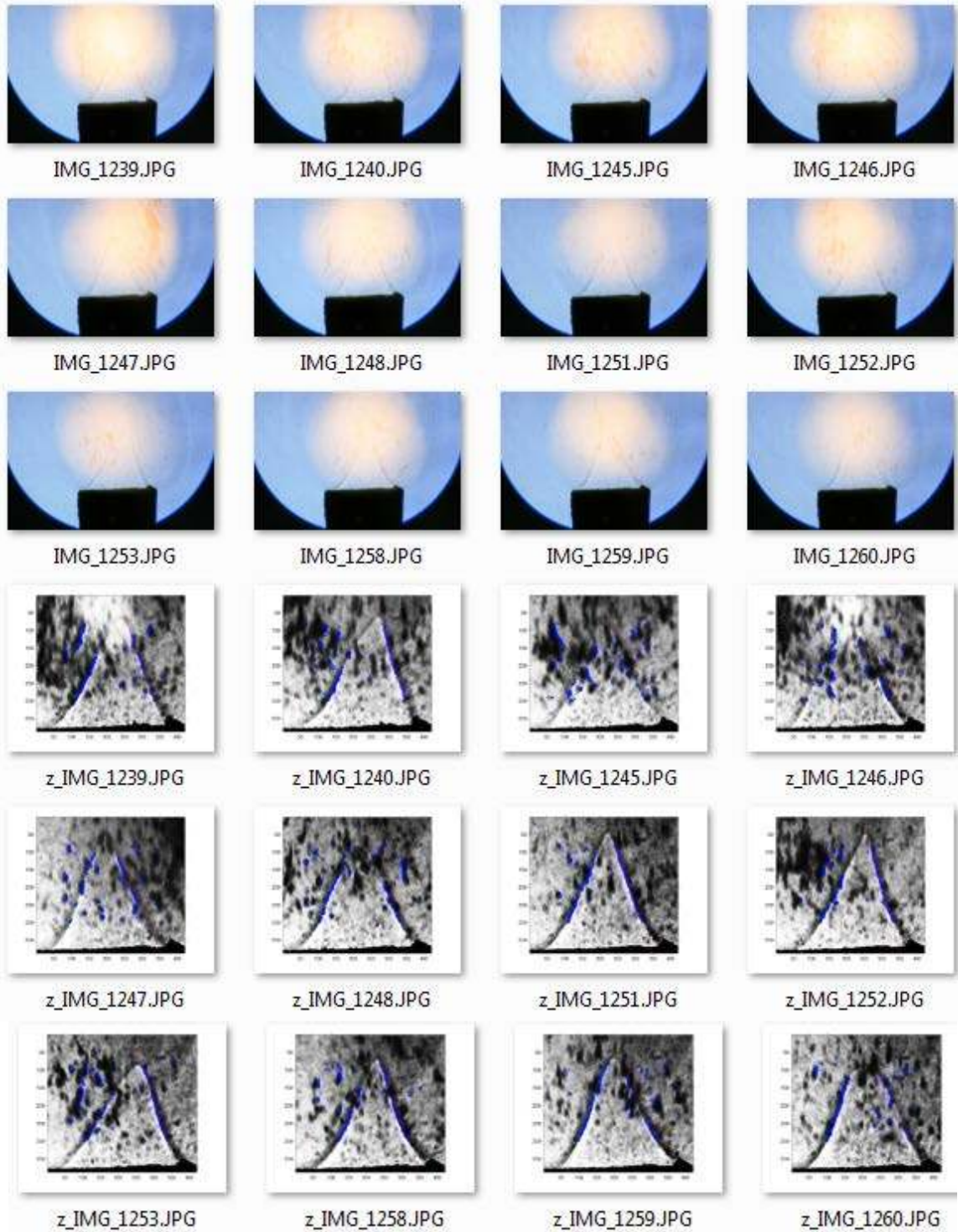
z_IMG_1207.JPG

Experiment NO. 8



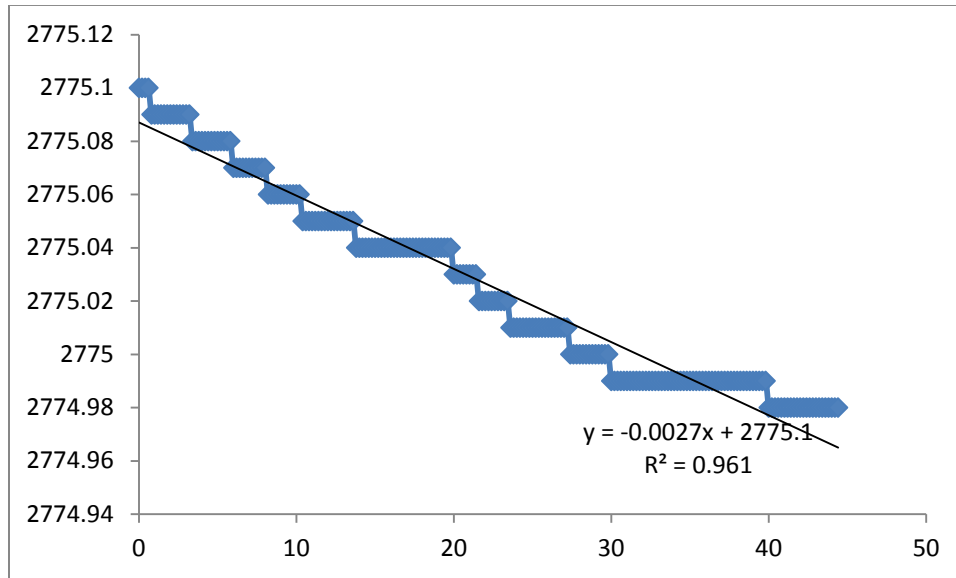
Air Flow Rate		Fuel Flow rate		Volume flow rate	nozzle width	U	Phi
SLPM	mole/sec	SLPM	mole/sec	m ³ /s	m	m/sec	
2.5	0.001732	0.21	0.000145	4.51E-05	0.010744	0.497869	0.79968

Entrainment Rate
3.30E-03 g/sec
Concentration
73.11 g/m³



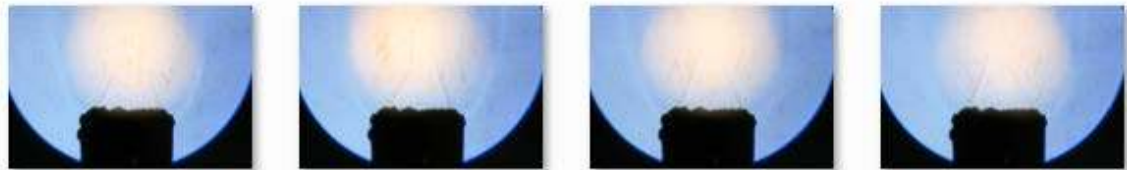
4.2 $\phi=0.85$; Flow Rate: Air 2.5 SLPM; Methane 0.223 SLPM

Experiment NO. 5



Air Flow Rate		Fuel Flow rate		Volume flow rate	nozzle width	U	Phi
SLPM	mole/sec	SLPM	mole/sec	m ³ /s	m	m/sec	
2.5	0.001732	0.223	0.000155	4.54E-05	0.010744	0.500255	0.849184

Entrainment Rate
 2.70E-03 g/sec
 Concentration
 59.53196 g/m³

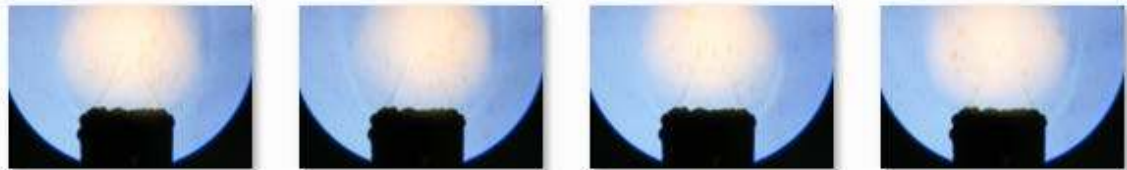


IMG_0856.JPG

IMG_0857.JPG

IMG_0858.JPG

IMG_0861.JPG



IMG_0863.JPG

IMG_0864.JPG

IMG_0865.JPG

IMG_0867.JPG

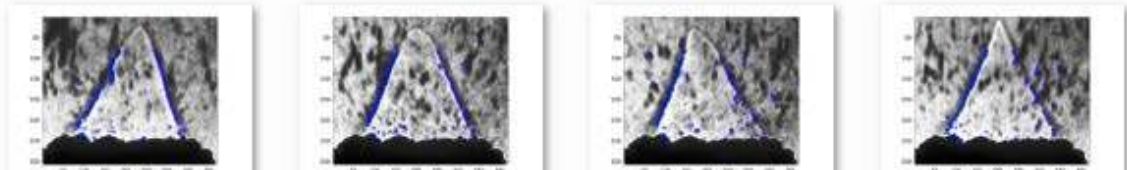


IMG_0869.JPG

IMG_0872.JPG

IMG_0873.JPG

z_IMG_0856.JPG

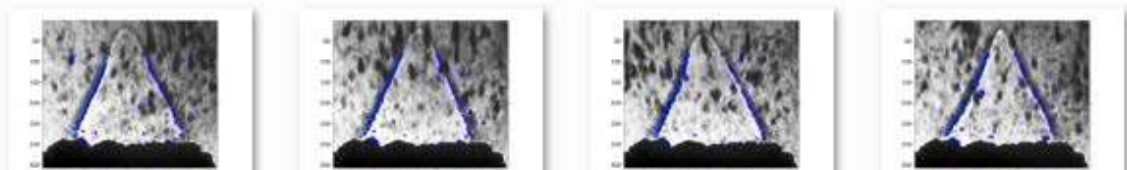


z_IMG_0857.JPG

z_IMG_0858.JPG

z_IMG_0861.JPG

z_IMG_0863.JPG



z_IMG_0864.JPG

z_IMG_0865.JPG

z_IMG_0867.JPG

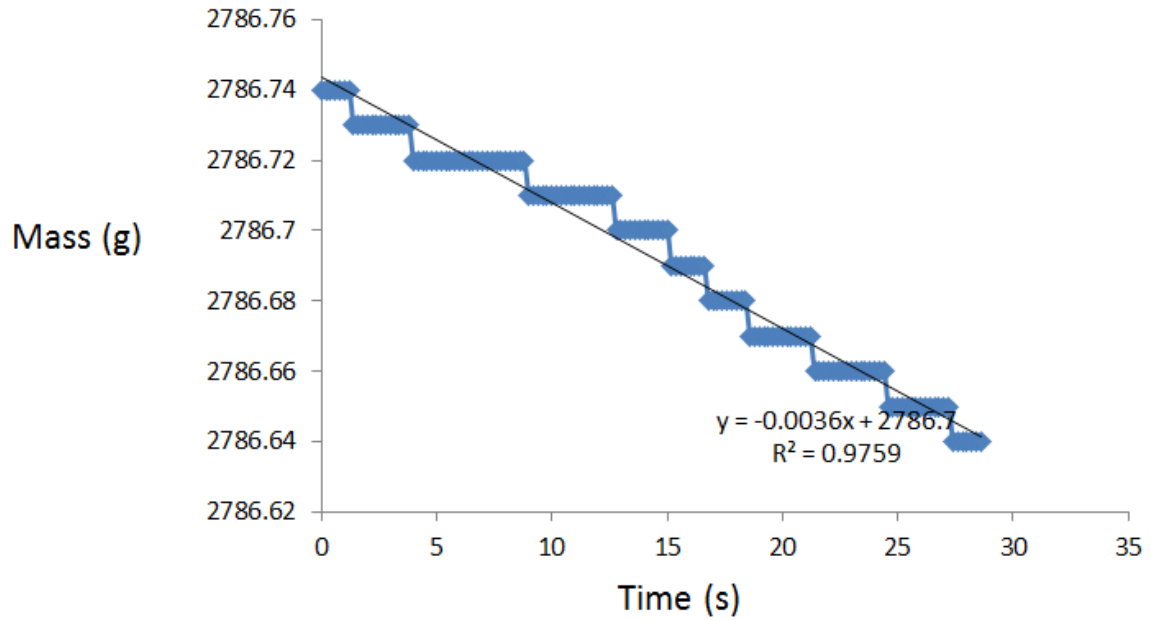
z_IMG_0869.JPG



z_IMG_0872.JPG

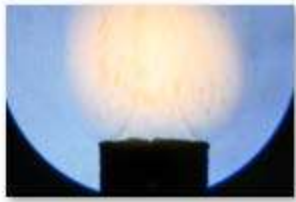
z_IMG_0873.JPG

Experiment NO. 10

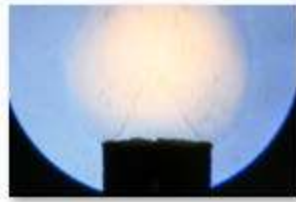


Air Flow Rate		Fuel Flow rate		Volume flow rate	nozzle width	U	Phi
SLPM	mole/sec	SLPM	mole/sec	m ³ /s	m	m/sec	
2.5	0.001732	0.223	0.000155	4.54E-05	0.010744	0.500255	0.849184

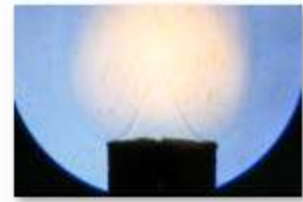
Entrainment Rate
3.60E-03 g/sec
Concentration
79.37594 g/m³



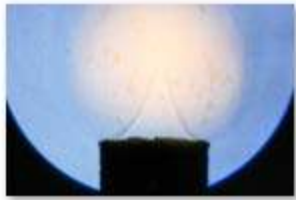
IMG_1019.JPG



IMG_1020.JPG



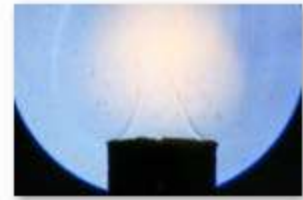
IMG_1021.JPG



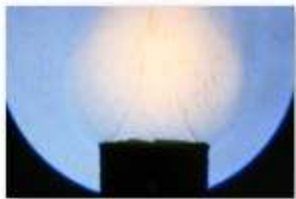
IMG_1022.JPG



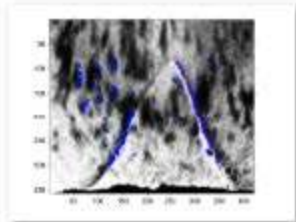
IMG_1023.JPG



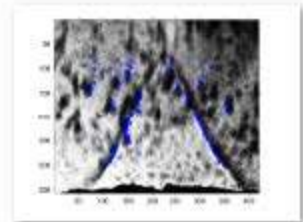
IMG_1024.JPG



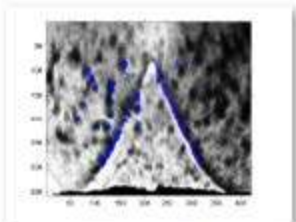
IMG_1025.JPG



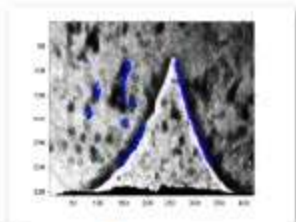
z_IMG_1019.JPG



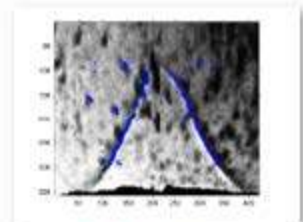
z_IMG_1020.JPG



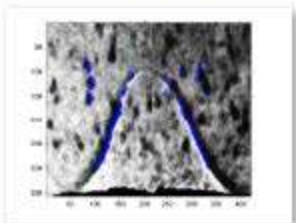
z_IMG_1021.JPG



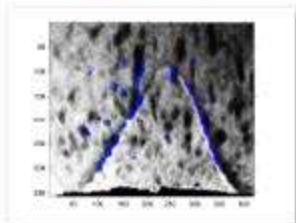
z_IMG_1022.JPG



z_IMG_1023.JPG

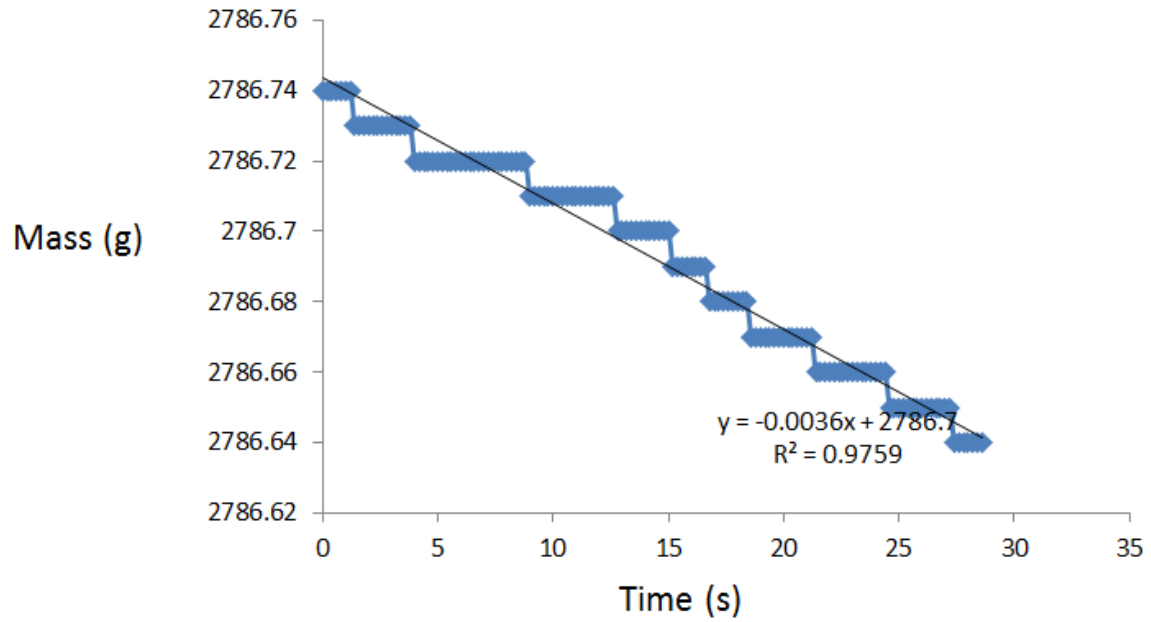


z_IMG_1024.JPG



z_IMG_1025.JPG

Experiment NO. 11



Air Flow Rate		Fuel Flow rate		Volume flow rate	nozzle width	U	Phi
SLPM	mole/sec	SLPM	mole/sec	m ³ /s	m	m/sec	
2.5	0.001732	0.223	0.000155	4.54E-05	0.010744	0.500255	0.849184

Entrainment Rate

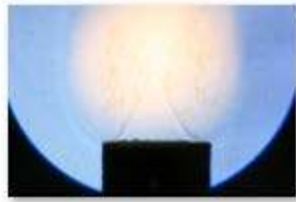
3.80E-03 g/sec

Concentration

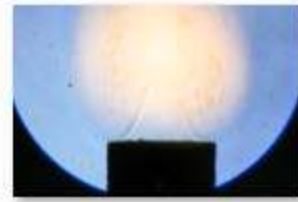
83.78572 g/m³



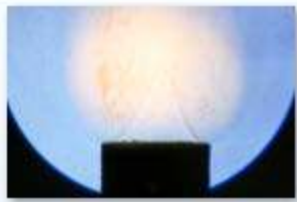
IMG_1035.JPG



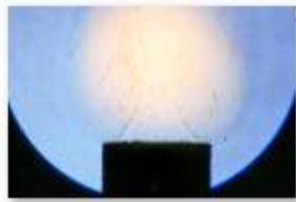
IMG_1038.JPG



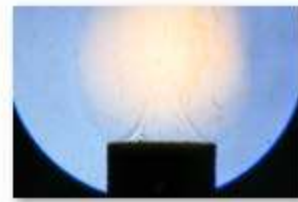
IMG_1039.JPG



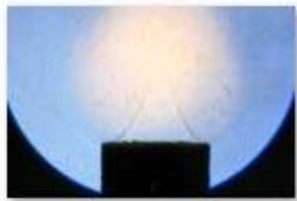
IMG_1042.JPG



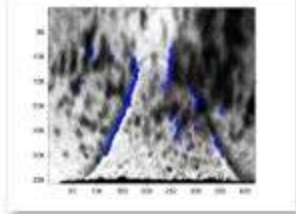
IMG_1044.JPG



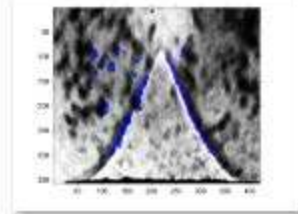
IMG_1054.JPG



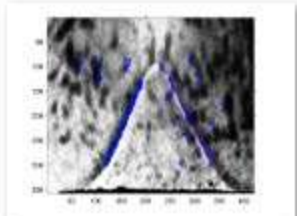
IMG_1058.JPG



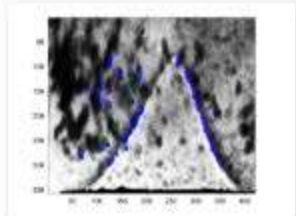
z_IMG_1035.JPG



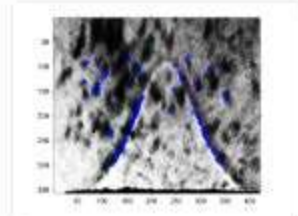
z_IMG_1038.JPG



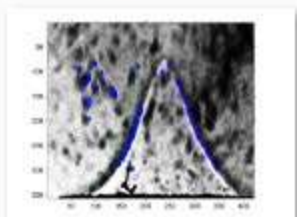
z_IMG_1039.JPG



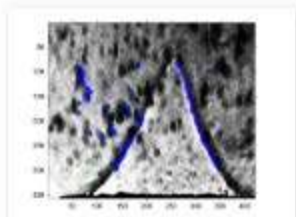
z_IMG_1042.JPG



z_IMG_1044.JPG

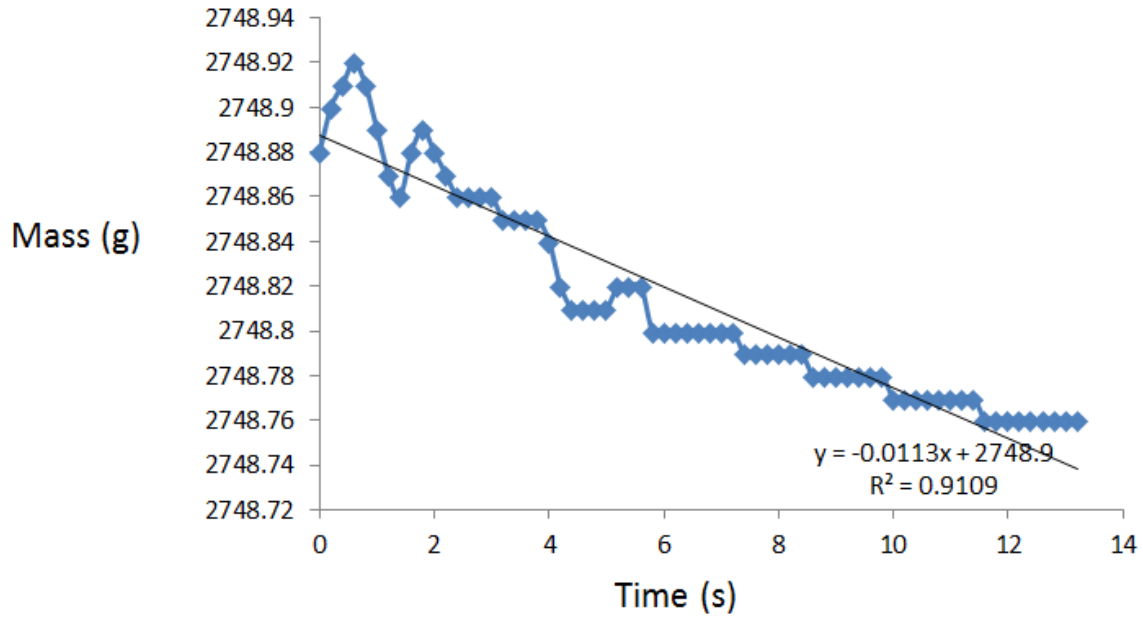


z_IMG_1054.JPG



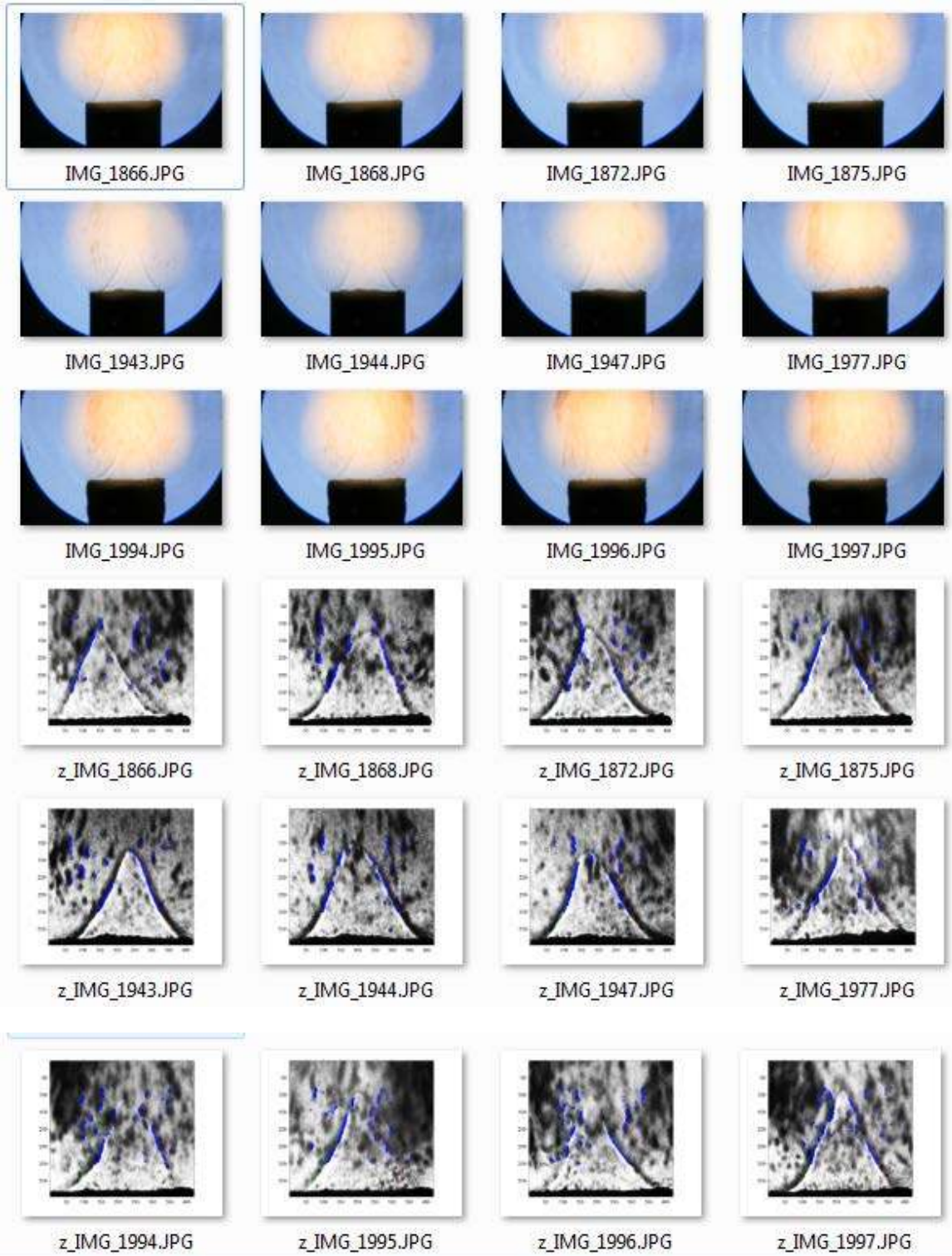
z_IMG_1058.JPG

Experiment NO. 17



Air Flow Rate		Fuel Flow rate		Volume flow rate	nozzle width	U	Phi
SLPM	mole/sec	SLPM	mole/sec	m ³ /s	m	m/sec	
2.5	0.001732	0.223	0.000155	4.54E-05	0.010744	0.500255	0.849184

Entrainment Rate
1.13E-02 g/sec
Concentration
249.1523 g/m³



5. Coal Particles (0-25 μm)

5.1 $\phi=0.75$; Flow Rate: Air 2.0 SLPM; Methane 0.158 SLPM

Experiment NO. 3

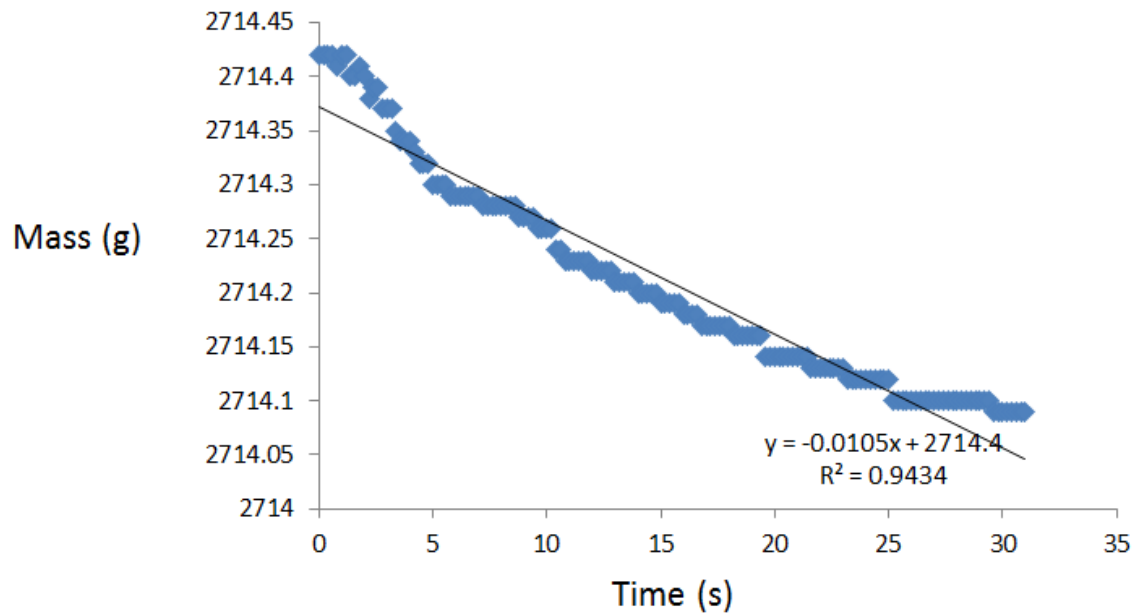
Air Flow Rate		Fuel Flow rate		Volume flow rate	nozzle width	U	Phi
SLPM	mole/sec	SLPM	mole/sec	m ³ /s	m	m/sec	
2	0.001386	0.158	0.000109	3.59E-05	0.010744	0.39646	0.75208

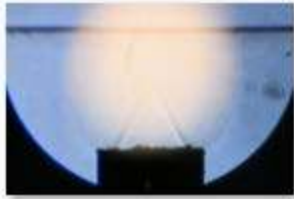
Entrainment Rate

1.05E-02 g/sec

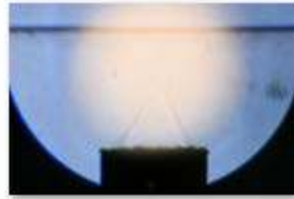
Concentration

292.1247 g/m³

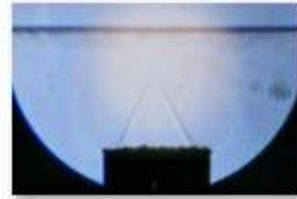




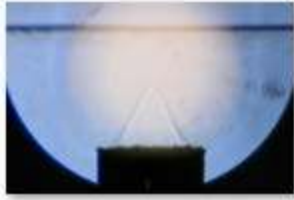
IMG_2968.JPG



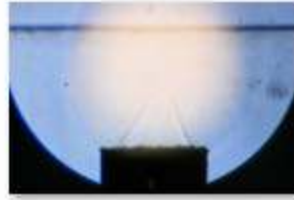
IMG_2976.JPG



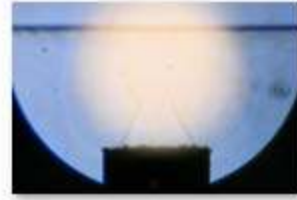
IMG_2977.JPG



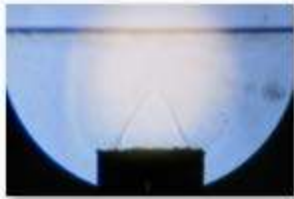
IMG_2978.JPG



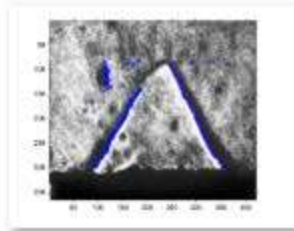
IMG_2981.JPG



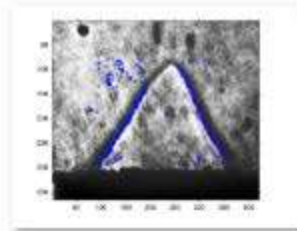
IMG_2982.JPG



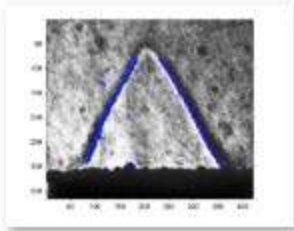
IMG_2983.JPG



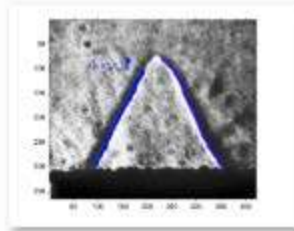
z_IMG_2968.JPG



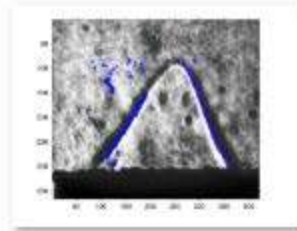
z_IMG_2976.JPG



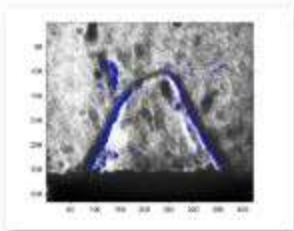
z_IMG_2977.JPG



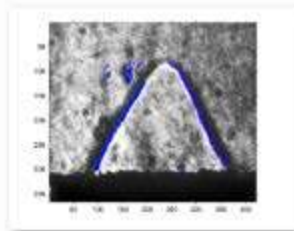
z_IMG_2978.JPG



z_IMG_2981.JPG



z_IMG_2982.JPG



z_IMG_2983.JPG